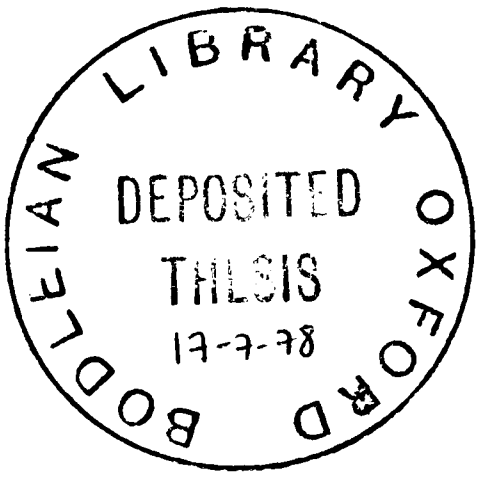
PHYSICAL PROPERTIES OF METALLOPORPHYRINS

by

PETER D. SKYTE

Dissertation submitted for the degree of Doctor of Philosophy
in the honour school of Physical Sciences (Chemistry),
University of Oxford.



The Queen's College

December, 1977

One view!

"HEME PROTEINS ARE MERELY LIGATED MODELS FOR STUDYING LIGATION PHENOMENA OF METALLOPORPHYRINS"

Alan D. Adler

ACKNOWLEDGMENTS

I should like to acknowledge the help of the following people, without whom this work would never have materialised.

Dr. H.A.O. Hill, for his guidance and supervision.

Dr. J. Büchler, Dr. A.K. Gregson, Dr. K.S. Murray, Professor G. Pellizer, Dr. D. Williams, Dr. N. Zarb-Adami, and members of the group, for general advice and valuable comments.

Mr. W.J. Murray and Mr. C. Webb for maintaining the N.M.R. instruments and livening up many long hours spent in the N.M.R. room.

Mr. D. Chapple and all the staff of the Inorganic Chemistry Laboratory.

Miss S. Toon, for converting my illegible scrawl into typed pages of scientific splendour.

The Science Research Council for their financial support for 2 years, and their lack of support for a 3rd year.

My parents, for their endless encouragement, devotion to duty during hours and hours of proof-reading, and doing their best to keep me in a frame of mind approximating to sanity.

CONTENTS

		Page
	List of Figures	viii
	List of Tables	xii
	Nomenclature and Abbreviations	xv
	Short Abstract	xvi
	Abstract	xvii
CHAPTER 1	INTRODUCTION	1
1.1	Porphyrins as Model Systems	1
1.2	Why Models?	4
	1. The influence of change in structure	5
	2. The influence of the porphyrin	8
	3. The influence of axial ligands	12
	4. The inter-relation of these influences	13
	5. Summary	16
1.3	The Ferric Ion in Complexes of Tetragonal Symmetry	16
	References	22
CHAPTER 2	THEORETICAL BACKGROUND OF PHYSICAL METHODS	26
2.1	Nuclear Magnetic Resonance Spectroscopy	26
	1. Theoretical basis of the NMR effect	26
	2. NMR spectroscopy of paramagnetic systems	28
	i) Fermi contact interactions	29
	ii) Pseudo-contact interactions	32
	iii) Applicability of Fermi contact and pseudo-contact term calculations	33
	3. Separation of contact and pseudo-contact interactions	36
	4. NMR instrumentation	37
2.2	Mössbauer Studies	38
	1. The isomer shift, δ	39
	2. The quadrupole splitting, Δ	39
	3. The magnetic hyperfine interaction	39
2.3	Electron Paramagnetic Resonance	40
	References	43

Page

CHAPTER 3 THE SPIN STATE EQUILIBRIUM IN FERRIC OCTAETHYLPORPHIN COMPLEXES 45

3.1 Introduction 45

1. Electronic crossover situations in iron porphyrin derivatives 45
2. Physical properties of spin equilibrium systems 50
   i) Electronic spectra 50
   ii) Infra-red spectra 54
   iii) Mössbauer effect 54
   iv) NMR spectra 55
   v) Paramagnetic susceptibilities 55
   vi) EPR spectra 56
3. Aim of the Work 56

3.2 Experimental 58

1. Apparatus and materials 58
   i) NMR measurements 58
   ii) Magnetic susceptibility and moment measurements 58
   iii) Electronic absorption spectroscopy 59
   iv) Mössbauer studies 60
   v) EPR measurements 60
   vi) Analysis of samples 60
2. Preparation of complexes 60
   i) Materials 60
   ii) Preparation 62

3.3 Results 64

1. N.M.R. results 64
2. Magnetic data 72
3. Electronic absorption spectroscopy 73
4. Mössbauer studies 77
5. EPR spectra 83

3.4 Discussion 85

1. General features 85
   i) NMR results 85
      a) Deviation of the temperature dependent plots from linearity 85
      b) Extrapolation anomalies in the temperature dependences of the observed shifts 86

Page

ii) Magnetic data 88

iii) Electronic absorption spectra 89

iv) Mössbauer studies 91

2. The spin equilibrium situation - a more complete description 93

3. Qualitative discussion of results of various physical methods 96

i) NMR results 97

ii) Magnetic data 98

iii) Electronic absorption spectra 99

iv) Mössbauer studies 101

4. Quantitative correlation between absorption spectra and magnetic moment data 102

5. Definitive treatment of the ferric porphyrin spin equilibrium 116

i) The magnetic model 116

ii) Magnetic data 117

iii) The isotropic PMR shifts 127

3.5 ADDENDUM: Preparation and PMR Spectroscopy of a Biscyano Ferric Porphyrin Complex 138

1. Introduction 138

2. Experimental 138

3. Results and Discussion 139

References 144

CHAPTER 4 PROTON MAGNETIC RESONANCE STUDIES OF SOME 'NATURAL' FERRIC PORPHYRIN COMPLEXES 147

4.1 Introduction 147

1. PMR spectroscopy and porphyrins 147

2. Spin delocalisation and electronic structure 151

3. Mechanisms of spin delocalisation 152

i) Ligand to metal charge transfer 154

ii) Metal to ligand charge transfer 154

iii) Spin delocalisation via M-L σ bonding 156

iv) Spin delocalisation via M-L π bonding 157

4. Theoretical models of delocalisation systems 160

5. Aim of the Work 161

Page

4.2 Experimental 162

1. Apparatus and materials 162
   i) NMR measurements 162
   ii) Solvents 163
   iii) Other materials 164
2. Preparation of compounds 164
   i) Esterification of ferric protoporphyrin chloride 164
   ii) Synthesis and purification of porphin 166
      a) Synthesis of pyrrole alcohol 166
      b) Synthesis of porphin 166
   iii) Insertion of iron into porphyrins 167

4.3 Results 169

1. Pyridinato complexes 169
2. Miscellaneous complexes 176
   i) Imidazole 176
   ii) Benzimidazole 179
   iii) Quinoline and isoquinoline 182

4.4 Discussion 185

1. Pyridinato complexes 185
   i) General features 185
   ii) Origin of shifts 187
   iii) Hyperfine shifts of the porphyrin ligand protons 190
   iv) Hyperfine shifts of the pyridinato ligand protons 197
   v) Non-Curie behaviour of chemical shifts 203
      a) Deviation of the temperature dependence plots from linearity 203
      b) Extrapolation anomalies in the temperature dependence plots 205
   vi) Bonding interactions in porphyrin complexes 206
      a) Porphyrin-metal bonding 206
      b) Pyridine-metal bonding 209
   vii) Substituent effects 213
2. Other complexes 215
3. Comparison with heme-proteins and enzymes 217

Page

4.5 ADDENDUM A: Studies on Piperidine Complexes of a Natural Porphyrin 220

1. Introduction 220
2. Experimental 221
3. Results 221
   i) NMR spectroscopy 221
   ii) Absorption spectroscopy 224
4. Discussion 227

4.6 ADDENDUM B: Studies on a Dipyridine Ferric Porphyrin Complex 228

1. Introduction 228
2. Experimental 229
3. Results 229
   i) NMR spectroscopy 229
   ii) Absorption spectroscopy 231
4. Discussion 233

References 238

CHAPTER 5 NUCLEAR MAGNETIC RESONANCE STUDIES OF SOME MIXED LIGAND FERRIC OCTAETHYLPORPHIN COMPLEXES 243

5.1 Introduction 243

1. Mixed ligand heme systems 243
2. Effect of axial ligands 245
   i) Cis and trans effects 245
   ii) Position of metal 246
3. Aim of the Work 248

5.2 Experimental 249

1. Apparatus and materials 249
2. Preparation of compounds 249

5.3 Results 249

1. Addition of pyridine to $Fe(OEP)(4\text{-}MePy)_2ClO_4$ 249
2. Addition of N-methylimidazole to $Fe(OEP)(4\text{-}MePy)_2ClO_4$ 254

5.4 Discussion 262

1. Equilibrium processes 262
2. NMR shifts 266
3. Cis and trans effects 268
4. Hyperfine shifts of the mixed ligand complex protons 271

Page

5. Position of iron atom 276

References 277

CHAPTER 6 NUCLEAR MAGNETIC RESONANCE STUDIES OF PORPHODIMETHENE FERRIC COMPLEXES 279

6.1 Introduction 279

1. Redox activities in the biological context 279
2. Redox properties of the porphyrin ligand 280
3. Oxo bridging in heme systems 285
4. NMR studies of oxo-bridged heme systems 286
5. Aim of the work 289

6.2 Experimental 290

1. Apparatus and materials 290
   i) NMR measurements 290
   ii) Solvents 291
2. Preparation of complexes 291

6.3 Results 291

1. Monomers 291
2. Dimers 302

6.4 Discussion 307

1. Monomers 307
2. Dimers 309
3. Comparison of monomers and dimers 310
4. Stereochemistry of the porphodimethene complexes 312
5. Effect of partial reduction of the porphyrin ring on electronic interaction 315
6. Relevance of the work to biological systems 320

References 323

Page

APPENDICES

APPENDIX I	FOURIER TRANSFORM NMR SPECTROSCOPY	325
APPENDIX II	OBSERVED ^1H NMR SHIFT DATA FOR FE(III)-OCTAETHYLPORPHIN X_2ClO_4 COMPLEXES	327
APPENDIX III	MAGNETIC SUSCEPTIBILITY DATA FOR FE(III)OCTAETHYLPORPHIN X_2ClO_4 COMPLEXES	333
APPENDIX IV	MAGNETIC MOMENT DATA FOR FE(III)OCTAETHYL-PORPHIN X_2ClO_4 COMPLEXES IN THE SOLID STATE	341
APPENDIX V	OBSERVED ^1H NMR SHIFT DATA FOR X_2FE(III)-PORPHYRIN DIMETHYL ESTER CHLORIDE COMPLEXES	342

LIST OF FIGURES

		Page
CHAPTER 1		
1.1	Structure of porphin	2
1.2	Structure of heme a	9
1.3	Structure of heme s	11
1.4	Structure of heme c	11
1.5	First order electrostatic, crystal field and spin-orbit coupling interactions of the sextet, quartet and doublet states of the d^5 configuration	19
1.6	Delineation of regions of different Fe(III) ground states	20
CHAPTER 3		
3.1	Potential energy curves in the crossover region	51
3.2	Absorption spectra of MbH_2O and MbCN	52
3.3	Absorption spectra of MbN_3 and MbOH	53
3.4	DN 704 cryostat	61
3.5	Ferric octaethylporphin complex	66
3.6	PMR spectrum of $Fe(OEP)(Py)_2ClO_4$ at various temperatures	67
3.7	Temperature dependence of observed NMR shifts of $Fe(OEP)(Py)_2ClO_4$	68
3.8	PMR spectra of some $Fe(OEP)(X\text{-}Py)_2ClO_4$ complexes at 200°K	71
3.9	Absorption spectrum of $Fe(OEP)(3\text{-}ClPy)_2ClO_4$ at 300°K and 217°K	74
3.10	Absorption spectrum of $Fe(OEP)(4\text{-}AcPy)_2ClO_4$ at 294°K and 218°K	75
3.11	Absorption spectrum of $Fe(OEP)(Py)_2ClO_4$ at 302°K and 213°K	76
3.12	Mössbauer spectrum of $Fe(OEP)(3\text{-}ClPy)_2ClO_4$ at 300°K and 77°K	79
3.13	Mössbauer spectrum of $Fe(OEP)(Py)_2ClO_4$ at 300°K and 77°K	80
3.14	Mössbauer spectrum of $Fe(OEP)(4\text{-}NH_2Py)_2ClO_4$ at 300°K and 77°K	81
3.15	Mössbauer spectrum of $Fe(OEP)(4\text{-}AcPy)_2ClO_4$ at 77°K	82
3.16	EPR spectrum of $Fe(OEP)(N\text{-}MeIm)_2ClO_4$ at liquid helium temperature	84
3.17	Simulated high spin and low spin absorption spectrum of $Fe(OEP)(3\text{-}ClPy)_2ClO_4$	112
3.18	Simulated high spin and low spin absorption spectrum of $Fe(OEP)(4\text{-}AcPy)_2ClO_4$	113

		Page
3.19	Simulated high spin and low spin absorption spectrum of $Fe(OEP)(Py)_2ClO_4$	114
3.20	Regions of parameter space defining different ground states for d^5 ferric ion	118
3.21	Temperature variation of theoretical and experimental magnetic moments of $Fe(OEP)(3\text{-}ClPy)_2ClO_4$	122
3.22	Ordering of the energy levels in $Fe(OEP)(3\text{-}ClPy)_2ClO_4$ against their magnetic moments at 320°K	123
3.23	Temperature dependent isotropic shifts of the β-pyridine proton resonances in $Fe(OEP)(4\text{-}AcPy)_2ClO_4$	131
3.24	PMR spectrum of $(CH_3CH_2CH_2CH_2)_4N^+Fe^-(OEP)(CN)_2$ at 298°K	140
CHAPTER 4		
4.1	Energy level diagram for metal-ligand bond formation	153
4.2	Spin transfer mechanisms	155
4.3	Relative energies of metal d orbitals and ligand σ, π (filled) and π* (vacant) molecular orbitals	158
4.4	PMR spectra of (a) 2,6-d_2-pyridine; (b) pyridine	165
4.5	Porphyrin structures and assignment nomenclature	170
4.6	PMR spectra of Fe-porphin chloride (A) and Fe-etioporphyrin chloride (B) + 4-methylpyridine at 225°K	171
4.7	PMR spectra of Fe-protoporphyrin dimethyl ester chloride + 3-methylpyridine and 4-methylpyridine at 219°K	172
4.8	PMR spectra of Fe-protoporphyrin dimethyl ester chloride + 2,6-d_2-pyridine, d_5-pyridine and pyridine at 219°K	173
4.9	PMR spectra of Fe-protoporphyrin dimethyl ester chloride (A), Fe-mesoporphyrin dimethyl ester chloride (B), Fe-deutero-porphyrin dimethyl ester chloride (C), and Fe-etioporphyrin chloride (D) + pyridine at 219°K	175
4.10	PMR spectrum of Fe-mesoporphyrin dimethyl ester chloride + 3-methylpyridine at various temperatures	177
4.11	Temperature dependence of observed PMR shifts from spectrum of Fe-mesoporphyrin dimethyl ester chloride + 3-methyl-pyridine	178
4.12	PMR spectra of Fe-porphin chloride (A) and Fe-mesoporphyrin dimethyl ester chloride (B) + imidazole at 246, 252°K respectively	180
4.13	Temperature dependence of observed PMR shifts from spectrum of Fe-mesoporphyrin dimethyl ester chloride + imidazole	181

		Page
4.14	PMR spectrum of Fe-mesoporphyrin dimethyl ester chloride + benzimidazole at various temperatures	183
4.15	PMR spectra of Fe-protoporphyrin dimethyl ester chloride + 5,6-dimethyl-benzimidazole (A) and benzimidazole (B) at 216°K	184
4.16	PMR spectra of Fe-mesoporphyrin dimethyl ester chloride (A) and Fe-protoporphyrin dimethyl ester chloride (B) + isoquinoline at 200°K	186
4.17	Top-filled and lowest empty π orbitals of iron(III)-porphyrin complexes	207
4.18	PMR spectrum of Fe-protoporphyrin dimethyl ester chloride + piperidine at 212°K	223
4.19	Absorption spectra of complexes of piperidine with Fe-proto-porphyrin dimethyl ester chloride	226
4.20	PMR spectrum of Fe-mesoporphyrin dimethyl ester chloride + 4,4'-dipyridyl at 223°K	230
4.21	Absorption spectra of complex of 4,4'-dipyridyl with Fe-mesoporphyrin dimethyl ester chloride	234

CHAPTER 5

5.1	Effect of additions of pyridine on -20 to -25 ppm region of PMR spectrum of $Fe(OEP)(4\text{-}MePy)_2ClO_4$ at 216°K	250
5.2	PMR spectrum of $Fe(OEP)(4\text{-}MePy)_2ClO_4$ + N-methylimidazole	255
5.3	Effect of additions of N-methylimidazole on -20 to -25 ppm region of PMR spectrum of $Fe(OEP)(4\text{-}MePy)_2ClO_4$ at 221°K	257
5.4	Titration of pyridine into $Fe(OEP)(4\text{-}MePy)_2ClO_4$	264
5.5	Titration of N-methylimidazole into $Fe(OEP)(4\text{-}MePy)_2ClO_4$	265

CHAPTER 6

6.1	Structures of chlorins and phlorins	283
6.2	Stereoisomers of folded complexes $(OEPR_2)MX$	284
6.3	PMR spectrum of μ-oxo-bis ferric protoporphyrin IX dimethyl ester at 308°K	288
6.4	PMR spectrum of $(OEPMe_2)FeOMe$ at 297°K	292
6.5	α,γ-Dialkyl-α,γ-dihydroferric octaethylporphin complex structures and assignment nomenclature	293
6.6	PMR spectrum of FeOEPCl at 302°K	294

		Page
6.7	PMR spectrum of $(OEPEt_2)FeOMe$ at 299°K	296
6.8	PMR spectrum of $(OEPPr_2)FeOMe$ at 299°K	297
6.9	PMR spectrum of $(OEPi\text{-}Pr_2)FeOMe$ at 299°K	298
6.10	PMR spectra of $\lfloor(OEPR_2)Fe\rfloor_2O$ complexes at 291°K	303
6.11	Deconvoluted PMR spectra of $\lfloor(OEPEt_2)Fe\rfloor_2O$ (A) and $\lfloor(OEPPr_2)Fe\rfloor_2O$ (B) at 291°K	306

LIST OF TABLES

Page

CHAPTER 1

1.1 Oxidation potentials of Fe(II) porphyrins 12

1.2 C-O stretch frequencies of heme carbonyls in reconstituted hemoglobins and myoglobins 15

CHAPTER 3

3.1 Effective magnetic moments of some ferrihemoglobin and ferrimyoglobin complexes 46

3.2 Analytical data for ferric octaethylporphin complexes 63

3.3 Diamagnetic susceptibility data 72

3.4 Mössbauer parameters of $Fe(OEP)(X\text{-}Py)_2ClO_4$ complexes 78

3.5 Relationship between basicity of axial ligand and magnetic moment of ferric octaethylporphin complex 89

3.6 Thermodynamic and physical parameters calculated for a high spin-low spin spin equilibrium in $Fe(OEP)X_2ClO_4$ complexes 107

3.7 Various parameters of the spin-state transition for ferrimyoglobin, ferrihemoglobin and ferriperoxidase complexes 109

3.8 Magnetic parameters for several ferric octaethylporphin derivatives 124

3.9 Representative experimental and theoretical isotropic shift data for some ferric octaethylporphin complexes 132

3.10 Observed NMR shift data for the $(CH_3CH_2CH_2CH_2)_4N^+ Fe^-(OEP)(CN)_2$ complex in deuterochloroform 142

3.11 Observed NMR shifts for the diamagnetic $(CH_3CH_2CH_2CH_2)_4N^+\bar{C}lO_4$ complex in deuterochloroform at 298°K 143

CHAPTER 4

4.1 Analytical data for porphyrin compounds 168

4.2 Diamagnetic porphyrin shifts relative to TMS 188

4.3 Isotropic shifts of protons in $(X\text{-}Py)_2Fe(III)$-porphyrin chloride complexes in $CDCl_3$ at 200°K 191

4.4 Calculated pseudocontact shifts of porphyrin protons in $(X\text{-}Py)_2Fe(III)$-porphyrin chloride complexes at 200°K 192

4.5 Hyperfine shifts of porphyrin protons in $(X\text{-}Py)_2Fe(III)$-porphyrin chloride complexes in $CDCl_3$ at 200°K 194

		Page
4.6	Hyperfine interaction data for some porphyrin protons of $(X\text{-}Py)_2Fe(III)$-porphyrin chloride complexes in $CDCl_3$ at 200°K	195
4.7	Diamagnetic shifts of pyridine protons of pyridinatocobalt-(III) porphyrin complexes	197
4.8	Isotropic shifts of pyridine protons in $(X\text{-}Py)_2Fe(III)$-porphyrin chloride complexes in $CDCl_3$ at 200°K	198
4.9	Calculated pseudocontact shifts of pyridinato protons in $(X\text{-}Py)_2Fe(III)$-porphyrin chloride complexes at 200°K	199
4.10	Hyperfine shifts of pyridinato protons in $(X\text{-}Py)_2Fe(III)$-porphyrin chloride complexes in $CDCl_3$ at 200°K	200
4.11	Hyperfine interaction data for some pyridinato protons of $(X\text{-}Py)_2Fe(III)$-porphyrin chloride complexes in $CDCl_3$ at 200°K	201
4.12	Values of T_c observed for $(X\text{-}Py)_2Fe(III)$-porphyrin dimethyl ester chloride complexes	203
4.13	Relative spin density distributions in molecular moieties	210
4.14	Comparison of ligand basicity with spin density for particular $(X\text{-}Py)_2Fe(III)$-porphyrin chloride complexes	214
4.15	Calculated pseudocontact shifts of protons in $Im_2Fe(III)$-porphyrin chloride complexes at 200°K	216
4.16	Hyperfine interaction data for some porphyrin protons of $Im_2Fe(III)$-porphyrin complexes in $CDCl_3$ at 200°K	216
4.17	PMR shift data for ferric protoporphyrin dimethyl ester chloride in the presence of piperidine	225
4.18	PMR shift data for ferric mesoporphyrin dimethyl ester chloride in the presence of 4,4'-dipyridyl	232

CHAPTER 5

5.1	Examples of heme-porphyrin complexes with mixed axial ligands	244
5.2	Spectral data for cyanoprotohemins in aqueous pyridine	246
5.3	PMR shift data for $Fe(OEP)(4\text{-}MePy)_2ClO_4$ + pyridine	253
5.4	PMR shift data for $Fe(OEP)(4\text{-}MePy)_2ClO_4$ + N-methylimidazole	260
5.5	Hyperfine parameters for $Fe(OEP)(4\text{-}MePy)(Py)ClO_4$ mixed ligand complex at 200°K	272
5.6	Comparison of spin density distributions at various axial ligand positions	275

Page

CHAPTER 6

6.1	Oxidation potentials of some non-metallic porphyrin derivatives	281
6.2	Reduction potentials of some non-metallic porphyrin derivatives	281
6.3	Observed PMR shift data for some α,γ-dialkyl-α,γ-dihydroferricporphin complexes	301
6.4	Observed PMR shift data for some α,γ-dialkyl-α,γ-dihydroferric porphin μ-oxo bridged dimers	304
6.5	Representative isotropic shift data for some α,γ-dialkyl-α,γ-dihydroferricporphin and high-spin ferric porphyrin chloride complexes	316
6.6	Observed PMR shift data for some oxo-bridged α,γ-dialkyl-α,γ-dihydroferricporphin and ferric porphin dimer complexes	319

NOMENCLATURE AND ABBREVIATIONS

PROTO	Protoporphyrin IX dimethyl ester
MESO	Mesoporphyrin IX dimethyl ester
DEUTERO	Deuteroporphyrin IX dimethyl ester
ETIO	Etioporphyrin III
OEP	Octaethylporphin
TPP	Tetraphenylporphin
Hb	Hemoglobin
Mb	Myoglobin
CCP	Cytochrome C peroxidase
Py	Pyridine
Im	Imidazole
Iq	Isoquinoline
Bz	Benzimidazole
Pip	Piperidine
Dipy	4,4'-dipyridyl
Me	Methyl
Et	Ethyl
Pr	n-propyl
i-Pr	iso-propyl
TMS	Tetramethylsilane
NMR	Nuclear magnetic resonance
PMR	Proton magnetic resonance
ESR	Electron spin resonance
EPR	Electron paramagnetic resonance
B.M.	Bohr magneton
FOZ	First order Zeeman
SOZ	Second order Zeeman
+/-	Upfield/downfield

Physical Properties of Metalloporphyrins

Peter D. Skyte

The Queen's College,
Oxford.

D.Phil. (Physical Sciences)

Michaelmas Term 1977

Short Abstract

In this work, a number of physical techniques are used to study the behaviour and properties of different metalloporphyrin systems under varying conditions. The behaviour of these systems is interpreted so far as is possible in terms of relations between structure, both geometrical and electronic, and function.

In Chapter 1, a general survey of porphyrin structure, activity, properties and relevance is provided as an introduction. The significance of porphyrins in the biological context is briefly discussed, and arguments are presented to justify the scope of model systems in providing an understanding of larger biological systems.

Chapter 2 is concerned with the basic theory and practice of the physical techniques employed.

In Chapter 3, the electronic properties of iron porphyrin derivatives in which spin crossover phenomena are present are studied. With certain derivatives, unusual and anomalous features manifest themselves in the magnetic moment and PMR, Mössbauer and electronic absorption spectroscopic data. These results are discussed and interpreted in terms of a number of theories of increasing sophistication.

In Chapter 4, PMR studies of some 'natural' ferric porphyrin complexes are described. Paramagnetic spectral shift data are obtained, analysed and interpreted in terms of a valid spin delocalisation theory. The effect of substituents on the porphyrin ring and on the axial ligand upon the bonding interactions is observed.

In Chapter 5, some mixed ligand ferric octaethylporphin derivatives are studied by means of PMR spectroscopy. Hyperfine interaction data are obtained and partially rationalised in terms of spin density distribution at particular axial ligand positions.

In Chapter 6, some monomer and oxo-bridged dimer porphodimethene ferric complexes are studied by means of PMR spectroscopy in order to examine the effect of partial saturation at the porphyrin periphery on bonding interactions, and on electron spin transfer from the iron atom.

ABSTRACT

This work is concerned with the physical properties of metalloporphyrins. A number of physical techniques are used to examine the behaviour of different metalloporphyrin systems, overwhelmingly those containing iron as the central metal, under varying conditions. The behaviour of these systems is interpreted so far as is possible in terms of relations between structure, both geometrical and electronic, and function.

In Chapter 1, a general survey of porphyrin structure, activity, properties, and relevance is provided to serve as an introduction to the thesis. The significance of porphyrins in the biological context is briefly discussed. Pertinent arguments are presented to justify the nature of and reliance on model systems as a means of examining and evaluating larger biological systems. The perturbation of the free ion states of the ferric ion by near neighbour atoms in molecular complexes is also discussed, with particular reference to complexes of tetragonal symmetry. Using a strong crystal field model, the regions delineated in crystal field parameter space in which the ferric ion can exist as a particular state are illustrated.

Chapter 2 is concerned with the basic theory of the physical techniques employed in this work. Some of the factors which influence the parameters measured by the nuclear magnetic resonance, Mössbauer and electron paramagnetic resonance spectroscopic techniques are outlined.

In Chapter 3, the electronic properties of iron porphyrin derivatives in which spin crossover phenomena are present are studied. It is found with certain derivatives that unusual and anomalous features manifest themselves in the experimental data measured. Thus from the PMR spectroscopy, it is noted that plots of observed shift against

reciprocal of the absolute temperature show a non-Curie dependence. Over the same temperature range, the magnetic moments of the corresponding complexes measured in solution are found to vary appreciably. Mössbauer and electronic absorption spectra of certain of the derivatives also demonstrate a marked change as the temperature is varied.

These results are discussed and an interpretation qualitatively in terms of a doublet-sextet spin-state equilibrium is firstly advanced to account for the anomalous experimental effects observed. A quantitative correlation between the magnetic moment and absorption spectral data is put forward, and values of the thermodynamic and physical parameters obtained are seen to compare favourably with various ferric hemeproteins thought to involve spin-state transitions. Finally, a definitive theoretical treatment of the ferric porphyrin system is undertaken using a fairly sophisticated model of the magnetic behaviour. This theoretical approach is able, with some refinement of the model which invokes the employment of temperature dependent ligand field parameters, to reproduce closely the experimental magnetic moment and PMR shift data over a range of circumstances. Values of the hyperfine coupling constants are calculated for various protons in the porphyrin complex. The hyperfine coupling constants of the protons in the pyridine adduct are consistent with a σ spin delocalisation mechanism of spin distribution.

In an addendum to Chapter 3, the preparation and PMR spectroscopy of a biscyano ferric octaethylporphin complex are described.

In Chapter 4, proton magnetic resonance studies of some 'natural' ferric porphyrin complexes are described. The features of the resonance spectra are highlighted, and the shifts are analysed with reference to contact and pseudocontact contributions. The temperature dependence

of the shifts is non-Curie in behaviour and provides evidence for a low-spin/high-spin equilibrium. For most protons the pseudocontact contribution to the isotropic shift is found to be too significant to be ignored.

Hyperfine coupling constants are calculated and the experimental results interpreted in terms of a valid spin delocalisation theory. The main mechanism for spin delocalisation at the pyrrole ring carbon atoms is deduced to be charge transfer from porphyrin π orbitals to the iron. Spin delocalisation to the pyridine moiety is considered to be transmitted through a σ-bonding framework, the actual spin density distribution being influenced by $\sigma-\pi$ spin polarisation within the pyridine orbitals and also by a measure of π back bonding from the metal. Theoretical INDO spin density calculations support this analysis. The effect of substituents on the porphyrin ring and on the axial ligand upon the bonding interactions is observed.

In the two addenda to Chapter 4, studies on two unusual porphyrin complexes are described. In Addendum A, the existence of a bispiperidine ferric porphyrin complex, hitherto proposed as being unobtainable, is reported. PMR and absorption spectroscopy are used to establish the presence of this complex at low temperatures. In Addendum B investigations into a dipyridine ferric porphyrin complex are undertaken. Reasonable evidence from the PMR and absorption spectra supports the assertion that polymeric ferric porphyrin species bridged by the dipyridine ligand are present.

In Chapter 5 some mixed ligand ferric octaethylporphin derivatives are studied by means of PMR spectroscopy. Cis and trans effects are monitored and the PMR shifts are analysed, with the introduction of a number of assumptions, in terms of contact and pseudocontact contributions. Hyperfine interaction data are interpreted and partially rationalised in terms of spin density distribution at

particular axial ligand positions. In themselves the experimental observations are incapable of providing any means of establishing the metal position relative to the porphyrin plane.

In Chapter 6 some porphodimethene ferric complexes are studied by means of PMR spectroscopy in order to examine the effect of a degree of saturation at the porphyrin periphery on bonding interactions, and the effect of this on electron spin transfer from the iron atom. Both monomer and oxo-bridged dimer complexes are examined and the spectra compared. It is suggested that the dimethyl derivative may possibly be of different configuration to the other alkyl derivatives studied, and the dependence of bonding interactions on the angle of folding of the porphyrin macrocycle is commented upon. Superficial indications seem to suggest that full conjugation throughout the porphyrin ring periphery is not essential for effective transmission of the unpaired electron spin to orbitals of predominantly ligand character; break in full conjugation of the porphyrin ring π-electron system does not significantly affect the metal-ligand bonding interactions.

CHAPTER 1

INTRODUCTION

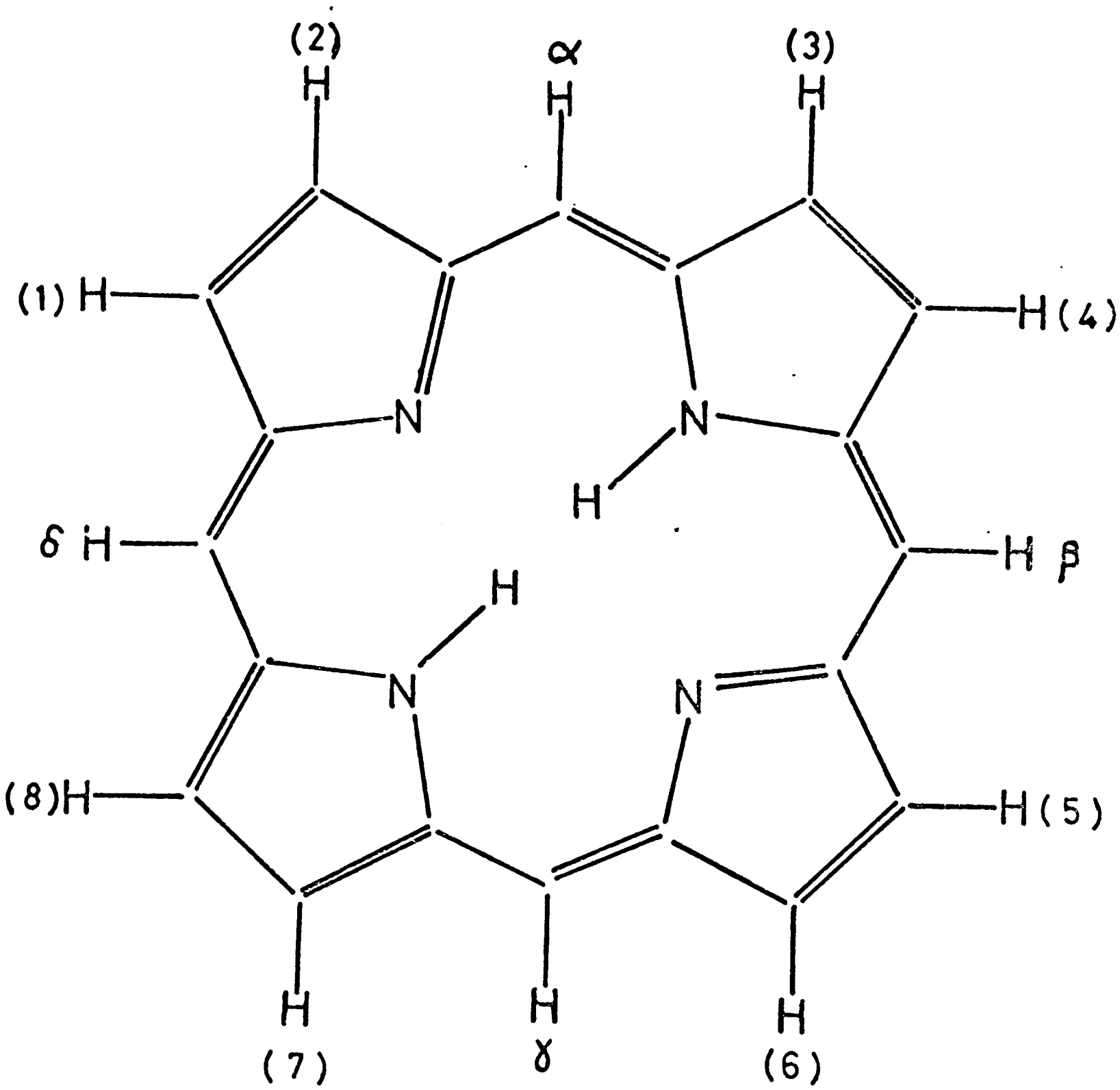
1.1 Porphyrins as Model Systems

Porphyrins are macrocyclic molecules of tetrapyrrole structure, derived formally from porphin (Figure 1.1) by substitution of some or all of the eight pyrrole hydrogen atoms and/or some or all of the four methene protons by various side-chains and groups[1]. The commonly occurring porphyrins have trivial names, which are nevertheless always used, and Roman numerals are used to distinguish the various positional isomers which occur when a porphyrin has more than one different side chain (e.g. protoporphyrin IX is 1,3,5,8-tetramethyl-2,4-divinyl porphin-6,7-dipropionic acid).

A very large number of variations of the basic porphin structure can be prepared and thus there is a large variety of structural types to choose from, to compare and to contrast. The best known examples of these materials found naturally are the chlorophylls and the heme prosthetic groups of heme proteins, but many other structures can be derived from these by appropriate reactions. Octa-alkyl and methene substituted (ms-) porphyrins[2] can be produced in great variety, and azaporphins[3] can also be prepared synthetically (the phthalocyanines[4] are examples of this class). Furthermore, there are obtainable, either synthetically or naturally, a number of related structures, e.g. corrins[5] (exemplified by vitamin B_{12}), bile pigments[6,7], quatrenes[8], tetra-pyridyls, etc.

These structures range from relatively low to relatively high molecular weights, from highly covalent to highly ionic materials, and from highly symmetric to highly anisotropic structures. In addition they show a wide range of chemical reactivity: metal chelation and ligand co-ordination; acid-base reactivity in both the central nitrogens and on

FIG. 1.1



PORPHIN

Structure of Porphin

various side chain derivatives; redox changes in the pyrrole rings (e.g. chlorins), in the methene bridges (e.g. phlorins), and in the oxidation states of the various metalloderivatives; aromatic reactivity on the central macrocyclic ring structure; and the tendency to form molecular complexes of various kinds and to aggregation.

Porphyrins and porphyrin derivatives also have a wide range of physical properties and there are many ways of studying and following the physical behaviour of these molecules[9]. They are intensely coloured and show selective and strong absorption in a large range of spectroscopies[1]. Variations found in the highly aromatic porphyrin ligand and in metallo atoms are characterised by changes in such properties as visible - U.V., Mössbauer, nuclear magnetic resonance, electron paramagnetic resonance, I.R., far I.R., and optical rotatory dispersion - circular dichroism (O.R.D. - C.D.) spectra and magnetic susceptibilities.

These materials are active surfactants and form good films[10,11]. They can be studied as crystals, films, solutions, liquids[12] (at high temperature and pressure) and in the gas phase[13] (at elevated temperatures in the absence of oxygen). Some forms are luminescent[14], some are paramagnetic[1], and some are active catalysts or photosensitizers[1,6,15]. They show organic semiconduction, photoconduction, and a number of other types of solid state behaviour[4,16], and have relatively good mechanical, thermal and radiation stability[1,4]. A number of porphyrin structures have been well characterised by X-ray analysis[17], and a detailed approach to the theory of their spectra is available[18].

Porphyrins, porphyrin derivatives and porphyrin-like materials play a large number of well-diversified and well-established biological roles[1,6,19,20]. The significance and importance of these biological functions has always been well emphasised, more especially in those physiological processes associated with photosynthesis and hemeprotein phenomenology. The varied chemical and physical properties are reflected

in the biological significance of porphyrinic materials in pigmentation, photosynthesis, cellular respiration, gas transport, enzymatic catalysis, metabolic regulation and control, emulsification, electron transport, etc.[6,15,21-27] Changes or modifications of general porphyrin metabolism are associated with cancer, drug metabolism, ageing and specific disease syndromes such as the porphyrias[19,28] and the hemoglobinopathies[29].

The unusually large number of observable variables of potential value for elucidation of structure and reaction mechanisms has made the iron porphyrins particularly promising for detailed study, more especially since they also serve as prosthetic groups for the hemeprotein class of proteins and enzymes. These proteins can exhibit distinctly different functions which include reversible oxygen binding for transport (hemoglobins) or storage (myoglobins) of oxygen, oxygen reduction to the level of water (cytochrome c oxidase), mixed-function oxidation with oxygen (e.g. cytochrome P-450), electron-transfer (cytochromes b and c), and hydrogen peroxide utilisation (catalases and peroxidases)[30].

Thus, porphyrins have an intriguing bioinorganic chemistry, not only because of their critical biological roles but also owing to the challenge of being able to correlate a large number of independent observable physical parameters with those aspects of structure which determine biological functions.

1.2 Why Models?

It is a truism that hemoproteins, which all contain a heme unit as a kernel, have a wide variety of physiological and biological actions, although in essence the structures do not vary radically. Obviously subtle changes in structure produce important changes in character of these molecules, and as the heme unit is the core in every case, it seems appropriate to investigate how certain structural and electronic features of this unit affect overall physical and electronic properties.

The raison d'être of a particular biological system is that each specialised site has the peculiar merit of performing a specific function (or functions) in a distinct manner. These specific functions are the result of an exact combination of factors, the inter-dependence of which controls the role of the system. The purpose of model systems is then to reduce the number of variable factors in order that the inter-relation of a small number of these factors can be monitored under controlled circumstances. Ideally, the larger systems would be "stripped" of their superfluous sections and only the essential sections examined.

If the multifarious activities of hemoproteins in vivo are to be accounted for and understood, a number of problems must be posed which can be answered by study in vitro. Some of the problems which might be posed are:

1. The influence of change in structure on the electronic properties of the iron atom.
2. The influence of the porphyrin on particular properties of the system.
3. The influence of axial ligands on particular properties of the system.
4. The inter-relation of these influences.

1. <u>The influence of change in structure</u>

The structure of the iron-porphyrin unit, and in particular the position of the iron atom with regard to the centre of the porphyrin "hole", is intimately related to the spin state and redox state of the iron atom. The extent to which the iron atom lies outside the plane of the porphyrin ligand is dependent on the nature of the ligands to which the iron is bound perpendicular to this plane. In model complexes two main factors will be relevant - electron donation from the ligand to the metal, which can affect the spin state of the iron, and steric hindrance between the incoming ligand group and the planar porphyrin ligands. This causal link between the position relative to the porphyrin ligand plane,

the spin state and the redox state of the iron atom is of critical importance in biological systems, and is best illustrated by reference to a few examples.

The distance of each pyrrole nitrogen from the centre of the grouping is given by the radius of the central hole of the porphyrin, Ct-N. The radius of this cavity is limited by the cyclic structure of the porphyrin and has been found to be 2.015 $\pm$ 0.007 Å for all metalloporphyrins. The metal lies in the plane of the nitrogens only if the metal-nitrogen bond distance can be equal to Ct-N. Consistent with the ionic radius for octahedral high-spin Fe(III)[31], the Fe-N bond distances for the high-spin hemes lie within the range of 2.061 $\pm$ 0.012 Å which is clearly larger than the radius of the central hole. Low-spin planar complexes are feasible because of the 1.91 Å Fe-N bond distance predicted for low-spin iron[31].

Protein X-ray studies can determine the plane of the porphyrin but not the plane of the pyrrole nitrogens. The iron atom is about 0.3 Å out of the plane of the porphyrin in all the Fe(II) and Fe(III) high-spin myoglobin derivatives[32-38] whose X-ray structures have been determined. In hemoglobin the iron is also displaced about 0.3 Å from the plane of the porphyrin toward the proximal histidine in the high-spin Fe(III) complexes[39-41]. However, for deoxyhemoglobin, the displacement of the iron is about 0.75 Å [41-44], consistent with the even larger radius for high-spin Fe(II) than for high-spin Fe(III) and the lack of any ligand in the sixth position to pull the iron toward the plane of the porphyrin. In certain low-spin Fe(III) hemoglobins there is an indication that the iron may lie in the plane of the porphyrin[45,46]. These results imply that the iron may move as much as 0.75 Å when oxygen is bound to hemoglobin, and it has been proposed that this movement may trigger heme-heme interaction in hemoglobin[47,48].

Reversible binding of molecular oxygen by these hemoproteins can only take place when the iron is in the Fe(II) oxidation state. Furthermore, there is a close balance between the energies of the low-spin and high-spin states so that a change at just one coordination position is able to drive the complex from one state to the other. Thus, deoxyhemoglobin and deoxymyoglobin are both high-spin paramagnetic complexes[49,50] while complexing with ligands such as O_2, CO and NO produces low-spin diamagnetic complexes[49-51]. The absence of any ligand in the sixth coordination position of the high-spin Fe(II) deoxy-complexes could well be due to the inability of the iron to make a "good" bond distance with both the four heme-nitrogens and two histidine nitrogens. The iron is therefore partly pulled from the plane of the heme to make a reasonably "good" bond with one histidine and partly excluded from the porphyrin hole on size grounds. On the addition of oxygen the iron changes to low-spin and its size is now such that it can be accommodated into the plane of the porphyrin. It also demands, as do all low-spin Fe(II) complexes, that the O_2 and the ligands in the fifth and sixth coordination positions should be at reasonable bond distances.

The hemoproteins involved in electron transfer processes, the cytochromes, undoubtedly utilise Fe(III)/Fe(II) redox characteristics which are inherently favourably balanced in these complexes. An extremely fine balance in the structure achieved around the iron atom is capable of exerting a great effect on the redox couple and oxidation state. Thus, in cytochrome c, various physical and electronic properties, for instance magnetic moments, have been interpreted as implying a spin-state equilibrium between high-spin and low-spin Fe(III). The two forms presumably have somewhat different metal-ligand bond distances and thus the ligands bound to the iron (III) must be able to adjust their positions relative to the iron very easily. The low-spin Fe(II) form of the enzyme has a different

structure from the predominantly low-spin Fe(III) form, emphasising the ease of structural change. In addition, the redox potentials of cytochromes c, +0.25 to +0.35 volts, are very high for a heme-complex, suggesting that the Fe(III) form is relatively unstable.

2. The influence of the porphyrin

The highly conjugated porphyrin macrocycle interacts very strongly with the iron atom in all hemoproteins, and differences in substituents on the periphery of the porphyrin ring have been found to have significant effects on the properties of the metal and the complex as a whole, for both model and natural systems[52-57]. The role of the porphyrin must therefore be examined. Essentially three classes of hemes are established in living systems which are labelled as heme a, heme b and heme c, since they are associated with the a, b and c type cytochromes.

Heme a serves as the site of oxygen reduction in cytochrome c oxidase with a critical function in mitochondrial reduction of molecular oxygen for the production of cellular energy[21,27]. The heme a structure (see Figure 1.2) is such that a formyl and a vinyl group are present, in addition to the 1-hydroxy-2-(trans,trans farnesyl)ethyl C_{17} side chain.

Heme b is the most extensively studied natural heme and is found in many proteins such as hemoglobins, myoglobins, cytochrome P-450, catalases and peroxidases as well as b-type cytochromes. The porphyrin ligand of this heme is protoporphyrin IX (for structure see Figure 4.5). Heme a differs from heme b only by the 1-hydroxy-2-(trans,trans farnesyl)ethyl and formyl groups at positions 2 and 8 in place of vinyl and methyl groups respectively. The heme b proteins perform a variety of roles as oxygen carriers, hydroxylation agents and electron transfer agents.

Spirographis or chlorocruoroheme, which has been called heme s[30], is a well-characterised natural heme (see Figure 1.3). It is found in certain sea worms and differs from heme b only by a formyl in place of vinyl at

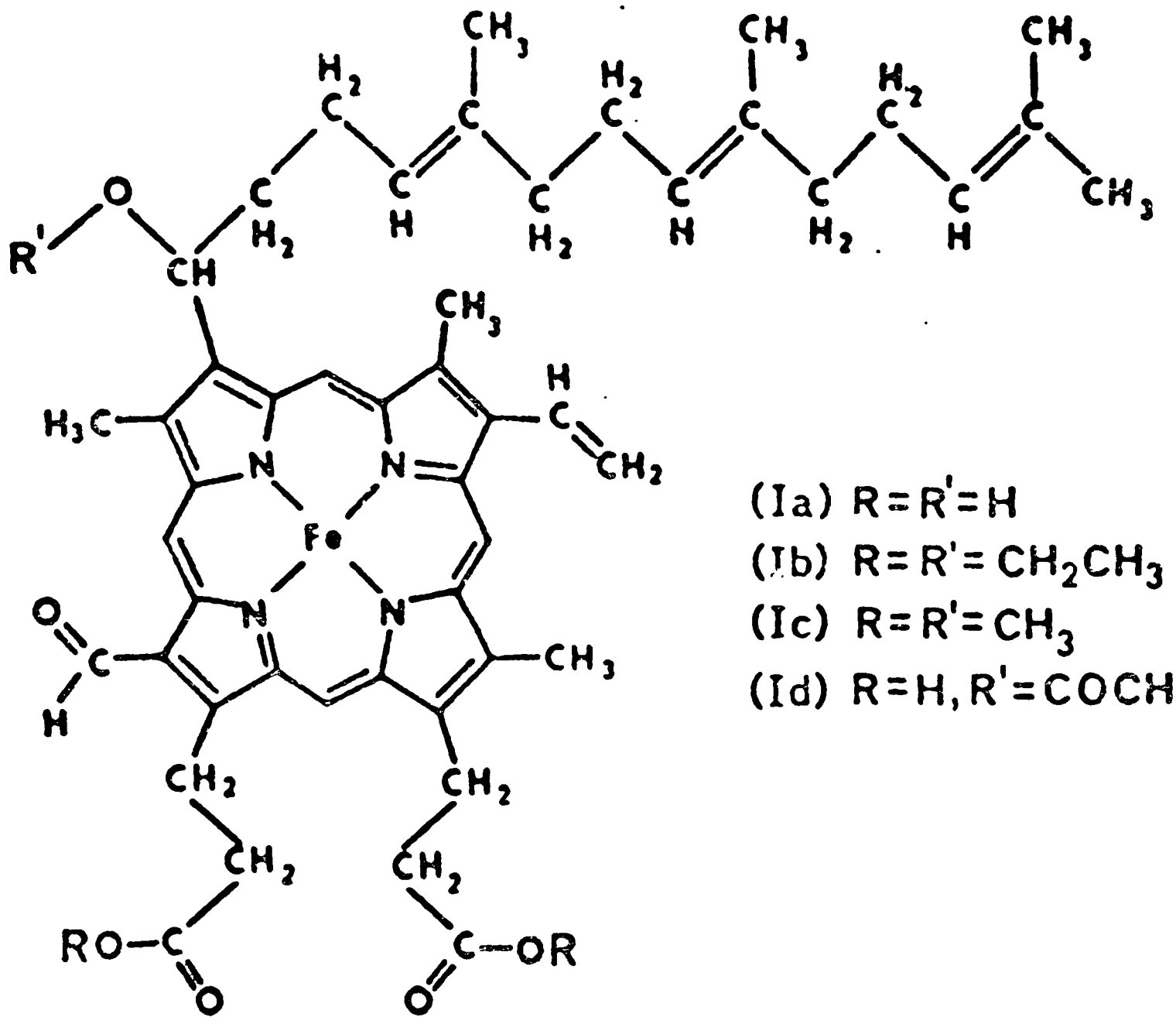


FIG. 1.2 Structure of heme a.

position 2. Heme c (Figure 1.4) has thioether linkages to cysteines at 1'-carbons of 2,4-ethyl groups with the remainder of the structure as in heme b. Heme c is found in cytochrome c, which functions as an electron transfer protein.

Sufficient data have been obtained on substituent effects with structural analogues to permit fairly accurate estimates of the effects of several of the structural differences found among the natural hemes a, b, c and s. Thus replacement of an 8-methyl or 2-vinyl by a formyl as is the case for heme a or heme s, respectively, compared with heme b has the effect of introducing a much more strongly electron-withdrawing substituent. Other reactions of the formyl (e.g. with protein) have been suggested but certainly not established. A particularly striking difference between hemes a and b is the unsaturated C_{17} side chain as opposed to a vinyl group. Possible roles for heme a in the electron-transport and oxidative phosphorylation functions of cytochrome c oxidase merit consideration[53,58,59]. The trans-trans farnesyl ethyl groups may form conformations in which the isolated double bonds can couple with each other and with porphyrin to serve in electron or energy transfer to or from the porphyrin ring or in which the terminal C_{12}-C_{13} double bond can participate in reactions at iron[53].

The redox behaviour of the Fe(III)/Fe(II) couple is varied by factors introduced by the substituents of the porphyrin ring, but generally the more highly oxidised state is stabilised with respect to the Fe(III) state of the hydrated inorganic ferric-ferrous couple. Electron-donating substituents (increasing the negative ring charge and the porphyrin basicity) lower the Fe(III)/Fe(II) potential, whereas electron-accepting substituents raise it. This has been shown to be true by many examples, and Table 1.1 below gives a good example where the effect of the two vinyl groups of protoporphyrin on the central iron in heme is substantiated.

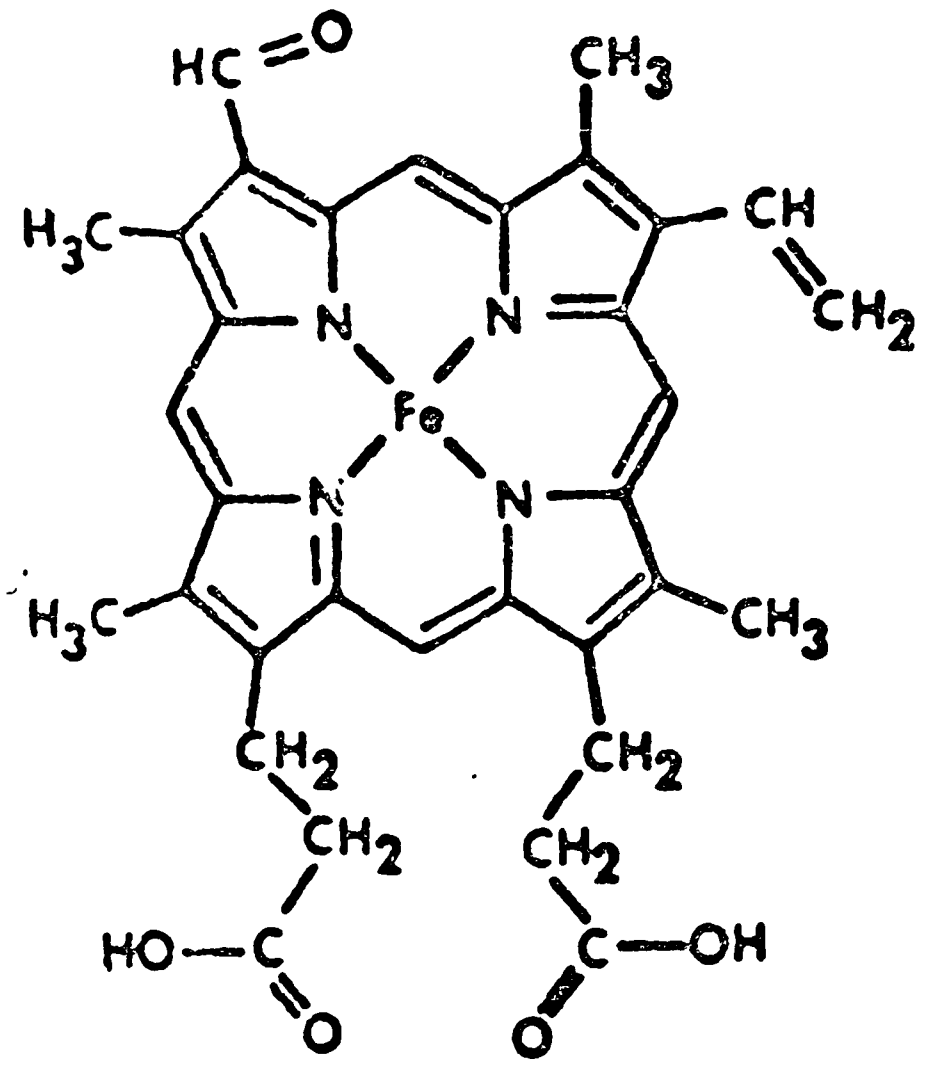


FIG. 1.3 Structure of heme s.

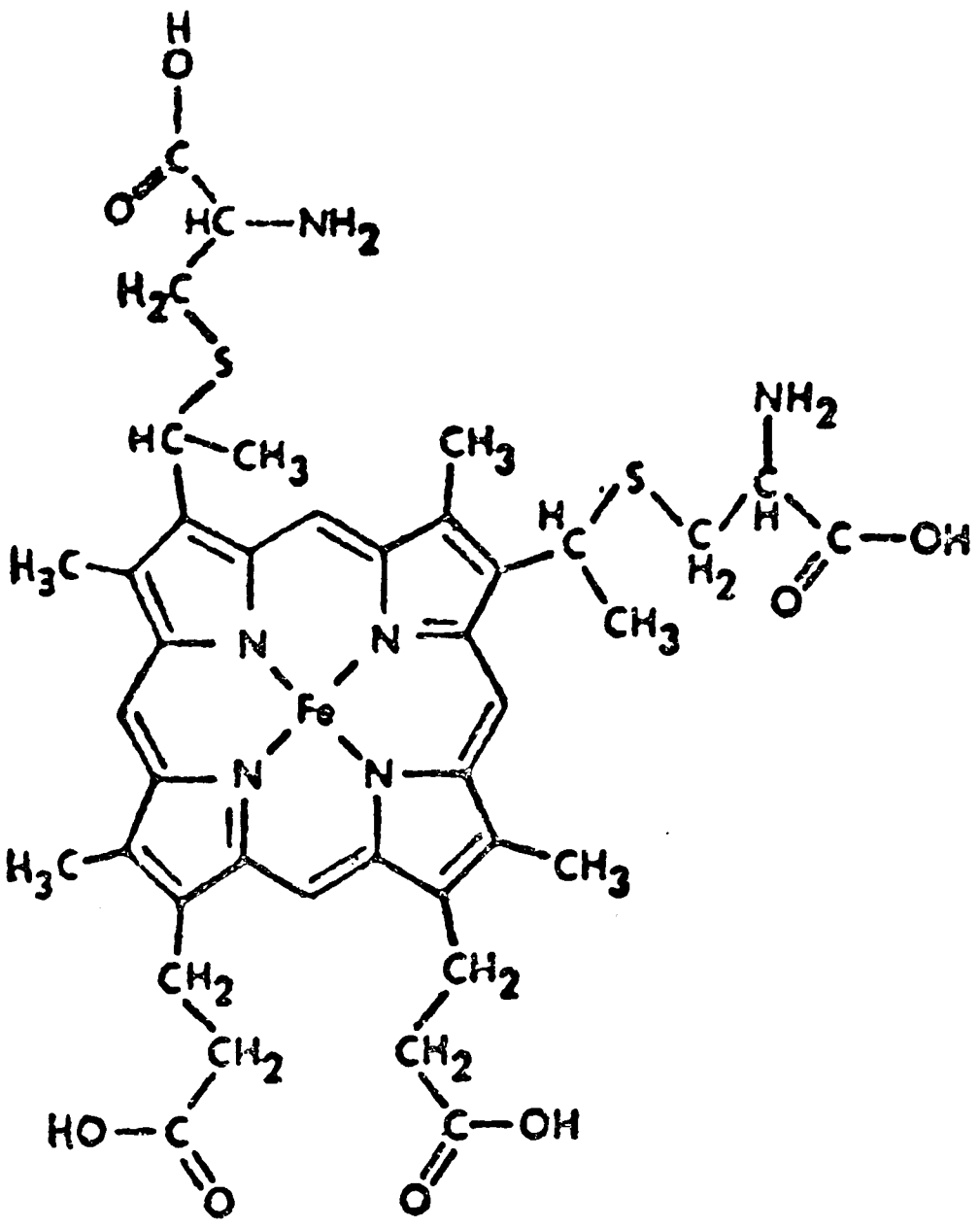


FIG. 1.4 Structure of heme c.

TABLE 1.1

Oxidation potentials[78] of Fe(II) porphyrins in alkaline solution (pH = 9.6)

Ferroporphyrin	$(Py)_2$ complex	$(CN^-)_2$
MESO	-0.30	-0.47
HEMATO	-0.24	-0.44
PROTO	-0.22	-0.42

Tetraphenyl-porphyrins, chlorophylls and phthalocyanines all yield higher potentials than the corresponding prototypes of porphyrins[78], indicating that electrostatic interaction with the bound metal ion is less effective.

3. The influence of axial ligands

The nature of axial ligand(s) can have a considerable influence on the behaviour and function of iron porphyrin units, although this influence has been more studied in artificial synthetic systems than in natural systems. The basicity of the axial ligand(s) plays an important role by conditioning the redox potential of the Fe(III)/Fe(II) couple to an energy range which is critical for biological systems. Electron-donating substituents (increasing the basicity) decrease the Fe(III)/Fe(II) potential whilst electron-accepting substituents increase it. The relationship between potentials and the pK_a of various bases added to the central Fe(II) ion (e.g. pyridine, nicotine, histidine, etc.) is essentially linear[1,22].

In addition to influencing the redox potential of the Fe(III)/Fe(II) couple, an axial ligand on one side of the heme plane is found to exert a considerable effect on binding of an axial ligand at the sixth coordination site. This is the result of mutual interaction between the two coordination sites on opposite sides of the metal known as the trans effect.

The binding of CO is known to be very sensitive to this trans ligand.

Thus, a mixed hemochrome in which one ligand is a base-like pyridine and the other ligand is CO is much more stable than complexes in which ligands at the fifth and sixth coordination positions are identical[22,60,61]. In fact, CO cannot be bound to both axial positions. Furthermore, replacing pyridine by the less basic H_2O ligand at the fifth position decreases the affinity of heme for CO by an order of magnitude.

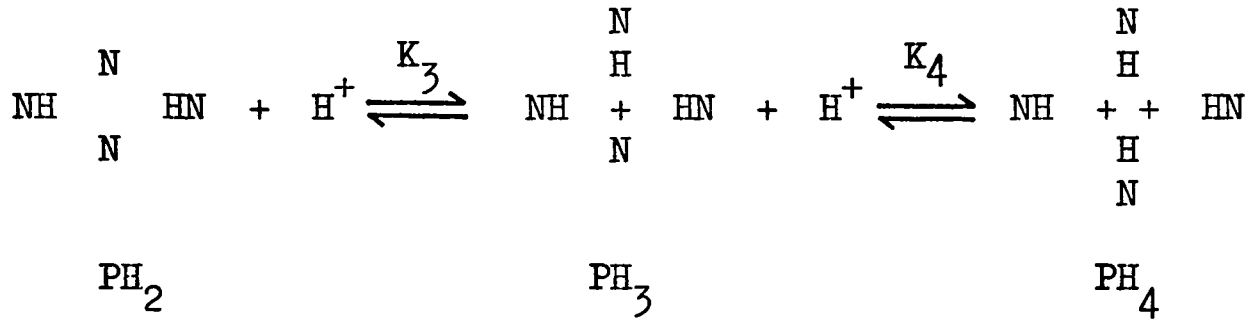
The ligand at the fifth coordination position, which is trans to O_2 in HbO_2 and MbO_2, is a part of the polypeptide chain. The only such proteins in which this ligand is not an imidazole ring are two genetically abnormal hemoglobins[62,63], M Iwate[64,65] and M Hyde Park[66,67]. In both cases histidines of the α and β chains, respectively, are replaced by less basic tyrosine residues. The abnormal sub-units do not reversibly bind oxygen but are oxidised instead, although this phenomenon is not solely attributable to the trans effect.

4. <u>The inter-relation of these influences</u>

The factors described above which may be invoked to account for the functions and properties of proteins are not of course operating independently and it is the combination of these factors that determines the role of a particular hemeprotein. Changes in axial ligand affect the strength of binding interactions between the metal and porphyrin. Conversely changes in electron-withdrawing or electron-donating character of a group at the periphery of the porphyrin ring are effectively transmitted across the porphyrin to influence the basicity of the central porphyrin nitrogen atoms. These in turn affect bonding between the porphyrin and the metal, and the bonding between metal and axial ligands. Such cis effects have been observed in hemeproteins and studied with a wide variety of physical methods in iron-porphyrin model complexes.

The ORD and electronic spectra of hemoglobin complexes such as HbO_2 and HbCO which are in the same oxidation state and spin state depend on

the axial ligand[68-70]. It has also been possible to study the effect of the porphyrin on the axial ligands of hemoglobin and myoglobin by using proteins reconstituted with different heme groups. The basicity of the central porphyrin nitrogen atoms can be evaluated with metal-free porphyrins in terms of equilibria for protonation of the imine-type nitrogen of the neutral species (PH_2) to form the "acid salts" (PH_3 and PH_4).



The carbon monoxide stretching frequency in heme carbonyls (ν_{CO}) is sensitive to porphyrin substituents at positions 2 and 4[53,71-73] (Table 1.2). As porphyrin basicity decreases, ν_{CO} increases. An increase in ν_{CO} indicates a higher C-O bond order, but a lower Fe-C bond order, and therefore weaker CO bonding to heme; decreased porphyrin basicity renders iron (II) a poorer π-donor to CO.

Relative oxygen affinities of these reconstituted hemoglobins and myoglobins follow a similar order ethyl > hydrogen > hydroxyethyl > vinyl[74]. This order is the reverse of that found for the negative induction effects of these groups, suggesting the importance of the π-electron density of the porphyrin in regulating the oxygen affinity of hemoglobin. It has, therefore, been proposed that the withdrawal of π-electron density from the porphyrin ring strengthens iron to porphyrin π-bonding and thereby weakens the π-bonds of the iron to axial ligands[54,74].

The above represent only a few of the many experimentally observed changes in physical properties of hemoproteins which can be correlated with changes in bonding between iron and axial ligand and between iron

TABLE 1.2

C-O stretch frequencies of heme carbonyls in reconstituted hemoglobins and myoglobins[53,71-73]

		ν_{CO} (cm^{-1})
Hemoglobin A		
Native		1951.0
Reconstituted with substituted deuteroheme		
2,4-vinyl		1951.0
2,4-hydrogen		1948.5
2,4-ethyl		1946.0
Myoglobin, sperm whale		
Native		1944.0
Reconstituted with substituted deuteroheme		
2,4-vinyl		1944.0
2,4-hydrogen		1941.0
2,4-ethyl		1939.0
In bromoform with 0.12M pyridine		
Substituted deuteroheme	pK_3[56,57]	
2,4-ethyl	5.8	1973.0
2,4-hydrogen	5.5	1975.1
2,4-vinyl	4.8	1976.6
2,4-acetyl	3.3	1983.7

and porphyrin. A reciprocal process operates in which a stronger iron-axial ligand bond results in weaker iron-porphyrin bonds and vice versa, with iron serving as a σ- and π-acceptor from both axial ligand and porphyrin ligand.

5. Summary

The above statements serve to indicate how nature tailors hemoproteins to perform a specific task or tasks. By variation of the porphyrin substitution pattern, by formation of mixed complexes with two different well-defined axial ligands from the protein core and by design of structure, factors such as oxidation potential, spin-state, position and bonding interactions of the central iron atom are manifestly capable of exerting a close control on the electronic, physical and biological properties of the system. The general aim of this work is to attempt to study some of these factors under model conditions, such that particular features may be "isolated" and examined in the absence of undue influence from extraneous factors. It is hoped that some light may be cast on the causes of particular effects.

1.3 The Ferric Ion in Complexes of Tetragonal Symmetry

Ferric ion has a $3d^5$ free ion ground state configuration with a ^6S ground state. When placed in a regular array of nearest neighbours to form a complex molecule or ion, free ion states are perturbed and mixed and there is the possibility that the lowest energy states of the ferric ion under certain conditions will be quartet or doublet states. In addition, if spin-orbit coupling is considered, it is also possible that the ground and low-lying states will be substantially spin-mixed states, i.e. states for which spin is no longer a good quantum number, and which are composed of mixtures of sextet, quartet and doublet components.

As the nature of these perturbed ferric ion states changes, so will the behaviour of the localised properties of the complex which can be associated primarily with the electronic and spin states of the ferric ion. The properties of particular relevance are the effective magnetic moment, the magnetic field energy and the electric field gradient of the ferric ion. In all ferric heme compounds the ferric ion is under such perturbed conditions that small changes in the local environment can cause significant changes in the nature of the ground and low-lying states. It then seems reasonable that a simple localised model for the hemin prosthetic group with parameters used in a consistent manner can explain and correlate the observed behaviour of the ferric ion and its dependence on the local environment.

The d^5 Fe(III) ion possesses a total of 43 high, low and intermediate spin multiplet states in a crystal field of cubic symmetry. Using the strong field approach, the pure orbitals t_{2g} and e_g form the basis for five electron configurations $t_{2g}^n\ e_g^{5-n}$, all derived from the original free ion configuration $3d^5$. In D_{4h} symmetry the 12 lowest strong cubic field states considered by Harris[75] become 21 states when split by a tetragonal field. Using the four quantum numbers ShmΘ (where S is the total spin of the state, m the z component of the total spin, h the irreducible representation of the group to which the state belongs and Θ the component of that representation, complex components 1,0,-1 being used for the threefold T_1 and T_2 representations and 1,-1 for the E representation), the original set of 12 strong cubic field multiplets become a total of 66 states. Harris[75,76] has shown that only the $^2T_{2g}$ (t_{2g}^5), the lowest lying $^4T_1$ $(t_{2g}^5\ e_g)$ and the $^6A_1$ $(t_{2g}^3\ e_g^2)$ strong field terms mix significantly via spin-orbit coupling. Thus, in describing the properties of ferric ion states due to a strong tetragonal crystal field and spin-orbit coupling, effectively it is only necessary to consider 24 states, the 12 components of the $^4T_1$, the 6 components

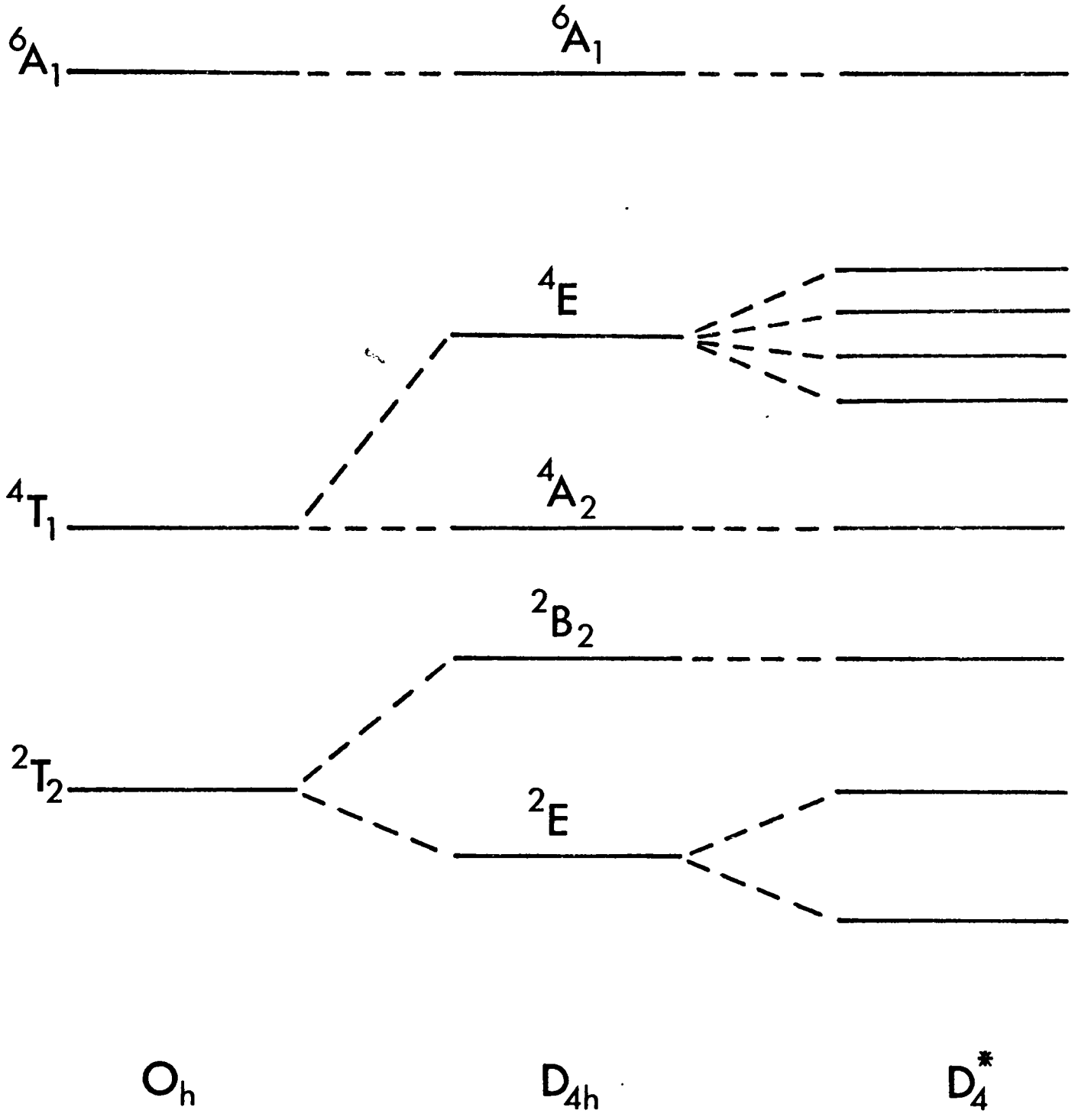
of $^2T_{2g}$ and the 6 components of $^6A_1$.

In a crystal field of strongly tetragonal symmetry the cubic field $^2T_{2g}$ term splits into $^2B_2$ and ^2E while the $^4T_1$ term splits into ^4E and $^4A_2$, the $^6A_1$ remaining orbitally nondegenerate. (Figure 1.5.) The energies of the resulting five electronic states in D_{4h} symmetry can be found in terms of the crystal field parameters Δ_{O_h}, C' and μ' defined by Harris, using methods outlined by Griffith[77]. Δ_{O_h} is the cubic crystal field splitting parameter and arises from the averaged effect of all the ligands of a given complex, Δ_{O_h} then varying with any change in the complex. Both C' and μ' relate to differences between axial and in-plane field strengths, positive when the in-plane interactions exceed the axial ones and negative when the axial interactions are greater. In this model, C' and μ' vary together so defining $C' = f\mu'$, the two tetragonal parameters become C' and f where C' now measures the magnitude of the tetragonal orbital distortion and f determines the ratio of the t_{2g} and e_g tetragonal splittings.

Using this strong crystal field model with tetragonal symmetry and allowing spin-orbit coupling among the sextet, quartet and doublet states which are possible, it is possible to delineate regions in crystal field parameter space in which ferric ion can exist as a sextet, quartet, doublet or spin-mixed state. Since all of the states are somewhat spin-mixed, due to spin-orbit coupling, a pure spin state has been defined as one for which the components are composed of 98% or more of the components of one total spin state or another, i.e. sextet, doublet or quartet. The remainder of the states are then "substantially" spin-mixed, i.e. more than 2%.

The delineation of regions of different ground states as a function of cubic and tetragonal field strength[75] is illustrated in Figure 1.6. For cubic field strengths $\Delta_{O_h} \leqslant 31000\ cm^{-1}$, a doublet ground state exists under conditions of strong axial fields. As the axial inter-

Figure 1.5: First order electrostatic, crystal field and spin-orbit coupling interactions of the sextet, quartet and doublet states of the d^5 configuration.



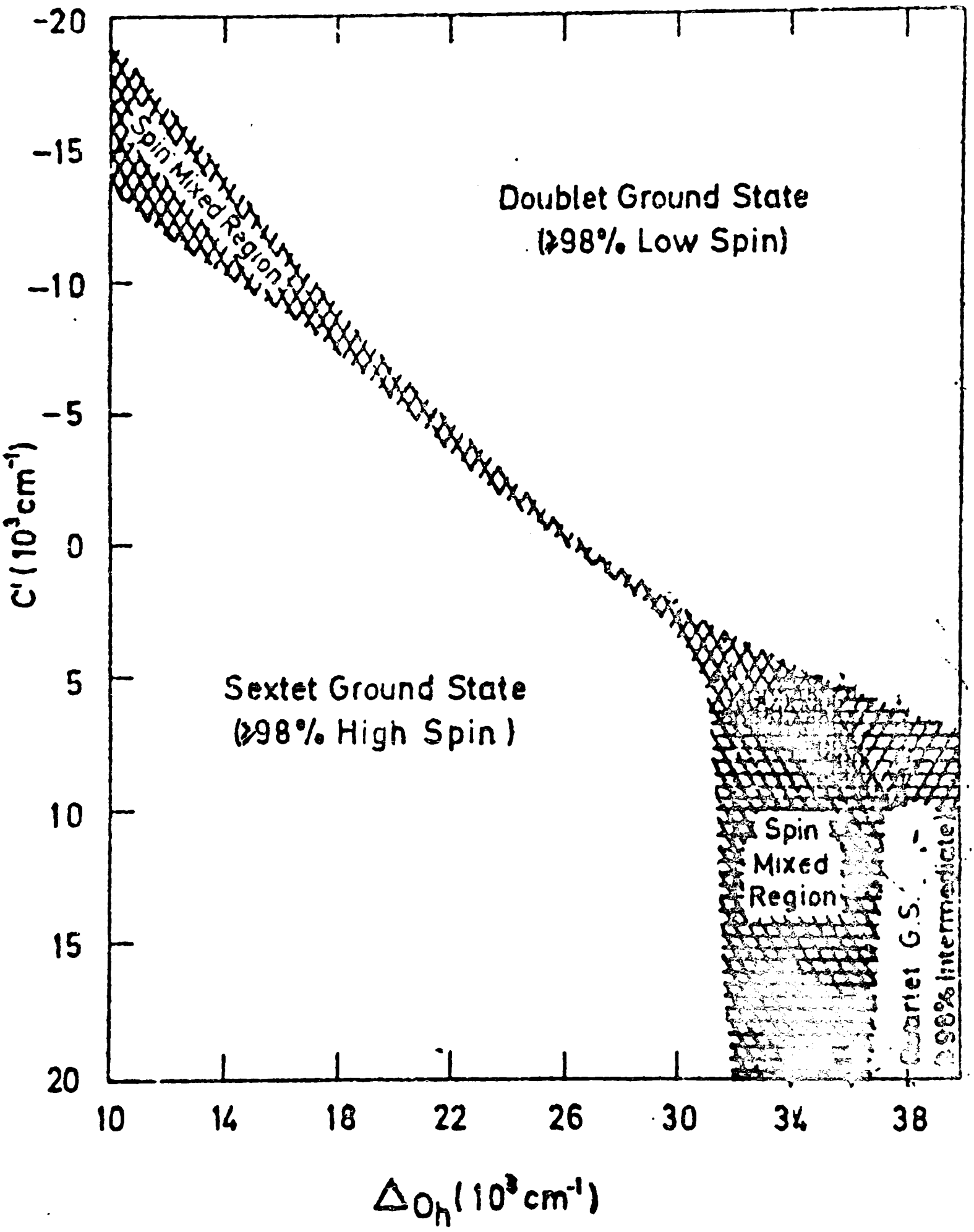


FIG. 1.6 Delineation of regions of different Fe(III) ground states.

actions decrease, there is a relatively narrow range of tetragonal parameter values in which ferric ion ground and low-lying states are substantially spin-mixed. This spin mixing primarily involves doublet and sextet states but has some quartet state character. As the axial field strength further decreases, pure sextet ground states occur.

For cubic field strengths from 31000 to 36000 cm^{-1}, doublet ground states again occur at the high axial field interaction conditions, and the states become spin-mixed as this interaction decreases. However, in this region of cubic field strengths a pure sextet state is no longer possible for the weakest axial fields considered. This is as a result of the increased quartet state mixing in the region of weaker axial fields at these higher overall field strengths. In this cubic field parameter region there is thus a rather wide range of axial field conditions for which the ferric ion states are substantially spin-mixed states.

Finally, at cubic field strengths $\geq$ 36000 cm^{-1} only doublet and quartet states are possible, the former with strong and the latter with weak axial fields. There is also a transition region between these two pure spin regions in which ferric ion states are again substantially spin-mixed, primarily involving doublet-quartet mixing.

REFERENCES

1. J.E. Falk. "Porphyrins and Metalloporphyrins", Elsevier, Amsterdam, 1964.

2. A.D. Adler, F.R. Longo, J.D. Finarelli, J. Goldmacher, J. Assour and L. Korsakoff. J. Org. Chem., 1967, 32, 476.

3. R.P. Linstead. J. Chem. Soc., 1953, 2873.

4. F.H. Moser and A.L. Thomas. "Phthalocyanine Compounds", Reinhold, New York, 1963.

5. D. Dolphin, A.W. Johnson and R. Rodrigo. Ann. N.Y. Acad. Sci., 1964, 112, 510.

6. R. Lemberg and J.W. Legge. "Hematin Compounds and Bile Pigments", Interscience, New York, 1949.

7. C.H. Gray. "The Bile Pigments", Methuen, London, 1953.

8. W.H. Brown and W.N. French. Can. J. Chem., 1958, 36, 371.

9. A.D. Adler. J. Polym. Sci. (C), 1970, 29, 73.

10. A.E. Alexander. J. Chem. Soc., 1937, 1813.

11. H.N. Dunning, J.W. Moore and M.O. Denekas. Indust. Eng. Chem., 1953, 45, 1759.

12. A.D. Adler, F.R. Longo and J.P. Heidere: unpublished observation.

13. J.A. Mullins, A.D. Adler and R.H. Hochstrasser. J. Chem. Phys., 1965, 43, 2548.

14. G.P. Gurinovitch, A.N. Sevchenko and K.N. Solov'ev. Soviet Physics Uspekhi, 1963, 6, 67.

15. P. Vernon and G.R. Seely. "The Chlorophylls", Academic Press, New York, 1966.

16. F. Gutmann and L.E. Lyons. "Organic Semiconductors", Wiley, New York, 1967.

17. J.L. Hoard. Science, 1971, 174, 1295.

18. M. Gouterman. J. Mol. Spec., 1961, 6, 138.

19. A. Vannotti. "Porphyrins", Hilger and Watts Ltd., London, 1954.

20. T.W. Goodwin. "Porphyrins and Related Compounds", Academic Press, New York, 1968.

21. B. Chance, R.W. Estabrook and T. Yonetani. "Hemes and Hemeproteins", Academic Press, New York, 1966.

22. J.E. Falk, R. Lemberg and R.K. Morton. "Hematin Enzymes", Pergamon Press, Oxford, 1961.

23. D. Keilin. "The History of Cell Respiration and Cytochrome", C.U.P., Cambridge, 1966.

24. G.S. Marks. "Heme and Chlorophyll", van Nostrand, London, 1969.

25. E.I. Rabinowitch. "Photosynthesis", Interscience, New York, 1945.

26. H. Tamiya. "Mechanism of Photosynthesis", Macmillan, New York, 1963.

27. K. Okunuki, M. Kamen and J. Sekuzu. "Structure and Function of Cytochromes", University of Tokyo Press, Tokyo, 1968.

28. A. Goldberg and C. Rimington. "Diseases of Porphyrin Metabolism", Thomas, Springfield, 1962.

29. J. Jonxis and J. Delafresnaye. "Abnormal Haemoglobins", Blackwell, Oxford, 1959.

30. W.S. Caughey, in "Inorganic Biochemistry", Ed. G.L. Eichhorn, Elsevier, Amsterdam, 1973, p.797.

31. L. Pauling. "The Nature of the Chemical Bond", Cornell University Press, Ithaca, 1960.

32. J.C. Kendrew, R.E. Dickerson, B.E. Strandberg, et al. Nature, 1960, 185, 422.

33. H.C. Watson. "Progress in Stereochemistry", Vol. 4, Butterworths, London, 1968.

34. J.C. Kendrew. Science, 1963, 139, 1259.

35. C.L. Nobbs, H.C. Watson and J.C. Kendrew. Nature, 1966, 209, 339.

36. C.L. Nobbs, in B. Chance, R.W. Estabrook and T. Yonetani, "Hemes and Hemoproteins", Academic Press, New York, 1966, p.143.

37. B. Chance, in B. Chance, T. Yonetani and A.S. Mildvan, "Probes of Structure and Function of Macromolecules and Membranes", Vol. 2, Academic Press, New York, 1971, p.321.

38. Ref. 6, p.149.

39. M.F. Perutz, M.G. Rossman, A.F. Cullis, H. Muirhead, G. Will and A.C.T. North. Nature, 1960, 185, 416.

40. M.F. Perutz, H. Muirhead, J.M. Cox and L.C.G. Goaman. Nature, 1968, 219, 131.

41. M.F. Perutz. Nature, 1970, 228, 726.

42. W. Bolton and M.F. Perutz. Nature, 1970, 228, 551.

43. H. Muirhead and J. Greer. Nature, 1970, 228, 516.

44. W. Bolton, J.M. Cox and M.F. Perutz. J. Mol. Biol., 1968, 33, 283.

45. E.A. Padlan and W.E. Love. Ref. 7, p.187.

46. E.A. Padlan and W.E. Love. Nature, 1968, 220, 376.

47. J.L. Hoard. "Structural Chemistry and Molecular Biology", Eds. A. Rich and N. Davidson; W.H. Freeman, San Francisco, 1968, p.573.

48. J.L. Hoard, M.J. Hamor, T.A. Hamor and W.S. Caughey. J. Amer. Chem. Soc., 1965, 87, 2312.

49. C.D. Coryell, F. Stitt and L. Pauling. J. Amer. Chem. Soc., 1937, 59, 633.

50. N. Nakano, J. Otsuka and A. Tasaki. Biochim. Biophys. Acta, 1971, 236, 222.

51. R.C.C. St. George and L. Pauling. Science, 1951, 114, 629.

52. W.S. Caughey. Ann. Rev. Biochem., 1967, 36, 611.

53. W.S. Caughey. Advan. Chem. Ser., 1971, 100, 248.

54. W.S. Caughey, H. Eberspaecher, W.H. Fuchsman, S. McCoy and J.O. Alben. Ann. N.Y. Acad. Sci., 1969, 153, 722.

55. W.S. Caughey, W.Y. Fujimoto and B.P. Johnson. Biochemistry, 1966, 5, 3830.

56. J.N. Phillips. Rev. Pure Appl. Chem., 1960, 10, 35.

57. J.N. Phillips, in "Comprehensive Biochemistry", Vol. 9, Eds. M. Florkin and E.H. Stolz, Elsevier, Amsterdam, 1963, p.34.

58. G.A. Smythe and W.S. Caughey. J. Chem. Soc., 1970, 809.

59. R.A. Bayne, G.A. Smythe and W.S. Caughey, in "Probes of Structure and Function of Macromolecules and Membranes", Vol. II, Eds. B. Chance, T. Yonetani and A.S. Mildvan, Academic Press, New York, 1971, p.613.

60. A. Nakahura and J.H. Wang. J. Amer. Chem. Soc., 1958, 80, 6526.

61. J.H. Wang, A. Nakahura and E.B. Fleischer. J. Amer. Chem. Soc., 1958, 80, 1109.

62. J.F. Perutz and H. Lehmann. Nature, 1968, 219, 902.

63. H. Morimoto, H. Lehmann and M.F. Perutz. Nature, 1971, 232, 408.

64. T. Miyaji, I. Iuchi, S. Shibata, I. Takeda and A. Tamura. Acta Haematol. Japan, 1963, 26, 538.

65. N. Hayashi, Y. Mutokawa and G. Kikuchi. J. Biol. Chem., 1966, 241, 79.

66. P. Heller, R.D. Coleman and V. Yakulis. J. Proc. 11th Congr. Int. Soc. Haematol., Govt. Printer, Sydney, 1966, p.427.

67. A. Hayashi, T. Suzuki, A. Shimuzu, K. Imai, et al. Arch. Biochem. Biophys., 1968, 125, 895.

68. A.J. Osbahr and G.L. Eichhorn. J. Biol. Chem., 1962, 237, 1820.

69. T. Samejima and K. Masako. J. Biochem. (Tokyo), 1969, 65, 759.

70. T-K. Li and B.P. Johnson, Biochemistry, 1969, 8, 3638.

71. W.S. Caughey, J.O. Alben and C.A. Beaudreau, in "Oxidases and Related Redox Systems", Eds. T.E. King, H.S. Mason and M. Morrison, John Wiley, New York, 1965, p.97.

72. J.O. Alben and W.S. Caughey. Biochemistry, 1968, 7, 175.

73. W.S. Caughey. Ann. N.Y. Acad. Sci., 1970, 174, 148.

74. Y. Sugita and Y. Yoneyama. J. Biol. Chem., 1971, 246, 389.

75. G. Harris. Tneor. Chim. Acta., 1968, 10, 119.

76. G. Harris. Theor. Chim. Acta., 1968, 10, 155.

77. J.S. Griffith. "The Theory of Transition Metal Ions", Cambridge University Press, 1961, Chapter 9.

78. J-H. Fuhrhop. Structure and Bonding, 1974, 18, 1.

CHAPTER 2

THEORETICAL BACKGROUND OF PHYSICAL METHODS

2.1 Nuclear Magnetic Resonance Spectroscopy

1. Theoretical basis of the N.M.R. effect

Nuclear magnetic resonance (N.M.R.) spectroscopy is the study of absorption of electromagnetic radiation, involving transitions occurring in the radio frequency region of the spectrum between nuclear energy levels of nuclei situated in a magnetic field[1-7]. All nuclei with odd, and some with even mass number, possess the property of spin, and the possession of both spin and charge confers on the nucleus a magnetic moment μ_N which is proportional to the magnitude of the spin.

$$\mu_N = \gamma_N \frac{hI}{2\pi} = g_N \beta_N I \qquad (2.1)$$

where γ_N is the nuclear gyromagnetic ratio in radians $sec^{-1} gauss^{-1}$, β_N is the nuclear Bohr magneton, g_N is the nuclear g factor and I is the value of the spin angular momentum vector. Quantum theory demands that the allowable nuclear spin states are quantised and the component M_I of the nuclear spin vector in any given direction can only take up one of a set of discrete values which are +I, I-1, ..., -I.

In the absence of a magnetic field the energy of an isolated nucleus is independent of M_I. When a magnetic field H is applied, there is an interaction between the field and the magnetic moment μ_N which may be represented by the spin Hamiltonian

$$\mathcal{H} = -\mu_N . H = \frac{-h}{2\pi} . \gamma_N H_o I_z = -g_N \beta_N H_o I_z \qquad (2.2)$$

where the static field H_o is chosen to lie along the z direction. The wave functions associated with the allowable nuclear spin states are represented as $|M_I>$ and solution of the Hamiltonian equation (2.2) gives eigenvalues of $-g_N \beta_N H_o M_I$. Thus in this situation there is a set of (2I+1) non-degenerate energy levels corresponding to the (2I+1) values of M_I, each separated by $g_N \beta_N H_o$.

These energy levels are normally observed by measuring the energy difference ΔE of transitions between two states. From transition probability theory, by considering the electromagnetic radiation as a perturbation on the system it can be shown that matrix elements of the type

$$| \langle \Psi_m | I_x | \Psi_n \rangle |^2 \qquad (2.3)$$

are zero unless $|m-n| = 1$ and the electromagnetic radiation is normal to the applied field. In expression (2.4) Ψ_m and Ψ_n are wave functions describing the m^{th} and n^{th} nuclear or electronic states. The Hamiltonian representing the interaction of the radio frequency ν with the system is given by

$$\mathcal{H} = -g_N \beta_N H(I_x \cos 2\pi \nu t - I_y \sin 2\pi \nu t) \qquad (2.4)$$

Thus transitions may be induced between the levels by applying an oscillating electromagnetic field of frequency ν perpendicular to the steady field H_o provided ν satisfies the resonance condition

$$\Delta E = h\nu = g_N \beta_N H_o \qquad (2.5)$$

The above discussion assumes that the presence of the sample does not perturb the magnetic field since the Hamiltonian given in (2.2) refers to an isolated nucleus. In fact, the nucleus is part of an atom or molecule which also contains electrons and the induced orbital motions of these electrons in the applied magnetic field produces a secondary magnetic field at the nucleus.

Thus

$$H_{effective} = H_o(1 - \sigma) \qquad (2.6)$$

where σ is defined as the screening constant. Since the shielding effect is caused by electronic environment, values of σ will vary with the position of the nucleus in the molecule, and factors that affect electron density will also affect σ .

The Hamiltonian given in (2.2) may be written as

$$\mathcal{H} = -g_N\beta_N(1 - \bar{\sigma})H_oI_z \qquad (2.7)$$

where $\bar{\sigma}$ is a tensor with principal values σ_x, σ_y, σ_z. In solution the average value is measured

$$\sigma = {}^1/_3 (\sigma_x + \sigma_y + \sigma_z) \qquad (2.8)$$

In practice, it is convenient to refer the chemical shift to that of a standard.

$$\text{Thus,} \quad \delta = \sigma - \sigma_{\text{reference}} = \frac{H_o - H_o^{\text{ref}}}{H_o^{\text{ref}}} \qquad (2.9)$$

2. N.M.R. spectroscopy of paramagnetic systems

In principle, any process giving rise to the formation of time dependent magnetic fields at the nuclear spins of a molecule will influence the N.M.R. spectrum[8,9]. Thus the presence of paramagnetic ions, with their unpaired electrons, in the vicinity of nuclei under investigation will affect the nature of the signal obtained.

Interactions between nuclei and unpaired electrons are manifested in changes in nuclear relaxation times[10], in nuclear spin polarisation (Overhauser effect)[11,12], in resonance field shifts in metals induced by coupling between nuclei and conduction electrons (Knight shift)[13], in shifts induced by macroscopic polarisation effects[14], and in shifts caused by isotropic hyperfine contact interactions and pseudo-contact interactions[15]. These phenomena are of interest because they provide further insight into the details of nucleus-electron interactions, and lead to a greater knowledge of the electronic structures of molecules and solids.

The very large chemical shifts in resonances of atoms, often shown by complexes containing a paramagnetic metal ion[16] are attributed to hyperfine interactions between the electron and nuclear spin (s) represented by the hyperfine Hamiltonian

$$\mathcal{H} = -g_N\beta_N(1-\sigma)HI + \bar{A}.\hat{I}.\hat{S}. \qquad (2.10)$$

where $\bar{A}$ is the hyperfine interaction tensor with principal values A_x, A_y, A_z, and $\hat{I}$ and $\hat{S}$ are nuclear and electron spin operators respectively. It is usual to subdivide[17] this additional hyperfine Hamiltonian into two contributions from (i) the Fermi contact interactions and (ii) the dipolar or pseudocontact interactions.

$$\text{i.e. } \mathcal{H}^{HYP} = \bar{A}.\hat{I}.\hat{S} = \mathcal{H}_1 + \mathcal{H}_2 \qquad (2.11)$$

(i) Fermi contact interactions

The isotropic hyperfine interaction between the magnetic moments of the electrons and the magnetic moment of the nucleus was first proposed by Fermi[18] and it is this interaction that leads to hyperfine splittings in the e.p.r. spectra of free radicals. In paramagnetic metal complexes this interaction term, derived by Fermi from relativistic quantum mechanics, involves a change in the effective magnetic field, ΔH, at the nucleus given by

$$\Delta H = \frac{a_i.h.S_z}{g_N\beta_N} \qquad (2.12)$$

where a_i is the contact hyperfine coupling constant measured in hertz, and is given by

$$a_i = \frac{8\pi}{3h}\, g.g_N.\beta.\beta_N \left[\psi(0)\right]^2 \qquad (2.13)$$

where g and g_N are the electronic and nuclear g values, β and β_N the Bohr and nuclear magnetons, and $\psi(0)$ the wave function describing the distribution of electrons at the nucleus.

In order that the transverse relaxation time, T_2, is long enough for the N.M.R. resonance to be observable, one of the following conditions[15] must be fulfilled:

$$T_{1e}^{-1} \gg a_i \qquad (2.14)$$

$$T_e^{-1} \gg a_i$$

where T_{1e} is the electron spin-lattice relaxation time, T_e is the electron spin exchange time and a_i is the hyperfine interaction constant for the i^{th} nucleus. Then the nucleus i will see a single average hyperfine magnetic field proportional to $< S_z >$, the time averaged value of S_z. Equation (2.12) then becomes

$$\Delta H = \frac{a_i h}{g_N \beta_N} < S_z > \qquad (2.15)$$

In general, $< S_z >$ is given by the Boltzmann distribution law

$$< S_z > = \sum_n S_{zn} \exp(-E_n/kT) / \sum_n (-E_n/kT) \qquad (2.16)$$

where E_n and S_{zn} are the energies and spin eigenvalues of the electronic state $|n>$. Evaluation of these summations can be difficult, but a simplified form of (2.15) can be obtained for those complexes in which all thermally accessible states belong to a single spin state S. Then

$$\left[\frac{\Delta H}{H_o}\right]^c = \Delta_i^c = - \frac{2\pi a_i}{3\beta\gamma_N} \left[\frac{\chi_{xx}}{g_{xx}} + \frac{\chi_{yy}}{g_{yy}} + \frac{\chi_{zz}}{g_{zz}} \right] \qquad (2.17)$$

where H_o is the applied magnetic field, χ_{xx}, χ_{yy}, χ_{zz} are the principal axis components of the magnetic susceptibility tensor, and g_{xx}, g_{yy} and g_{zz} are the principal axis components of the g tensor.

For axial symmetry, (2.17) becomes:

$$\left[\frac{\Delta H}{H_o}\right]^c = \Delta_i^c = - \frac{2\pi a_i}{3\beta\gamma_N} \left[\frac{\chi_{\parallel}}{g_{\parallel}} + \frac{2\chi_{\perp}}{g_{\perp}} \right] \qquad (2.18)$$

where $\chi_{\parallel}$, $\chi_{\perp}$ and $g_{\parallel}$, $g_{\perp}$ are the components of the susceptibility tensor and g tensor parallel and perpendicular to the principal axis of the molecule.

In order for the Fermi contact shift to be non-zero there must be a finite probability of finding the unpaired electron(s) at the nucleus i, a_i being given by (2.13). The problem of explaining the observation of hyperfine coupling and contact shifts in molecules where the unpaired

electron is in an orbital which has nodes at all nuclei (e.g. a π orbital) can be overcome by proposing a wave function

$$\Phi = \left\| \psi_1^{\alpha} \; \psi_1'^{\beta} \; \ldots\ldots \; \psi_n^{\alpha} \; \psi_n'^{\beta} \; \psi_o^{\alpha} \right\| \qquad (2.19)$$

in which electrons of α and β spin occupy independent orbitals ψ_o, ψ_1 .... ψ_n and ψ_1' ..... ψ_n', respectively. The unpaired electron density, ρ , at any point is then given by

$$\rho = |\psi_o|^2 + \sum_1^n \left[|\psi_i|^2 - |\psi_i'|^2 \right] \qquad (2.20)$$

so that if $|\psi_o|^2$ is zero, ρ can still be non-zero if an inequality in $|\psi_i|^2$ and $|\psi_i'|^2$ exists. Such an inequality can arise from the effect of "spin correlation" (otherwise called "exchange interaction" or "spin polarisation") between the unpaired electron in ψ_o and the electrons in ψ and ψ'. Consider for example an aromatic $\diagdown\!\!\diagup$CH fragment with the unpaired electron in a carbon p orbital. The ground state wave function Ψ can then be represented by $\Psi = \| \sigma\sigma' p \| (\alpha\beta\alpha)$, where σ and σ' are two σ-CH bonding orbitals; the minimum energy of this function will be attained when the α CH σ-bonding electron is described as being in an orbital, σ , preferentially concentrated nearer the carbon atom and the β electron in σ' as being localised to a greater extent near the proton (this distribution will minimise the exchange interactions represented by $\langle \sigma p | e^2/r | p\sigma \rangle$ which are less for a symmetric 2-electron spin wave function than for an antisymmetric spin wave function*). The relationship

$$a_H = Q_H \cdot \rho_C^{\pi} \qquad (2.21)$$

where a_H is the hyperfine coupling constant, ρ_C^{π} is the unpaired spin density centred on the carbon pπ orbital, and Q is a proportionality constant has been shown to hold[15]. Q must possess a negative sign since

*For a quantitative treatment of spin correlation effects, see references 15, 21, 22.

the spin density centred on carbon and that induced at the hydrogen nucleus are of opposing sign; theory and experiment concur in assigning to Q a value of -22.5 gauss or -6.5×10^7 sec^{-1} [23,24].

Hyperfine coupling is not restricted to aromatic protons and it is commonly observed in the protons of methyl groups bonded to aromatic carbon atoms. However, in such cases, coupling may arise not only from spin polarisation effects (transmitted along two σ-bonds) but also by direct spin transfer in which the methyl protons sense the $p\pi$ spin density by a hyperconjugative mechanism involving direct delocalisation of the $p\pi$ electron to the hydrogen 1s orbitals[25,26]. Both mechanisms would lead to spin density on the protons of the same sign as the spin density on the ring atom. If spin polarisation effects predominate, a relationship of the type

$$a_H = Q_{CH_3} \cdot \rho_c^{\pi} \qquad (2.22)$$

where Q_{CH_3} is positive and constant should hold by analogy with (2.21). However, the observation[21] that Q_{CH_3} is not a true constant but depends on the charge on the radical suggests that hyperconjugation effects are more important as these would be expected to vary with the energy of the π-orbital containing the unpaired electron. In this situation an expression analogous to (2.21) cannot be written as the $C-CH_3$ fragment must be considered as part of the extended π system and not as an isolated unit.

(ii) Pseudo-contact interactions

An isotropic nuclear resonance shift can arise from certain electron-nucleus interactions for which the term pseudo-contact has been employed. These interactions do not involve delocalisation of electron-spin but arise from the combined effects of electron spin-orbit interaction, (electron-orbit)-(nuclear spin) dipolar coupling and (electron-

spin)-(nuclear spin) dipolar coupling[27,28]. Since the contribution to the shift depends on the inverse cube of the distance of the electron from the nucleus under study, the effect of unpaired spin in a p orbital centred on the ligand nucleus can, in principle, be quite large, even though the unpaired spin density is itself quite small. For proton NMR studies the unpaired spin centred on the proton resides in an s orbital, and to a good approximation this contribution to the shift vanishes. The contribution arising from the unpaired spin in orbitals centred on the metal is in general the most important and, using a point dipole model, an expression for this contribution may be derived in terms of the components of the magnetic susceptibility tensor.

$$\left[\frac{\Delta H}{H_o}\right]_i^D = \frac{1}{2R^3}\left[(1 - 3\cos^2\theta)(\tfrac{2}{3}\chi_{zz} - \tfrac{1}{3}\chi_{xx} - \tfrac{1}{3}\chi_{yy}) + \sin^2\theta\cos 2\Omega\,(\chi_{yy} - \chi_{xx})\right] \qquad (2.23)$$

where R is the distance between nucleus i and the unpaired electron (considered to be localised on the metal ion), θ is the angle between the z axis and the vector along the line joining the metal and nucleus i and Ω is the angle between x axis and the projection of this vector in the xy plane.

For axial symmetry, (2.23) becomes

$$\left[\frac{\Delta H}{H_o}\right]_i^D = -\frac{1}{3R^3}(3\cos^2\theta - 1)(\chi_{\parallel} - \chi_{\perp}) \qquad (2.24)$$

where $\chi_{\parallel}$ and $\chi_{\perp}$ are the components of the magnetic susceptibility tensor parallel and perpendicular to the principle axis of the molecule.

(iii) Applicability of Fermi contact and pseudo-contact term calculations

Equations (2.18) and (2.24) for the contact and pseudo-contact contributions to the paramagnetic shift have been derived in terms of magnetic susceptibility tensor components. These equations are of more general applicability than the more common derivation in terms of the g

tensor components: Kurland and McGarvey[20] have discussed the limitations of this latter approach and criticised the classical expressions of McConnell and Chesnut[15] and McConnell and Robertson[29] for the contact and pseudo-contact contributions, respectively, on the following grounds.

Firstly, it was assumed that the complex had only one thermally populated energy level (in the absence of the magnetic field), and the states of this ground level could be assigned a spin quantum number, S. Secondly, it was implicitly assumed that for $S \gg 1$, splittings of the ground level in the absence of the field (zero field splittings) could be ignored; and thirdly, that the orbital contribution to the isotropic NMR shift could be taken into account indirectly through the use of g-tensor components. This last assumption requires that there be at most only a first order orbital contribution to the magnetic moment of the complex, brought about by spin-orbit mixing of the ground level with non-populated excited states.

Many complexes do not satisfy one or other of these assumptions. Complexes with a T_1 or T_2 ground term may, by virtue of spin-orbit coupling effects, have an appreciable orbital contribution to the magnetic moment and several thermally accessible excited levels (e.g. octahedral low-spin Fe(III)). Moreover, a number of tetragonal Fe(III) complexes are known to have relatively large zero field splittings.

Jesson[19] attempted to include the contribution of thermally populated excited states in his calculations on octahedral Co(II)complexes, but he neglected the significant contribution from the Zeeman mixing of these states. Four possible limiting cases were considered, depending on the relative values of the Zeeman anisotropy energy (ZAE), the correlation time for tumbling of the molecule τ, and the electron spin relaxation time T_{1e}. The form of equations (2.18) and (2.24) corresponds to the "solid state" case (Jesson's case a), for which $\tau^{-1} \ll$ ZAE; $T_{1e} \ll \tau$,

and under these conditions the Boltzmann distribution between the spin levels is preserved over the rotation of the molecule. For iron porphyrins, the complexes of interest in this thesis, NMR line widths of the order of about 30 Hz yield an electron spin relaxation time $T_{1e} \sim 8 \times 10^{-12}$ sec by the method of Bloembergen and Morgan[30]. Dielectric relaxation studies[31] of hemin have indicated that $\tau \sim 5 \times 10^{-10}$ sec while e.s.r. data[32] yield $ZAE \sim 2 \times 10^{11}$ sec^{-1} at 23.5 k.gauss. Thus $\tau^{-1} \ll ZAE$ and $T_{1e} \ll \tau$, satisfying Jesson's case a. Recent theoretical considerations, moreover, have revealed that the dipolar shift should be independent of the relative values of τ, T_{1e} and ZAE, and that only the "solid state" equations are in fact valid[33].

Golding[34] has derived equations for the contact shift in octahedral complexes taking into account thermally populated excited states and the Zeeman mixing of these states. However his assumption that the spin density is the same for all the thermally populated states does not necessarily apply to many complexes that have been studied.

The point dipole assumption, made by Jesson, may not be applicable in all cases, for the calculation of the pseudo-contact shift. McGarvey and Pearlman[35] have suggested that this may be the reason that the ^{14}N NMR pseudo-contact shifts found in ferric cyano complexes are much larger than predicted.

If meaningful estimates of the distribution of unpaired electrons in paramagnetic complexes are to be obtained from isotropic NMR shifts, a theory is required which is not limited by the restrictive assumptions discussed above. Moreover it may be particularly important in analysing isotropic NMR shifts of nuclear species other than protons to consider the orbital contribution from unpaired electrons in orbitals centred at the ligand nucleus[36,37]. This orbital contribution cannot be taken into account simply by use of the g tensor of the complex.

The general equations (2.18) and (2.24) which do not involve these restrictive assumptions will be used as the basis for developing appropriate expressions for contact and pseudo-contact contributions to the observed paramagnetic shift according to the exigencies of the particular system, in subsequent chapters.

3. Separation of contact and pseudo-contact interactions

A study of the relative contributions of the contact and pseudo-contact terms to the total paramagnetic shift can yield two types of information. The pseudocontact shift is a direct function of the geometry of the complex, and NMR studies may yield information on this. In addition, the mechanism by which unpaired spin on the metal ion reaches ligand nuclei may be indicated by the spin density distribution on the ligand, and insight into the electronic structure and bonding of the ligand obtained from the latter.

The separation of the two terms has been attempted in a number of ways. Comparison of solution and polycrystalline solid spectra of vanadocene[38] has been used to establish the pseudo-contact effect, and shifts were found to be contact in origin. The method has not been further exploited because of the excessive widths of NMR lines of polycrystalline solids.

The most generally used arguments to establish or disprove polar contributions have been based on experimental data on the presence or absence of magnetic isotropy in a complex. Horrocks et al.[39-43] described a "ratio method" applicable to two series of complexes differing only in central metal ion, where the modes of spin delocalisation are identical and one member is isotropic. This was applied with some success to complexes of octahedral or near-octahedral Co(II) and Ni(II), but it was later pointed out[43] that second order Zeeman terms were not negligible and measurements of the anisotropy of the magnetic susceptibility rather

than of the g-tensor should be considered.

Pseudocontact shifts can be estimated directly from equations (2.23) and (2.24) with a knowledge of magnetic susceptibility components or principle g-values (obtainable from e.p.r. measurements) and the molecular geometry (obtainable from X-ray crystallography). Quantitative results so derived are probably not completely reliable because of lack of detailed information on the electronic ground state, although it is probable that many of the qualitative conclusions made will not be substantially altered by refinements in theory.

4. NMR instrumentation

^{1}H NMR spectra were obtained on the following instruments:

i) A Japan Electronics Optics Laboratory (J.E.O.L.) J.N.M.-C-60HL High Resolution N.M.R. Spectrometer (continuous wave) at 60 MHz. The spectra were recorded on precalibrated chart paper using tetramethyl silane (T.M.S.) as an internal standard. Chemical shifts were calibrated with reference to a solution containing chloroform (τ value 2.67), methylene chloride (4.70), dioxan (6.37), trichloroethane (7.26), acetone (7.87), cyclohexane (8.57) and tetramethyl-silane (10.0) for 9 ppm and 18 ppm sweep widths, and with reference to the 4 KHz audio frequency modulation sideband for 90 ppm sweep widths.

The temperature of the sample was varied using a J.E.O.L. J.E.S.-V.T.-3 temperature controller, the desired temperature being attained by passing a regulated stream of hot air (for temperatures in excess of +30°C), cold nitrogen gas (0 → -100°C), or warmed nitrogen gas (0 → +30°C) over the sample. The temperature was measured by recording the chemical shift difference between the methyl and hydroxylic protons of a sample of dry methanol. Above 40°C, when methanol begins to vaporise appreciably, 1,3-propanediol was used as a high temperature calibration sample. The chemical shift difference, $\Delta\nu$ Hz, of the two resonances of the methanol

or glycol was substituted in the appropriate relation[44] below:

SAMPLE	EQUATION	RANGE OF USE
Methanol	$T°K = 478.6 - 1.906\|\Delta\nu\|$	220 - 280°K
Methanol	$T°K = 464.0 - 1.775\|\Delta\nu\|$	260 - 320°K
Glycol	$T°K = 466.0 - 1.694\|\Delta\nu\|$	310 - 410°K

All recorded temperatures are considered to be accurate to 1°K.

ii) A Bruker HX90 90 MHz spectrometer with Nicolet B-NC 12 Fourier transform* computer.

iii) A Bruker WH90 90 MHz spectrometer with Nicolet B-NC 12 Fourier transform* computer.

iv) A Bruker 270 MHz spectrometer using the modified Bruker HFX-90 console and 64 K.gauss superconducting magnet (Oxford Instruments Ltd.) with a Nicolet 1085 Fourier transform* computer.

All the Bruker spectrometers have thermostatted probes, and facilities for variable temperature measurement using warmed or cooled nitrogen gas. A digital print-out of the resonance peak position is given by the computer.

2.2 Mössbauer Studies

Mössbauer spectroscopy is the resonant absorption of gamma rays from a gamma ray emitter. Resonance is obtained by adjusting the energy of gamma rays by a kinetic energy change in the gamma ray source. As the emission and absorption of gamma radiation affects the nucleus it is a useful technique for obtaining information about certain nuclei in molecules. ^{57}Fe of 2% natural abundance has an excited state lying 14.4 KeV above the ground state and gamma-ray absorption is obtained using a ^{57}Co as source.

*A summary of the theory of Fourier transform spectroscopy is given in Appendix I.

The absorption of gamma radiation by the nucleus is influenced by:

(i) the isomer shift

(ii) the quadrupole splitting

(iii) the magnetic hyperfine interactions.

1) The isomer shift, δ

The nucleus of an atom is surrounded and penetrated by electric charge with which it interacts. As the ground and excited states of the nucleus have different radii these interactions are different for the two states. The difference between the energies of the transitions for the absorber and some arbitrary standard, often sodium nitroprusside, is called the isomer shift and if $\Psi(0)_s$ and $\Psi(0)_a$ are the electronic wave functions at the origins of the source and absorber nuclei then

$$\delta = kz\ (R_e^2 - R_g^2)\left[|\Psi(0)_a|^2 - |\Psi(0)_s|^2\right] \qquad (2.25)$$

where z is the nuclear charge and R_e and R_g are the radii of the excited and ground states. As $\Psi(0)$ is non-zero only for s electrons this gives a measure of the s electron density at the nucleus.

2) The quadrupole splitting, Δ

A nucleus with a spin $\geqslant 1$ possesses a quadrupole moment Q which is a measure of the distortion of the nuclear volume from spherical symmetry. Interaction of this quadrupole moment with the electric field gradient from the anisotropic electrostatic environment causes the 2I+1 degeneracy to be partly lifted and the quadrupole splitting is given by

$$\Delta = \pm \frac{e^2Qq}{4}\ (1 + \eta^2/3)^{\frac{1}{2}} \qquad (2.26)$$

where eq is the principal component of the electric field gradient and η is an asymmetry parameter.

3) The magnetic hyperfine interaction

This is the Zeeman splitting of the nuclear levels in a magnetic field, giving energy levels:

$$E_m = -g_N \beta_N H_o M_I \qquad (2.27)$$

where M_I may have discrete values from -I to +I. The hyperfine field is the sum of contributions from the interactions of the nucleus with the orbital and spin moments of the electrons and the interaction of the nuclear and electron spins.

2.3 Electron Paramagnetic Resonance

Electron paramagnetic resonance is concerned with transitions between Zeeman levels which arise when a paramagnetic substance is placed in a magnetic field and at the same time exposed to electromagnetic radiation[45,46]. An alternating field of frequency ν is applied at right angles to a magnetic field of strength H. According to the selection rule $\Delta M_s = \pm 1$ allowed magnetic dipole transitions are produced between the Zeeman components of the same, usually the lowest, electronic level.

The energy separation of the components and thus the resonance condition for transitions between the two states is given by

$$\Delta E = h\nu = g\beta H \qquad (2.28)$$

In EPR experiments ν is held constant and H varied, which gives rise to resonance lines characterised by different values of g.

The total energy of a paramagnetic system may be described by a general Hamiltonian, which in turn is composed of terms describing all energy contributions, and may be written as

$$\mathcal{H} = \mathcal{H}_0 + \mathcal{H}_{LF} + \mathcal{H}_{LS} + \mathcal{H}_{SS} + \mathcal{H}_N + \mathcal{H}_H \qquad (2.29)$$

where $\mathcal{H}_0$ is the Hamiltonian for the free ion, $\mathcal{H}_{LF}$ describes the perturbation by an electrostatic ligand field, $\mathcal{H}_{LS}$ and $\mathcal{H}_{SS}$ describe the magnetic interactions between the electron spin moment and the moments of its orbit and other electron spins, $\mathcal{H}_N$ describes the hyperfine interaction of the nuclear moment with orbital and spin moments and $\mathcal{H}_H$ describes interaction of the electrons with an external magnetic field.

The g factor can be considered as a quantity characteristic of the molecule in which the unpaired electrons are located. g is caused to deviate from the free electron value of 2.0023 by local magnetic fields, the principal source being an orbital magnetic moment introduced into the ground state by mixing with excited states. For most molecules the admixture of excited states is not isotropic and this anisotropy is summarised in the form of the second rank tensor referred to a principal axis system XYZ

$$g = \begin{vmatrix} g_{XX} & 0 & 0 \\ 0 & g_{YY} & 0 \\ 0 & 0 & g_{ZZ} \end{vmatrix}$$

If X, Y and Z are equivalent as in octahedral, tetrahedral or cubic symmetry, then $g_{XX} = g_{YY} = g_{ZZ}$ and the g factor may be represented by a single value. This latter statement is also true if molecular tumbling removes the g factor anisotropy. If the molecular system contains a single threefold or higher symmetry axis Z, then X and Y are equivalent and $g_{XX} = g_{YY} \neq g_{ZZ}$ for axial symmetry. In this case $g_{XX} = g_{YY}$ is designated as $g_{\perp}$ and g_{ZZ} as $g_{\parallel}$.

The signal obtained from a particular sample has an intensity and line width determined by a number of different effects. Broadening may occur by interaction between the electron spins and the motion of the lattice or exchange interaction and dipole-dipole interaction of electron spins and these two processes are homogeneous or inherent in the line itself and irrespective of orientation. Zeeman anisotropy and electron dipole-nuclear dipole interaction are inhomogeneous broadening processes.

To observe the optimum EPR spectrum these effects must be minimised. Spin-lattice interaction may be reduced by lowering the temperature of the sample. T_1, the spin-lattice relaxation time, is thereby lengthened. Exchange and spin-spin interactions are generally reduced by dilution

of the sample in a diamagnetic medium, and in general concentrations of the order of 10^{-3}M are employed for EPR work. The Zeeman anisotropy may be reduced by lowering the frequency at which measurement is made. Interaction between electron dipoles and nuclear dipoles is usually removed by observation of liquid samples in which the time averaged momentum becomes zero because of the molecular tumbling.

REFERENCES

1. E.M. Purcell, H.C. Torrey and R.V. Pound. Phys. Rev., 1946, 69, 37.
2. F. Bloch, W.W. Hansen and M.E. Pickard. Phys. Rev., 1946, 69, 127.
3. J.E. Wertz. Chem. Rev., 1955, 55, 829.
4. J.A. Pople, W.G.Schneider and H.J. Bernstein. "High Resolution Nuclear Magnetic Resonance", McGraw-Hill, New York, 1959.
5. A. Abragam. "The Principles of Nuclear Magnetism", Clarendon Press, Oxford, 1961.
6. C.P. Slichter. "Principles of Magnetic Resonance", Harper and Row, New York, 1963.
7. G.E. Pake. Solid State Review, 1956, 2, 1.
8. Reference 4, p.218.
9. Reference 5, p.424.
10. N. Bloembergen, E.M. Purcell and R.V. Pound. Phys. Rev., 1948, 73, 679.
11. A.W. Overhauser. Phys. Rev., 1953, 91, 476.
12. A.W. Overhauser. Phys. Rev., 1953, 92, 411.
13. W.D. Knight. Phys. Rev., 1949, 76, 1259.
14. W.C. Dickinson. Phys. Rev., 1951, 81, 717.
15. H.M. McConnell and D.B. Chesnut. J. Chem. Phys., 1958, 28, 107.
16. D.R. Eaton. "Physical Methods in Inorganic Chemistry", Edited by H.A.O. Hill and P. Day, Interscience, 1968, pp. 514-529.
17. B. Bleaney and K.W.H. Stevens. Rep. Prog. Phys., 1953, 16, 108.
18. E. Fermi. Z. Physik., 1930, 60, 320.
19. J.P. Jesson. J. Chem. Phys., 1967, 47, 579.
20. R.J. Kurland and B.R. McGarvey. J. Mag. Res., 1970, 2, 286.
21. A.D. McLachlan. Mol. Phys., 1960, 3, 233.
22. D.R. Eaton and W.D. Phillips. Adv. Mag. Res., 1965, 1, 103.
23. S.I. Weissman, T.R. Tuttle and E. de Boer. J. Phys. Chem., 1957, 61, 28.
24. I. Bernal, P.H. Rieger and G.K. Fraenkel. J. Chem. Phys., 1962, 37, 1489.
25. A.D. McLachlan. Mol. Phys., 1958, 1, 233.

26. D.B. Chesnut. J. Chem. Phys., 1958, 29, 43.

27. N. Bloembergen and W.C. Dickinson. Phys. Rev., 1950, 79, 179.

28. W.C. Dickinson. Phys. Rev., 1951, 81, 717.

29. H.M. McConnell and R.E. Robertson. J. Chem. Phys., 1958, 29, 1361.

30. N. Bloembergen and L.O. Morgan. J. Chem. Phys., 1961, 34, 842.

31. D.A. Pitt and C.P. Smyth. J. Phys. Chem., 1959, 63, 582.

32. G.N. La Mar and F.A. Walker. J. Amer. Chem. Soc., 1973, 95, 1782.

33. A.J. Vega and D. Fiat. Pure Appl. Chem., 1972, 32, 307.

34. R.M. Golding. Mol. Phys., 1964, 8, 561.

35. B.R. McGarvey and J. Pearlman. J. Mag. Res., 1969, 1, 178.

36. K.W.H. Stevens. Proc. Roy. Soc., 1953, A219, 542.

37. W. Marshall. "Paramagnetic Resonance". Ed. W. Low, Academic Press, New York, 1963, Vol. 1, p.347.

38. H.M. McConnell and C.H. Holm. J. Chem. Phys., 1958, 28, 749.

39. W. de W. Horrocks Jr., R.C. Taylor and G.N. La Mar. J. Amer. Chem. Soc., 1964, 86, 3031.

40. R.W. Kluiber and W. de W. Horrocks, Jr. J. Amer. Chem. Soc., 1965, 87, 5350.

41. R.W. Kluiber and W. de W. Horrocks, Jr. J. Amer. Chem. Soc., 1966, 88, 1399.

42. R.W. Kluiber and W. de W. Horrocks, Jr. Inorg. Chem., 1967, 6, 166.

43. W. de W. Horrocks, Jr. Inorg. Chem., 1970, 9, 690.

44. A.L. van Geet. Anal. Chem., 1968, 40, 2227.

45. H.M. Assenheim. "Introduction to Electron Spin Resonance", Hilger and Watts, 1966.

46. A. Carrington and A.D. McLachlan. "Introduction to Magnetic Resonance", Harper and Row, 1967.

CHAPTER 3

THE SPIN STATE EQUILIBRIUM IN FERRIC OCTAETHYLPORPHIN COMPLEXES

3.1 Introduction

1. Electronic crossover situations in iron porphyrin derivatives

The existence of temperature dependent equilibria between isomers of differing spin multiplicity is now well established[1], since the first and perhaps most striking example of an equilibrium involving magnetically isomeric species was discovered by Cambi et al.[2-6] in the period 1931-1933 with a series of iron (III) N,N-dialkyldithiocarbamates. Examples of spin state crossover phenomena are quite numerous, and the physical properties of such systems have been studied by a variety of physical techniques.

It has been suggested that the important biological functions of some iron-containing biological molecules, in particular those of the iron-porphyrin group, are due to unusual physical properties which are a consequence of unusual electronic structure[7]. The magnetic properties of many iron-porphyrin complexes such as hemoglobin, myoglobin, peroxidase, catalase, cytochromes, etc., have been studied to elucidate the nature of the chemical binding in biologically important systems. The original studies of Pauling and Coryell[8,9] revealed that the difference in energy between high- and low-spin states of iron (II) hemoglobin was probably small; for example, ferrohemoglobin in the natural physiological condition with a water molecule coordinated in the sixth position is high-spin ($S=2$, μ_{eff} = 5.46 Bohr magnetons) but it becomes diamagnetic ($S=0$) if an oxygen molecule substitutes water in the sixth position (oxygenated ferrohemoglobin).

Taube[11] drew attention to the rather similar close balance which exists between the energies of "inner orbital" and "outer orbital" complexes encountered in iron (III) porphyrin systems. Some data (see Table 3.1)

compiled by Schoffa[12] reveal that the effective magnetic moments of certain ferrihemoglobin and ferrimyoglobin complexes vary between 5.9 and 2.3 B.M. and tend to decrease along the series of axial ligands $F^- > H_2O > \ldots\ldots\ldots > CN^-$. In these complexes the central Fe^{3+} ion is surrounded by four porphyrin nitrogen atoms and a fifth axial nitrogen atom from the imidazole portion of the protein, which leaves the sixth axial position free to accommodate a diversity of monodentate ligands.

TABLE 3.1:

Effective Magnetic Moments of Some Ferrihemoglobin and Ferrimyoglobin Complexes

Ligand	Horse Hemoglobin		Horse Myoglobin	
	pH	μ_{eff} B.M.	pH	μ_{eff} B.M.
F^-	7.10	5.76	6.84	5.77
H_2O	6.36	5.65	6.44	5.73
HCO_2^-	6.92	5.44	6.54	5.69
$CH_3CO_2^-$	6.84	5.44	6.98	5.70
OCN^-	7.58	5.40	9.60	4.41
SCN^-	6.60	5.06	6.62	5.47
OH^-	9.73	4.66	11.60	5.04
NO_2^-	6.84	4.13	6.63	5.12
$SeCN^-$	6.91	3.88	7.36	4.89
Imidazole	6.92	2.87	6.81	2.44
CN^-	6.72	2.50	7.41	1.96
N_3^-	6.72	2.35	6.80	3.30

Taube noted that ligands of low polarisability (e.g. F^- or H_2O) in the sixth position produced high spin complexes, whereas highly polarisable ligands (e.g. HS^- or CN^-) quench the moment to low-spin

values. However, the hydroxide ion of polarisability between these extremes produces a complex of intermediate magnetic moment, μ_{eff} = 4.47 B.M.[10] Pauling et al.[10] had suggested the possibility that this value would be predicted if the spin were half-quenched by the hydroxide ion, i.e. corresponding to a net spin of S = $^3/_2$. Taube foreshadowed the alternative possibility of closely balanced inner orbital and outer orbital forms in equilibrium with one another.

Theorell and Ehrenburg[13] independently reached a closely related conclusion. These workers had observed that both the magnetic susceptibility and the electronic absorption spectrum of hemoglobin hydroxide were strictly intermediate between the corresponding properties of the hydroxide of myoglobin (predominantly high spin) and the hydroxide of horseradish peroxidase (predominantly low spin). Accordingly they suggested that all four iron atoms in hemoglobin hydroxide were not necessarily alike and that two might be held by "covalent" bonds and two by "ionic" bonds so that equal proportions of high- and low-spin iron atoms would obtain.

Pauling's proposal of a ground state of intermediate spin was subsequently regarded as unfavourable in the light of a later comparison of the relative energies of the three possible ground states, S = $^1/_2$, S = $^3/_2$, S = $^5/_2$, in terms of their respective orbital and mean pairing energies[14,15]. Griffith demonstrated that for octahedral d^5 complexes the intermediate S = $^3/_2$ spin state is energetically unfavoured, although he also indicated that intermediate spin states would in principle be possible for complexes with lower symmetry. In spite of the symmetry of the hemoproteins being lower than cubic, Griffith concluded from crystal field theory that a ground state of intermediate spin is energetically improbable and accordingly supported the alternative postulate of a thermal equilibrium between molecules with S = $^1/_2$ and S = $^5/_2$.[16] This interpretation has been elegantly confirmed[17] by

extensive measurements of magnetism and electronic spectra, and of their temperature dependence, for the hydroxides of a number of ferrihemoproteins. If the assumption is made that the hydroxides are mixtures of high- and low-spin forms, the magnetic and electronic spectral properties can then be quantitatively correlated.

It now seems certain that the crossover phenomenon occurs with many other systems of biological importance, especially of the hemoglobin, catalase and peroxidase types, and in the cytochromes. For example, the azide ion, like the hydroxide ion, appears to generate ligand fields which place certain hemoproteins close to the crossover position. Thus the magnitudes of the magnetic moments of ferricatalase azide, μ_{eff} = 5.36 B.M., and ferrihemoglobin azide, μ_{eff} = 2.84 B.M., lie between the values expected for high- and low-spin complexes[10,18]. The data contained in Table 3.1 confirm that in all of these compounds, the field strengths and symmetries must be close to the spin-transition region, because small changes in these conditions are enough to make the ground state of the ferric ion a sextet state, a doublet state, or be somewhere in between.

An alternative explanation for the difference in magnetic moments of the ferric ion in ferrihemoglobin derivatives has been put forward by Harris[19]. Under certain conditions provided by strong ligand fields, there is the possibility of low-lying quartet or doublet energy states. In addition, spin-orbit coupling is capable of spin-mixing the ground and low-lying states. For these states, spin can no longer be regarded as a good quantum number, and they are composed of mixtures of sextet, quartet and doublet components. With this model, small changes in crystal field parameters lead to variations in the nature of the ferric ion states, and thus variations in the manner of electron population of the states. Such conditions simulate in a reasonable fashion the effect of a change

in one ligand in a series of heme derivatives.

Theoretical crystal field calculations[20,21], compatible with the spectroscopic data, provide support for the existence of mixed-spin ground states, composed of components of different states, the variable magnetic moment being due to the character of "mixing-in" to the ground state. Harris has established the conditions for a spin-mixed ferric ion ground state in complexes of tetragonal symmetry, in addition to sextet, quartet and doublet ground states. For this symmetry, which of these states occurs as the ground state in a given complex is determined by the magnitude of the average cubic field strength (Δ_{O_h}) and the axial distortions present (C). Such regions have been delineated and the changing nature of the wave-functions described (Figure 1.6). Recent magnetic studies[22] on the protein Chromatium ferricytochrome c' have been explained by postulating an admixture of electronic states, in accordance with Harris. In addition, anomalous resonance Raman spectra for cytochrome c' from Rhodopseudomanas palustris have been interpreted[23] by proposing an intermediate S = $^3/_2$ spin state.

Until these above proposals, it had been generally accepted that there existed a thermal equilibrium between spin state forms in most (possibly all) ferric hemoproteins and their derivatives[24]. Evidence of spin equilibria in smaller "model" systems such as Fe(III) - porphyrins has also been found. Thus the temperature dependence of chemical shifts in the NMR spectra of bis-pyridinato iron (III) - porphyrin complexes has been observed[25,26] to be consistent with a spin-state equilibrium, and the position of the equilibrium found to be dependent[26] on both the basicity of the pyridine ligand and of the porphyrin. However, further investigations[27] of the temperature dependence of the magnetic susceptibilities and absorption spectra of these complexes in solution suggested that the high-spin form was possibly the intermediate S = $^3/_2$ state and not the expected S = $^5/_2$ state.

2. Physical properties of spin equilibrium systems

The effect of a spin equilibrium situation, where there are two thermally accessible electronic states with differing spin multiplicities, on the physical properties of such a system has been extensively studied[1], more especially in the case of the iron (III) dithiocarbamates[28]. The electronic crossover mechanism can affect the physical property considered in two ways, depending on whether the spin state interconversion time is faster than, or slower than, the characteristic time for a transition to occur in the physical property under investigation.

(a) A superimposition of signals is obtained when the spin state interconversion time is slower than the characteristic time for a transition to occur in the physical property under investigation.

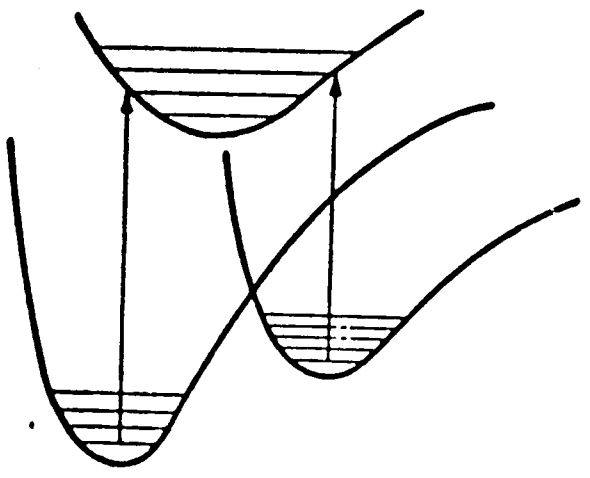
(b) An average value of the physical property of the spin states being measured is obtained when the spin state interconversion is fast in relation to the transition time in the physical property.

The experimental time scales of various physical techniques and the form of information expected are given below.

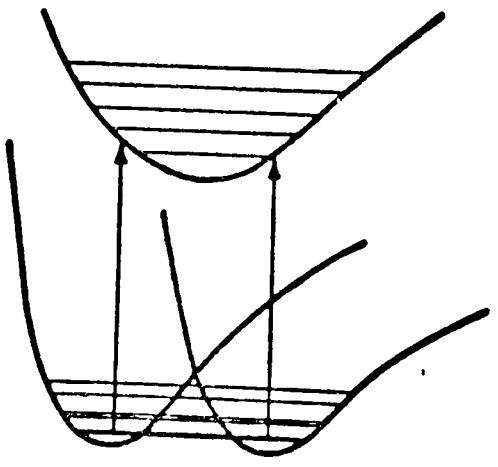
(i) Electronic spectra

Normally the electronic spectrum of a crossover system will consist of the superposition of separate peaks which characterise each spin state rather than an "averaged" spectrum, since the spin state interconversion time is likely to be long compared with the time required for an electronic transition (cf. Fig. 3.1(a)). In this event, a lower limit for the period of dynamic interconversion of 10^{-13} sec. can be set, since metal-ligand nuclear oscillations are of this order.

N.B. It is possible that separate peaks may not be observed in cases where the zero-point energies of the crossing-states are equal.



(a)



(b)

Figure 3.1: Potential energy curves in the crossover region. The double potential energy minimum would require two stacks of vibrational levels in the ground state, and application of the Franck-Condon principle would then lead to the expectation of broad averaged electronic absorption bands (cf. Fig. 3.1(b)).

Figure 3.2 shows the spectra of metmyoglobin (MbH_2O) and ferrimyoglobin cyanide (MbCN), which may be taken as examples of porphyrins with the ferric ion in the $S = {}^5/_2$ and $S = {}^1/_2$ state respectively. The latter has a fairly typical metalloporphyrin spectrum, although the α-band is rather weak and there is a new, weak band in the near infra-red. The spectrum of MbH_2O is completely different. The bands between 590 nm and 530 nm are similar in position to the α- and β-bands of the cyanide, but there are new bands at around 1000, 625 and 500 nm.

Figure 3.3 shows the spectra of MbOH and MbN_3. These are apparently

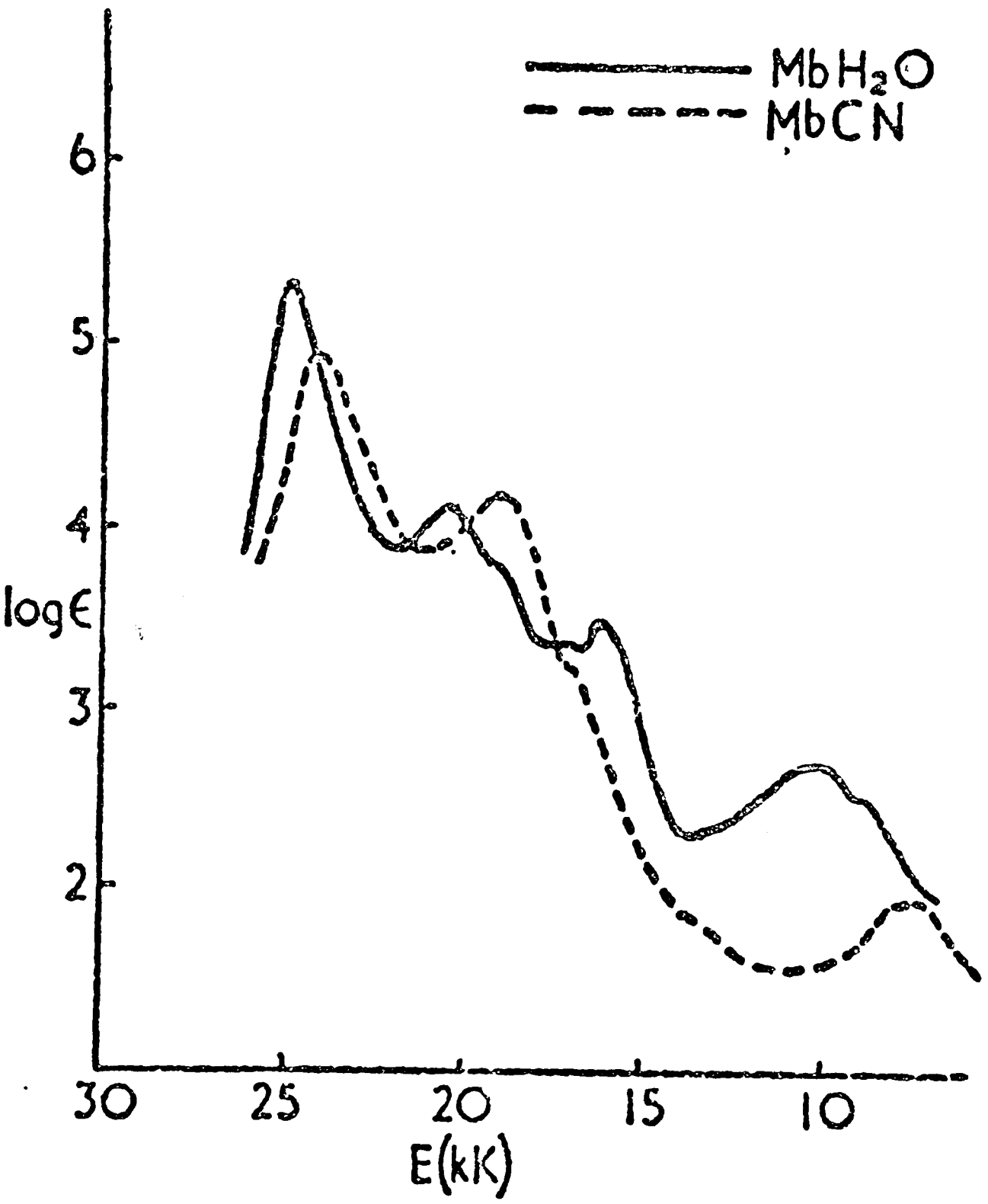


FIG. 3.2 Absorption spectra of MbH_2O and MbCN.

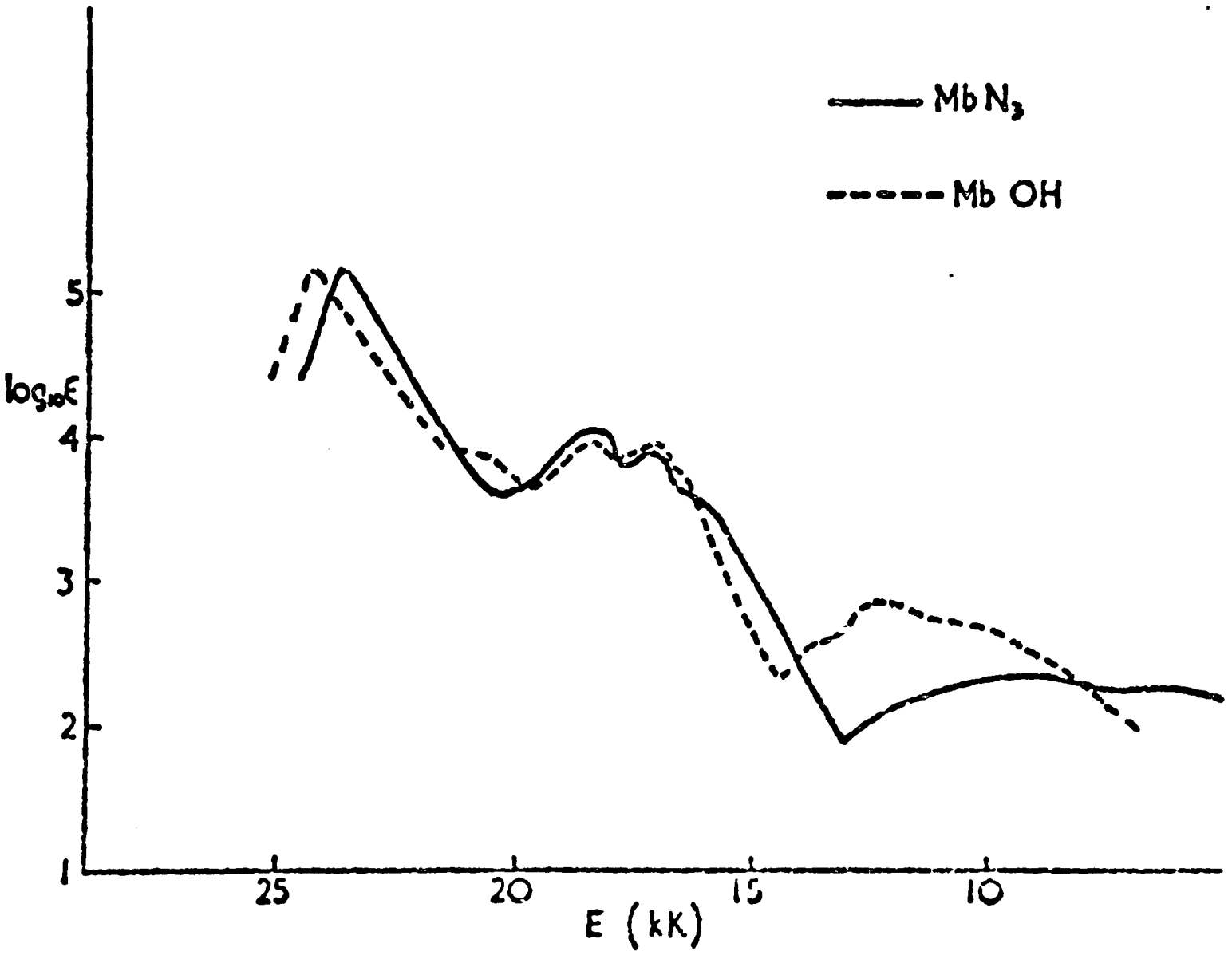


FIG. 3.3 Absorption spectra of MbN_3 and MbOH.

superpositions of the MbH_2O and MbCN types of spectra, with a weak band at 625 nm and well-developed α- and β-bands. The magnetic moments of these derivatives indicate that a spin equilibrium situation is present.

(ii) Infra-red spectra

Metal-ligand vibration frequencies are expected to differ in the different spin states. For a crossover system the metal-ligand vibrations are expected to conform to one of the following patterns:

(a) If the potential barrier between the crossing states is high, absorption bands of the different spin-states should be superimposed. The relative intensities of the two sets of peaks should display the expected response to changes of temperature and pressure.

(b) If the zero-point energies of the two states are equal, and if the potential barrier is small, an averaged vibrational spectrum should be obtained. However, vibrational doubling should occur (cf. Fig. 3.1(b)) and the temperature dependence of the spectrum will differ from that expected for situation (a).

(iii) Mössbauer effect

In order for Mössbauer studies to show simultaneous existence of two electronic species, the spin state crossover must be slower than the lifetime of the excited state of ^{57}Fe. Spin states are usually characterised in terms of the isomer shift and quadrupole splitting effects and providing that the effective quadrupole period for each spin state is less than the lifetime of the ^{57}Fe metastable state ($I = {}^3/_2$), i.e. 1.45×10^{-7} sec., then two situations involving Mössbauer spectra may be envisaged.

(a) If the relaxation time to change from one spin state to the other is much greater than the effective quadrupole period, then a resolved superposition of the characteristic spectrum of each spin state should obtain.

(b) If the correlation time for electronic relaxation between the spin states is much less than the effective quadrupole period, then the iron nucleus experiences an averaged electric field gradient, the magnitude of which is determined by the relative populations of the spin states.

(iv) NMR spectra

The conditions necessary for observation of contact interaction shifts in the NMR spectroscopy of paramagnetic systems, as described in Chapter 2, are either that the electronic spin-lattice relaxation time or a characteristic electron exchange time must be short compared with the isotropic hyperfine contact interaction constant a_i. Values commonly observed for this constant lie in the range 10^5 - 10^7 Hz, so that the observation of separate contact shifted resonances for each spin state requires a spin-state interconversion time of less than 10^{-5} - 10^{-7} sec. Such a situation has not been observed for most of the spin-equilibria ferric systems studied by NMR, and in general only "averaged" spectra have been observed.[25,29,30]

(v) Paramagnetic susceptibilities

The paramagnetic susceptibility χ_M^P is of great value in determining the relative proportions of two spin states approximately. However, when the observed susceptibility is close to the higher-spin or lower-spin limits, it is difficult to decide whether or not the data are consistent with a 100% higher-spin or lower-spin compound; the presence of only a few percent of one form could be crucial, for example in mechanistic arguments. For instance, in a low-spin compound with magnetic moment (μ_{eff}) of 2.2, it is not easy to say whether the discrepancy between 2.2 and the "spin-only" value of 1.73 is entirely due to the orbital contribution, or indicates the presence of a few percent of the high spin form.

(vi) EPR spectra

In principle mixtures of spin states should be detectable from EPR spectra, and a number of such observations on spin equilibrium systems have been made. The spectra of the different spin forms are usually quite distinct, e.g. a number of hemoproteins in the high-spin ($S = {}^5/_2$) state have $g'_{\parallel} = 2$ and $g'_{\perp} = 6$ while the low-spin ($S = {}^1/_2$) ferric bisimidazole complexes of a number of synthetic porphyrins have g values $g_x \sim 1.5$, $g_y \sim 2.3$ and $g_z \sim 2.9$.

However there are two serious drawbacks. First the sharpness of EPR signals depends largely on relaxation processes which are difficult to correlate with molecular structure and E.S.R. signals may be broad and difficult to find. Thus the absence of low-spin signals does not necessarily imply that the compound is completely high-spin. The second difficulty is that EPR spectra of Fe^{3+} systems, particularly low-spin, almost always have to be measured at rather low temperatures, usually $77^{\circ}K$ or lower. Since the position of equilibrium between the spin states is likely to be temperature-dependent, information about spin states obtained at low temperatures is not necessarily relevant to the situation at room temperature. It appears that lowering the temperature usually favours the lower spin form.

3. Aim of the work

From the foregoing introduction, it is apparent that the physical properties of hexa-coordinated ferric-porphyrin complexes are not well characterised. The anomalous magnetic moments of some of these complexes have been interpreted both in terms of a spin equilibrium system and in terms of a mixed-spin ground state. The observed physical properties of some systems have been explained by reference to the intermediate $S = {}^3/_2$ spin state.

The aim of this chapter is to provide a more complete explanation

of the properties of ferric porphyrin complexes than has hitherto been expounded. Further light will be cast on the phenomenon of anomalous magnetic moments in some ferric-porphyrin systems. It will be shown that previous explanations involving the postulate of a spin-equilibrium between two different spin states or the Harris treatment employing mixed-spin ground and excited states are not necessarily alternative theories but explicable in relation to a particular electronic model.

Although hemin complexes previously employed have served as useful models for the heme proteins, the low symmetry of the natural heme coupled with the lack of knowledge of the location of the in-plane magnetic axes has proved difficult in determination of, e.g., dipolar NMR shifts. Whilst many bis adducts of ferric porphyrins are known in solution, thus far very few have been isolated as solids. A clearer picture would be expected if data were available for structurally better characterised and more symmetrical heme complexes.

Accordingly, in order to improve understanding of the electronic structure of the natural heme complexes, as well as heme proteins, bis-amine adducts of ferric octaethyl porphin perchlorate have been isolated in this work. The advantages of using these model systems are:

(a) isolation of the solid permits identification and an exact analysis of the complex,

(b) improved solubility and stability in solution over wide temperature ranges allows a more detailed characterisation of the temperature dependence of physical properties,

(c) axial symmetry and X-ray structural data are available,

(d) axial ligand substituents can be varied so as to introduce probes for electronic structure and bonding.

The electronic properties of these ferric octaethylporphin bis-amine perchlorate complexes will be analysed by reference to:

(i) ^{1}H NMR spectroscopy, as a probe of the ligands.

(ii) Magnetic susceptibility data.

(iii) Electronic absorption spectroscopy.

(iv) Mössbauer effects, as a probe of the Fe nucleus.

The results will be studied firstly in terms of a simple spin state equilibrium theory and secondly in terms of a more sophisticated electronic model and a theoretical basis for the experimental data proposed. The unusual electronic properties of these complexes will show that they are particularly apt models for complex biological systems.

3.2 Experimental

1. Apparatus and Materials

i) NMR measurements

^{1}H NMR spectra were recorded on the JEOL J.N.M.-C-60HL spectrometer at 60 MHz.

$CDCl_3$, isotopic purity 99.8% D, as supplied by C.I.B.A. Ltd., was used as solvent in all cases. Solutions used were 50 mM (^{1}H spectra) in porphyrin. Tetramethylsilane, supplied by Stohler Isotope Chemicals, was used as reference compound. Chemical shifts are quoted in parts per million relative to the internal standard, negative values indicating low field shifts.

ii) Magnetic susceptibility and moment measurements

Magnetic susceptibilities of the samples were measured by the method described by Evans[33] utilising a coaxial NMR cell. The cell consisted of a precision ground inner tube held centrally in an outer NMR tube by a Teflon cap[34,35]. A 2% solution of TMS in $CDCl_3$ was syringed into the inner tube and a solution of known concentration of

sample in 2% TMS/$CDCl_3$ was placed in the outer tube. Two resonance lines were obtained from the methyl protons of TMS in the two solutions, owing to the difference in their volume susceptibilities, with the line from the paramagnetic solution at higher field. The separation of the TMS peaks was measured over the temperature range 200-320°K and the mass susceptibility, χ_g, of the sample found from the relation

$$\chi_g = \frac{3\Delta\nu}{2\pi\nu_o m} + \chi_o \qquad (3.1)$$

(neglecting density changes on adding solute to solvent)

where $\Delta\nu$ is the frequency separation between the two lines in Hz, ν_o is the frequency at which the protons are being studied in Hz, m is the concentration of substance in solution in kg. per l, and χ_o is the mass susceptibility of the solvent. The mass susceptibility can be converted to molar susceptibility, χ_m, by multiplying χ_g by the molecular weight of the paramagnetic substance. The molar paramagnetic susceptibility, χ_m^p, is found by subtracting the molar diamagnetic susceptibility, which can be quite accurately represented as a sum of contributions from the individual atoms and groups in the molecule, from χ_m and the magnetic moment of the complex is then given by

$$\mu_{eff} = \left[\frac{3kT\ \chi_m^p}{\mu_o N\beta^2}\right]^{\frac{1}{2}} = 25.25\left[\chi_m^p\ T\right]^{\frac{1}{2}} \qquad (3.2)$$

where k is the Boltzmann constant, T is the absolute temperature, β is the Bohr magneton, N is the Avogadro number, μ_o is the vacuum permeability and χ_m^p is in S.I. units.

Solid state susceptibility measurements were kindly undertaken by Dr. H. Lücken.

iii) Electronic absorption spectroscopy

Spectra were recorded on a Cary 17 spectrophotometer fitted with a Universal Absorbance-% Transmittance Slidewire, giving eight absorbance

ranges. Variable temperature measurements were made by utilising an Oxford Instruments DN 704 Cryostat (see Fig. 3.4) in conjunction with an Oxford Instruments Manual Temperature Indicator Controller SCL 1939. Variable temperatures were obtained by balancing the heat input to a heat exchange block against the cooling power available from a liquid nitrogen cooling unit, the cooling power being regulated by opening or closing a gas exhaust valve. The temperature was determined by monitoring a thermocouple with reference to a temperature/e.m.f. calibration chart: accuracy is considered to be $\pm$ 1°K. The solutions used were either 10^{-4}M (800-450 nm region) or 10^{-5}M (450-350 nm) with respect to the complex.

iv) Mössbauer studies

Mössbauer spectra were obtained by Dr. B. Dale using the facilities at AERE Harwell.

v) E.P.R. measurements

The E.P.R. spectra were recorded on a Varian E.9 instrument at 4.2°K operating at a frequency of ~ 9.4 GHz with 100 KHz modulation. The spectra were calibrated with reference to a diphenyl picryl hydrazil radical marker, DPPH, which has a sharp resonance at g = 2.0036.[36]

vi) Analysis of samples

All the complexes were analysed for carbon, hydrogen and nitrogen by standard microanalytical methods.

2. Preparation of complexes

i) Materials

Chloroform (AR), silver perchlorate, pyridine, 4-aminopyridine and 4-methylpyridine as supplied by B.D.H. Chemicals Ltd. 4-Methylpyridine was purified as in Chapter 4. Silver perchlorate was dried for 72 hrs. on a vacuum line.

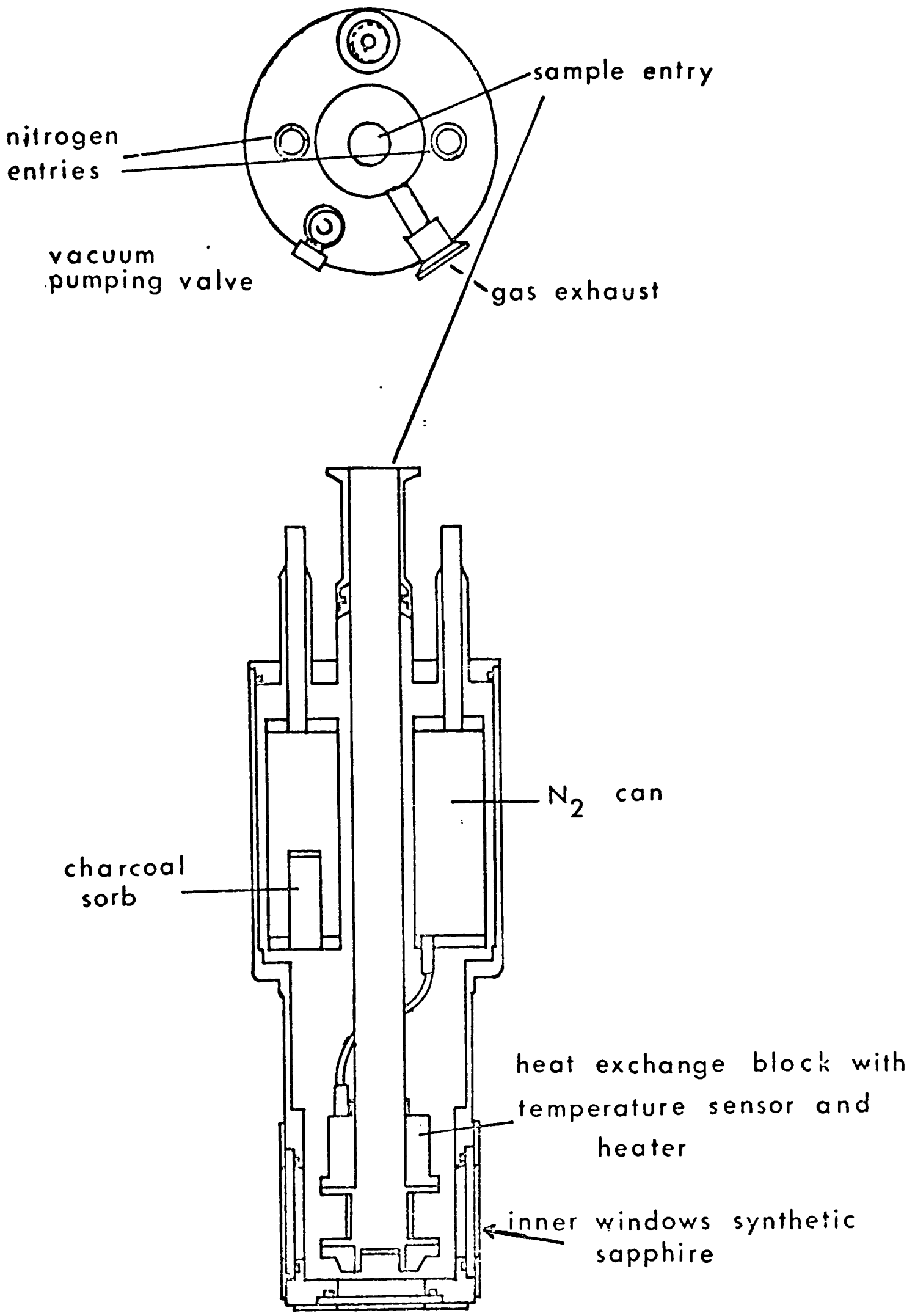


FIG. 3.4

DN 704 CRYOSTAT

Benzene as supplied by B.D.H. Chemicals Ltd., petroleum ether (60-80°) as supplied by Harrington Brothers Ltd., 3-chloropyridine and 4-acetylpyridine as supplied by Ralph N. Emanuel Ltd., 3-acetylpyridine as supplied by Koch-Light Laboratories Ltd., and N-methylimidazole as supplied by Fluka A.G.

Ferric octaethylporphin chloride, Fe(OEP)Cl, was a gift from Dr. J.W. Buchler.

ii) Preparation

Bis-amine complexes of ferric octaethylporphin perchlorate, $Fe(OEP)X_2ClO_4$ were prepared according to the following method of Ogoshi et al.[37] Silver perchlorate (100 mg) was added to Fe(OEP)Cl (120 mg) in benzene (50 ml) and the mixture refluxed for 20 mins. The desired amine (0.9 ml or 90 mg) was added dropwise, either neat or dissolved in the minimum quantity of benzene, and the reaction mixture refluxed for 45 mins. The mixture was cooled to room temperature and left to stand and crystallise. The solid material thus obtained was washed with water several times, dried and then extracted with chloroform. After removal of the bulk of chloroform, recrystallisation from a chloroform/petroleum ether mixture produced dark red, purple or maroon crystals in the majority of cases.

TABLE 3.2

Analytical Data for Ferric Octaethylporphin Complexes

COMPLEX	FORMULA	REQUIRED (%)			FOUND (%)		
		C	H	N	C	H	N
$Fe(OEP)(3\text{-}Cl\text{-}Py)_2ClO_4$	$C_{46}H_{52}N_6Cl_3FeO_4$	60.4	5.68	9.20	59.1	5.58	9.22
$Fe(OEP)(3\text{-}Ac\text{-}Py)_2ClO_4$	$C_{50}H_{58}N_6ClFeO_6$	64.5	6.24	9.04	64.3	6.08	8.43
$Fe(OEP)(4\text{-}Ac\text{-}Py)_2ClO_4$	$C_{50}H_{58}N_6ClFeO_6$	64.5	6.24	9.04	64.9	6.63	8.61
$Fe(OEP)(Py)_2ClO_4$	$C_{46}H_{54}N_6ClFeO_4$	65.3	6.38	9.93	65.2	6.25	9.90
$Fe(OEP)(4\text{-}Me\text{-}Py)_2ClO_4$	$C_{48}H_{58}N_6ClFeO_4$	65.9	6.68	9.61	64.4	6.63	9.21
$Fe(OEP)(4\text{-}Am\text{-}Py)_2ClO_4$	$C_{46}H_{56}N_8ClFeO_4$	63.1	6.40	12.79	62.9	6.14	12.29
$Fe(OEP)(N\text{-}Me\text{-}Imid)_2ClO_4$	$C_{44}H_{56}N_8ClFeO_4$	62.0	6.57	13.15	60.7	6.76	13.30

3.3 Results

1. N.M.R. Results

In contrast with the N.M.R. spectra of the bis-amine complexes of natural hemins in Chapter 4, the absence of uncomplexed free base in bulk solution ensures cleaner spectra and better resolution of the resonances. All of the expected resonances are observed, and their variation of half-width and shift with temperature can be monitored over a wide range of temperature.

The PMR spectrum of $Fe(OEP)(pyridine)_2ClO_4$ comprises 6 resonances, and as there are 6 different proton types, it seems fair to assume that each signal represents a different proton type. Three resonances would be expected from the porphyrin ligand, that is from the methyl protons (24), the methylene protons (16) and the methene protons (4). Three resonances would be expected from each pyridine ligand, that is from the α-protons (2), the β-protons (2) and the γ-proton (1). The two most intense resonances are thus assigned to the porphyrin methyl and methylene protons, the more intense of these two at higher field being assigned to the methyl protons.

The resonances of the β- and γ-pyridine proton resonances are assigned by comparison of the pyridine complex spectrum with those of the 3-acetyl and 4-methyl pyridine complexes. With the 3-acetylpyridine complex, one of the resonances is reduced in intensity by approximately 50% in comparison with the corresponding resonance of the pyridine complex, and this can thus be assigned to the β-protons. Similarly, the use of the 4-methylpyridine complex results in the disappearance of one resonance, at around 10-12 ppm downfield from TMS, present in the spectrum of the pyridine complex and this resonance in the pyridine complex spectrum is thus assigned to the γ-proton. The two remaining signals upfield from TMS in the pyridine complex are thus those of the porphyrin methene protons and α-pyridine protons. The broadness of the upfield signal is

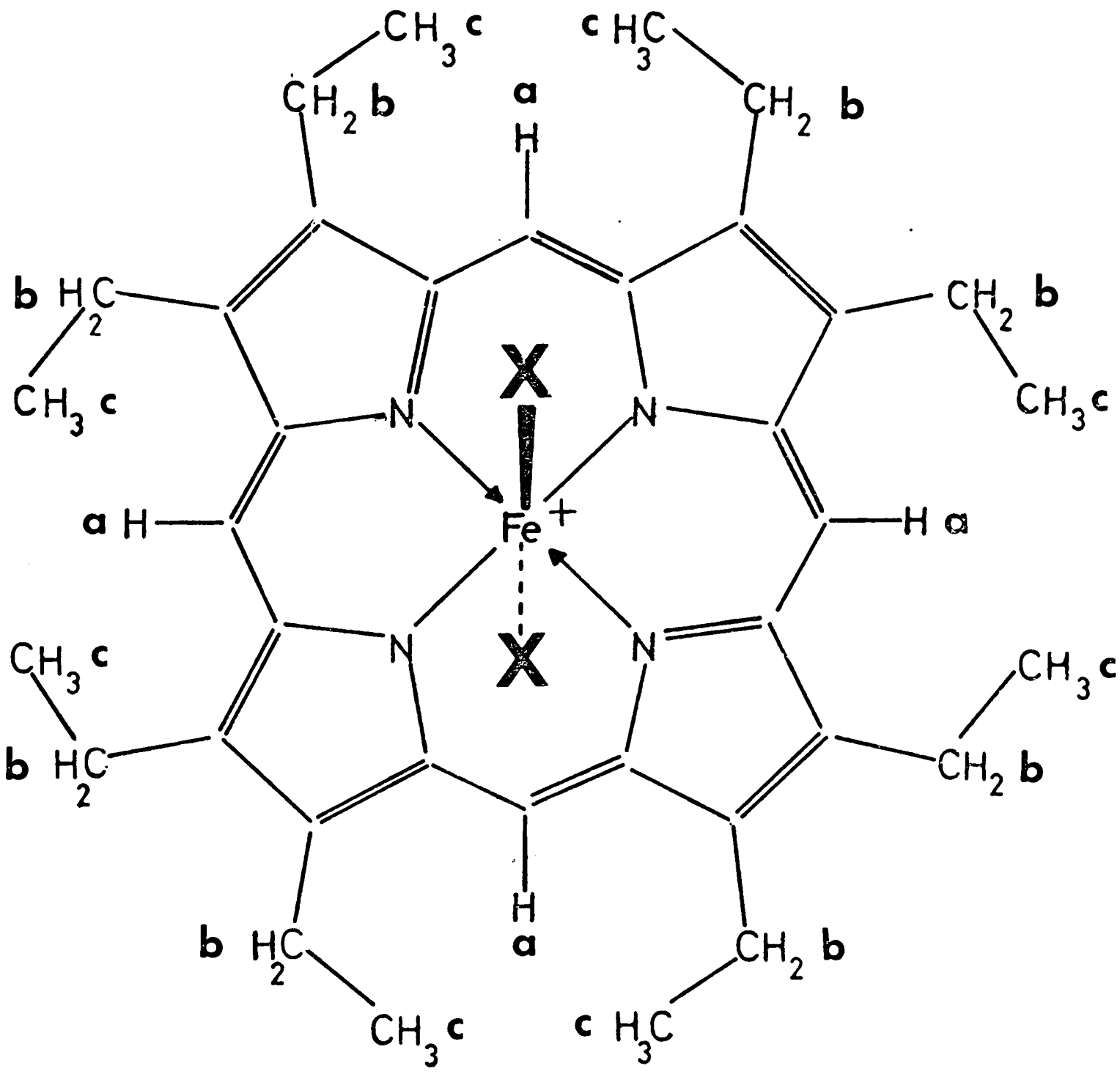
taken to be caused by the proximity of the protons resonating to the metal. In view of the fact that the metal-proton distance of the pyridine α-protons is 3.0 Å as against 4.5 Å for the porphyrin methene protons, this broad signal is attributed to the pyridine α-protons. The other remaining signal is thus assigned to the porphyrin methene protons.

These assignments are supported by the relative intensities of the signals. If the most intense signal is integrated as corresponding to 24 protons, then the resonances of the pyridine protons represent 4, 4 and 2 protons respectively for α-, β- and γ-protons. This proves that the investigated species in solution is the bispyridinato iron (III)-octaethylporphin perchlorate complex, and this is evident throughout the temperature range studied.

The PMR spectrum of $Fe(OEP)(pyridine)_2ClO_4$ at a variety of temperatures is illustrated in Figure 3.6, the assignment labels being given in Figure 3.5. The temperature dependence of the observed N.M.R. shifts is illustrated in Figure 3.7 from the data in Appendix II.D. The observed shifts of other substituted pyridine complexes and the N-methylimidazole complex of ferric octaethylporphin perchlorate are given in Appendix II, and a comparison of the spectra of some of the complexes at 200°K is given in Figure 3.8.

In order to conclusively prove that the species present in solution is in all cases a bispyridinato complex, excess of the appropriate pyridinato ligand was added to the solution and the PMR spectrum re-run. In all cases, no change in the spectrum of the complex was observed, vis-à-vis intensity and position of the resonances, even at the higher temperatures and with the thermodynamically less favoured complexes such as the 3-chloropyridine one. Exchange broadening effects caused by fast exchange between complexed and uncomplexed base, which complicate the spectra of the ferric complexes of natural porphyrins formed in situ in solution are thus absent in the system under observation here.

FIG. 3.5



Ferric Octaethylporphin Complex

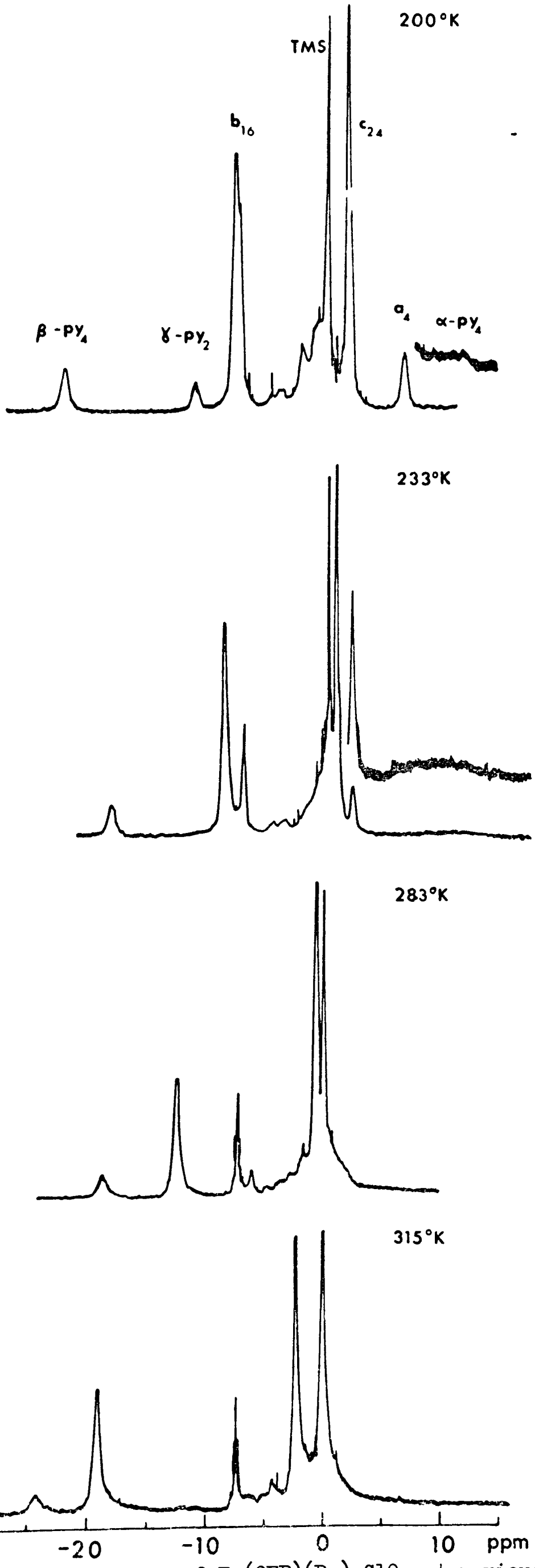


FIG. 3.6 PMR spectrum of $Fe(OEP)(Py)_2ClO_4$ at various temperatures.

FIGURE 3.7(i) TEMPERATURE DEPENDENCE OF N.M.R. SHIFTS OF $Fe(OEP)(PYRIDINE)_2ClO_4$

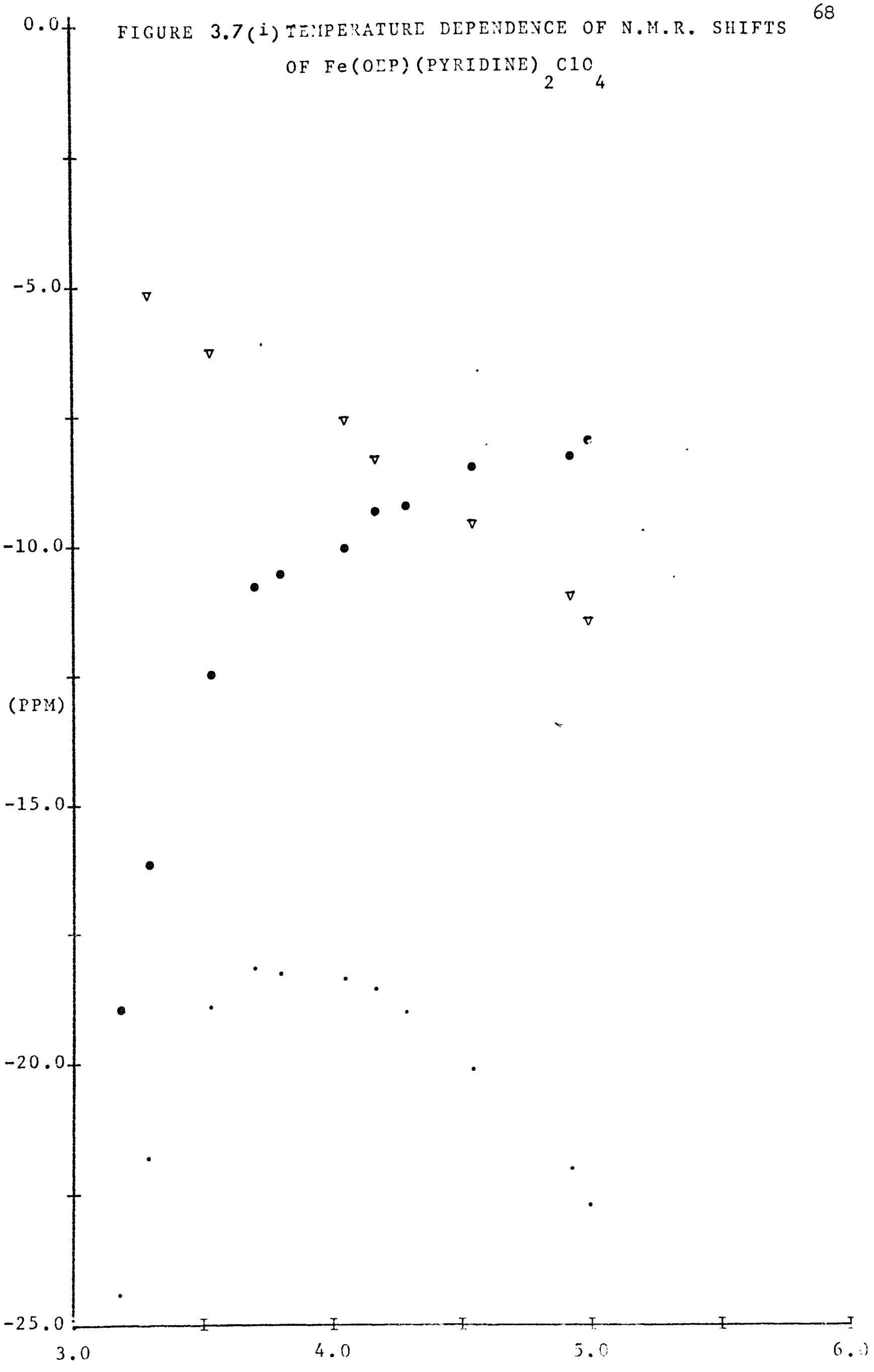
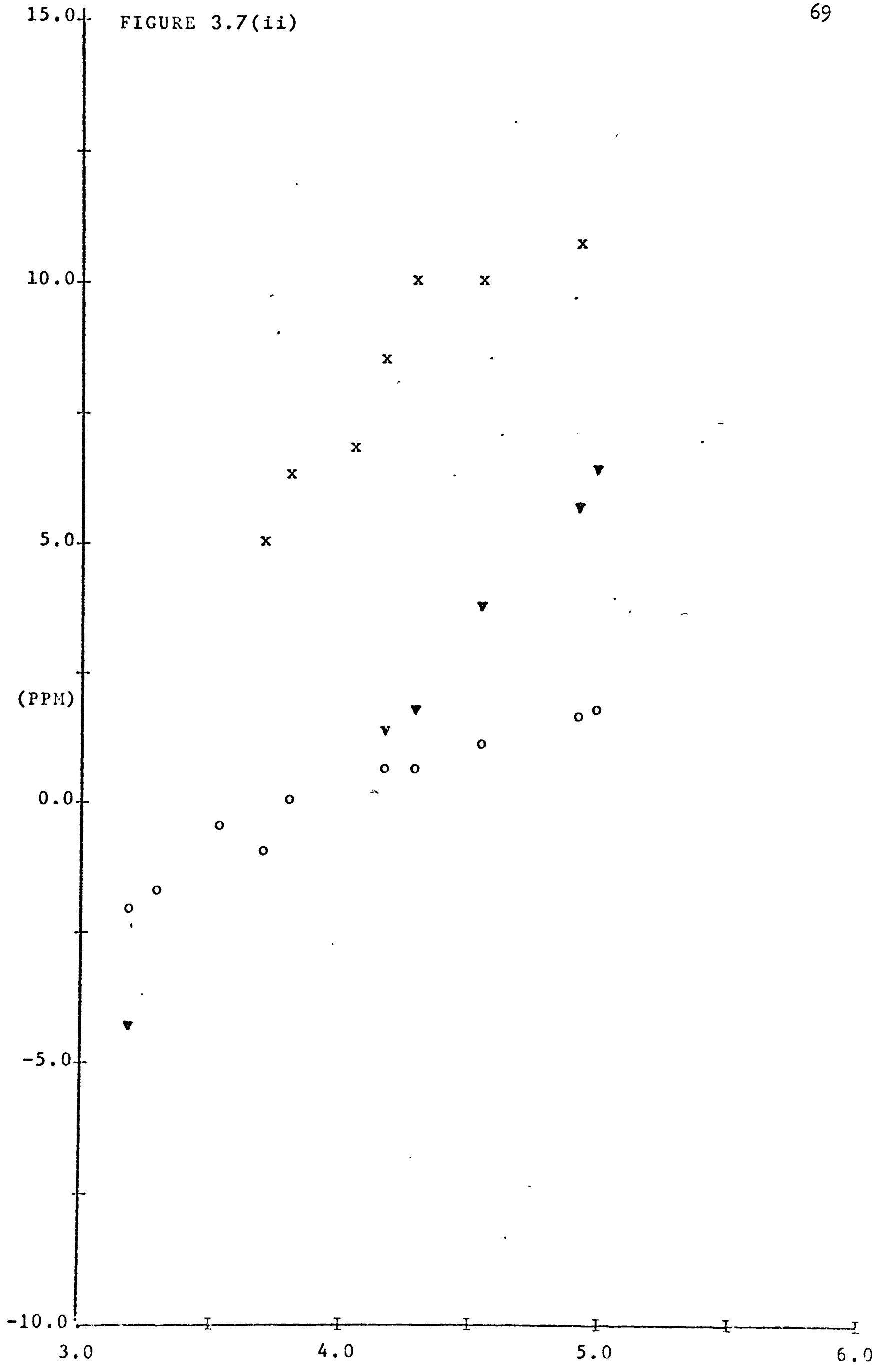


FIGURE 3.7(ii)

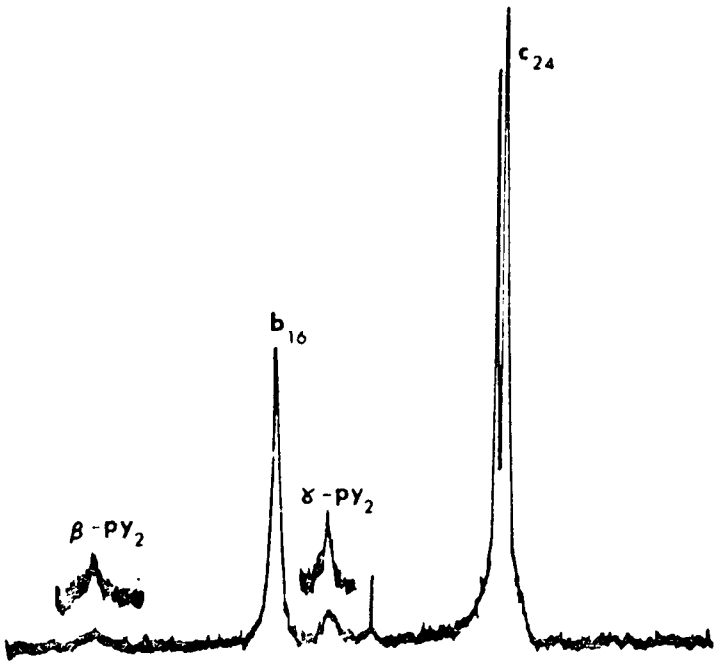


The extra resonances due to substitution in the pyridine ligand were assigned for the various complexes by comparison with the bis-pyridine complex spectrum and by relative intensities of the signals. For all spectra the four methene protons (a) are equivalent, as are protons of the eight ethyl groups (b and c), a not unexpected result given the D_{4h} symmetry of the molecular geometry. The resonances of the pyridine α-protons which are found in the region 6 to 12 ppm upfield from TMS are broadened in every case and indeed in most cases are difficult to observe. The β-proton resonances are in the region expected by analogy with the results for the hemin complexes (Chapter 4) and the γ-proton resonances, obscured by free base in the hemin complexes, are well-defined here in the region -7 to -12 ppm downfield from TMS.

The position of a particular resonance is seen to be markedly dependent on the axial ligand, as is the line width, and both of these vary considerably with temperature, in general the line widths increasing with increase in temperature. Thus all the resonances of the 3-chloropyridine complex are broadened at higher temperatures, so much so that resonances of amine protons are only observed at lower temperatures. In contrast, for most of the other complexes, amine proton resonances are observed throughout the temperature range used. With the N-methylimidazole complex, resonances of the imidazole ring protons are exceedingly broad. Positive assignments and determination of observed shifts are not possible, although the N-methyl resonance is well-defined, integrating as 6 protons and showing that as with the bispyridinato complexes, the complex is present as the bis N-methylimidazole form.

All of the plots of observed shift against the reciprocal of the absolute temperature (T^{-1}), excepting that for the bis N-methylimidazole complex, show considerable deviations from linear behaviour. This non-linear behaviour is most marked for β-protons of the axial pyridine ligand, for which the slope of the temperature plot changes sign. The

FIG. 3.8 PMR spectra of some $Fe(OEP)(X\text{-}Py)_2ClO_4$ complexes at 200°K.



temperature plots of resonances a, c and α have positive slopes whilst that of resonance γ has a negative slope. The slope of resonance β changes sign with temperature, except for the 4-aminopyridine and N-methylimidazole complexes for which the slope is consistently negative over the temperature range studied.

2. Magnetic data

The susceptibility data for various complexes of ferric octaethylporphin perchlorate are given in Appendix III, the molar paramagnetic susceptibilities being calculated on the basis of the diamagnetic susceptibilities given in Table 3.3.

TABLE 3.3

Diamagnetic Susceptibility Data[38]

Atom or Group	Molar diamagnetic susceptibility ($m^{-3}kg^{-1}mole^{-1} \times 10^{-8}$)
Fe^{3+}	-13
OEP	-671
Pyridine	-60
ClO_4^-	-43

The change in diamagnetic susceptibility calculated with values for substituted pyridines or N-methylimidazole was found to be negligible in comparison with the total molar diamagnetic susceptibility, and so the molar diamagnetic susceptibility value for pyridine was used throughout. The values quoted are considered accurate to $\pm$ 0.2 B.M.

The effective magnetic moments (μ_{eff}) for ferric octaethylporphin complexes in the range 200-320°K can be seen to vary appreciably according to the particular axial ligand complexed. The extremes are represented by the bis 3-chloropyridine complex (μ_{eff} = 4.2 at 324°K) and the bis N-methylimidazole complex (μ_{eff} = 2.4 at 324°K). Furthermore,

the change in value of the magnetic moment over the temperature range does not increase in a constant manner over the series from the N-methylimidazole complex to the 3-chloropyridine complex. Thus the change in moment over the temperature range is ca. 1.6 B.M. for ferric octaethylporphin bis 3-chloropyridine perchlorate, ca. 1 B.M. for the 3-acetyl- and 4-acetylpyridine complexes diminishing to 0.2 B.M. for the N-methylimidazole complex.

To ensure that the magnetic data referred to the bis-amine complex and not to some dissociation product of the equilibrium

$$Fe(OEP)(X)_2ClO_4 \rightleftharpoons Fe(OEP)X\ ClO_4 + X$$

the magnetic measurements were repeated for the 3-chloropyridine complex in the presence of excess 3-chloropyridine. This would have the effect of driving the above equilibrium in the direction of the bis complex. In the event, the presence of excess amine is seen to have negligible effect on the magnetic data, allowing for experimental error (see Appendix III.A).

Indeed the magnetic moments calculated with magnetic susceptibility measurements obtained from the compounds in the solid state are not substantially different from the magnetic moments obtained by solution measurements. These magnetic moments are set out in Appendix IV. Whilst there are variations between the magnetic moments measured for the solid and in solution, the same trends in the magnetic moment change with temperature are observed. This must conclusively prove that the changes in magnetic moments as the temperature is varied do not arise from solution effects such as dissociation to any significant degree.

3. Electronic absorption spectroscopy

The absorption spectrum of Fe(OEP)(3-chloropyridine)$_2$ClO$_4$ at 300°K and 217°K is shown in Figure 3.9, the absorption spectrum of Fe(OEP)(4-acetylpyridine)$_2$ClO$_4$ at 294°K and 218°K in Figure 3.10, and the

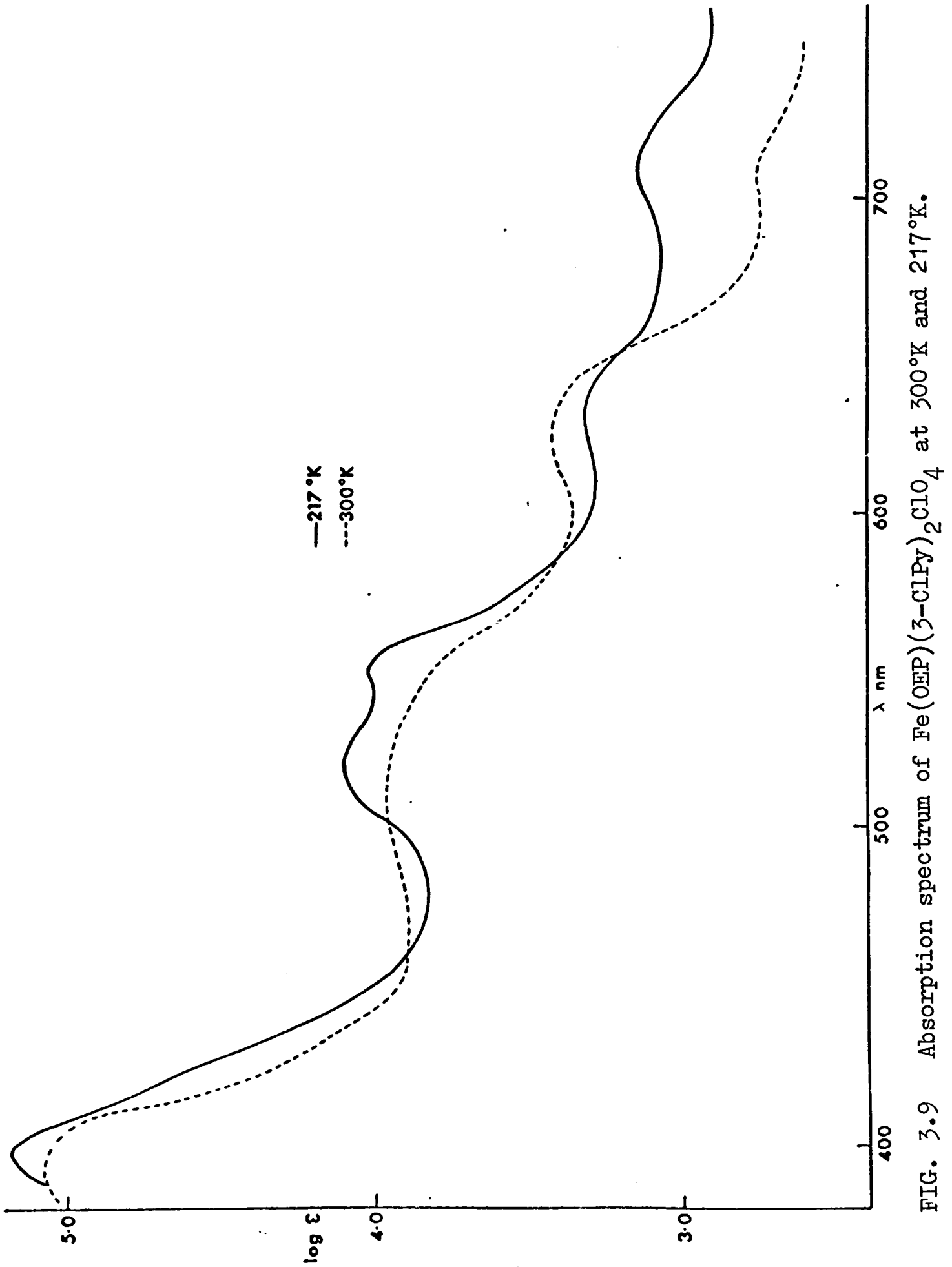


FIG. 3.9 Absorption spectrum of $Fe(OEP)(3\text{-}ClPy)_2ClO_4$ at 300°K and 217°K.

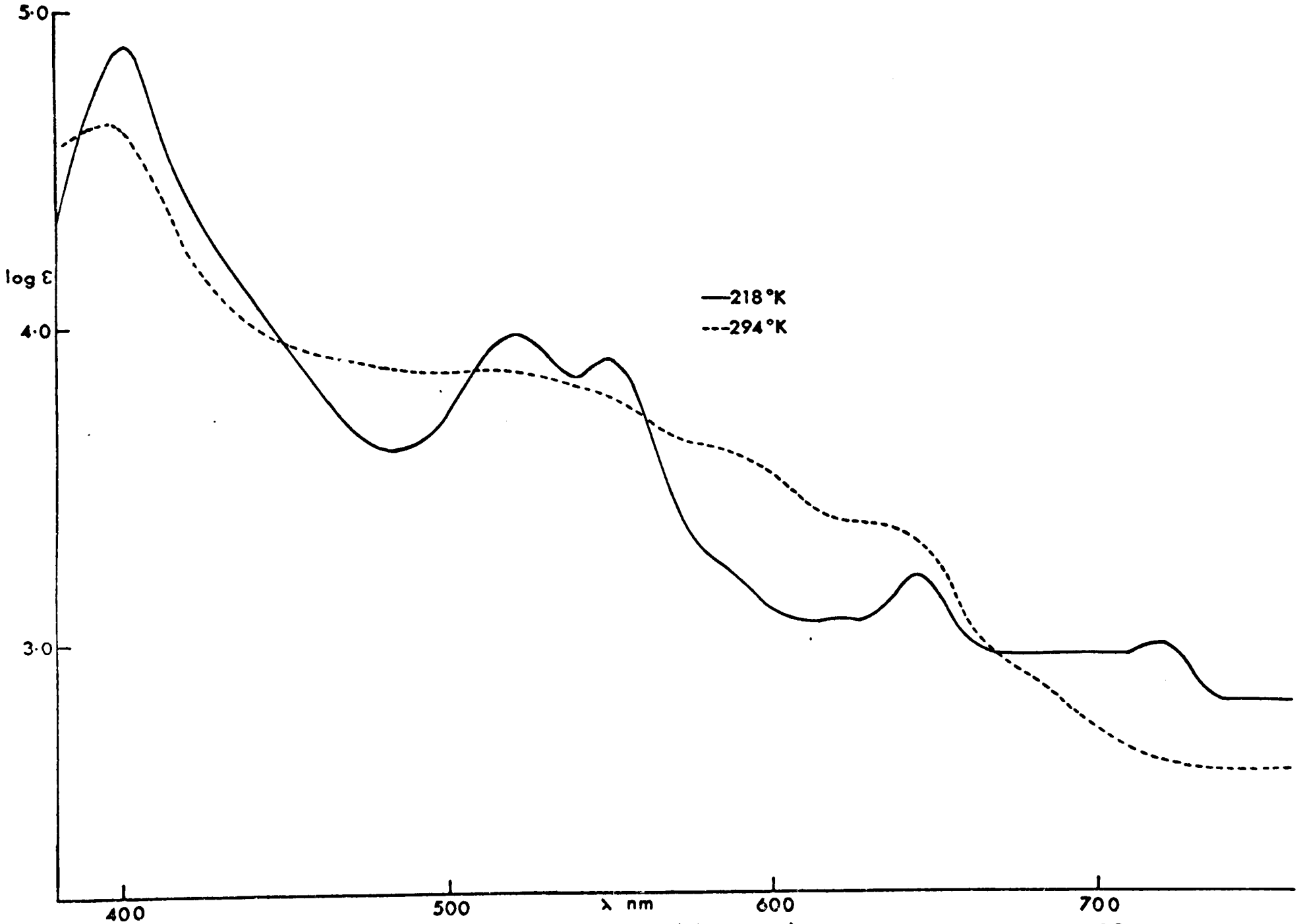


FIG. 3.10 Absorption spectrum of $Fe(OEP)(4\text{-}AcPy)_2ClO_4$ at 294°K and 218°K.

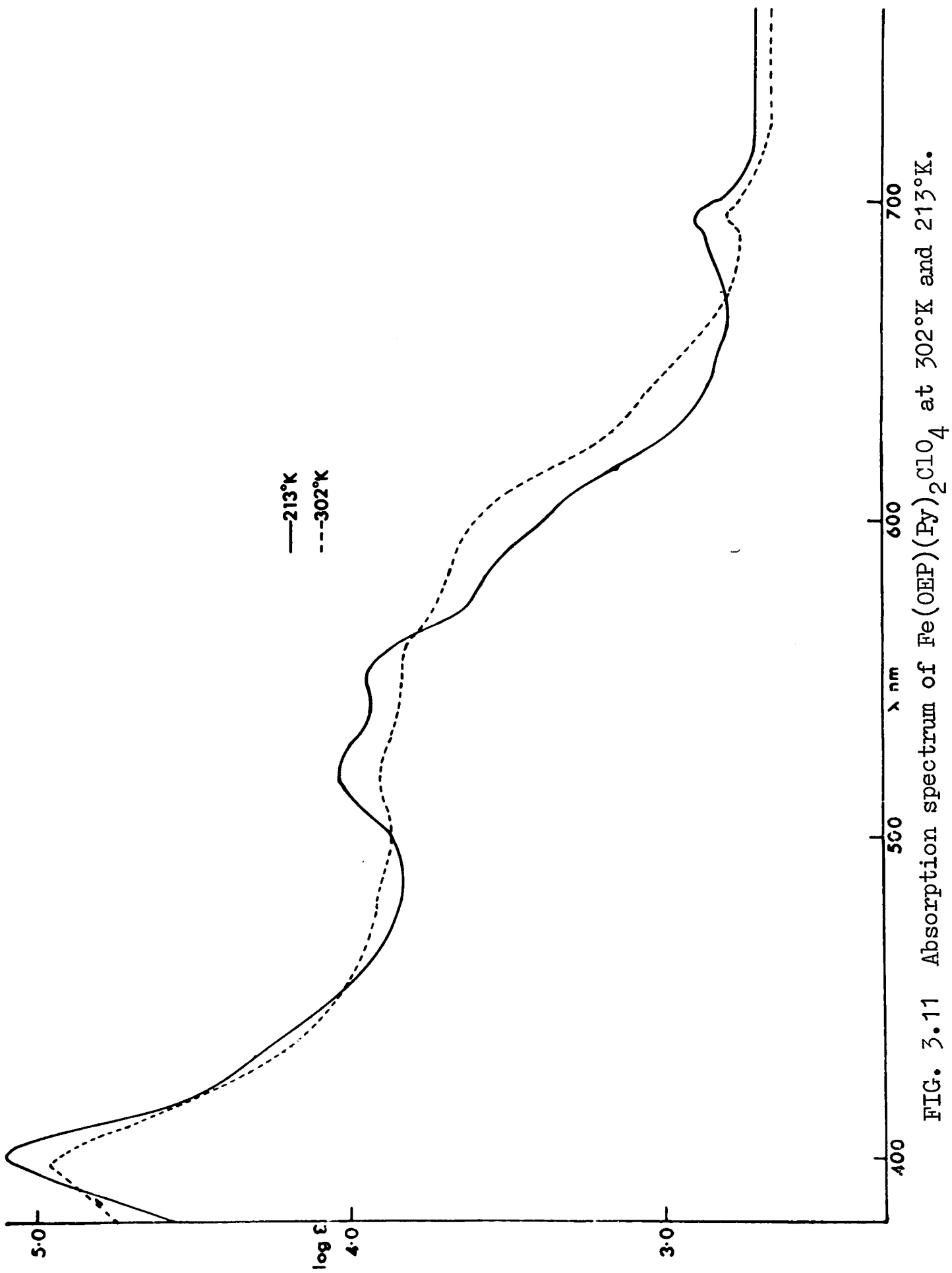


FIG. 3.11 Absorption spectrum of Fe(OEP)(Py)$_2$ClO$_4$ at 302°K and 213°K.

absorption spectrum of $Fe(OEP)(pyridine)_2ClO_4$ at 302°K and 213°K in Figure 3.11. The spectra at a common temperature show a certain similarity in the 350-800 nm region studied for all 3 complexes. However, for a particular complex, a quite dramatic change in the spectrum is observed on cooling from room temperature to 218°K.

At room temperature, the spectrum consists of a number of ill-defined diffuse bands at about 500, 550-600 and 600-650 nm. At 218°K, the spectrum shows bands at 520, 550 and 700-730 nm. The intense Soret band decreases in intensity and shifts to lower wavelength by about 5 nm on increasing the temperature from 218°K to room temperature. The position of the bands shows a small dependence on the axial ligand, being more pronounced at higher temperatures.

It was found that at the dilutions employed ($\sim 10^{-5}$ moles l^{-1}), the dissociation

$$Fe(OEP)(X\text{-}Py)_2ClO_4 \rightleftharpoons Fe(OEP)(X\text{-}Py)ClO_4 + X\text{-}Py$$

was very much in evidence. It was therefore necessary to add excess pyridine base to drive the equilibrium back to the bispyridinato complex in all cases.

Aliquots of the appropriate substituted pyridine were added to the solution until no change in the absorption spectrum was observed, in order to ensure that the species under investigation was the bis pyridinato complex.

4. Mössbauer studies

The Mössbauer spectra of some bis pyridinato ferric octaethylporphin perchlorate complexes at 300°K (room temperature) and 77°K (liquid nitrogen temperature) are shown in Figures 3.12 to 3.14. The Mössbauer spectrum of ferric octaethylporphin bis 4-acetylpyridine perchlorate at 77°K is shown in Figure 3.15, but no Mössbauer spectrum could be observed

for this complex at 300°K. The isomer shifts and quadrupole splittings for the complexes at 300°K and 77°K are given in Table 3.4 below.

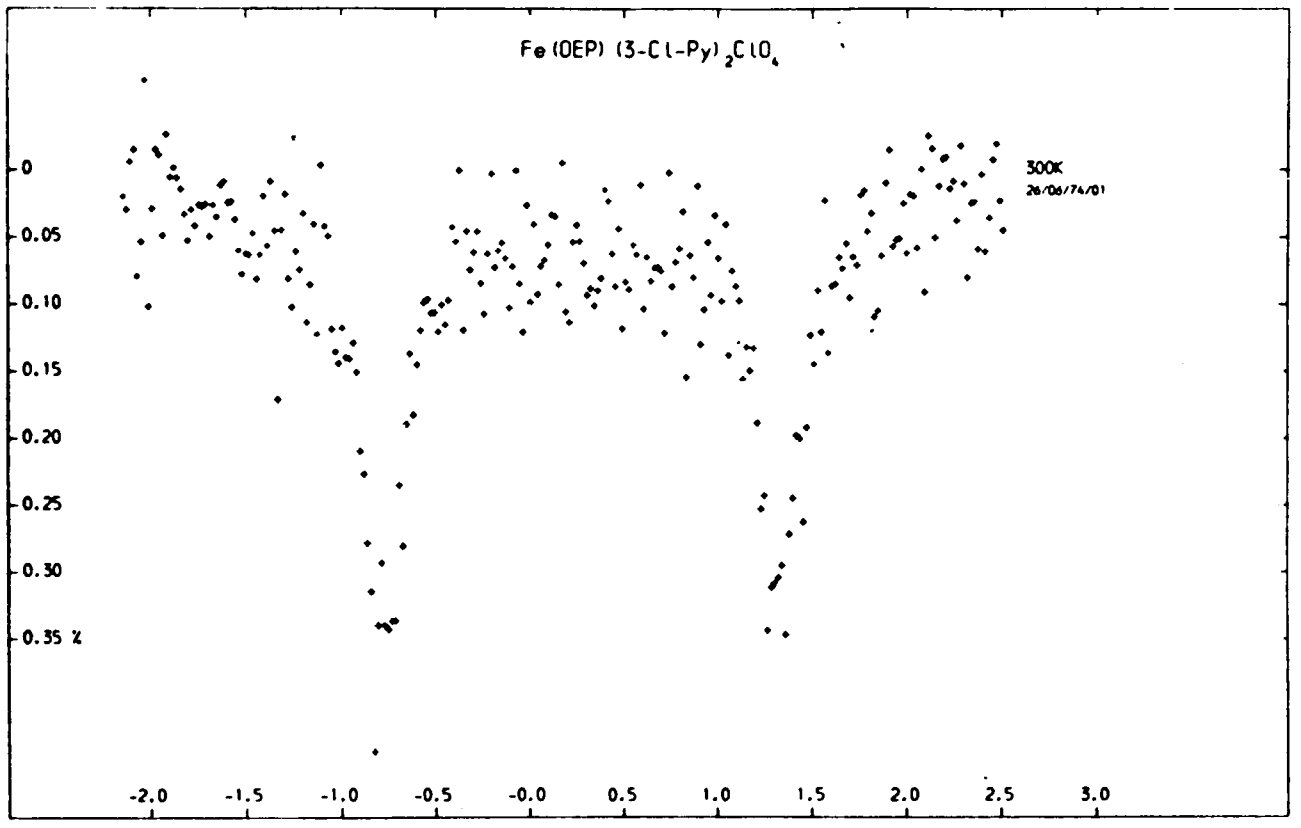
TABLE 3.4

Mössbauer Parameters of $Fe(OEP)(X\text{-}Py)_2ClO_4$ Complexes

Axial Ligand	Isomer shift (mm/sec)		Quadrupole splitting (mm/sec)	
	300°K	77°K	300°K	77°K
3-Chloropyridine	+0.26	+0.30	2.07	2.00
4-Acetylpyridine		.0.23		2.03
Pyridine	+0.21 +0.18	+0.25	1.93	1.90
4-Aminopyridine	+0.22	+0.26 +0.37	1.91	2.43 +0.45
(Chromatium Cytochrome cc'	+0.08 (205°K)	+0.11	1.97 (205°K)	2.27
(Chromatium Cytochrome c_{552}	-0.05 (205°K)	-0.03	2.22 (205°K)	2.14

All the spectra show sharp doublets with a quadrupole splitting of about 2 mm sec^{-1}. These doublets are reasonably symmetric at 300°K but are much less so at 77°K. The isomer shifts are in the region 0.2 - 0.3 mm sec^{-1}, increasing in magnitude as the temperature is lowered. The quadrupole splittings appear to decrease slightly for the 3-chloropyridine and pyridine complexes between 300°K and 77°K, but the quadrupole splitting for the 4-aminopyridine complex increases substantially at the lower temperature.

A less well-defined doublet with a small quadrupole splitting is present to a greater or lesser extent in all cases at the higher temperature. This is most clearly observed for the pyridine complex, although the splitting is better resolved in the case of the 4-aminopyridine complex. For the latter, the quadrupole splitting is around 0.45 mm sec^{-1} at 77°K.



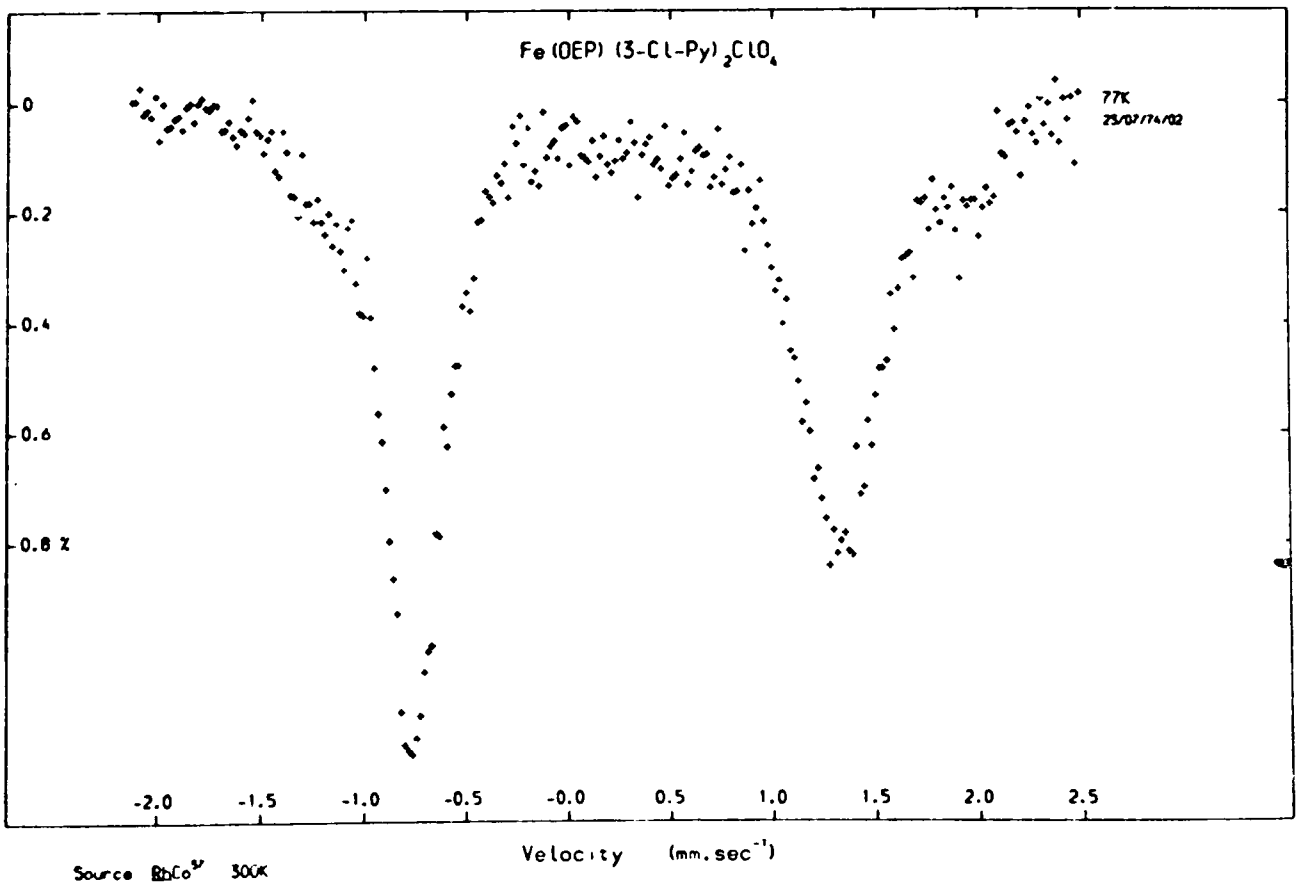


FIG. 3.12 Mössbauer spectrum of Fe(OEP)(3-ClPy)$_2$ClO$_4$ at 300°K and 77°K.

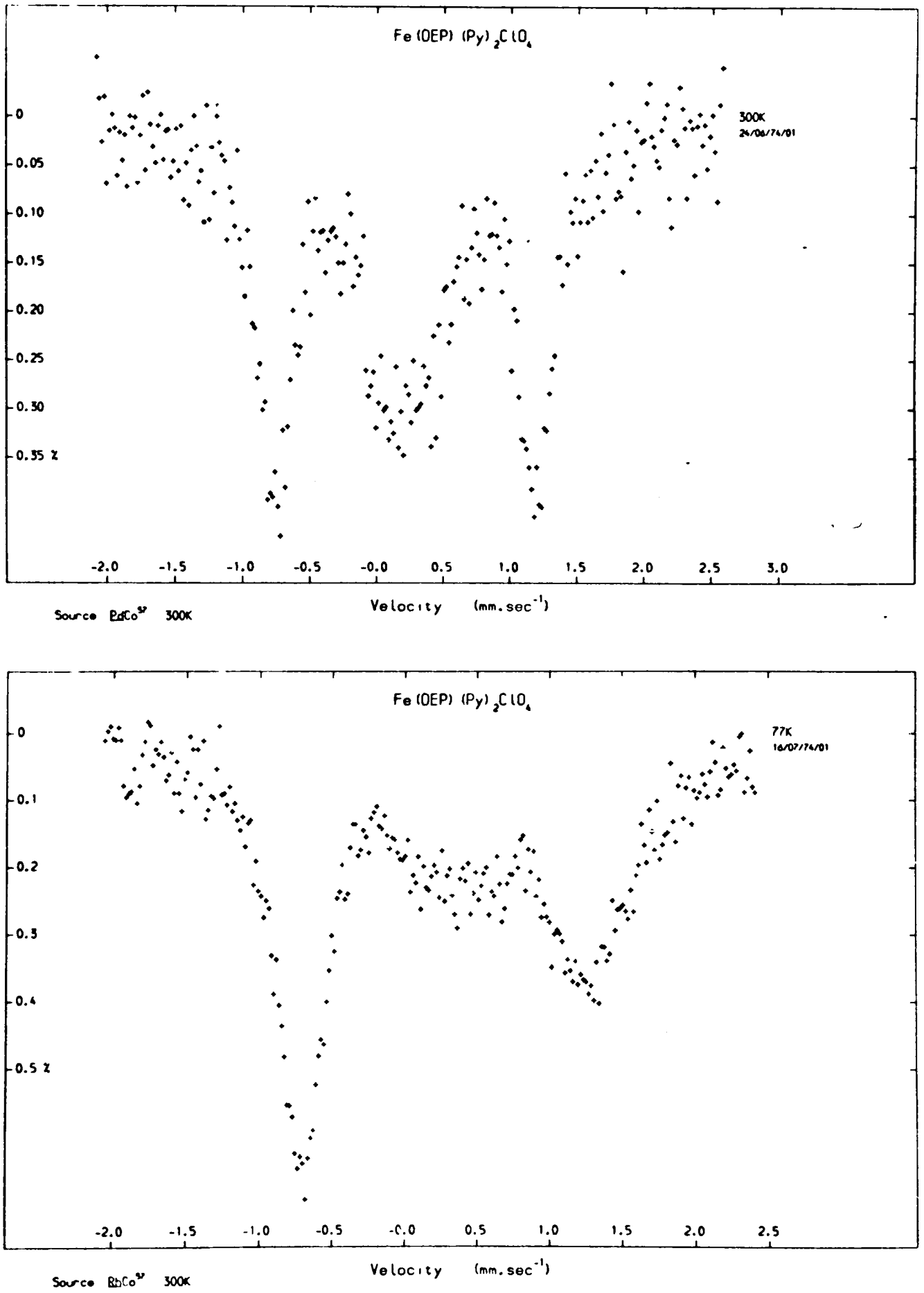
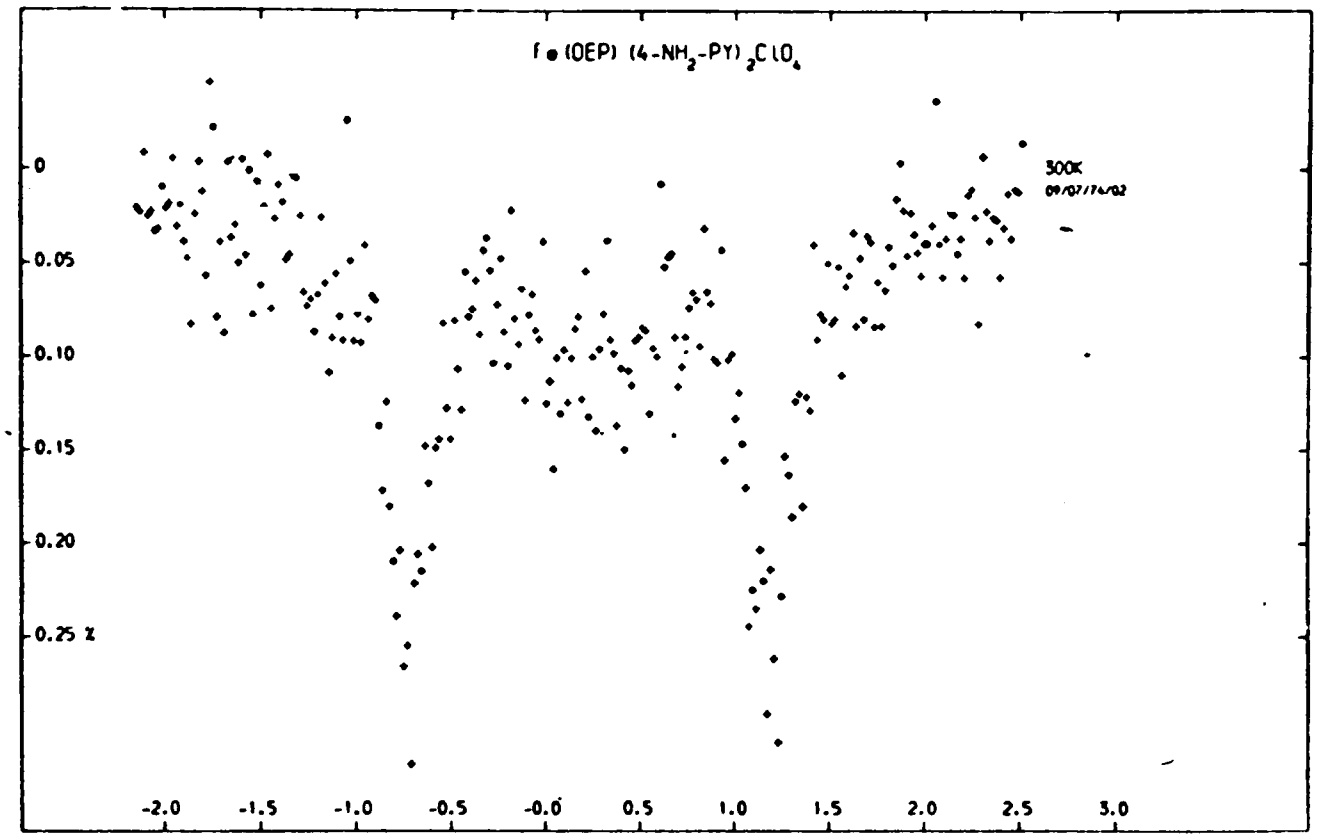


FIG. 3.13 Mössbauer spectrum of $Fe(OEP)(Py)_2ClO_4$ at 300°K and 77°K.



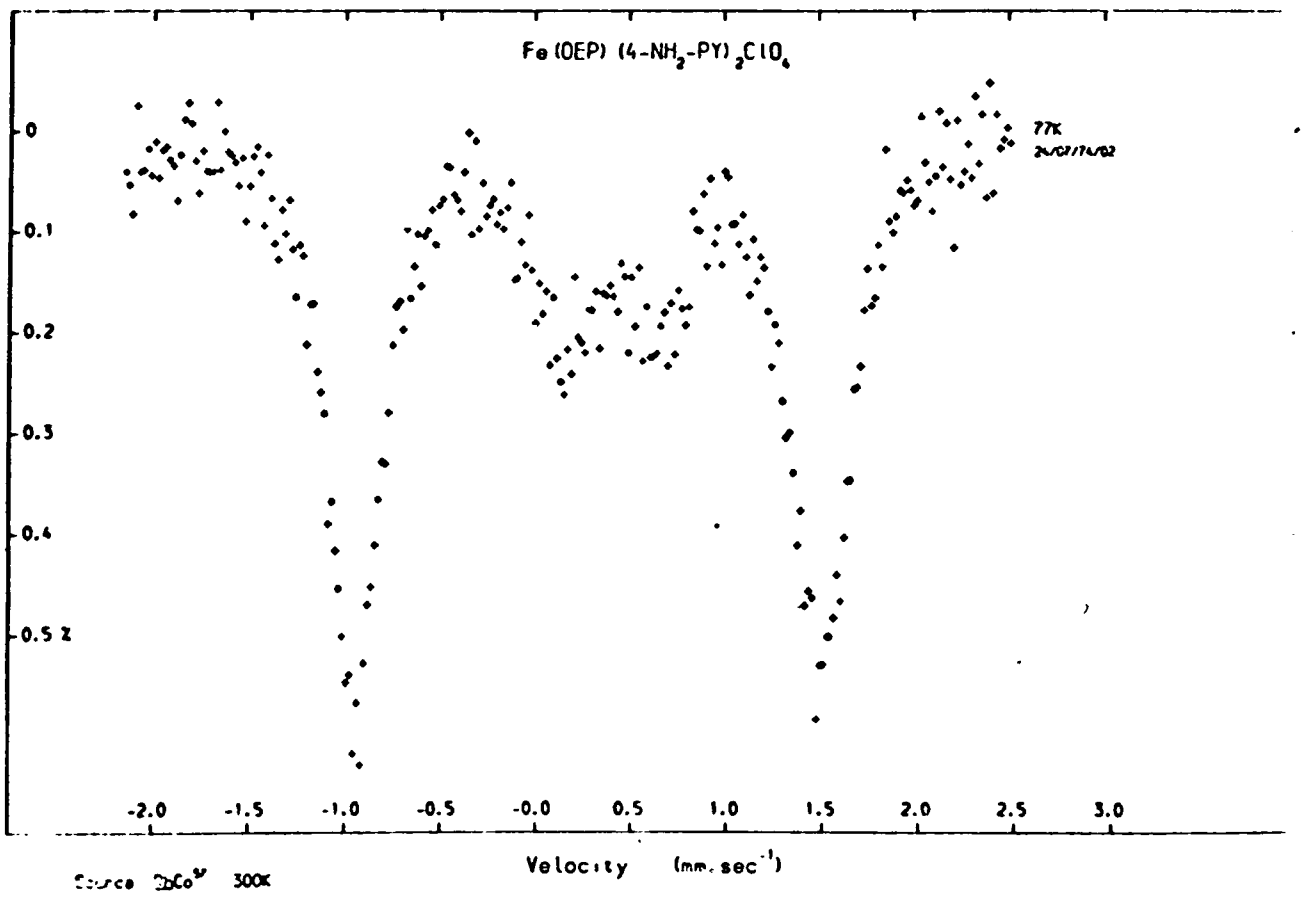


FIG. 3.14 Mössbauer spectrum of $Fe(OEP)(4\text{-}NH_2Py)_2ClO_4$ at 300°K and 77°K.

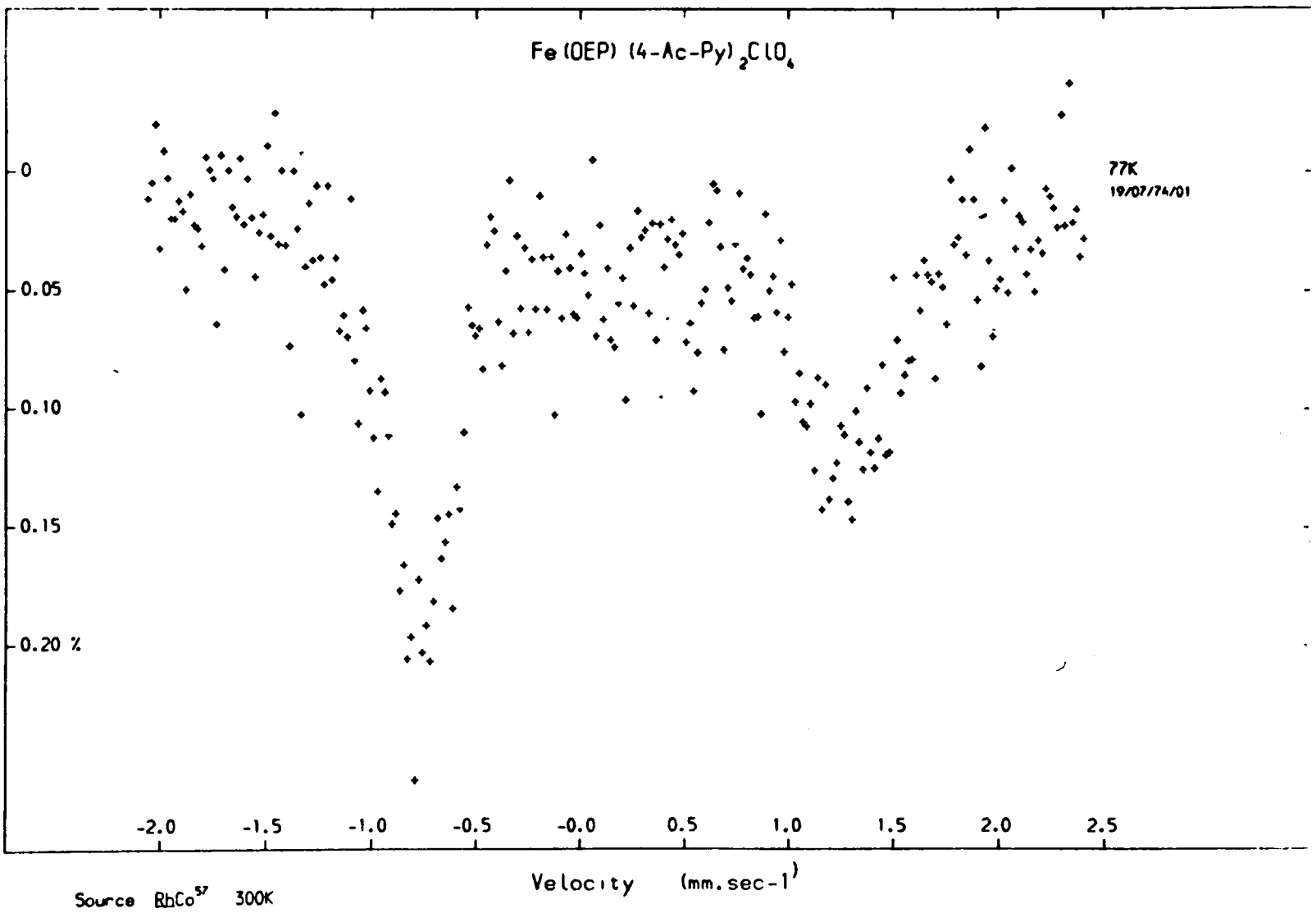


FIG. 3.15 Mössbauer spectrum of Fe(OEP)(4-AcPy)$_2$ClO$_4$ at 77°K.

5. E.P.R. Spectra

The E.P.R. spectra of the bispyridine and bis N-methylimidazole complexes of ferric octaethylporphin perchlorate were obtained in frozen solution in $CHCl_3$ at liquid helium temperature. The spectrum of the pyridine complex was found to exhibit one signal at a field which corresponded to a g value of 3.4. No other signal within the field range of the magnet was observed, and it is a reasonable assumption that with a stronger magnet, a signal at a field corresponding to a g value of 0.58 would be observed. This would be analogous to the EPR spectrum of the bispyridine complex of iron (III)-protoporphyrin IX chloride (Chapter 4), whose g values were measured as $g_{\parallel} = 3.4$ and $g_{\perp} = 0.58$, typical of an axially symmetric complex with large anisotropic g values.

The spectrum of the N-methylimidazole complex, shown in Figure 3.16, exhibits three signals and must therefore possess a lower symmetry than D_{4h}, possessing large in-plane magnetic anisotropy. The g values, $g_x = 1.48$, $g_y = 2.28$, $g_z = 3.04$, are similar to those reported[39-42] for a number of other low-spin ferric hemes, where a static rhombic distortion is present in the form of highly asymmetric peripheral substituents, and to those reported[43] for the bisimidazole ferric complex of tetraphenylporphin.

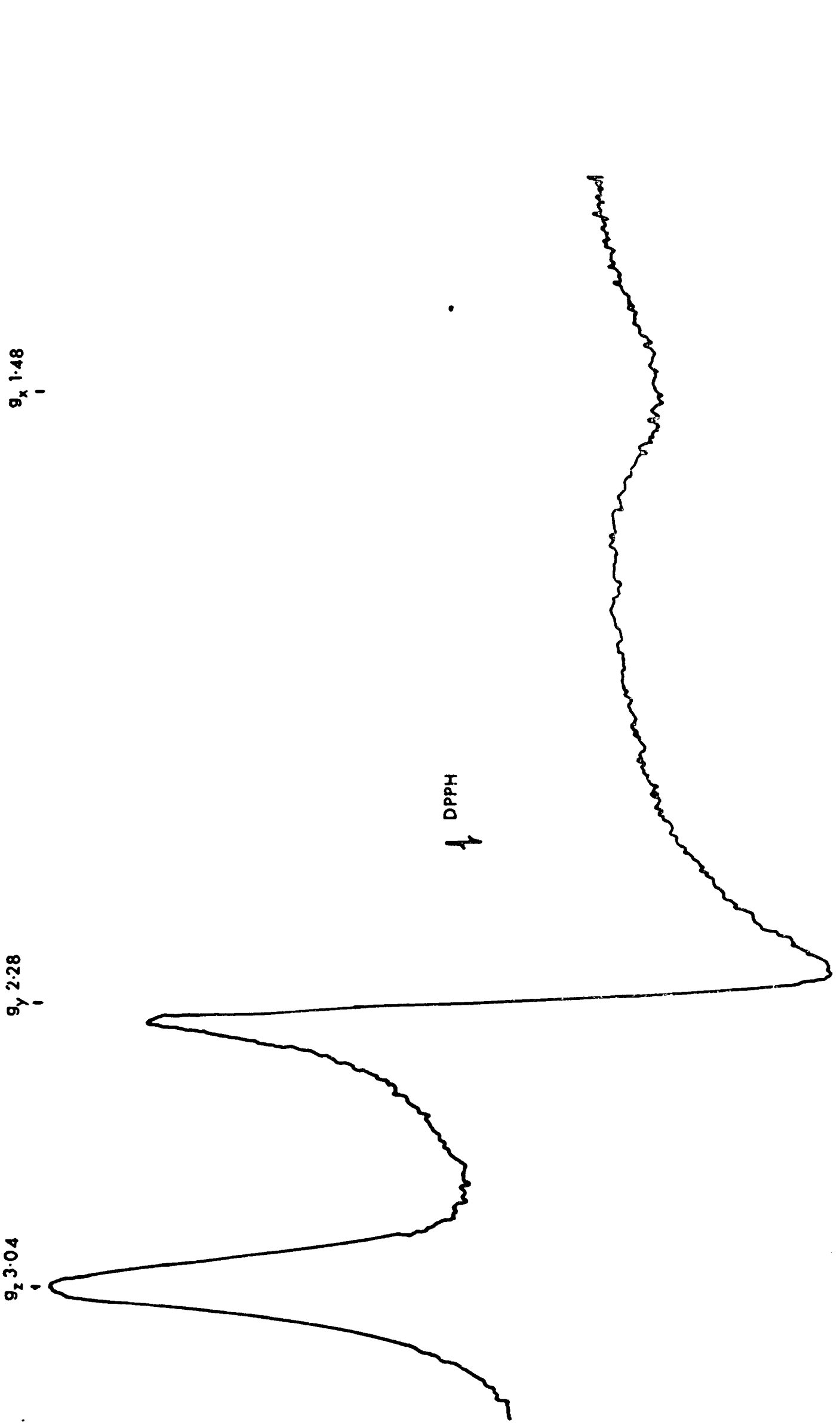


FIG. 3.16 EPR spectrum of $Fe(OEP)(N\text{-}MeIm)_2ClO_4$ at liquid helium temperature.

3.4 Discussion

1. General features

i) NMR results

In all the complexes studied, excepting the $Fe(OEP)(3\text{-}ClPy)_2ClO_4$ at higher temperatures, resonances corresponding to bound pyridine ligand protons are observed over the full temperature range studied. The relative integration of porphyrin and pyridine resonances demonstrates that the bispyridinato complex is present throughout. The resonances of protons a, b and c on the porphyrin ligand shift to higher field with increase in basicity of the axial ligand, at a given temperature. Thus, in order of magnitude the observed shifts follow the order 3-chloropyridine < 4-acetylpyridine < 3-acetylpyridine < pyridine < 4-methylpyridine < 4-aminopyridine. A similar effect can be observed for some of the resonances of the 'natural' porphyrins (see Appendix V).

All of the plots of observed shift against reciprocal of the absolute temperature demonstrate a non-Curie dependence in deviating from the linear behaviour expected and in that the isotropic shifts do not extrapolate to zero at infinite temperature, i.e. as $T^{-1} \longrightarrow 0$.

a) Deviation of the temperature dependence plots from linearity

The non-linear behaviour is most apparent for the β-protons of the pyridinato ligand, as remarked earlier, although evident for all the protons. Furthermore, the resonances of the various protons within a particular complex exhibit different temperature dependences. As no resonances corresponding to uncomplexed ligand are observable, it must follow that either exchange effects are absent completely, or that the rate of change is fast compared with the NMR time scale. It would therefore not seem plausible for the non-linear behaviour of these plots to arise from exchange effects.

The observations are, however, consistent with some form of equilibrium between the various accessible spin states of the ferric

ion. The contact shift contribution will in fact be represented by a complex function with a different hyperfine coupling constant for each state arising from a different orbital configuration. In addition, the contribution of different spin multiplet states to the susceptibility tensor has the effect that anisotropy in susceptibility as a function of temperature can vary greatly. In these circumstances a non-Curie dependence is not surprising, and further reference to the experimental relationship of observed shift with temperature will be made later in this work.

b) Extrapolation anomalies in the temperature dependences of the observed shifts

Basic theory based on relationships between contact shift and temperature (equation 2.18) and pseudocontact shift and temperature (equation 2.24) predicts that for this Curie behaviour, a plot of isotropic shift against T^{-1} should approach zero as T^{-1} approaches zero. More usually stated, a plot of observed shift against T^{-1} should approach the value of the shift observed in a corresponding diamagnetic complex as T^{-1} approaches zero.

This relationship is not found for the complexes under investigation, in general the value of the isotropic shift being negative as T^{-1} is approached. Again this non-Curie behaviour could be consistent with the electronic population of a number of spin states, and hence the dependence with temperature of the averaged coupling constant. However, as was pointed out in Chapter 2, a number of assumptions are inherent in the derivation of relationships such as (2.18) and (2.24).

It is known that taking into account the orbital contribution to the isotropic NMR shift indirectly by means of g-tensor components requires that at most there be only a first order orbital contribution to the magnetic moment of the complex, brought about by spin-orbit mixing of the ground level with non-populated excited states. Unfortunately this

analysis neglects the second-order Zeeman (SOZ) terms in the expression derived by Van Vleck for paramagnetic susceptibility, and these terms may contribute substantially to the magnetic susceptibility. Furthermore the SOZ effect contributes more heavily to $\chi_{\perp}$ than to $\chi_{\parallel}$ indicating that g tensor and susceptibility anisotropy are not strictly proportional.

From studies and calculations performed on a series of low-spin hemin systems[70], it was found that as g-tensor anisotropy decreased, SOZ contributions first counteracted, then became negligible and finally augmented the FOZ anisotropy contributions. In this way it is clear that estimation of dipolar shifts directly from g-tensor anisotropy data without inclusion of SOZ effects or excited state contributions can lead to either over-estimations or under-estimations depending on the anisotropy of the system. The authors also found evidence in the most anisotropic case of a non-Curie behaviour of the total axial anisotropy arising from three sources:

i) a SOZ anisotropy contribution which is opposite in sign from the FOZ term and relatively independent of temperature;

ii) thermal depopulation of the lowest Kramers doublet which increases with temperature;

iii) thermal population of the first excited Kramers doublet which has a FOZ anisotropy opposite in sign from that of the ground doublet.

Effects (ii) and (iii), which amplify one another, can cause significant non-Curie behaviour even in the absence of SOZ effects. Non-Curie behaviour in the FOZ contribution is expected to become less pronounced and at the same time the increasingly positive SOZ contribution causes the intercept of the total anisotropy on the T^{-1} axis to become negative as g-tensor anisotropy decreases.

These findings suggest that neglect of the factors discussed above in any theoretical treatment is bound to mean that non-Curie behaviour will be observed, and also any experimentally measured quantities, such

as observed shifts, obviously contain contributions from effects like SOZ which are specifically excluded from the basic theoretical relationship. In the ferric octaethylporphin complexes studied here, g-tensor anisotropy is significant and the dipolar shift is therefore overestimated in the theoretical treatment.

For a constant value of a_i, the contact contributions to the observed shifts are expected to be proportional to the function $(\chi_{\parallel}/g_{\parallel} + 2\chi_{\perp}/g_{\perp})$ as is seen from (2.18). The temperature dependence of this function leads to a negative intercept on the T^{-1} axis. It is therefore understandable in qualitative terms why experimentally it is found for the ferric octaethylporphin complexes that the value of the isotropic shift is negative as T^{-1} is approached.

ii) Magnetic data

The values of the magnetic moments themselves are unusual in that for the most part they do not correspond to the values expected for low-spin ($S = {}^1/2$) in the region 2.2 - 2.6 B.M., nor to those expected for high-spin ($S = {}^5/2$) in the region of 5.9 B.M. The values for the moments of the 3-chloropyridine complex and the 4-acetylpyridine complex at higher temperatures in the region 3.9 - 4.3 B.M. could be explained by postulating the existence of the $S = {}^3/2$ state as the ground state. The remaining complexes have values for the most part intermediate between this value and that expected for a low-spin ($S = {}^1/2$) complex. These results are explicable by postulating the presence of a spin-equilibrium, and are consistent with the atypical PMR results mentioned above.

The magnetic moments of all the complexes measured are found to change appreciably over the temperature range considered. This feature can be readily interpreted if low-lying electronic states of differing spin multiplicity to the ground state are thermally accessible. Change in temperature leads to a change in the Boltzmann distribution over these

energy levels, thus affecting the magnetic susceptibility and magnetic moment. Similar results have been observed for a number of ferric porphyrin hemichromes in the solid state[44], and these were interpreted in terms of a thermal equilibrium between the S = $^1/_2$ state and a higher spin state.

There is a fairly direct relationship between basicity of the axial ligand and magnetic moment value. As the basicity of the axial ligand increases, the value of the magnetic moment at a given temperature decreases. This effect is demonstrated in the Table below.

TABLE 3.5

Relationship between basicity of axial ligand and magnetic moment of ferric octaethylporphin complex

Ligand	pK_a[45]	μ_{300} (B.M.)
3-ClPy	2.81	4.03
3-AcPy	3.18	3.41
4-AcPy	3.51	3.68
Py	5.17	2.65
N-MeIm	7.25	2.35
4-AmPy	9.12	2.96

(Magnetic moments at 300°K)

Excepting the anomalous values of the bis-3-acetylpyridine and bis-4-aminopyridine complexes, there is a general diminution in the value of the magnetic moment found at 300°K as the basicity of the axial ligand increases. There would thus appear to be an increased contribution from higher spin states as the basicity of the axial ligand decreases.

iii) Electronic absorption spectra

The spectra at low temperatures bear much resemblance to those of low-spin ferric porphyrin and protein species having an intense Soret band at about 400 nm and a weaker $\alpha-\beta$ system at 500-600 nm. These

typical low-spin spectra have been interpreted as involving $\pi \rightarrow \pi^*$ transitions. A model in which the highest energy filled π-orbitals have an angular momentum about the fourfold axis of $L = \pm 4$ has been proposed[46]. The lowest empty π^* orbitals had $L = \pm 5$, so that the lowest-lying $\pi \rightarrow \pi^*$ transitions corresponded to $\Delta L = \pm 1$ and ± 9. The former is strongly allowed and the latter forbidden, in agreement with the observation of an intense Soret band and a weaker $\alpha - \beta$ system.

Gouterman and his co-workers[47-51] have extensively discussed the electronic structure of the electronic π-system and explained the positions and intensities of the $\alpha - \beta$ and Soret bands in terms of a "four-orbital" model. The lowest-lying excited states are deemed to arise only from configurations involving the two highest energy filled orbitals, designated a_{1u} and a_{2u} under D_{4h} symmetry, and the two lowest energy empty orbitals, which are e_g. Contributions from other configurations are considered to be negligible. The two excited states arising from the excitations $a_{1u} \longrightarrow e_g$ and $a_{2u} \longrightarrow e_g$ are both of E_u symmetry and should be nearly degenerate, but for the fact that configuration interaction mixes them and drives them apart. The transition to the higher of the two excited states can be shown to be more intense and corresponds to the Soret band. The lower excited state gives rise to the α-β system. The α- and β-bands are believed to be the 0-0 and 0-1 components of a vibrational progression. The effects of axial substitution at the metal can be discussed in terms of the donor ability of the ligand, and its effect on the charge on the metal. Unfortunately, the complexity of the system and the superposition of bands corresponding to different spin states makes any characterisation of the bands in terms of pK_a and π-donor ability virtually impossible.

The visible spectra of high-spin and mixed-spin ferric porphyrin and protein species are much more complex than those of the low-spin compounds. The high-spin ferric hemeprotein spectra have been interpreted on the basis that there is configuration interaction between a charge transfer

state and a π^* state[24]. The bands 500 nm and 625 nm in these cases arise from transitions to excited states which can be regarded as involving both charge transfer and $\pi - \pi^*$.

Some of these points could be appropriate to the spectra of the bis-pyridinato ferric octaethylporphin complexes, especially at the upper end of the temperature range studied. Thus the 3-chloropyridine complex contains a band at about 630 nm and a broad band at ca. 510 nm. This latter band could be characteristic of another spin-state complex, or may simply be a superimposition of the α-β bands of a low-spin complex on the higher temperature spectrum. Similarly, the 4-acetylpyridine complex contains broad bands at the higher temperatures which bear a resemblance in intensity and wavelength to those of ferric hemeproteins which are classically referred to as "high-spin", or "intermediate-spin" complexes.

It is not possible to discuss the absorption spectra observed in any great detail due to the broadness of the bands and the quite striking variation of these with temperature. However, there is definitely evidence for the existence of more than one electronic species in that the spectra appear to consist of superimpositions of separate spectra characteristic of particular electronic species. The similarity of some of these spectra with those of ferric porphyrin and protein complexes, and the behaviour with respect to variation in temperature, leads to the conclusion that some form of spin equilibrium is present. A more detailed analysis of the spectra will be attempted later.

iv) Mössbauer studies

The Mössbauer parameters given in Table 3.4 would in the first instance approximate to some of those previously reported for ferric porphyrin and protein complexes[44,52-55]. The quadrupole splittings are of the same magnitude as those assigned to low-spin ($S = {}^1/2$) ferric complexes, although the isomer shifts are slightly less than those reported for $S = {}^1/2$ ferric complexes.

The presence of the less intense resonance is not so easy to explain. High spin ($S = {}^{5}/_{2}$) ferric complexes in D_{4h} or lower symmetry are expected to show small quadrupole splittings. One explanation for these resonances could be that they are due to small amounts of either the monopyridinato complex, or the initial ferric octaethylporphin perchlorate material, in both of which the ferric ion would be expected to be in the $S = {}^{5}/_{2}$ state. Alternatively, these resonances could arise from the presence of a "higher" spin-state ferric complex present at higher temperatures, the proportion of which diminishes as the temperature is lowered. This invokes the idea of a spin-equilibrium and this system would differ essentially from the ferric bisdithiocarbamate system in that two separate signals are observed here whereas only an averaged signal is observed for the latter system. Hence it would follow that here the correlation time for electronic relaxation between the spin states is greater than the effective quadrupole period.

A number of features of the spectra do not however agree with this second analysis. Thus for the 3-chloropyridine complex there is very little evidence of the second resonance corresponding to the higher spin-state whereas it is for this complex that the resonance would be anticipated to be most pronounced. For the 4-aminopyridine complex, the resonance in question becomes more in evidence at the lower temperature, contrary to the prediction of a spin-equilibrium theory. The 4-aminopyridine complex is anomalous in that the quadrupole splitting of the intense doublet increases considerably with decrease in temperature, and it could be in fact that this complex is behaving in a different way to the other complexes on all counts.

A spin equilibrium system in which the correlation time for electronic relaxation between the spin states is much less than the effective quadrupole period would manifest itself in terms of an

averaged Mössbauer spectrum. It may be that the spectra under consideration represent this situation and the less intense, poorly resolved resonance indicates an impurity in the test compound. The quadrupole splitting of the more intense doublet, except in the case of the 4-aminopyridine complex, does not change appreciably between 300°K and 77°K, although such a change would be expected if the Mössbauer characteristics of the different spin states involved were radically dissimilar. Possibly the electric field gradients relating to the states that are involved in the spin equilibrium are not widely varying.

The higher energy quadrupole line (toward positive source velocity) generally broadens most rapidly as the temperature is lowered. This broadening of the higher energy line, caused by interaction between the unpaired electron spin and the nuclear spin, indicates a positive nuclear quadrupole coupling constant.

2. <u>The spin equilibrium situation - a more complete description</u>

Before commencing a detailed analysis of the experimental results, it is important at this juncture to examine more closely the concept of a temperature dependent equilibrium between isomers of differing spin multiplicity, commonly described as a "spin-equilibrium" situation. Simple theory has it that for two states in equilibrium, the physical properties of that system should be given simply by the value of the property for each of the states weighted by the appropriate Boltzmann factor. The first model put forward in explanation of the physical properties of the iron (III) dithiocarbamates was found to account for these reasonably well. A Boltzmann distribution over two states, each represented by a well-defined spin quantum number and hence a well-defined spin multiplicity, close enough in energy for the upper state to be appreciably populated, could reproduce qualitatively the empirical dependence of particular physical properties on temperature.

Whilst in octahedral fields it is emphasised that two states in their

equilibrium geometries cannot be mixed appreciably by spin-orbit coupling, in the region of ligand-field strengths where the potential energy curves actually cross, the position is complicated by the fact that matrix elements of spin-orbit coupling between certain eigenfunctions do not vanish. In this region, the concept of spin-multiplicity becomes ill-defined and the physical properties of the system are no longer adequately described by weighting each multiplet property by an appropriate Boltzmann factor. This is understood to be called spin-mixing of states, in that the various eigenfunctions cannot be labelled by pure quantum numbers but represent mixtures with components of different states, that is the irreducible representations under the particular double group symmetry contain species of the correct symmetry for mixing.

With tetragonal symmetry, the situation becomes even more complex, since there are matrix elements for spin-orbit coupling linking states of the D_4 symmetry group. Allowing these states to interact by introducing the spin-orbit coupling operator produces 12 eigenvalues and 12 doubly degenerate eigenfunctions which cannot be adequately described in terms of pure quantum numbers. Thermal population over these states then accounts for the electronic properties associated with a particular system. Thus the simple description invoked above certainly cannot be utilised in the tetragonal case.

Several refinements in the simple model can explain quantitative differences between theory and experiment. Thus, using a simple model to describe the octahedral d^5 case such as for the ferric dithiocarbamates, metal-ligand vibration frequencies should differ in the $^6A_1$ and $^2T_2$ states and the consequences of this can be of sufficient magnitude to account for much of the deviation between theory and experiment. Thus vibrational partition functions should be incorporated into the theory,

as the relative populations of the states will in part be determined by these.

A model treating electronic states as separate entities described in terms of "good" quantum numbers is therefore simplistic and inadequate. A more complete picture is described by allowing for a quantum mechanical admixture of states, which refers to a situation in which the wavefunction representing a particular electronic configuration contains substantial contributions from a number of different electronic states. In fact spin-orbit coupling can simply be regarded as a perturbation of the basic electronic states of, in this case, the ferric ion, and is one of a number of factors together with ligand field, electrostatic and symmetry parameters, which serve to represent the electronic behaviour of the ferric ion in each particular environment. Since all electronic states in a tetragonal environment are to some extent spin-mixed due to spin-orbit coupling, in order to define terms, a "pure" spin state is designated as one for which the components are composed of 98% or more of the components of one total spin state or another, i.e. sextet, doublet or quartet. The remainder of the states are then "substantially" spin-mixed, i.e. more than 2%[20].

Thermal population over the various energy levels available accounts for the electronic properties of the system. Thus the apparent change of "spin-state" of a particular complex observed by monitoring the variation of some electronic or physical property with temperature is due to a change in Boltzmann distribution over the thermally accessible levels. The apparent changes in "spin-state" observed in a similar fashion for a series of closely related complexes, e.g. for the bispyridinato iron (III) octaethylporphin complexes studied here, can occur with internally consistent and rather small variations in ligand field parameters. Thus the notion of spin-equilibrium systems and spin-mixed systems, which tend to be regarded as separate entities in much of the literature, is a somewhat nebulous one. The extreme limiting cases are thus represented as a

Boltzmann distribution over a series of non-interacting spin states and one involving interacting levels connected by spin-orbit coupling. Formally the former corresponds to the possibility of individual molecules having different ground states, whereas the latter corresponds to a single-ion property, defined by reference to molecular dimensions. Usually, however, a particular system operates in the intermediate region between the limiting cases and then the concepts of spin equilibrium and spin mixed systems are not mutually exclusive but interdependent. Furthermore, the use of the term "change in spin-state" to denote a change in population and order of the ground state and low lying electronic states is obviously meaningless if the states considered are not pure but spin mixed states.

To illustrate the shortcomings of a simple theoretical treatment of the electronic properties of ferric porphyrins, some of the experimental results in section 3.3 will be treated on the basis that they arise from the fact that although the ground state is a doublet state, thermally accessible states of different spin multiplicity are present. The population of these latter states is a function of variation in temperature and/or ligand field parameters. Throughout this treatment, the electronic states will be regarded as being pure states and as such, each can be represented by one total spin state. This basic approach will then be compared with a more sophisticated quantitative approach, in which several of the factors discussed in this introduction will be introduced and their effects monitored.

3. Qualitative discussion of results of various physical methods

On the assumption that all electronic states can be regarded as pure states according to the definition given above, then for the ferric ion in a tetragonal ligand field, only doublet, quartet and sextet excited states need be considered. Treating the phenomena of the

electronic properties as resulting from a simple equilibrium between two pure spin states, and proceeding on the basis that the ground state of the ferric ion is a doublet ($S = {}^1/2$) state in all cases, then the spin equilibrium can be either doublet-quartet (${}^1/2 \longrightarrow {}^3/2$) or doublet-sextet (${}^1/2 \longrightarrow {}^5/2$) equilibrium. Evidence that a doublet state is indeed the ground state is provided by the solution magnetic susceptibility data. The magnetic moments of all the complexes studied are below a value of 3.0 B.M. at the low temperature end of the range, and many of them are within the spread of values of magnetic moments commonly associated with doublet spin states, that is 2.2 - 2.6 B.M.

A superficial examination of the data produced by the various physical methods employed does not categorically determine which of the two upper spin states is the more appropriate representation of the electronic phenomena. The results will therefore be examined in somewhat more detail in order to distinguish which of the two spin equilibria provides the more apposite representation of the electronic processes occurring.

i) <u>NMR results</u>

Only one set of resonances for each chemically inequivalent set of protons is observed. This represents a spectrum consisting of resonances "averaged" between positions corresponding to each of the two spin states. Thus a spin state interconversion time of less than 10^{-5} - 10^{-7} sec. is indicated. The effect of these observations is that the NMR results are of little help in distinguishing which of the two spin equilibria types is a better representation of the system under study. However, attempts have been made by Iizuka[59,60] to separate these averaged shifts into contributions from high-spin ($S = {}^5/2$) and low-spin ($S = {}^1/2$) components in the case of ferric myoglobin and hemoglobin derivatives, but with few meaningful conclusions.

ii) Magnetic data

The magnetic moments of those complexes for which the spin-state equilibrium appears to favour the higher spin state, namely the $Fe(OEP)(3\text{-}ClPy)_2ClO_4$ and $Fe(OEP)(4\text{-}AcPy)_2ClO_4$ complexes, have respectively values of 4.2-4.3 and 3.9 B.M. at the highest temperature recorded (ca. 330°K). The plot of μ_{eff} against T for these complexes tends to show a slight "flattening" of the curve as a value of 3.9 B.M. for μ_{eff} is approached in certain cases, but in no case is a limiting value of around this figure found.

The spin only limiting magnetic moment of the quartet state is 3.87 B.M., whilst that of the sextet state is 5.92 B.M. In the spin-state equilibrium observed[61] for the five coordinate cobalt (II) complex of N-R-N-2-(diphenylphosphino)ethyl-N',N'-diethylethylenediamine (R=H), limiting values of 2.16 and 4.50 B.M. were assumed for the doublet-quartet equilibrium, since a number of moments over 4.0 B.M. were calculated at temperatures over 300°K. An orbital contribution of at least 0.6 B.M., or contributions from higher excited states, would have to apply here to account for the observed magnetic moments.

Whilst the magnetic moment of 4.3 B.M. associated with the 3-chloro-pyridine derivative could represent the contribution of a spin quartet state to the equilibrium, nevertheless alone this is not sufficient to conclude that the upper state in the spin equilibrium is the quartet state, particularly as the plot of μ_{eff} against T does not level off at this limiting value. (Indeed it will be demonstrated later that a roughly constant magnetic moment of between 4.0 and 4.5 B.M. is possible with a spin sextet first excited state, and therefore not necessarily indicative of a spin quartet first excited state.)

On the basis of the magnetic susceptibility and moment results, therefore, it is not possible to state which of the quartet or sextet spin states contributes to the likely spin equilibrium process. The results are capable of being interpreted in favour of either system,

and it will be necessary to examine the experimental results determined by other physical methods in order to arrive at a more unambiguous interpretation.

iii) Electronic absorption spectra

By comparing the electronic spectra of some of the complexes studied with electronic spectra of ferric hemoprotein derivatives, a number of similarities are immediately apparent. Considering a known low-spin protein such as cyanoferrimyoglobin, with, for example, the $Fe(OEP)(Py)_2ClO_4$ complex at low temperature, a number of features common to both electronic spectra are observed. Two bands occur between 500 and 560 nm, with no other distinct bands in the region from 560 to 700 nm. A slight absorption is recorded at about 700 nm in the case of the bispyridine porphyrin complex but not in the case of the cyanide hemoprotein.

Considering a protein such as aquo myoglobin (magnetic moment 5.73 at room temperature) and the $Fe(OEP)(3\text{-}ClPy)_2ClO_4$ and $Fe(OEP)(4\text{-}AcPy)_2ClO_4$ complexes at about $300^{\circ}K$, a number of features common to all three electronic spectra are found. Broad ill-defined bands are observed in the regions 500-550 nm and 600-650 nm, and Soret bands rather broader than those of the low-spin complexes are observed. Possibly the most illuminating comparison is between spectra where two spin-states co-exist, for example ferrihemoglobin hydroxide and $Fe(OEP)(3\text{-}ClPy)_2ClO_4$. On progressively lowering the temperature at which the spectra are obtained, a number of changes occur. The Soret band is found to increase in intensity and move to higher wavelength. The two bands occurring at 500-560 nm become more pronounced, and the broad ill-defined absorption at 600-650 less so.

Strekas and Spiro, in their resonance-Raman study of cytochrome c' from Rhodopseudomonas Palustris, suggested that the oxidised protein

exhibited anomalous spectra at lower pH characteristic of the intermediate spin state ($S = {}^{3}/_{2}$) species[23]. Visible absorption spectra of this cytochrome c' species at lower (ca. 7.0) pH were also investigated, and it is therefore possible to compare the spectrum of this species with the visible spectra produced in the case of the ferric octaethylporphin complexes under study in this case.

The visible spectrum of the cytochrome c' species at pH 7.0 contains absorbance bands at ca. 390 nm (Soret band), ca. 500 nm and 640 nm, with a shoulder at about 550 nm. This spectrum bears a superficial resemblance to the spectrum of the 3-chloropyridine derivative measured at 300°K, but does not show the same resemblance with the other visible spectra of the bis-pyridinato complexes.

As the spectra of spin equilibrium systems represent a superimposition of those absorption bands characteristic of each state and as most of these bands are broad, the result tends to be that these systems produce ill-defined spectra which are difficult to interpret. Whilst there is a similarity between the spectra of the 3-chloropyridine derivative and the Rps. palustris cytochrome c' species which could be suggestive of the influence of a quartet species, the favourable comparison of these ferric porphyrin spectra with those of, for example, ferrihemoglobin hydroxide, implies that similar electronic processes are present. The fact that the spectra of known high-spin ($S = {}^{5}/_{2}$) ferric hemeproteins are superficially similar to those of some of the porphyrin complexes studied is not conclusive proof that a doublet-sextet spin equilibrium is present. However, in view of the observation that many of the experimental visible spectra are close to the spectra of the ferrihemoglobin hydroxide system, it is suggested that a doublet-sextet spin equilibrium is present for many of the systems, although the possible influence of a quartet state cannot be entirely excluded from consideration.

iv) Mössbauer studies

It is of interest to compare the Mössbauer spectra of the ferric octaethylporphin complexes with those of hemeproteins, in order to observe whether any common features are present. In theory Mössbauer studies should be capable of distinguishing between different spin states of the Fe(III) ion. Typically, low spin ($S = {}^1/2$) ferric heme complexes exhibit Mössbauer spectra with quadrupole splittings in the range 1.9-2.3 mm/sec and an isomer shift of 0.4-0.5 mm/sec; high spin ($S = {}^5/2$) ferric heme complexes display small quadrupole splittings generally less than 1 mm/sec, with isomer shifts of 0.4-0.8 mm/sec.

The Mössbauer spectra of methemoglobin and cytochrome cc' exhibit quadrupole splittings (>2.0 mm/sec) in the oxidised state which are much wider than those observed for typical high-spin ferric compounds[58]. The higher energy quadrupole line (towards positive source velocity) in the methemoglobin spectrum broadens most rapidly as the temperature is lowered, while for cytochrome cc' the lower energy line broadens most rapidly. The Mössbauer spectra of chromatium cytochrome c_{552}, on the other hand, in the oxidised form show a wide (> 2.0 mm/sec) quadrupole splitting, small isomer shift and temperature dependent line broadening as seen with other low-spin Fe(III) heme proteins.

It would thus seem that there are a number of features common to the Mössbauer spectra of the ferric octaethylporphin complexes and the heme proteins mentioned above. Indeed it is clear that a wide quadrupole splitting is possible for both low spin and high spin complexes and the Mössbauer characteristics of these spin states may not be too different. It may then be the case that where there is a spin state equilibrium, only one set of Mössbauer lines is observed, due to superposition of the lines corresponding to each state with similar Mössbauer parameters. In this situation, the question of whether the correlation time for electronic relaxation between the spin states is more or less than the effective

quadrupole period will not materially affect the observed spectra.

It is of interest that methemoglobin hydroxide and cytochrome cc' have been considered as examples of heme proteins which exist in thermal mixtures of electronic spin states, since the magnitude of the quadrupole splitting is much more temperature dependent than is usual for pure high-spin ferric compounds. None of these display more than one pair of Mössbauer quadrupole lines over the temperature range 4 - 270°K.

The possible involvement of the intermediate ($S = {}^{3}/_{2}$) ferric state cannot be ruled out without a closer study of the data. Mössbauer parameters for several intermediate spin bis-(N,N-dialkyldithiocarbamato) iron(III) halides have been published[56,57]. The isomer shifts of these complexes are in the region 0.4-0.5 mm/sec and the quadrupole splittings in the region 2.6-2.9 mm/sec. These quadrupole splittings are larger than found for porphyrin complexes, but this is not altogether surprising as the electric field gradient for five coordinate complexes might be expected to be considerably greater than for the higher symmetry six-coordinate porphyrin complexes.

However, in view of the close similarity between the Mössbauer spectra of the ferric octaethylporphin complexes and those of both methemoglobin and c-type cytochromes that contain iron spin states of $S = {}^{1}/_{2}$, $S = {}^{5}/_{2}$ or a spin-state equilibrium between the two, it is considered that the spectra of the porphin complexes reflect a doublet-sextet spin state equilibrium.

4. Quantitative correlation between absorption spectra and magnetic moment data[17,46,47]

Assuming a thermal equilibrium between high-spin and low-spin states of the form

$$\underset{1-\alpha}{\text{high spin}} \overset{K}{\rightleftharpoons} \underset{\alpha}{\text{low spin}} \qquad (3.3)$$

then

$$K = \frac{\alpha}{1-\alpha} \qquad (3.4)$$

where α and $1-\alpha$ are relative fractions of the low-spin and high-spin forms present, and K is the equilibrium constant. Throughout the use of the term high-spin will be taken to refer to a spin-state of greater spin multiplicity than the doublet low-spin state, and as such therefore refers to either a quartet or a sextet spin-state.

At any particular temperature T, the observed mean magnetic moment for a complex is given by

$$\mu_{obs}^2 = \alpha\mu_L^2 + (1-\alpha)\mu_H^2 \qquad (3.5)$$

where μ_H and μ_L are the magnetic moments of the high-spin and low-spin forms respectively. The terms contain μ^2 since the additive magnetic property is the molar susceptibility, χ_m^p, which is related to μ by the expression $\mu = 25.25\left[\chi_m^p T\right]^{\frac{1}{2}}$.

At a given wavelength the mean extinction coefficient of a complex, ε, is also determined by the fraction α according to the relation

$$\varepsilon = \alpha\varepsilon_L + (1-\alpha)\varepsilon_H \qquad (3.6)$$

where ε_H and ε_L are the extinction coefficients of the high- and low-spin forms at this particular wavelength. Since μ and ε are known experimental quantities, and since reasonable values can be adopted for μ_H and μ_L, these equations can be used to evaluate ε_H and ε_L, and hence obtain the absorption spectra of the high- and low-spin components. In order to obtain the individual spectra of these forms, an independent determination of the fractions present at the two temperatures is required. At any two temperatures T_1 and T_2

$$\varepsilon_1 = \alpha_1\varepsilon_L + (1-\alpha_1)\varepsilon_H \qquad (3.7)$$

$$\varepsilon_2 = \alpha_2\varepsilon_L + (1-\alpha_2)\varepsilon_H \qquad (3.8)$$

leading to

$$\varepsilon_L = \frac{\varepsilon_2(1-\alpha_1) - (1-\alpha_2)\varepsilon_1}{\alpha_2 - \alpha_1} \qquad (3.9)$$

and

$$\varepsilon_H = \frac{\varepsilon_1\alpha_2 - \alpha_1\varepsilon_2}{\alpha_2 - \alpha_1} \qquad (3.10)$$

Now $$\alpha = \frac{\mu^2_{obs} - \mu^2_H}{\mu^2_L - \mu^2_H} \qquad (3.11)$$

Thus substituting (3.11) in (3.9) and (3.10) gives values of ε_L and ε_H at any particular wavelength, and by measuring the observed absorption at a number of wavelengths, the complete spectra of the high-spin and low-spin components can be obtained.

According to Boltzmann distribution the populations of the low-spin state and high-spin state are proportional to

$$W_L e^{-E_L/kT} \quad \text{and} \quad W_H e^{-E_H/kT}$$

where E_L and W_L are the energy and the effective statistical weight of the low-spin state, respectively, and E_H and W_H are the corresponding quantities of the high-spin state. Hence the relative concentration of the low-spin state is given by

$$\alpha = \frac{W_L e^{-E_L/RT}}{W_L e^{-E_L/RT} + W_H e^{-E_H/RT}} \qquad (3.12)$$

As far as W_L and W_H are concerned, only the ratio of W_H/W_L is of importance as regards subsequent calculation. Considering only the degree of freedom of spin, and assuming that for each high-spin and low-spin state only one spin multiplet may be considered, then

$$\frac{W_H}{W_L} = \frac{(2S+1)_H}{(2S+1)_L} \cdot \Upsilon = p \cdot \Upsilon \qquad (3.13)$$

where Υ represents the different effectiveness in the high-spin and low-

spin states of contributions from various degrees of freedom in the molecule other than that of spin. By use of $W_H/W_L = p\gamma$ and $\varepsilon = E_H - E_L$ (the energy difference between high-spin and low-spin states), α and K can be written as

$$\alpha = \frac{1}{1 + p\gamma e^{-\varepsilon/kT}} \qquad (3.14)$$

$$K = (p\gamma)^{-1} e^{-\varepsilon/kT} \qquad (3.15)$$

Thermodynamic quantities can be derived from the following equations

$$\Delta G^\circ = -RT \ln K = \Delta H^\circ - T\Delta S^\circ \qquad (3.16)$$

$$\therefore \ln K = -\frac{\Delta H^\circ}{RT} + \frac{\Delta S^\circ}{R} \qquad (3.17)$$

assuming that ΔH° is independent of temperature. Thus,

$$\Delta H^\circ = -N\varepsilon \qquad (3.18)$$

$$\Delta S^\circ = -Nk \ln p\gamma \qquad (3.19)$$

The temperature which gives $\Delta G^\circ = 0$ is given by the relation

$$\frac{\varepsilon}{kT_c} = \ln p\gamma \qquad (3.20)$$

From relation (3.17), a plot of lnK versus T^{-1} should be a straight line and from the gradient and intercept can be found values for ΔH° and ΔS° respectively, and hence values for ε, γ and T_c.

However, there are several reasons why calculations on this basis are only approximations. Although the sextet spin state can be assigned a magnetic moment of 5.92 B.M., the theoretical spin contribution of five unpaired electrons, the value for quartet and doublet states is open to argument as some contribution from orbital angular momentum may have to be taken into account. Secondly, the moment of the low-spin (doublet) form could differ appreciably from one complex to another, but, in the absence of independent evidence, the same value for μ_L will

be used throughout as 2.24 B.M.

Values for the various quantities above have been found for $Fe(OEP)(3\text{-}ClPy)_2ClO_4$, $Fe(OEP)(4\text{-}AcPy)_2ClO_4$ and $Fe(OEP)(Py)_2ClO_4$ using high-spin values of both $S = {}^3/_2$ and $S = {}^5/_2$, i.e. for Υ values of 2 and 3. For the quartet state, an upper value of μ_H of 4.3 was taken. The results are set out in full in Table 3.6.

Plots of lnK versus T^{-1} are reasonably linear for a sextet/doublet equilibrium but not so for a quartet/doublet equilibrium. Values of $\Delta H°$ and $\Delta S°$ have been ascertained for each complex assuming both a quartet/doublet and a sextet/doublet equilibrium. A large entropy change seems to cancel a large enthalpy change at the temperature T_c where $\Delta G° = \Delta H° - T\Delta S° = 0$, as both are negative in sign. Thus conversion from a high-spin to a low-spin form is favoured by the enthalpy change, but is appreciably hindered by the entropy change. In other words, with respect to their heats of formation the low-spin form is the more stable, whereas in terms of their entropies the high-spin form is the more stable. As the fraction of the low-spin form increases, $\Delta S°$ assumes more negative (unfavourable) values, while $\Delta H°$ assumes more negative (favourable) values. This trend in $\Delta S°$ could be associated with a greater structural rigidity in the vicinity of the iron atom of the low-spin form.

ε and Υ are physical parameters which characterise the tendency of thermal mixing between high-spin and low-spin states. Though values of ε, which represents the difference in energy of the low-spin and high-spin states, are fairly large compared with the thermal energy kT at room temperature (ca. 200 cm^{-1}), large values of Υ make the thermal mixing observable. All the values of ε are positive, indicating that the low-spin state is the ground state in all cases. The values of ε are to some extent a reflection of both the pK_a of the axial ligand and the proportion of low-spin form present at any given temperature for a particular complex. Thus, comparing the complexes with axial ligands

TABLE 3.6

Thermodynamic and physical parameters calculated for a high-spin⟶low-spin equilibrium in $X_2Fe(OEP)ClO_4$ complexes

A. Quartet/doublet equilibrium

X	T	$T^{-1} \times 10^3$	μ (B.M.)	α	1-α	K	lnK	ΔH° (joules)	ΔS° (joules deg^{-1})	$T_c/^\circ K$	ε/cm^{-1}	Υ
3-ClPy	323	3.10	4.19	0.07	0.93	0.08	-2.59	-19860	-80.5	247	1660	8.077×10^3
	300	3.33	4.04	0.16	0.84	0.19	-1.66					
	270	3.70	3.66	0.38	0.62	0.61	-0.49					
	246	4.07	3.32	0.55	0.45	1.22	0.20					
	217	4.63	2.88	0.76	0.24	3.17	1.15					
4-AcPy	321	3.12	3.93	0.23	0.77	0.30	-1.21	-11550	-43.3	267	966	91.6
	295	3.39	3.61	0.41	0.59	0.69	-0.36					
	270	3.70	3.32	0.55	0.45	1.22	0.20					
	236	4.24	3.05	0.68	0.32	2.13	0.75					
	218	4.59	2.96	0.72	0.28	2.57	0.94					
Py	319	3.13	3.12	0.65	0.35	1.86	0.62	-34080	-99.9	341	2850	8.3×10^4
	301	3.32	2.66	0.85	0.15	5.67	1.73					
	269	3.71	2.34	0.97	0.03	32.3	3.48					
	254	3.94	2.29	0.98	0.02	49.0	3.89					

(Cont.)

Table 3.6 (Cont.): B. Sextet/doublet equilibrium

X	T	$T^{-1} \times 10^3$	μ (B.M.)	α	1-α	K	lnK	ΔH^o (joules)	ΔS^o (joules deg^{-1})	$T_c/^oK$	ε/cm^{-1}	γ
3-ClPy	323	3.10	4.19	0.58	0.42	1.38	0.32	-9790	-28.2	347	818	9.9
	300	3.33	4.04	0.62	0.38	1.63	0.49					
	270	3.70	3.66	0.72	0.28	2.57	0.94					
	246	4.07	3.32	0.80	0.20	4.00	1.39					
	217	4.63	2.88	0.89	0.11	8.09	2.09					
4-AcPy	321	3.12	3.93	0.65	0.35	1.86	0.62	-7680	-18.0	427	642	2.9
	295	3.39	3.61	0.73	0.27	2.70	0.99					
	270	3.70	3.32	0.80	0.20	4.00	1.39					
	236	4.24	3.05	0.86	0.14	6.14	1.81					
	218	4.59	2.96	0.88	0.12	7.33	1.99					
Py	319	3.13	3.12	0.84	0.16	5.25	1.66	-29600	-78.0	380	2480	3.95×10^3
	301	3.32	2.66	0.93	0.07	13.3	2.59					
	269	3.71	2.34	0.98	0.02	49.0	3.89					
	254	3.94	2.29	0.99	0.01	99.0	4.60					

3-chloropyridine and pyridine, the former has a smaller values of ε, smaller pK_a and a greater proportion of the high-spin form as evidenced by its larger magnetic moment at any given temperature in comparison with the latter. However, some sort of conformational change will almost certainly occur with transitions between states of different spin, so that "higher states" are not necessarily purely electronic excited states corresponding to the same fixed values of ligand field parameters. In this sense the excitations may be vibrational.

The values of the various thermodynamic and physical parameters in Table 3.6 compare very favourably with those of various ferric proteins which have anomalous magnetic moments and absorption spectra and are thought to involve spin-state transitions. Values for myoglobin (Mb), hemoglobin (Hb) and cytochrome c peroxidase (CCP) complexes are given below.

TABLE 3.7

Various parameters of the spin-state transition for ferrimyoglobin, ferrihemoglobin and ferriperoxidase complexes[62-64]

Complex	$\Delta H°$ (joules)	$\Delta S°$ (joules deg^{-1})	T_c (°K)	ε (cm^{-1})	γ
$Mb(Fe^{3+}).N_3^-$	-15660	-40.0	391	1310	40.1
$Hb(Fe^{3+}).OH^-$	-7880	-21.2	372	655	4.20
$Hb(Fe^{3+}).N_3^-$	-21290	-56.9	374	1770	3.02×10^2
$CCP(Fe^{3+}).OH^-$	-21820	-94.1	232	1830	2.58×10^4

Thus the data for $Fe(OEP)(3\text{-}ClPy)_2ClO_4$ ($^1/2 \rightarrow {}^3/2$ equilibrium) and $CCP(Fe^{3+}).OH^-$, $Fe(OEP)(4\text{-}AcPy)_2ClO_4$ ($^1/2 \rightarrow {}^5/2$ equilibrium) and $Hb(Fe^{3+}).OH^-$, and $Fe(OEP)(Py)_2ClO_4$ and $Hb(Fe^{3+}).N_3^-$ are comparable,

giving rise to the possibility that similar systems and transitions are present. Two explanations have been put forward[62], to take account of the large deviations of Υ from unity, involving different degrees of freedom of the molecule in proteins. Firstly, electronic energies may be temperature dependent due to the effects of anharmonicity of vibrational modes. It is then probable that high-spin and low-spin states correspond to more or less different conformations, so that the temperature dependence of electronic energies for these two states may be different, and the energy difference, ε , may be temperature dependent. Secondly, there is the possibility based on the idea that spin change is coupled with some other low-frequency degrees of freedom, probably those of internal rotations, in the protein molecule. When the spin of a hemoprotein molecule changes, the accompanying conformational change may give rise to quasi-rotational motion of a few parts of the molecule, for instance by utilising the energy for breaking hydrogen bonds.

Returning to the ferric porphyrin complexes, it is possible, in an analogous manner to the second explanation above, that spin change is accompanied by, for instance, rotation of one or both of the axial ligands, so that the planes of the two axial ligands are re-oriented with respect to one another. It would seem that the experimental magnetic susceptibility and absorption spectra data are better represented in terms of a doublet-sextet spin equilibrium, since the plots of $\ln K$ versus T^{-1} are linear whereas in the doublet-quartet case deviations from linear behaviour are quite apparent. It may be that ΔH° cannot be regarded as being independent of temperature, which is another manifestation of a change of conformation between the two spin states. It is also possible that a complex spin equilibrium involving a system such as $(S = {}^{1}/_{2}) \rightleftharpoons (S = {}^{3}/_{2}) \rightleftharpoons (S = {}^{5}/_{2})$ is present, which is feasible but not capable of treatment in terms of the simple theory

employed here. The only other explanation for deviations from linear behaviour would be that the measurements taken did not refer to equilibrium conditions, but reflected the rate of approach to equilibrium. The significance of T_c is that this is the temperature where α is equal to 0.5. Hence, the higher the value of T_c, the more the equilibrium tends to favour the low-spin form.

As discussed earlier, the complete spectra of high-spin and low-spin components of a thermal equilibrium of spin-states can be simulated by evaluating equations (3.9), (3.10) and (3.11). Taking the idea of a doublet-sextet spin-state equilibrium as providing the more apposite representation of the absorption spectra effects, and combining data from these spectra with magnetic susceptibility data, absorption spectra representing the contributions of the doublet and sextet states can be separated from the superimposed spectrum of the equilibrium distribution. This operation has been performed in the cases of the $Fe(OEP)(3\text{-}ClPy)_2ClO_4$, $Fe(OEP)(4\text{-}AcPy)_2ClO_4$ and $Fe(OEP)(Py)_2ClO_4$ complexes, and the results are shown in Figures 3.17 to 3.19. The high-spin ($S = {}^5/_2$) component spectra follow very closely the spectrum of aquoferrimyoglobin[24], which has a magnetic moment of 5.73 B.M. and can thus be regarded to all intents and purposes as solely comprising a sextet spin state ferric ion. Broad bands in the 450-500 nm and 600 nm ranges are common to all, and the Soret band has an extinction coefficient of less than 10^5. The low-spin ($S = {}^1/_2$) component spectra follow fairly closely the spectrum of cyanoferrimyoglobin[24], which has a magnetic moment of 1.96 B.M. and can thus be regarded as being entirely low-spin. A pair of well-defined bands occur in the region 500-550 nm for all, and the Soret band is more intense and at a slightly higher wavelength than for the high-spin component.

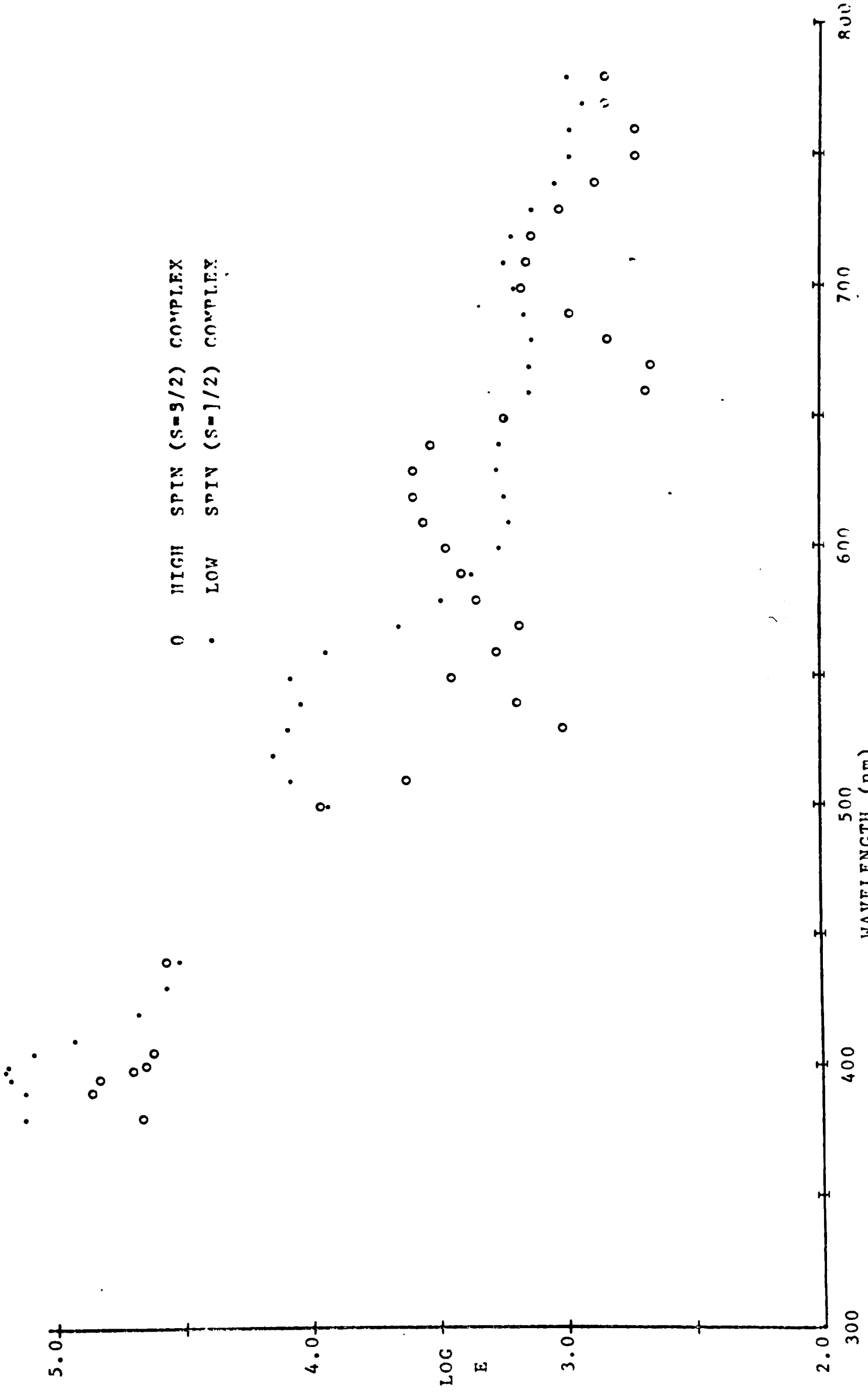


FIG. 3.17 Simulated high spin and low spin absorption spectrum of $Fe(OEP)(3\text{-}ClPy)_2ClO_4$

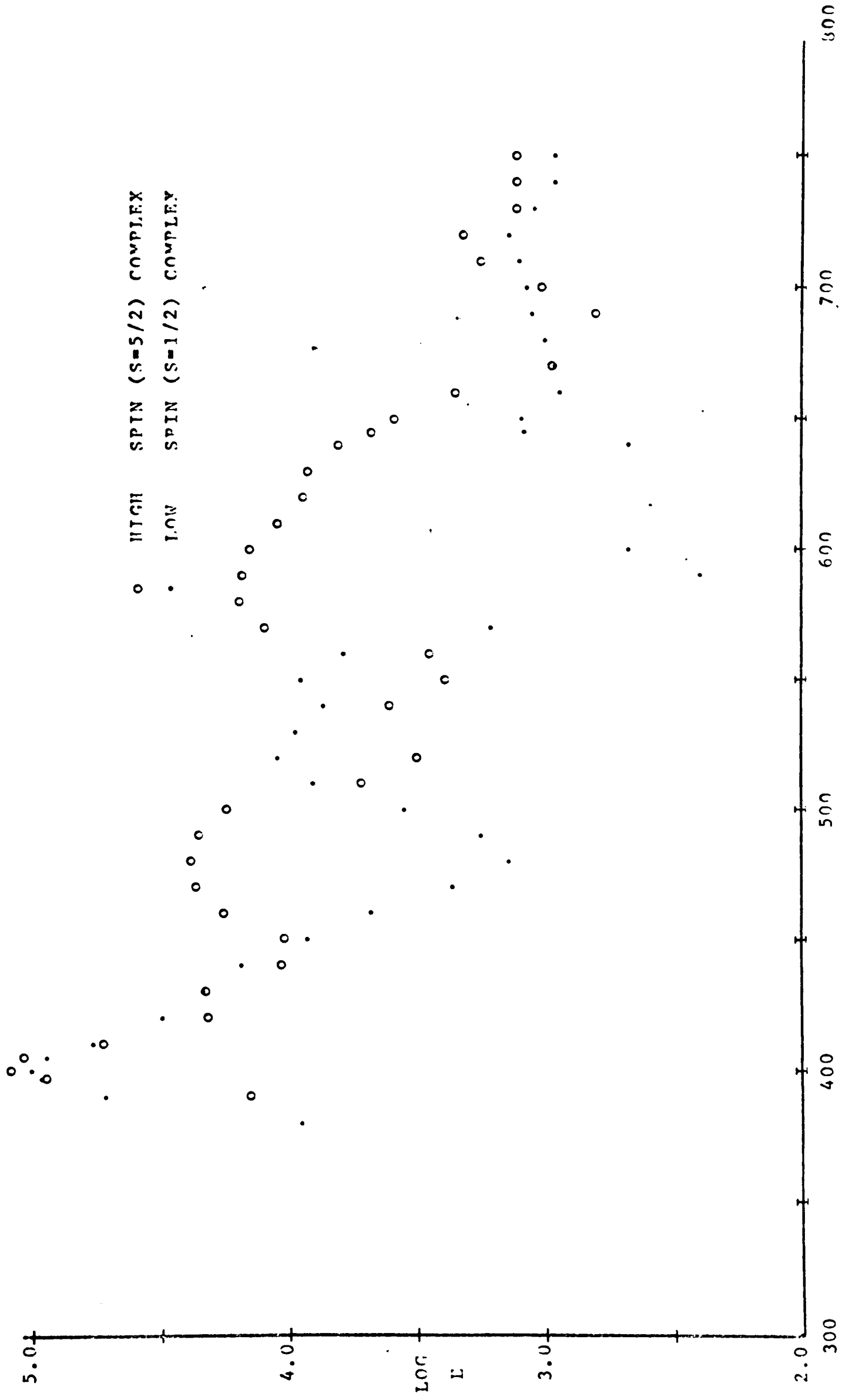
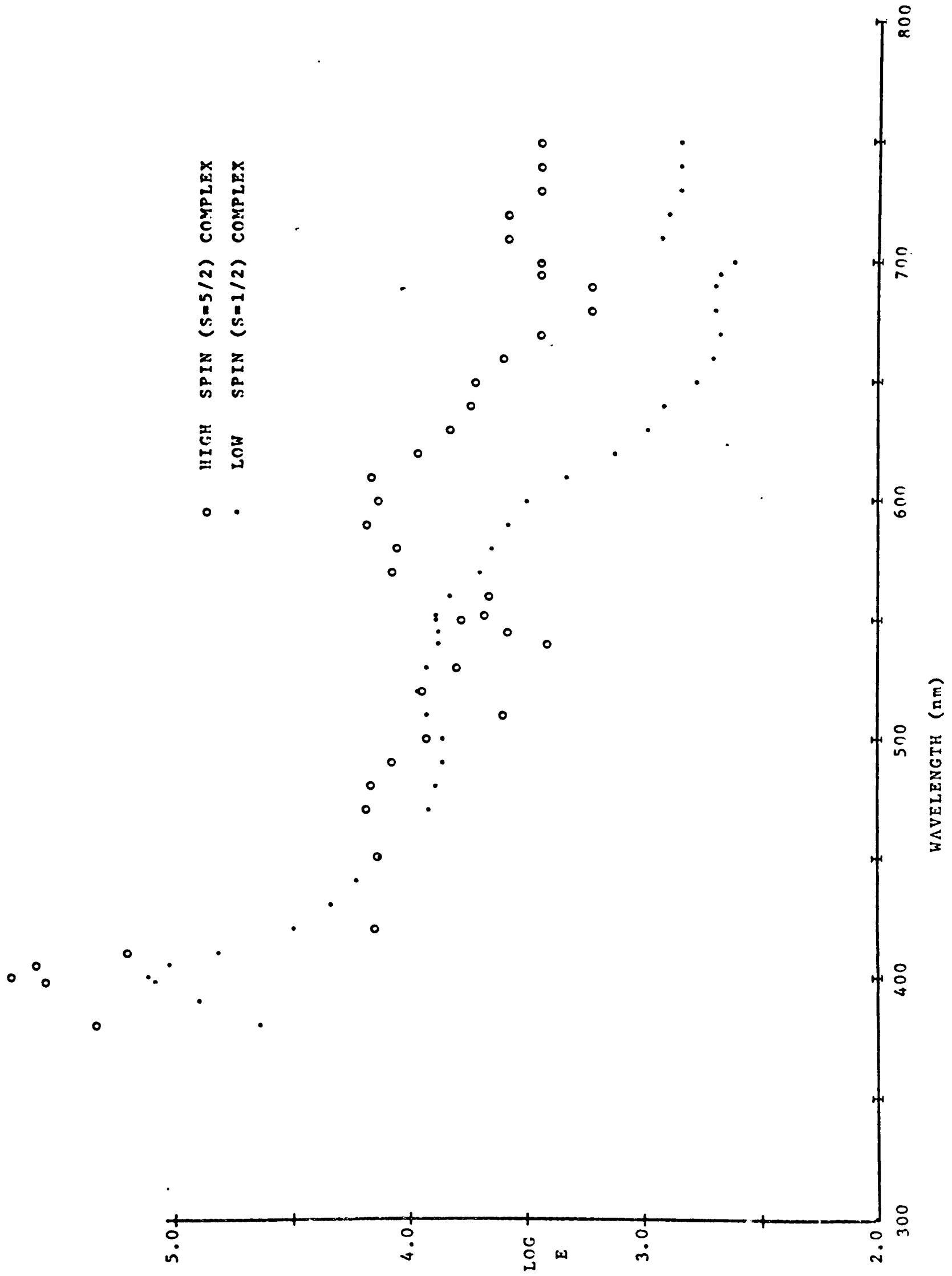


FIG. 3.18 Simulated high spin and low spin absorption spectrum of $Fe(OEP)(4\text{-}AcPy)_2ClO_4$

FIG. 3.19 Simulated high spin and low spin absorption spectrum of $Fe(OEP)(Py)_2ClO_4$



The overall conclusion of this simple theoretical approach is that proceeding on the assumption of an equilibrium between two spin-states of different spin multiplicities, the experimental results are in the main better represented in terms of a doublet-sextet equilibrium than a doublet-quartet equilibrium. The electronic spectra and Mössbauer results are better interpreted in light of the former representation. The magnetic susceptibility/magnetic moment data are inconclusive and are capable of being interpreted in terms of either system. The NMR spectra do not provide any information which can be interpreted in terms of either system.

Neither system provides a fully satisfactory interpretation of the experimental results, and indeed it would be surprising if such a model as described in the whole of this section were to represent fully the electronic effects and processes giving rise to the unusual and anomalous results observed. A model assuming that the states involved are "pure" states and capable of being symbolised as taking part in a simple equilibrium process is over-simplistic and naive, albeit the experimental results can be described adequately in these terms. A more complete model would take account of the factors and concepts embodied in Section 3.4.2, especially as the tetragonal field around the ferric ion might be expected to lead to "spin-mixed" as opposed to "pure" electronic wavefunctions and states. The simple model invoked throughout Section 3.4.3 will now be replaced by a more sophisticated and thorough approach, which it is hoped will be able to cater for all the physical electronic effects observed.

5. Definitive treatment of the ferric porphin spin-equilibrium

A more complete and sounder theoretical treatment of the experimental data will here be attempted. Although this is not always necessarily true, in general the soundness of a theoretical approach to empirical observation is dependent upon the ability to reproduce the experimental data in terms of the theory over a wide range of circumstances. As stated above, the rather naive model presented ignores certain salient features of the ferric system existing under tetragonal ligand fields.

i) The magnetic model

In cubic symmetry there are two possible ground states for the iron (III) ion, namely the high spin $^6A_1$ state or the low spin $^2T_{2g}$ state. In strongly tetragonal symmetry there are two possible low spin ground states arising from the splitting of the $^2T_{2g}$ state into ^2E and $^2B_{2g}$. An intermediate S = $^3/2$ state ($^4A_{2g}$) can also, in certain circumstances, become the ground state. This was detailed fully in Section 1.3.

Recently the magnetic properties of the d^5 configuration have been considered[65,66] taking account of the $^6A_{1g}$, $^4T_{1g}$ and $^2T_{2g}$ cubic field states which, in a strong tetragonal field, give rise to all the possible ground states. This work followed on from that of Harris[20,21] and included spin-orbit coupling between all states and full parameterisation of the ligand field in terms of the Racah parameters B and C and also the three parameters ΔO_h, C' and f. In all the calculations the free ion values for spin orbit coupling constant (420 cm^{-1}), B (1100 cm^{-1}) and C (3750 cm^{-1}) are used and f is normally given the value 1.0. This reduces the number of varying parameters that need to be used and as the parameters are interdependent, the effects of varying B, C, f etc. are incorporated in the other variable parameters.

The magnetic moments were calculated by Dr. A.K. Gregson using a generalised computer programme VVLECH based on the Van Vleck equation. One modification has been made for the present work. As the parameters of interest in the PMR shift question are also required, the conventional Van Vleck equation is set aside in favour of calculation of dE/dH directly, since the magnetic field of the NMR instrument is involved.

The regions of parameter space giving rise to the various possible ground states in the d^5 electronic configuration are illustrated in Figure 3.20. The states shown are the only ones which can have a significant effect on the ground state magnetic properties of an ion in this particular electronic state. There is only one possible situation where this is not strictly true and this occurs when the quartet spin state ($^4A_{2g}$) is lowest in energy. An excited ^4E state from a higher lying $^4T_1$ level can play a major role in determining the zero-field splitting properties of the $^4A_{2g}$ state but in the present situation with the dominating $^6A_{1g}$ state so near this feature of the d^5 electronic configuration will not be of concern.

ii) Magnetic data

The method of comparison of theory and experiment consists firstly of taking over from where the quantitative treatment in Section 3.4.4 above finishes and then introducing additional refinements to the theory which can be included in the computations. With magnetic moments ranging from 2.2 B.M. to ~ 4.2 B.M. the simplest treatment would be consideration of a non-interacting doublet-quartet equilibrium involving the $^2T_{2g}$ and $^4A_2$ states. This is easily achieved on the Harris model by removing all the spin-orbit coupling matrix elements connecting the doublet and quartet states and placing the $^6A_{1g}$ state at a very high energy such that it makes no contribution to the magnetic state of the

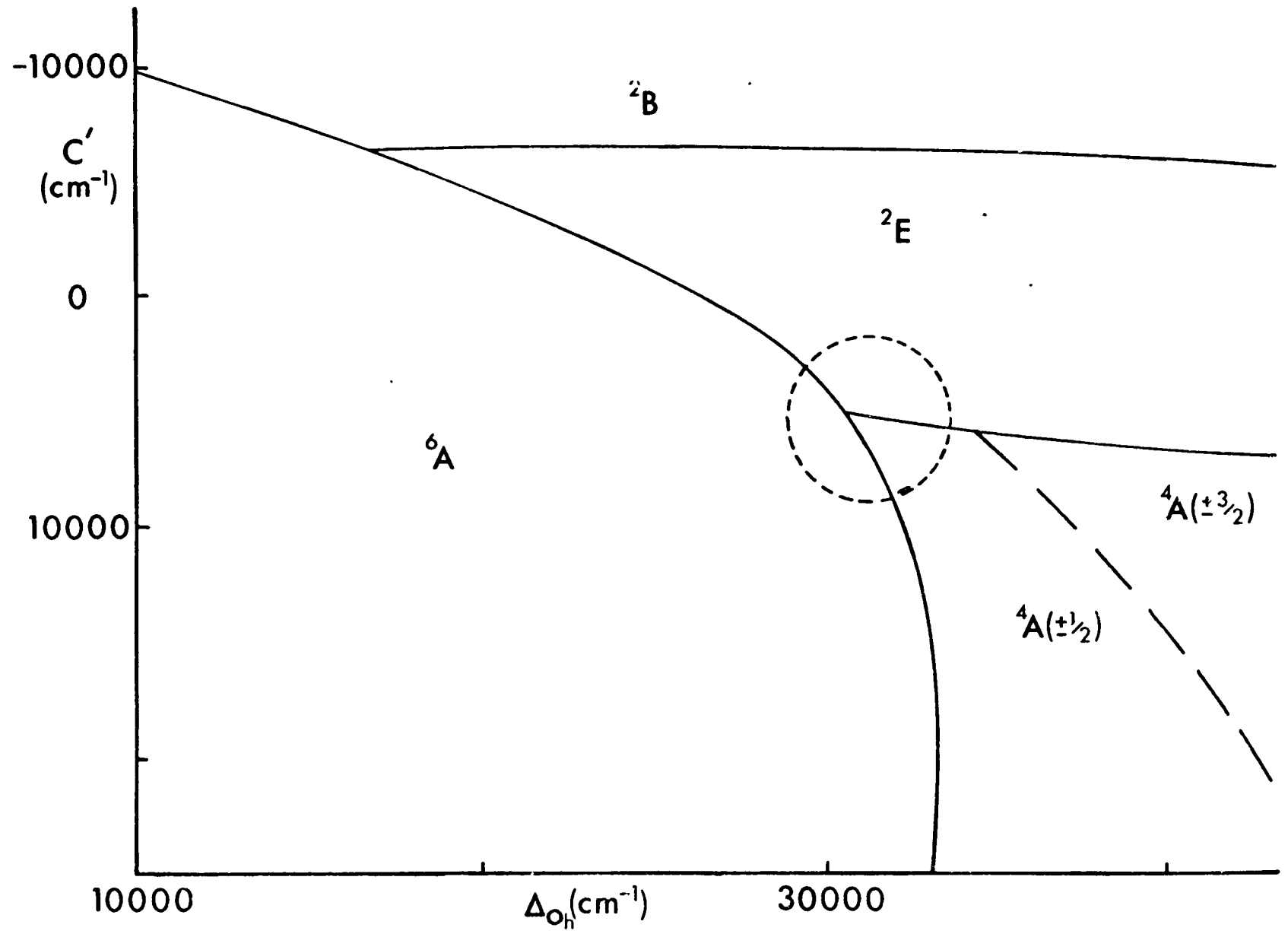


FIG. 3.20 Regions of parameter space defining different ground states for d^5 ferric ion.

ion. The parameters describing the $^2T_{2g}$ ground state can be deduced from a knowledge of the limiting magnetic moment of 2.2 B.M. for the N-methylimidazole and pyridine complexes. This value of μ_{eff} is compatible with an axial-field splitting of about 2000 cm^{-1}, the corresponding calculated g values being $g_{\parallel} = 3.9$ and $g_{\perp} = 0.3$ which are not far removed from those estimated from the EPR work on the bis-pyridine complex. Using a pure $^4A_2$ state as the excited state spin species, an upper limit of 4.0 B.M. is obtained for the average magnetic moment, even considering the splitting of the parental $^4T_1$ ground state to be small or zero. In order to account for the experimentally determined upper limit of 4.2 B.M. for the average magnetic moment, it is necessary to reckon for some influence of the $^6A_1$ state. Placing this sextet state approximately 800 cm^{-1} above the formal $^4T_1$ state reproduces the correct upper limit of μ_{eff}, that is the value of 4.2 B.M. obtained for the 3-chloropyridine complex.

The model is in need of refinement since the experimental observations can only be consistent with a set of ligand field parameters proximate to the region of Figure 3.20 where $^6A_{1g}$, $^4A_{1g}$ and ^2E_g are all close to being the ground state. This is further borne out by the fact that although the extrema in magnetic moments of 2.2 and 4.2 B.M. can be reproduced, the large magnetic moment change over the temperature range studied can not. The quantum mechanical spin-mixed model would seem more appropriate because if the three states in question are so close to each other in energy, the neglect of spin-orbit mixing between them is simply not realistic. Accordingly, it is necessary to examine the complete Harris model taking account of spin-orbit coupling and all the relevant ligand-field perturbations.

The 3-chloropyridine derivative is chosen first because it has the highest magnetic moment at 320°K (~ 4.22 B.M.) and also the largest

temperature variation, the moment decreasing to 2.7 B.M. by 205°K. Choosing the free-ion values for the spin orbit coupling constant and the parameters B and C given above and the values 31950 cm^{-1} and 4450 cm^{-1} for Δ_{O_h} and C' respectively predicts the correct value of ca. 4.22 B.M. at 320°K. The latter two values were arrived at by plotting the change in magnetic moment as a function of Δ_{O_h} and C' at 320°K and selecting the appropriate combination - an arbitrary but acceptable procedure. As with the non-interacting doublet-quartet equilibrium, the large drop in magnetic moment (~ 1.5 B.M.) over the temperature range 320-200°K cannot be reproduced theoretically. This problem applies in varying degrees to all the compounds whose magnetic moments were measured, as well as several of the temperature dependent isotropic PMR shifts.

There must be some factor lacking in the theoretical approach, since both the thermal and quantum mechanical mixing models are unable to account for the total magnetic moment variation with temperature, even qualitatively and attempting large scale variation of all possible parameters. A possibility could be the effect of a substantial zero-field splitting in the quartet and sextet states, since in related compounds such as manganese (II) phthalocyanine[66] and some hemoglobin derivatives[67,68] zero-field splittings of 40 cm^{-1} and 60 cm^{-1} respectively are found. Splittings of more than 100 cm^{-1} were tried and although this made a small difference in the correct direction, there was still a considerable disparity with the experimental data.

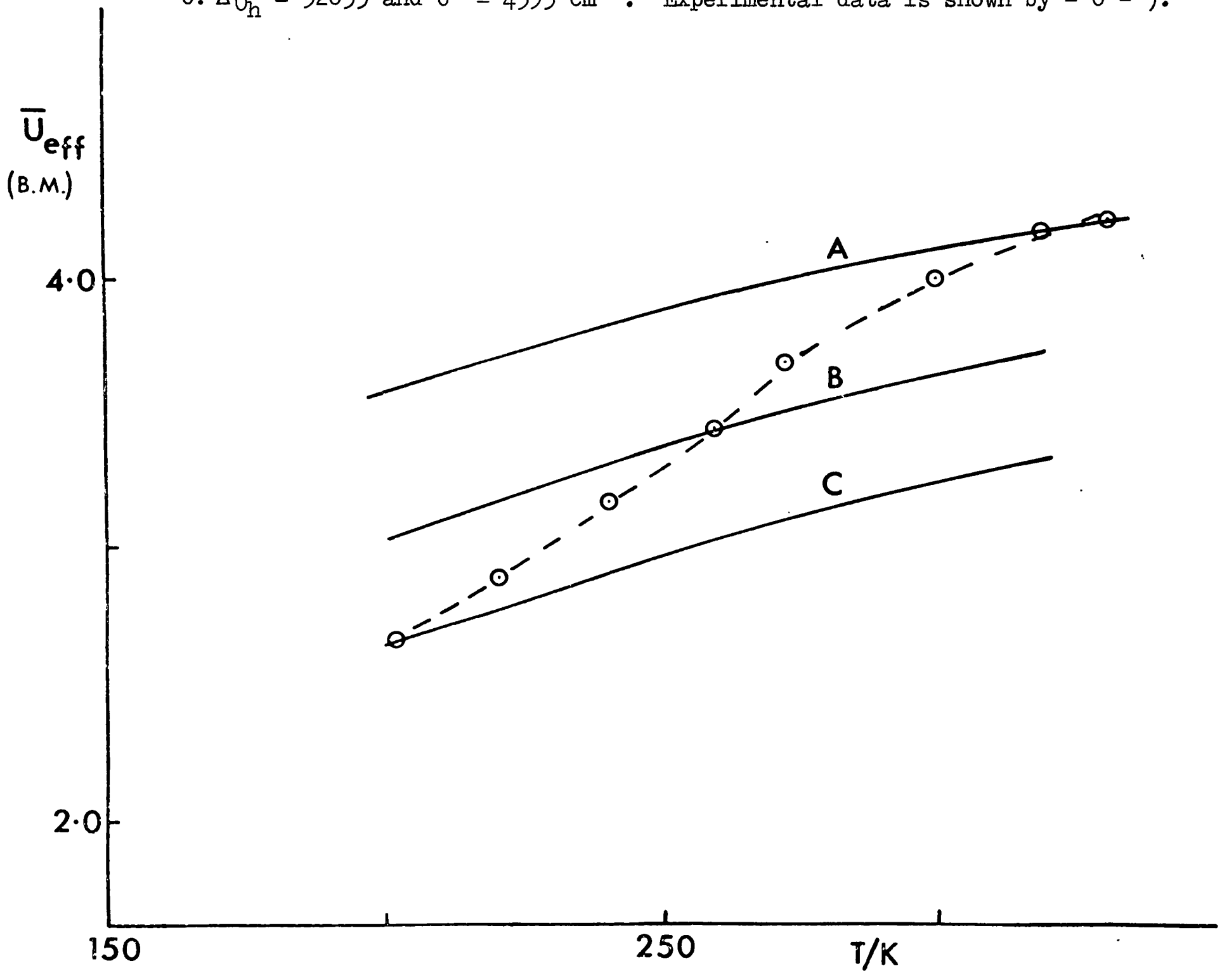
One assumption that has been made throughout is that the ligand field parameters are temperature independent. On further examination this appears to be a naive presumption. It would be unlikely for the molecular dimensions of a complex to remain constant over a temperature range of 130°K. Furthermore in this situation where the $^6A_{1g}$, $^4A_{1g}$ and ^2E_g states are all close together in energy, the change in population

with temperature would be expected to significantly affect the molecular dimensions given as a weighted average of the populated states. In view of the fact that the ligand-field parameters Δ_{O_h}, C' and f relate to the effect of the bound ligands, it would be surprising if these were not dependent on the absolute and relative molecular dimensions, and hence on temperature. Accordingly temperature dependent ligand field parameters were investigated.

Taking the highest magnetic moment of the 3-chloropyridine complex and using Δ_{O_h} = 31950 and C' = 4425 cm^{-1}, the measured value of μ_{eff} at 330°K can be reproduced. At 260°K the two varying parameters are 32000 and 4405 cm^{-1} respectively and at 200°K they are 32055 and 4395 cm^{-1} respectively. This is plotted in Figure 3.21 to clarify the magnetic moment variation with temperature for the three sets of parameters. If it is then assumed that Δ_{O_h} varies smoothly with temperature from 31950 to 32055 cm^{-1} and C' varies from 4425 to 4395 cm^{-1} the magnetic properties of the 3-chloropyridine derivative can be satisfactorily accounted for. The qualitative ordering of the various electronic states at 200 and 300°K is shown in Figure 3.22 for the 3-chloropyridine complex. Similar variations in the ligand field parameters can reproduce all the measured magnetic moments, the values appearing in Table 3.8.

In essence these findings mean that in lowering the temperature from 330 to 200°K the ligand field around the metal ion is becoming more cubic in the sense that the difference between in-plane and axial field strengths is slightly smaller because Δ_{O_h} is increasing and the tetragonality parameter is becoming smaller. This could quite possibly correspond to the iron atom moving closer towards the plane of the porphyrin ring as it is now recognised that conformational changes involving the position of the iron atom along the axis perpendicular to the heme plane are probably crucial in determining the properties of the high, low and intermediate spin iron proteins.

FIG. 3.21 Temperature variation of theoretical and experimental magnetic moments of $Fe(OEP)(3\text{-}ClPy)_2ClO_4$. (Solid lines calculated with A: ΔO_h = 31950 and C' = 4425 cm^{-1}; B: ΔO_h = 32000 and C' = 4405 cm^{-1}; C: ΔO_h = 32055 and C' = 4395 cm^{-1}. Experimental data is shown by - ⊙ -).



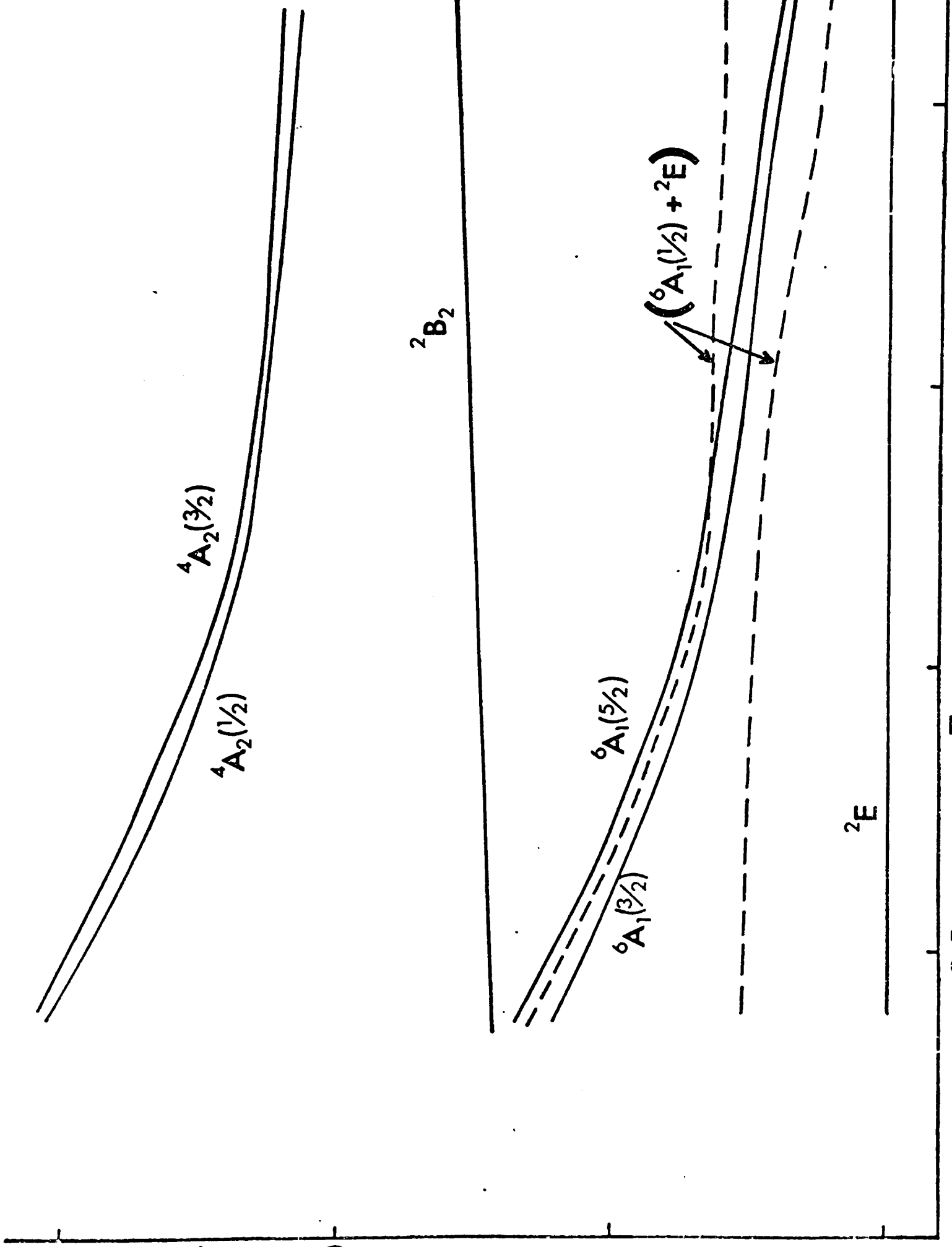


FIG. 3.22 Ordering of the energy levels in Fe(OEP)(3-ClPy)$_2$ClO$_4$ against their magnetic moments at 320°K.

TABLE 3.8

Magnetic parameters for several ferric octaethylporphin derivatives

Complex	T/K	$\mu_{\parallel}$/B.M.	$\mu_{\perp}$/B.M.	$\bar{\mu}$/B.M.	$\bar{\mu}_{exp}$/B.M.	$\Delta O_h/cm^{-1}$	C'/cm^{-1}
Fe(OEP)(3-chloropyridine)$_2$ClO$_4$	320	4.36	4.14	4.22	4.20	31950	4425
	260	3.90	3.18	3.44	3.50	32000	4405
	200	3.57	2.09	2.68	2.65	32055	4395
Fe(OEP)4-acetylpyridine)$_2$ClO$_4$	320	4.16	3.76	3.89	3.89	31970	4400
	260	3.79	2.94	3.25	3.23	32000	4380
	200	3.65	2.37	2.86	2.86	32000	4380
Fe(OEP)(3-acetylpyridine)$_2$ClO$_4$	320	4.04	3.53	3.70	3.70	32000	4400
	260	3.69	2.67	3.05	2.95	32000	4350
	200	3.57	2.13	2.69	2.60	32000	4350
Fe(OEP)(pyridine)$_2$ClO$_4$	320	3.66	2.76	3.09	3.10	32000	4300
	260	3.40	1.93	2.52	2.40	32050	4250
	200	3.39	1.61	2.35	2.30	32050	4250
Fe(OEP)(N-methylimidazole)$_2$ClO$_4$	320	3.24	1.91	2.43	2.43	32000	4000
	260	3.27	1.74	2.36	2.30	32000	4000
	200	3.29	1.57	2.29	2.25	32000	4000

It has also been suggested that in the ferricytochromes c' the several different intermediate values of magnetic moment arise from different spin state admixtures which in turn depend on the different distances the iron atom may be placed from the heme plane, and indeed the sense and direction of the resulting orbital energies obtained by Maltempo are very similar to those obtained in this work. If the magnetic properties are then dependent on such sensitive factors the fact that the position of the iron atom relative to the heme plane is only slightly temperature dependent appears not unreasonable. The magnitude of the parameter changes over the temperature range studied is also quite small, the maximum being only about 0.3% for ΔO_h and about 1% for C'. However even these quite small changes produce significant changes in the magnetic state of the iron atom because the spin mixed region ($^6A_{1g}$, $^4A_{2g}$ and ^2E_g in D_4 symmetry) appears to control the overall properties of the metal ion in question.

At this stage an examination in detail of the actual composition of the ground and excited states of the iron atom in these octaethylporphin complexes is considered useful. There are two distinctly different types of state (classified in the D_4 double group) for the d^5 ion in this environment, namely E' and E". In all cases the ^4E state always occurs at relatively high energies ($>10{,}000$ cm^{-1} above the ground state) so it will be neglected in the following discussicn. The E" state then contains the following components: $^6A_1$ ($\pm\,5/2$), $^6A_1$ ($\pm\,3/2$), $^4A_2$ ($\pm\,3/2$), ^2E ($\pm\,1/2$, $\mp\,1$) and $^2B_2$ ($\pm\,1/2$) while E' states are composed of $^6A_1$ ($\pm\,1/2$), $^4A_2$ ($\pm\,1/2$) and ^2E ($\pm\,1/2$, $\pm\,1$) components. The ground state is always E" and dominated by ^2E character. Not surprisingly, this increases from 77% (the $^6A_1$ ($^3/2$), $^4A_2$ ($^3/2$), $^2B_2$ ($^1/2$) and $^6A_1$ ($^5/2$) components contribute approximately 10, 8, 3 and 1 percent respectively) for the 3-chloropyridine derivative (μ_{eff} 4.22 B.M. at 320°K)

to 86% for the N-methylimidazole derivative (μ_{eff} 2.4 B.M. at 320°K). In addition, the change of ligand field parameters with variation in temperature leads to increased ^2E character in the ground state, mainly at the expense of the $^6A_1$ ($^3/2$) component.

The excited states are shown in Figure 3.22, and apart from the two that are mainly comprised of $^6A_1$ ($^1/2$) and ^2E ($\pm\ ^1/2, \pm 1$) they are all predominantly single component levels and are so labelled in Figure 3.22. The two E' states composed mainly of $^6A_1$ ($^1/2$) and ^2E ($\pm\ ^1/2, \pm 1$) have varying composition. For example the lower one (first excited state) comprises 85% $^6A_1$ and 6% ^2E for a magnetic moment of 4.2 B.M., whereas 96% ^2E character is predicted for a magnetic moment of 2.4 B.M., the amount of ^4A ($^1/2$) remaining approximately constant. The reverse occurs for the second E' state while the third E' state always remains predominantly $^4A_2$ ($^1/2$).

It is notable that the very different magnetic properties of the iron octaethylporphin derivatives can arise from an energy level diagram which is, qualitatively, remarkably similar for all the derivatives. The key would seem to lie in the composition of the first excited state and probably to a lesser degree its energy relative to the ground state. This is only possible in the complicated spin-mixed region. Although the first excited state is largely $^6A_1$ ($^1/2$) the calculated limiting magnetic moment for the 3-chloropyridine derivative at say 400°K is 4.4 B.M. and at 500°K it is still only 4.5 B.M. A roughly constant magnetic moment of between 4.0 and 4.5 B.M. is then not necessarily indicative of a spin quartet first excited state.

With this treatment of the unusual features of the magnetic properties of the present materials several points have to be emphasised. Firstly, it is fairly clear that the iron atom is in a spin equilibrium region where the $^6A_{1g}$, $^4A_{2g}$ and ^2E_g ground states are all close to each

other and all have some influence on the resultant ground state properties. If this is the case then spin-orbit coupling between all three must be included for a realistic description of the ground and excited state properties of the metal ion. It appears that many of the heme protein materials probably have the three different spin states close in energy, judging by the wide range of magnetic behaviour observed in these systems, i.e. high spin, low spin and all the intermediate variations, spin $^{5}/_{2}$ - spin $^{3}/_{2}$ equilibria and here a proposed spin $^{3}/_{2}$ - spin $^{1}/_{2}$ equilibrium with a little sextet character included, all depending on the nature of the axial ligands.

Secondly, the actual values of the quoted ligand field parameters are not unique and probably other combinations could reproduce the experimental data just as well. However, the important point is that temperature dependent parameters appear to be necessary and that this is probably quite reasonable given that the iron atom may not be firmly fixed in its coordination site but probably takes up a position of least resistance dependent on many small and subtle influences, including temperature. This factor may correspond to the entatic state of Vallee and Williams[69], which has been claimed to be responsible for a highly significant part of enzyme activity.

iii) The isotropic PMR shifts

Assuming that the systems under study possess axial symmetry, then the pseudocontact shift is given by equation 2.24. As stated in Chapter 2, this equation invokes a number of assumptions, the validity of which may or may not be reasonable depending on the particular situation. Although the complex may have a geometric four-fold axis, the ligand field and hence the susceptibility tensor is quite likely to be of lower symmetry and so the assumption breaks down. Low spin d^{5} systems are notoriously

low in symmetry, e.g. g_x, g_y and g_z in several porphyrin and hemin systems[70] and the orbitally non degenerate ^4A ground states of the $Fe(dtc)_2X$ system (where X = Cl, Br or I) show quite marked rhombic character[71]. However in the absence of any single crystal susceptibility data for the present series of compounds and also to reduce the already large uncertainty and ambiguity in describing the model, the assumption is made in everything which follows that axial symmetry exists. Again, the ligand contribution to the pseudocontact shift has been ignored. For low spin iron compounds this could be a serious omission but in the absence of more detailed data, the extra effort involved is not warranted at this stage.

To proceed from equation 2.24 it is common practice to represent the principal susceptibilities in terms of the principal g-values. Whilst this may be adequate for an orbitally non-degenerate ground state it is certainly not valid for orbitally degenerate ground states where there is a thermal population of several levels. The susceptibilities in this latter case are then a complicated function of all the ligand field parameters and temperature as described by the Van Vleck equation. This will apply particularly to the present situation where there are very many levels of different spin multiplicities all contributing in different ways to the susceptibility tensor.

Furthermore, the concept of the first and second order Zeeman effects also loses meaning when the magnitude of the "applied" magnetic field (of the NMR spectrometer) is considered. Again with many levels close together and including zero-field splitting the large magnetic field introduces differences between the results of the conventional Van Vleck equation based on perturbation theory and that involving $\delta E/\delta H$ directly. In the spin mixed region the magnitude of the magnetic field affects both the calculation of susceptibility and the contact

shifts given by equation (2.15) and Gregson is currently studying contact shifts as a function of resonance frequency[72].

The technique in the present series of iron (III) (OEP) complexes utilised by Gregson is to use the principal susceptibilities which give rise to the average magnetic moments described in the previous section together with the known geometric factors to calculate the pseudocontact shifts. With the differing amounts of high, low and intermediate spin contributions in the spin mixed region the anisotropy in susceptibility as a function of temperature can vary greatly and is often crucial in accounting quantitatively for the overall shifts.

In the calculation of the contact shift, the coupling constant associated with each state is allowed to differ because the different states arise from different orbital configurations. In practice, the calculation of $\sum_i A_i \langle S_{iz} \rangle$ is performed by an extra computer subroutine as part of the general susceptibility calculation of the programme VVLECH[72].

Using temperature independent ligand field parameters several of the unusual experimental isotropic proton shifts could not be reproduced by way of the above procedure and a qualitative examination indicated that this problem nearly exactly parallelled the difficulties encountered with the magnetic moments. Introducing the temperature dependent ligand field parameter values makes a significant difference to the values of the shifts calculated and allows a ready explanation of the experimental PMR shift data in certain instances.

The fact that this applies to particular resonances (e.g. the β-py_4 shifts of $Fe(III)(OEP)(4\text{-}AcPy)_2ClO_4$) probably illustrates the large degree of uncertainty in the actual coupling constants chosen to describe the contact part of the total shift. This is not unreasonable given the large flexibility which exists when three different coupling constants

(^6A; ^4A and ^4E; ^2E and ^2B) are used and which in many circumstances can probably absorb the temperature varying ligand field. In principle separate coupling constants could be assigned to each of the spin quartet and doublet states but to retain some semblance of control over the number of parameters this was not done.

The results of some representative resonances are given in Table 3.9. The experimental and theoretical isotropic PMR shifts for the β-py_4 resonances of $Fe(III)(OEP)(4\text{-}AcPy)_2ClO_4$ are illustrated in Figure 3.23, two sets of coupling constants being applied at each of the two temperatures chosen. It can readily be seen that the coupling constants chosen have a marked effect on the value of the isotropic shift calculated. The figure also dramatically demonstrates the need for a temperature dependent description of the environment in which the central iron atom is situated.

The calculated shifts of the α-pyridine protons in Table 3.9 are of particular interest. Although the observed isotropic shift is rather small the geometrical factor coupled with the large calculated anisotropy in susceptibility makes the pseudocontact contribution quite large and opposite in sign to the isotropic shift. As a consequence the contact part of the shift has to be large and of opposite sign and so the experimental shift and its temperature variation is a delicate balance between two large calculated values. This circumstance applies in fact to many of the resonances which were observed and fitted to the above model.

Ideally it would be of merit to compare the various coupling constants (i) between the different positions within each complex,

(ii) between corresponding positions in different complexes.

FIG. 3.23 Temperature dependent isotropic shifts of the β-pyridine proton resonances in $Fe(OEP)(4\text{-}AcPy)_2ClO_4$. (Two representative descriptions with A: Δ_{O_h} = 31970 and C' = 4400 cm^{-1}; B: Δ_{O_h} = 32000 and C' = 4380 cm^{-1}.)

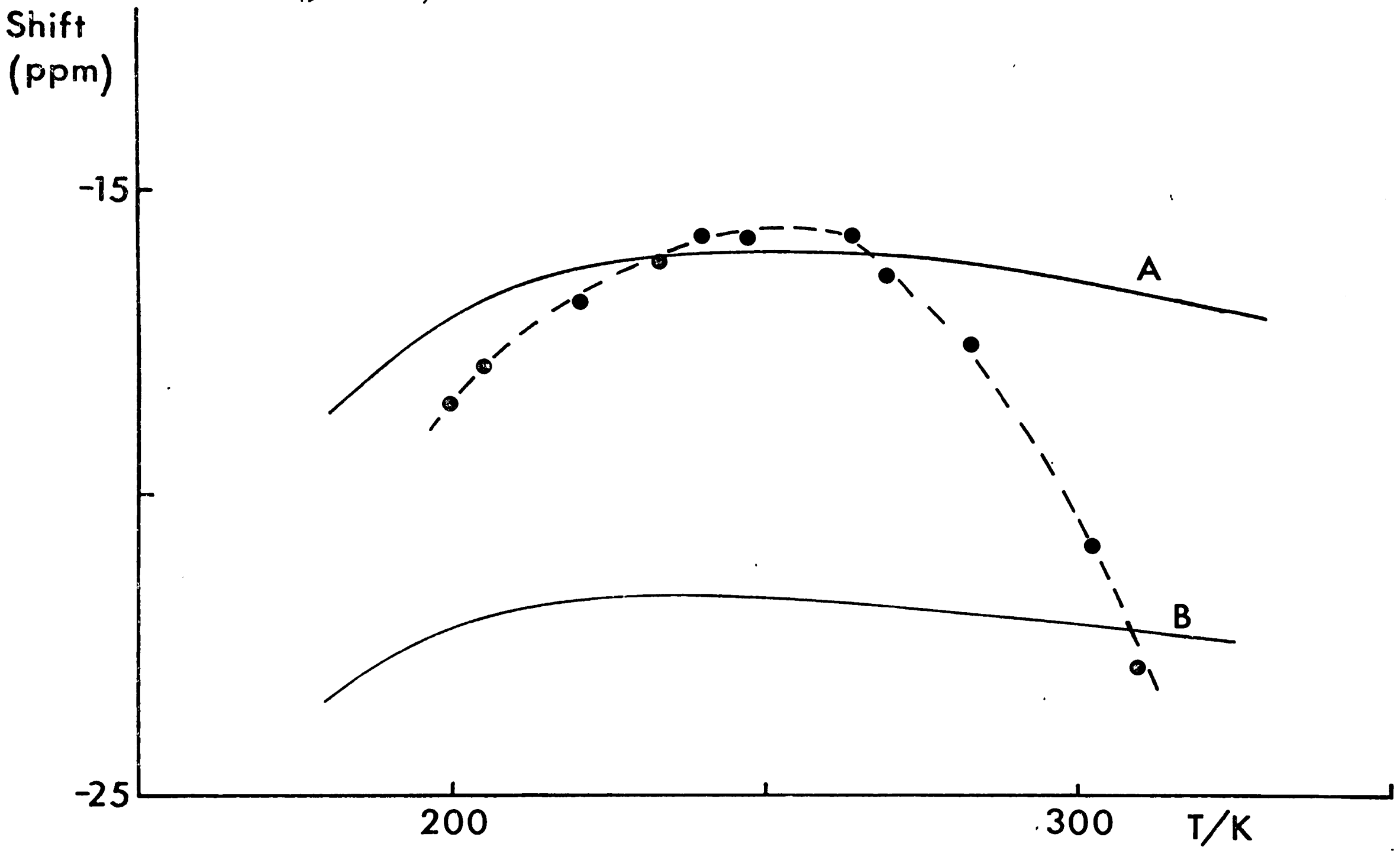


TABLE 3.9

Representative experimental and theoretical isotropic shift data for some ferric octaethylporphin complexes

(a) β-py protons

i) $Fe(OEP)(3\text{-}ClPy)_2ClO_4$

T/K	$K_{\parallel} - K_{\perp}/10^{-6}cm^3mol^{-1}$	ΔH_{DIP}/ppm	ΔH_{CON}/ppm	Total shift/ppm	Expt. shift/ppm
320	742	-4.5	-28.2	-32.7	
260	2461	-15.0	-8.9	-24.0	
200	5215	-31.8	12.3	-19.4	-19.0

$A(^6A_1) = 3.5$; $A(^4E, {}^4A) = 0.5$; $A(^2E, {}^2B) = -1.8$ all by 10^5 Hz.

ii) $Fe(OEP)(4\text{-}AcPy)_2ClO_4$

320	1327	-7.5	-16.3	-23.9	-24.2
260	2790	-17.0	0	-17.0	-15.7
200	5116	-29.3	12.4	-16.9	-17.5

$A(^6A_1) = 3.4$; $A(^4E, {}^4A) = 0.4$; $A(^2E, {}^2B) = -2.2$ all by 10^5 Hz.

iii) $Fe(OEP)(3\text{-}AcPy)_2ClO_4$

320	1518	-9.2	-13.4	-22.3	-22.9
260	3105	-18.9	2.9	-16.0	-15.5
200	5138	-31.3	14.3	-17.0	-18.5

$A(^6A_1) = 3.4$; $A(^4E, {}^4A) = 0.5$; $A(^2E, {}^2B) = -2.0$ all by 10^5 Hz.

(Cont.)

TABLE 3.9 (Cont.)

T/K	$K_{\parallel}$ $-K_{\perp}/10^{-6}cm^3mol^{-1}$	ΔH_{DIP}/ppm	ΔH_{CON}/ppm	Total shift/ppm	Expt. shift/ppm
iv)	$Fe(OEP)(Py)_2ClO_4$				
320	2267	-13.8	-5.3	-19.1	-19.7
260	3761	-22.9	9.6	-13.2	-13.6
200	5556	-33.8	16.4	-17.4	-18.0

$A(^6A_1) = 4.5$; $A(^4E, {}^4A) = 0.7$; $A(^2E, {}^2B) = -1.50$ all by 10^5 Hz.

(b) α-py protons

i)	$Fe(OEP)(3\text{-}AcPy)_2ClO_4$				
260		-35.0	41.0	6.0	6.0
200		-58.0	67.2	9.2	10.0

$A(^6A_1) = 3.0$; $A(^4A, {}^4E) = -1.0$; $A(^2E, {}^2B) = -6.0$ all by 10^5 Hz.

ii)	$Fe(OEP)(Py)_2ClO_4$				
260		-42.5	50.6	8.1	6.5
200		-62.7	73.0	10.3	10.7

$A(^6A_1) = 6.0$; $A(^4A, {}^4E) = -1.0$; $A(^2E, {}^2B) = -5.7$ all by 10^5 Hz.

(Cont.)

TABLE 3.9 (Cont.)

T/K	$K_{\parallel} - K_{\perp}/10^{-6}cm^3mol^{-1}$	ΔH_{DIP}/ppm	ΔH_{CON}/ppm	Total Shift/ppm	Expt. shift/ppm
(c) b_{16} protons					
i) $Fe(OEP)(3\text{-}ClPy)_2ClO_4$					
320	741	1.6	-30.3	-28.8	-28.6
260	2461	5.2	-24.5	-19.3	-20.5
200	5215	11.0	-20.2	-9.1	-9.0
$A(^6A_1) = 2.4$; $A(^4A, {}^4E) = 2.4$; $A(^2E, {}^2B) = 0.8$ all by 10^5 Hz.					
ii) $Fe(OEP)(4\text{-}AcPy)_2ClO_4$					
320		2.6	-22.9	-20.3	-20.8
260		6.5	-16.4	-9.9	-10.5
200		10.8	-16.9	-6.1	-6.2
$A(^6A_1) = 2.2$; $A(^4A, {}^4E) = 2.2$; $A(^2E, {}^2B) = 0.6$ all by 10^5 Hz.					
iii) $Fe(OEP)(3\text{-}AcPy)_2ClO_4$					
320		3.2	-23.6	-20.4	-19.5
260		6.5	-17.2	-10.7	-9.5
200		10.8	-16.4	-5.6	-5.1
$A(^6A_1) = 2.8$; $A(^4A, {}^4E) = 2.4$; $A(^2E, {}^2B) = 0.4$ all by 10^5 Hz.					

(Cont.)

TABLE 3.9 (Cont.)

T/K	$K_{\parallel} - K_{\perp}/10^{-6}cm^3mol^{-1}$	ΔH_{DIP}/ppm	ΔH_{CON}/ppm	Total shift/ppm	Expt. shift/ppm
iv) $Fe(OEP)(Py)_2ClO_4$					
320		4.8	-18.9	-14.1	-14.8
260		7.9	-14.2	-6.3	-6.3
200		11.7	-16.9	-5.2	-3.8
$A(^6A_1) = 3.2$; $A(^4A, {}^4E) = 2.6$; $A(^2E, {}^2B) = 0.9$ all by 10^5 Hz.					
v) $Fe(OEP)(N\text{-}MeIm)_2ClO_4$					
320	2679	5.6	-8.5	-2.8	-4.0
260	3678	7.7	-10.1	-2.4	-2.2
200	5260	11.1	-13.1	-2.1	-1.8
$A(^6A_1) = 3.5$; $A(^4A, {}^4E) = 2.6$; $A(^2E, {}^2B) = 0.8$ all by 10^5 Hz.					

Unfortunately such comparisons are not meaningful because there is no certainty that the parameters taken to fit the calculations are unique. Indeed it is highly probable that more than one set of parameters will produce the same or a similar theoretical answer. Precise experimental anisotropic susceptibility data are needed to choose a unique set of parameters. This is critical because it is apparent that even if the above model is only qualitatively correct the pseudo-contact shift makes a significant yet varying contribution to the total isotropic shift which in turn makes the calculation of coupling constants a rather arbitrary procedure.

It is however possible to make several qualitative observations. Although in principle dissimilar coupling constants for the same resonance position could be expected in differently substituted adducts (different donor properties, etc.), the effects must be relatively small because the results in Table 3.9 suggest that, in the main, the changing ligand field can account for the varying shifts.

Taking average values of the coupling constants for a particular derivative (pyridine) and neglecting the quartet spin states, because they contribute little to the observed properties, the following values ($\times 10^5$ Hz) for the various positions are found:

	^6A	^2E
α	6.0	-5.7
β	4.5	-1.5
γ	0	-1
a	1	1
b	3.2	0.9
c	0	0.5

The porphin a, b and c protons have rather small coupling constants, the c position being, predictably, very small. The rather smaller than perhaps expected values for the a position (in comparison with those of

the b position) may well reflect the predicted nodes (Hückel molecular orbital calculations[73]) at the methene bridge carbons in the porphin $3e_g$ orbitals. There does not appear to be any alternation in the sign of the coupling constants around the α, β and γ positions of the pyridine adduct, the values decreasing away from the metal ion. These observations are consistent with a σ delocalisation mechanism.

Over and above all the complications discussed so far there also remains the problem of possible conformational changes in solution when the temperature is altered. This influence on the magnetic properties of the metal ion has in effect been taken account of with the varying ligand field parameters but could quite easily lead to an extra variation of the contact and pseudo contact contributions to the isotropic shift. The possibly inequivalent adducts (with the iron atom out of the N_4 plane) could also lead to complications which may even contribute to the line broadening, making the resonances difficult to observe at the higher temperatures.

3.5 ADDENDUM

PREPARATION AND PMR SPECTROSCOPY OF A BISCYANO FERRIC PORPHYRIN COMPLEX

1. Introduction

In the main part of this Chapter, attention was focussed on, amongst other electronic properties, the PMR spectroscopic features of bis axial derivatives of ferric porphyrins. These derivatives involving pyridine and imidazole bases as axially bound ligands were isolated in the solid state. As was stated in Section 3 of the Introduction to this Chapter, very few bis adducts of ferric porphyrins have been isolated as solids.

A number of reports[31,39,74] have been published on PMR spectroscopic studies of biscyano ferric porphyrin complexes. Generally these studies have been undertaken on the biscyano complex formed in situ in solution without isolation and chemical analysis of the solid. In view of the success in preparing and isolating the bispyridinato derivatives, it was of interest to attempt to isolate a biscyano complex in order that further examination of the solid and solution electronic properties could be made.

2. Experimental

The essential strategy utilised to prepare and isolate a solid biscyano complex was to look for a large cation to be used as a counterion in an attempt to precipitate a bis cyano ferric porphyrin complex out of solution. Using the ferric octaethylporphin chloride complex, the tetrabutyl ammonium cation suggests itself as a possible counterion of appropriate size. Accordingly experiments were undertaken to find a solvent for ferric octaethylporphin chloride, tetrabutyl ammonium perchlorate and sodium or potassium cyanide. Of the common organic solvents, dimethylsulphoxide (DMSO) appeared to dissolve all three reactants most readily.

Ferric octaethylporphin chloride (23.2 mg) and sodium cyanide (45.6 mg) were each dissolved in the minimum quantity of DMSO and then mixed. The porphyrin dissolved with difficulty to give a brown solution. All of the solid remaining undissolved was immediately taken up on addition of the cyanide solution and the solution turned red (total bulk 10 ml). Tetrabutyl ammonium perchlorate (12.6 mg) in the minimum quantity of DMSO was added. The DMSO was evaporated on a vacuum line, the solid washed with water, extracted with chloroform leaving behind excess cyanide, and the solvent evaporated. The dicyano complex was recrystallised from a chloroform/carbon tetrachloride solvent mixture as dark red needles of the $Bu_4N^{+}{}^{-}Fe(OEP)(CN)_2$ complex (yield 6 mg).

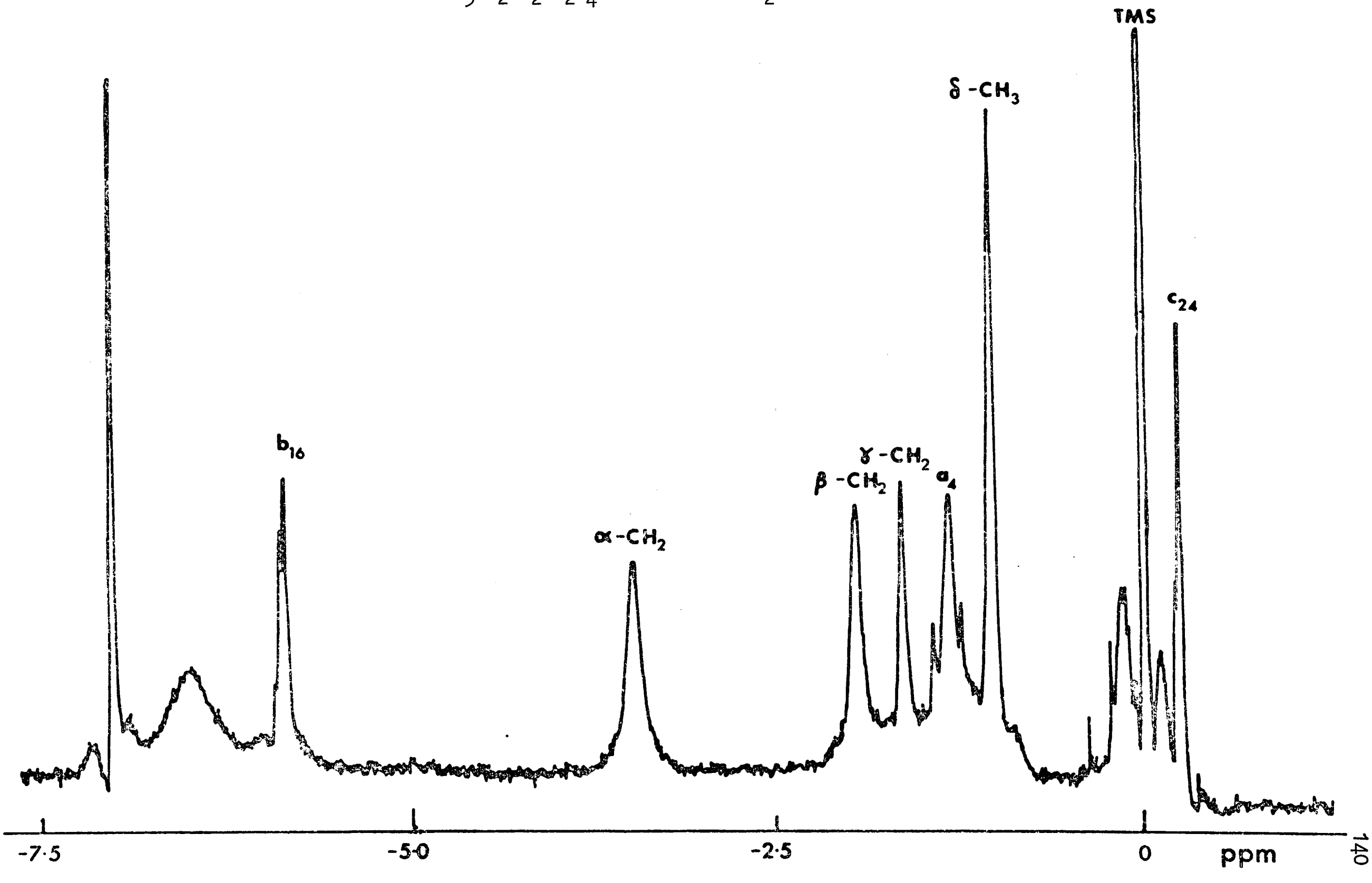
			C	H	N
Analysis	$Bu_4NFe(OEP)(CN)_2$	calculated (%)	73.5	9.06	11.1
		found (%)	72.74	8.89	11.35

3. Results and Discussion

The physical technique used to study the small amount of complex prepared as described above was PMR spectroscopy. The 270 MHz PMR spectrum of a 1.6 mM solution of the $Bu_4N^{+}{}^{-}Fe(OEP)(CN)_2$ complex in deuterochloroform at 298°K is shown in Figure 3.24. The porphyrin proton resonances are similarly shifted as those reported for other biscyano ferric porphyrin complexes[31,39,74]. Thus the split resonance at -6.07, -6.04 ppm arises from the b_{16} protons, the resonance at +0.26 ppm from the c_{24} protons and the resonance at -1.34 ppm from the a_4 protons, using the same nomenclature employed elsewhere in this Chapter. The remaining four peaks in the -4 to -1 ppm region can be attributed to the butyl protons, the α- CH_2 proton resonance being shifted to lowest field and the δ-CH_3 proton resonance being shifted least.

A broad peak is observed at -6.68 ppm. Using wider sweep widths of the spectrometer, further peaks are observed at lower field, that is shifted to -43.4 and -39.9 ppm. The shifts and form of these peaks

FIG. 3.24 PMR spectrum of $(CH_3CH_2CH_2CH_2)_4N^+$ $Fe^-(OEP)(CN)_2$ at 298°K.



are very similar to those observed in the spectrum of Fe(OEP)Cl[75]. It is fairly certain that these peaks signify the presence of a high-spin ferric porphyrin species, the peaks at about -40 ppm being assigned to the b_{16} protons and the peak at -6.68 ppm to the c_{24} protons. The presence of this high spin species may be accounted for by proposing equilibria as follows:

$$Bu_4N^+ {}^-Fe(OEP)(CN)_2 + S \rightleftharpoons Bu_4N^+ + CN^- + Fe(OEP)(CN)(S)$$

$$\Big\Vert S$$

$$+ \quad Fe(OEP)(S)_2 + CN^-$$

where S represents solvent.

This analysis is supported by observing the effect of addition of excess cyanide. The addition of 10 microlitres of a 2M solution of sodium cyanide in DMSO was found to affect the NMR spectrum, the peaks proposed as originating from a high-spin species disappearing. This is entirely expected, since the addition of excess cyanide would drive the above equilibria to the left, increasing the concentration of the biscyano low spin ferric complex at the expense of the high spin ferric porphyrin species.

Some preliminary studies of the effect of temperature variation on the NMR spectrum were made. The shifts at various temperatures are given in Table 3.10. These shift values do not show a Curie dependence, in that plots of observed shift against T^{-1} do not approach the diamagnetic values (see Table 3.11) as T^{-1} approaches zero. In the absence of more detailed studies it is not possible to gain any insight into the cause of this behaviour, although a contributory factor is likely to be the presence of the equilibria involving solvent as shown above.

Further studies on the $Bu_4N^+ {}^-Fe(OEP)(CN)_2$ complex by means of infra-red and EPR spectroscopy would be useful in characterising more fully the electronic properties. However, this preliminary study does

TABLE 3.10

Observed NMR shift data* for the $(CH_3CH_2CH_2CH_2)_4N^+$ $Fe(OEP)(CN)_2^-$ complex in deuterochloroform

T°K	$(b_{16})_{HS}$		$(c_{24})_{HS}$	b_{16}		$(\alpha\text{-}CH_2)_4$	$(\beta\text{-}CH_2)_4$	$(\gamma\text{-}CH_2)_4$	$(\delta\text{-}CH_3)_4$	c_{24}	a_4
331	-37.0	-34.5	-5.1	-6.01	-5.92	-3.55	-1.81	-1.44	-1.00	-0.23	-3.13
316				-6.05	-5.97						
298	-43.4	-39.9	-6.68	-6.07	-5.99	-3.55	-1.99	-1.66	-1.04	+0.26	-1.34
284	-46.6	-42.6		-6.09	-6.01	-3.71	-2.05	-1.79	-1.07	+0.42	-0.81
274	-48.5	-44.3		-6.07	-5.99	-3.71	-2.12	-1.89	-1.11	+0.60	-0.26
264	-50.8	-46.5	-7.91	-6.02	-5.94	-3.76	-2.20		-1.12	+0.80	
254	-53.3	-47.8	-8.35	-5.91		-3.91	-2.29		-1.17	+1.01	
244	-57.3	-51.4	-9.13	-5.81			-2.44		-1.22	+1.29	+1.81

*Observed shift in ppm from TMS

at least demonstrate that a solid biscyano ferric porphyrin complex can be prepared and isolated.

TABLE 3.11

Observed NMR shifts for the diamagnetic $(CH_3CH_2CH_2CH_2)_4N^+ \; ClO_4^-$ complex in deuterochloroform at 298°K

	$(\alpha\text{-}CH_2)_4$	$(\beta\text{-}CH_2)_4$	$(\gamma\text{-}CH_2)_4$	$(\delta\text{-}CH_3)_4$
	-3.26 -3.23	-1.65 -1.62	-1.48 -1.45	-1.04 -1.01
	-3.20		-1.43 -1.40	-0.98
Average	-3.23	-1.64	-1.44	-1.01

REFERENCES

1. R.L. Martin and A.H. White. Transition Metal Chemistry, 1968, 4, 113.
2. L. Cambi and A. Cagnasso. Atti. Accad. Naz. Lincei, 1931, 13, 809.
3. L. Cambi and L. Szegö. Ber. 1931, 64, 2591.
4. L. Cambi, L. Szegö and A. Cagnasso. Atti. Accad. Naz. Lincei, 1932, 15, 266.
5. L. Cambi, L. Szegö and A. Cagnasso. Atti. Accad. Naz. Lincei, 1932, 15, 329.
6. L. Cambi and L. Szegö. Ber., 1933, 66, 656.
7. M. Kotani. Rev. Mod. Phys., 1963, 35, 717.
8. L. Pauling and C.D. Coryell. Proc. Nat. Acad. Sci. U.S., 1936, 22, 159.
9. L. Pauling and C.D. Coryell. Proc. Nat. Acad. Sci. U.S., 1936, 22, 210.
10. C.D. Coryell, F. Stitt and L. Pauling. J. Amer. Chem. Soc., 1937, 59, 633.
11. H. Taube. Chem. Rev. 1952, 50, 69.
12. G. Schoffa. Advan. Chem. Phys. 1964, 7, 182.
13. H. Theorell and A. Ehrenburg. Acta. Chem. Scand. 1951, 5, 823.
14. J.S. Griffith. J. Inorg. Nucl. Chem. 1956, 2, 1.
15. J.S. Griffith. J. Inorg. Nucl. Chem. 1956, 2, 229.
16. J.S. Griffith. Proc. Roy. Soc. 1956, A235, 23.
17. P. George, J. Beetlestone and J.S. Griffith. "Haematin Enzymes", Pergamon Press, London, 1961, p.105.
18. H.F. Deutsch and A. Ehrenburg. Acta Chem. Scand. 1952, 6, 1522.
19. G.M. Harris. Theor. Chim. Acta, 1966, 5, 379.
20. G.M. Harris. Theor. Chim. Acta, 1968, 10, 119.
21. G.M. Harris. Theor. Chim. Acta, 1968, 10, 155.
22. M.M. Maltempo, T.H. Moss and M.A. Cusanovich. Biochim. Biophys. Acta, 1974, 342, 290.
23. T.C. Strekas and T.G. Spiro. Biochim. Biophys. Acta, 1974, 351, 237.
24. D.W. Smith and R.J.P. Williams. Structure and Bonding, 1970, 7, 1.
25. H.A.O. Hill and K.G. Morallee. J. Amer. Chem. Soc. 1972, 94, 731.
26. P.D. Skyte, Part II Thesis, Oxford, 1972.

27. H.A.O. Hill, C.M. Wernham and R.J.P. Williams. Unpublished observations.

28. A.H. White, P. Roper, E. Kokot, H. Waterman and R.L. Martin. Aust. J. Chem., 1964, 17, 294.

29. J.P. Jesson, S. Trofimenko and D.R. Eaton. J. Amer. Chem. Soc., 1962, 89, 3158.

30. R.M. Golding, W.C. Tennant, J.P.M. Bailey and A. Hudson. J. Chem. Phys., 1968, 48, 764.

31. K. Würtrich, R.G. Schulman, B.J. Wyluda and W.S. Caughey. Proc. Nat. Acad. Sci. U.S., 1969, 62, 636.

32. R.J. Kurland, R.G. Little, D.G. Davis and C. Ho, Biochem., 1971, 10, 2237.

33. D.F. Evans. J. Chem. Soc. 1959, 2003.

34. J.L. Deutsch and S.M. Poling. J. Chem. Educ. 1969, 46, 167.

35. L.N. Mulay and I.L. Mulay. Anal. Chem. 1966, 38, 501.

36. C.A. Hutchinson, R.C. Pastor and A.G. Kowalsky. J. Chem. Phys., 1952, 20, 534.

37. H. Ogoshi, E. Watanabe, Z. Yoshida, J. Kincaid and K. Nakamoto. J. Amer. Chem. Soc., 1973, 95, 2845.

38. Landolt-Bornstein, New Series II, Vol. 2, 1-16.

39. R.G. Shulman, S.H. Glarum and M. Karplus. J. Mol. Biol. 1971, 57, 93.

40. M. Kotani. Progr. Theor. Phys. Suppl., 1961, 17, 4.

41. H. Hori. Biochim. Biophys. Acta., 1971, 251, 227.

42. I. Salmeen and G. Palmer. J. Chem. Phys., 1968, 48, 2049.

43. G.N. La Mar and F.A. Walker. J. Amer. Chem. Soc., 1973, 95, 1782.

44. L. Bullard, R.M. Panayappan, A.N. Thorpe, P. Hambright and G. Ng. Bioinorg. Chem., 1974, 3, 161.

45. K. Schofield. "Hetero aromatic Nitrogen Compounds - Pyrroles and Pyridines", Butterworth, 1967, p.146.

46. W.T. Simpson. J. Chem. Phys., 1949, 17, 1218.

47. M. Gouterman. J. Chem. Phys., 1959, 30, 1139.

48. M. Gouterman. J. Mol. Spectrosc., 1961, 6, 138.

49. M. Gouterman, G.H. Wagniere and L.C. Snyder. J. Mol. Spectrosc., 1963, 11, 108.

50. C. Weiss, H. Kobayashi and M. Gouterman. J. Mol. Spectrosc., 1965, 16, 415.

51. W.S. Caughey, R.M. Deal, C. Weiss and M. Gouterman. J. Mol. Spectrosc., 1965, 16, 451.

52. L.M. Epstein, D.K. Straub and C. Maricondi. Inorg. Chem., 1967, 6, 1720.

53. G. Lang. Quart. Rev. Biophys., 1970, 3, 1.

54. M. Sharrock, E. Münck, P.G. Debrunner, V. Marshall, J.D. Lipscomb, I.C. Gunsalus. Biochem., 1973, 12, 258.

55. D.K. Straub and W.M. Connor. Ann. N.Y. Acad. Sci., 1973, 206, 383.

56. H.H. Wickman and A.M. Trozzolo. Inorg. Chem., 1968, 7, 63.

57. G.E. Chapps, S.W. McCann, H.H. Wickman and R.C. Sherwood. J. Chem. Phys., 1974, 60, 990.

58. T.H. Moss, A.J. Bearden, R.G. Bärtsch and M.A. Cusanovich. Biochem., 1968, 7, 1583.

59. T. Iizuka and I. Morishima. Biochim. Biophys. Acta., 1974, 371, 1.

60. I. Morishima and T. Iizuka. J. Amer. Chem. Soc., 1974, 96, 5279.

61. R. Morassi, F. Mani and L. Sacconi. Inorg. Chem., 1973, 12, 1246.

62. T. Iizuka and M. Kotani. Biochim. Biophys. Acta., 1969, 181, 275.

63. T. Iizuka and M. Kotani. Biochim. Biophys. Acta., 1969, 194, 351.

64. T. Iizuka, M. Kotani and T. Yonetani. Biochim. Biophys. Acta., 1968, 167, 257.

65. A.K. Gregson. Ph.D. Thesis, University of Melbourne, 1971.

66. C.G. Barraclough, A.K. Gregson and S. Mitra. J. Chem. Phys., 1974, 60, 962.

67. J.S. Griffith. Proc. Roy. Soc. (London), 1956, A235, 23.

68. J.F. Gibson, D.J.E. Ingram and D. Schonland. Disc. Farad. Soc., 1958, 26, 72.

69. B.L. Vallee and R.J.P. Williams. Proc. Nat. Acad. Sci. U.S., 1968, 59, 498.

70. W. de W. Horrocks and E.S. Greenberg. Mol. Phys., 1974, 27, 993.

71. S. Mitra. Unpublished results.

72. A.K. Gregson. To be published.

73. H.C. Longuet-Higgins, C.W. Rector and J.R. Platt. J. Chem. Phys., 1950, 18, 1174.

74. K. Wüthrich. Structure and Bonding, 1970, 8, 53.

75. F.A. Walker and G.N. La Mar. Ann. N.Y. Acad. Sci., 1973, 206, 328.

CHAPTER 4

PROTON MAGNETIC RESONANCE STUDIES OF SOME 'NATURAL' FERRIC PORPHYRIN COMPLEXES

4.1 Introduction

1. P.M.R. spectroscopy and porphyrins

Nuclear magnetic resonance spectroscopy has proved to be a powerful tool in helping to establish the electronic structure of paramagnetic centres of hemes and heme proteins. Ideally, investigations of iron porphyrins, and their role as hemes in hemoproteins, in solution would yield the same molecular structural details as have been obtained for the crystalline state by X-ray diffraction methods[2-10].

The parameters which describe NMR spectra provide a wealth of information on each magnetic nucleus. The chemical shift is sensitive to the electronic and molecular environment, the area of each resonance is proportional to the number of nuclei involved, the fine structure, characterised by coupling constants, describes interactions with neighbouring magnetic nuclei and the nuclear spin relaxation times, T_1 and T_2, depend on inter- and intramolecular magnetic dipole interactions.

In the past few years, there has been a great increase in the use of PMR spectroscopy in investigating structure and structure-function relationships in a variety of biological macromolecules containing paramagnetic metal ions[11,12]. Paramagnetism of the molecule can serve as a very sensitive and specific probe for the environment of the metal ion by causing large perturbations[13] on the normal diamagnetic line widths and chemical shifts of the protons. Since the interactions with the unpaired electrons are relatively short-range, only nuclei in the immediate vicinity of the metal ion are appreciably affected by the paramagnetism. If the exact origin of the proton-electron interaction is understood, considerable information on bonding and molecular configuration can be extracted from the line width and shift data. Although

a variety of protein systems have been investigated by PMR spectroscopy, the two classes of proteins which have received the most attention are the "iron-sulphur" proteins[12,14,15] (rubredoxin and ferridoxin[5]) and the iron-heme proteins (cytochrome c[16-19], hemoglobins[20-24] and myoglobins[25-32]). For the iron sulphur proteins, PMR spectroscopy has been instrumental in elucidating the anti-ferromagnetic coupling between irons in the two- and eight iron species.

For the heme-iron proteins, PMR data have proved valuable in the investigation of a variety of properties, such as detecting cooperativity and characterising mutations in hemoglobins[20-24], elucidating the iron environment and the tertiary structure of myoglobins[25-31], locating the in-plane magnetic axes in myoglobin[32], and characterising[17-19] the bonding, configuration and electron transfer properties of cytochrome c. The characteristic feature of the PMR spectra which facilitated these interpretations is that the paramagnetic (isotropic) shifts for the porphyrin and axial ligand protons are sufficiently large to move the peaks well outside the range of proton shifts commonly observed for analogous diamagnetic proteins[11], i.e. 0 to -10 ppm from TMS. Although considerable useful information has been derived from these observed shifts, a clear understanding of the iron-porphyrin bonding and the configuration about the metal ion can only be obtained if the electronic origins of the isotropic shifts are known[13].

Detailed PMR studies of molecules with paramagnetic metal ions have been largely restricted to the simpler inorganic complexes, in which structural data, high symmetry and also available supplementary spectroscopic data have permitted quantitative interpretations of the observed shifts in certain cases[33,34]. For the metal ions in proteins the reliability of interpretations of paramagnetic shift data is considerably enhanced by the detailed elucidation of the PMR spectra of model systems, which closely resemble the active site in the protein. To aid in understanding the protein spectra, a number of studies of simple iron complexes

of porphyrins have been carried out.

First reports on the NMR spectra of porphyrins[35-39] were concerned with elucidating the structure of porphyrins and related compounds, and marked effects of changes in structure on the spectra were interpreted in terms of long-range deshielding effects of magnetically anisotropic substituents and the effect of the ring-current field[40]. As porphyrins (in the form of cytochromes) are heavily implicated in biological electron transfer processes, delocalisation of the metal d electrons to the periphery of the ligand has received much attention. Early studies on hyperfine shifts of the high spin ($S = {}^{5}/_{2}$) states of iron (III) tetraphenylporphin[41] and chlorohemin[42] derivatives were interpreted in terms of an isotropic hyperfine interaction transmitted principally through the σ-bond system of the porphyrin ring, since in the latter case no high-field shifts were found.

In contrast, later work showed[43] that in the PMR spectra of high-spin ($S = {}^{5}/_{2}$) iron (III) deuteroporphyrin IX dimethyl esters with different axial ligands, certain protons of the porphyrin ligand exhibited large paramagnetic shifts to high and low field with a dependence on the axial ligand, the latter affecting the "interaction between the porphyrin nitrogens and the iron". It was suggested that π-type orbitals contributed significantly to the transmission of isotropic hyperfine interactions from the iron, a mechanism which was also proposed[44] to account for observed paramagnetic shifts in high-spin hemin derivatives.

These investigations of high-spin ($S = {}^{5}/_{2}$) forms of simple iron complexes with natural porphyrins indicated that the axial ligand can have pronounced effects on some proton shifts. Unfortunately, the proton resonances were found to be quite broad so that peak assignments were difficult and accurate determination of chemical shifts even harder. Detailed analysis of the electronic origin of the isotropic shifts in

these high-spin complexes was hampered by the low symmetry, which results in complex overlapping patterns. In addition, the relatively narrow temperature range of some of the solvents employed interfered with a quantitative assessment of the magnitude of the dipolar shifts. However, in more recent studies[45,46] of PMR spectra of high-spin iron (III) complexes with a variety of synthetic porphyrins, a quantitative separation of the observed shift into contact and dipolar contributions has been possible and a value determined for the zero field splitting parameter D. A dominant mechanism for spin transfer in terms of a π-system delocalisation has been described. Moreover, the authors demonstrated that the data obtained for these synthetic porphyrins were directly applicable to interpretation of the PMR spectra of iron complexes with natural porphyrins[42-44,47].

The combination of its favourably short electronic spin-lattice relaxation time and significantly anisotropic magnetic properties renders the low-spin ($S = {}^1/2$) iron (III) heme moiety a more potent probe of structure via high resolution P.M.R. than the high-spin form. High resolution P.M.R. experiments on low-spin hemes[11,48-51] and heme proteins[28,29] have measured temperature-dependent proton shifts, which can be related to the electron spin density distribution in the π-orbitals of the porphyrin ring. For the heme-iron proteins, in the main the PMR studies have been carried out on the low-spin ($S = {}^1/2$) ferric form of the protein formed by ligation of one or more CN^- ions. These species are magnetically anisotropic, as evidenced by some ESR spectra in glasses[52-54]. Efforts have been made to separate the component contributions of the paramagnetic shift in some cases, but the low symmetry and lack of magnetic data permit only qualitative separations.

Whilst the possible role of magnetic anisotropy was recognised in earlier studies, the initial interpretations favoured a negligible contribution of the dipolar term. Subsequent analyses of heme complexes

based on ESR data have demonstrated that dipolar shifts make significant contributions to the observed shifts, in some cases on a par with the contact contribution. It has been pointed out[55] that dipolar shifts should be correctly evaluated from magnetic susceptibility anisotropy data rather than directly from g tensor anisotropy, as has been customary because of a paucity of magnetic data. This approach has been verified by theoretical work[56,57] and by comparison with experimental data[58,59]. The procedure utilising g tensor anisotropy ignores all second order Zeeman contributions to the susceptibility anisotropy, which may be significant in many cases.

Studies[48,49] on low-spin iron complexes of natural porphyrins have been hampered by a lack of magnetic data and low symmetry, although it is now accepted that the dipolar term provides a sizeable contribution to the isotropic shifts for many ligand protons. Also, the lack of in-plane symmetry in the natural porphyrins makes an experimental determination of the in-plane magnetic axes necessary. However, recent[50,51] PMR spectra of low-spin iron (III) complexes of synthetic porphyrins have permitted a quantitative evaluation of dipolar shifts and the authors suggested that detailed analysis of shifts in synthetic porphyrins could serve to place the interpretation of the PMR spectra of the natural porphyrins on a more quantitative basis.

2. Spin delocalisation and electronic structure

Many transition metal complexes ML^{n+} can generally be described[60,61] as being comprised of a metal ion in a more-or-less defined oxidation state M^{q+} and a diamagnetic ligand system $L^{(n-q)+}$, which are relatively weakly coupled in comparison to the bond strengths within the polyatomic ligand. The ligand system usually, though not necessarily, consists of a number of closed shell, diamagnetic molecules, while the metal ion

may possess unpaired electrons in either its incompletely filled d or f orbitals. If any of the metal orbitals containing the unpaired electron(s) is involved in the metal-ligand bonding, the unpaired spins may find themselves in a new molecular orbital which may partially delocalise the spin onto the ligand. For ligands possessing magnetic nuclei ($I \neq 0$), this delocalised spin may interact with these nuclei via the Fermi contact interaction (see Chapter 2).

The determination of the distribution of the delocalised spin density over the ligand by observing the variation in coupling constants for the non-equivalent magnetic nuclei may lead to the characterisation of the molecular orbital containing the unpaired spin, and thereby lead to an improved understanding of the electronic structure of the particular complex.

Elucidation of the observed coupling constants in terms of the metal-ligand bonding involves three general areas of consideration:

(a) the relationship between the observed coupling constant for a given nucleus and the probability of finding the unpaired spin in an atomic orbital at the nucleus of interest and/or at a neighbouring nucleus[63-69], particularly as to how the coupling constant reflects the type (σ or π) of ligand molecular orbital containing the spin;

(b) evaluation of the mechanism by which the unpaired spin on the metal is transferred to the ligand[70];

(c) the qualitative and, where possible, the quantitative relationships between the fraction of total spin transferred and the M-L covalency[10,11].

3. Mechanisms of spin delocalisation

In the molecular orbital description of bonding in transition metal complexes, well-defined metal (ϕ_M) and ligand (ϕ_L) orbitals are mixed to give the molecular orbitals for the whole complex (ϕ_L is generally a symmetry-adapted ligand MO). In the interpretation of nuclear magnetic

resonance data, the primary concern is with the metal d orbitals, in whose antibonding linear combination the unpaired spins in a paramagnetic complex are generally placed.

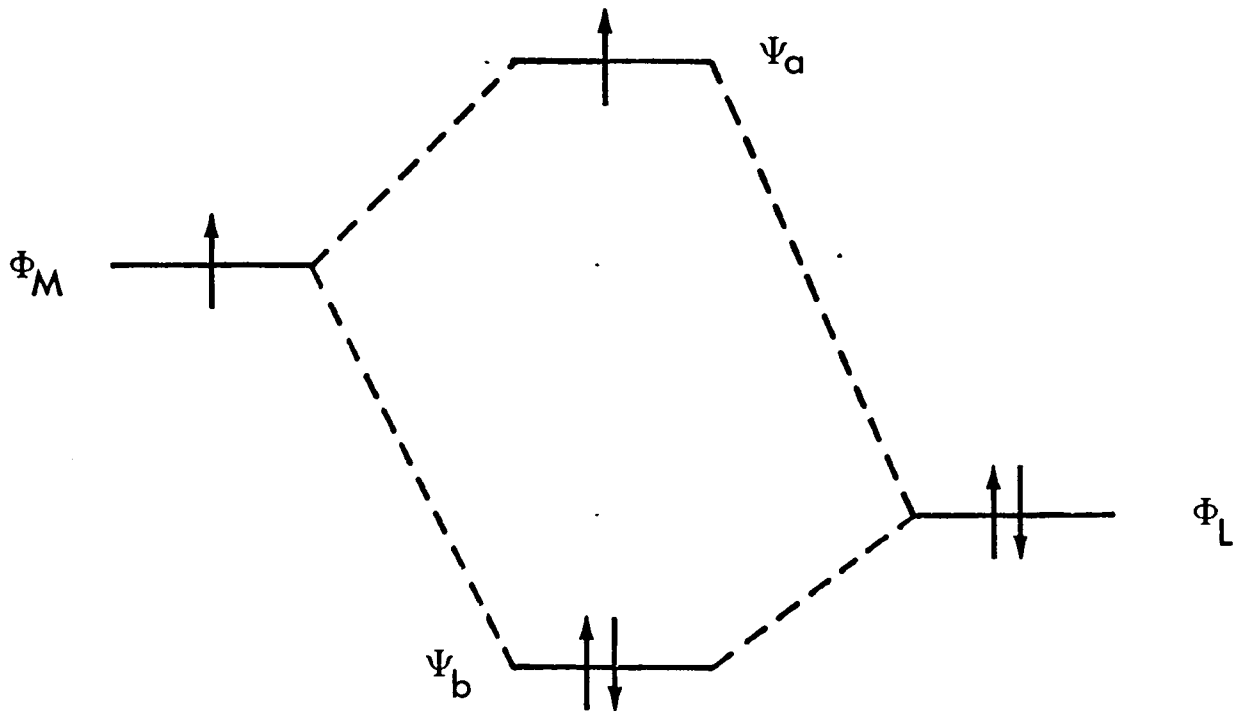


Figure 4.1: Energy level diagram for metal-ligand bond formation.

Due to the relatively high energy of the d levels and the relatively low energies of the filled ligand orbitals (Figure 4.1) the mixing[70] of the metal and ligand orbitals is such that the bonding MO

$$\Psi_b = N_b(\phi_L + \lambda_b d) \qquad (4.1)$$

where the normalisation constant $N_b = (1 + 2\lambda_b S + \lambda_b{}^2)^{-\frac{1}{2}}$ and the

overlap integral $S = \int d_M \phi_L d\tau$

is primarily ligand in character ($\lambda_b \ll 1$).

The antibonding combination

$$\Psi_a = N_a(d - \lambda_a \phi_L) \qquad (4.2)$$

where $N_a = (1 - 2\lambda_a S + \lambda_a{}^2)^{-\frac{1}{2}}$

on the other hand is primarily metal in character ($\lambda_a \ll 1$).

i) Ligand → metal charge transfer

With the assumption of diamagnetic ligands, ligand → metal charge transfer implies that ϕ_L is doubly occupied. In ϕ_b, however, bond formation leads to a transfer of λ_b^2 (↑) spin as well as λ_b^2 (↓) spin from ligand → metal, leaving an excess of λ^2 (↑) spin on the ligand, as depicted in Figure 4.2a. Hence the transferred λ^2 (↑) spin on the ligand should be associated with the hole rather than the electron in ψ_a. Thus the transfer of λ^2 charge from L → M results in the transfer of λ^2 (↑) spin from M → L.

If the bond formation occurs between a filled ϕ_L and a vacant d orbital on a transition metal ion which does possess unpaired spins in other d orbitals (which are symmetry forbidden from interacting with ϕ_L) it would initially be expected that the transfer of (↑) spin (Figure 4.2b) and (↓) spin (Figure 4.2c) in ψ_b would be equal, such that the net spin density in ϕ_L is zero. However, correlation favours[70,72,73] the transfer of (↑) spin from the ligand (Figure 4.2b), thereby leaving a net (↓) spin density in ϕ_L.

ii) Metal → ligand charge transfer

For a diamagnetic ligand, this requires a vacant ϕ_L and since vacant σ^* MO's are too high in energy to be important, only vacant π^* MO's need be considered. The case of a singly occupied d orbital is shown in Figure 4.2d. In the case where the d orbital is doubly occupied (though the metal possesses unpaired spins in noninteracting d orbitals), the transfer of ↓ (Figure 4.2e) from the filled d orbital to ϕ_L is favoured[70] over the transfer of ↑ spin (Fig. 4.2f) since the former case has the more favourable correlation energy.

In the cases depicted in Figures 4.2a and 4.2d, a fraction of the unpaired electron originally on the metal is actually placed into a MO which includes the ligand to some extent, with the fraction of transferred spin equal to the charge transfer (though not necessarily in the

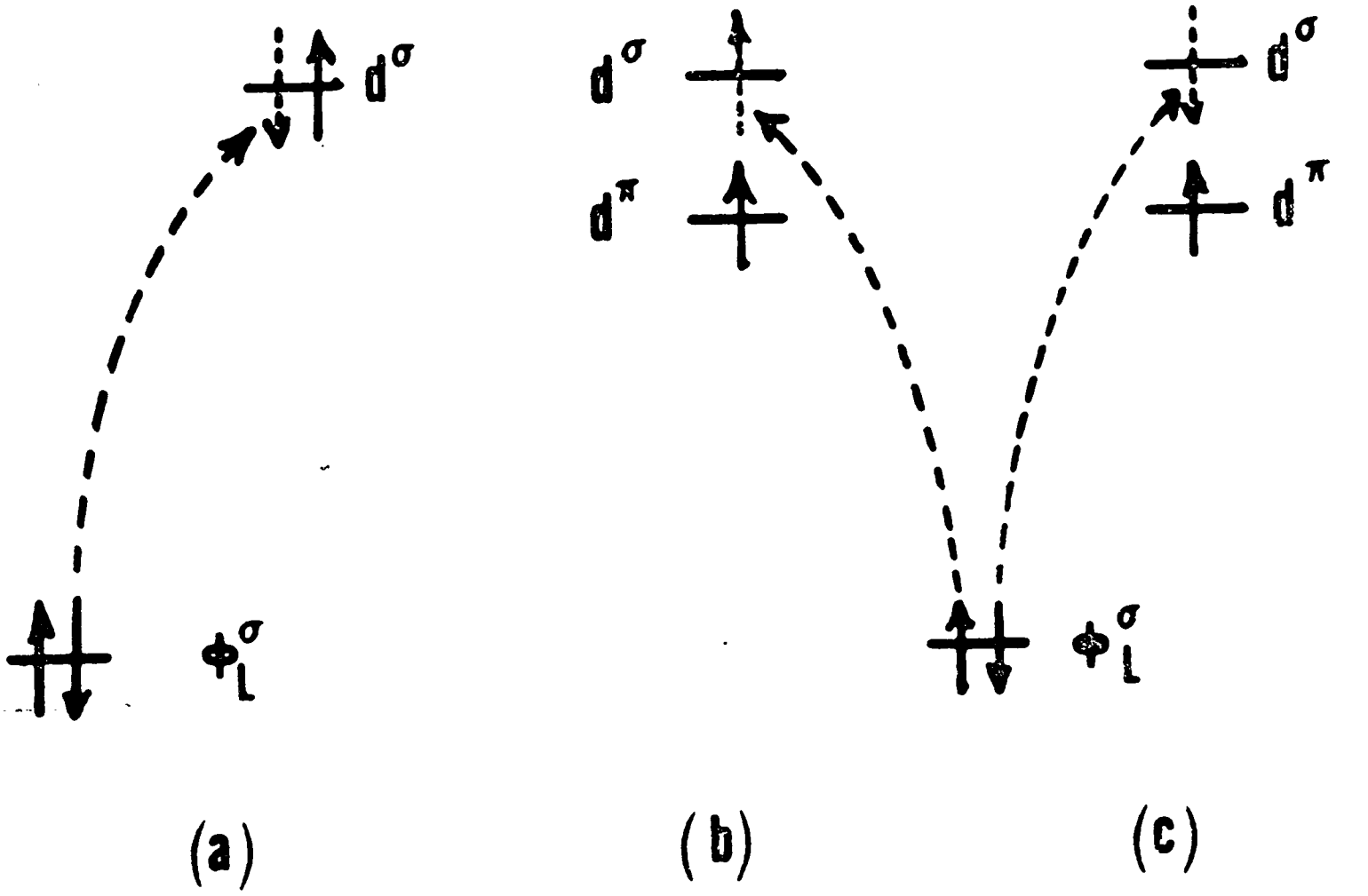


FIG. 4.2 Spin transfer mechanisms.

same direction). This mechanism thus involves direct spin delocalisation. In cases depicted in Figures 4.2b, c, e, f, however, the unpaired spin on the metal introduced a redistribution of the spin in an otherwise paired molecular orbital. This mechanism involves indirect spin delocalisation, more usually called spin polarisation.

iii) Spin delocalisation via M-L σ bonding

Although σ MO's had once been considered highly localised orbitals, theoretical calculations[74] as well as experimental data[74,75] have shown that lone pair electrons do exhibit significant delocalised character. Aromatic molecules, which may serve as ligands by bonding solely through a lone pair M-L σ bond, possess extended π systems which may or may not directly interact with any metal orbitals. The latter type may yield NMR spectra[76-80] indicative of spin density in the aromatic framework which gives some of the characteristics of a system for which the π system may directly participate in M-L π bonding.

For planar species σ and π systems are well defined and are strictly separable by symmetry. The π portion is comprised of an atomic basis of p_z orbitals normal to the plane and σ refers to the remainder of the electronic structure (in plane). In Happe and Ward's study[76] of pyridine-type ligands coordinated to $Ni(acac)_2$, the observed rapid attenuation of proton resonance shifts as the protons become further removed from the paramagnetic centre was attributed to σ spin delocalisation. This conclusion is supported by the fact that isotropic shifts for protons of saturated alkyl groups tend to fall off monotonically and quite rapidly with distance down the chain.

In systems exhibiting σ spin delocalisation, replacement of a proton by a methyl group quite often results in a methyl resonance shift in the same direction, but smaller in magnitude, than that of the proton.

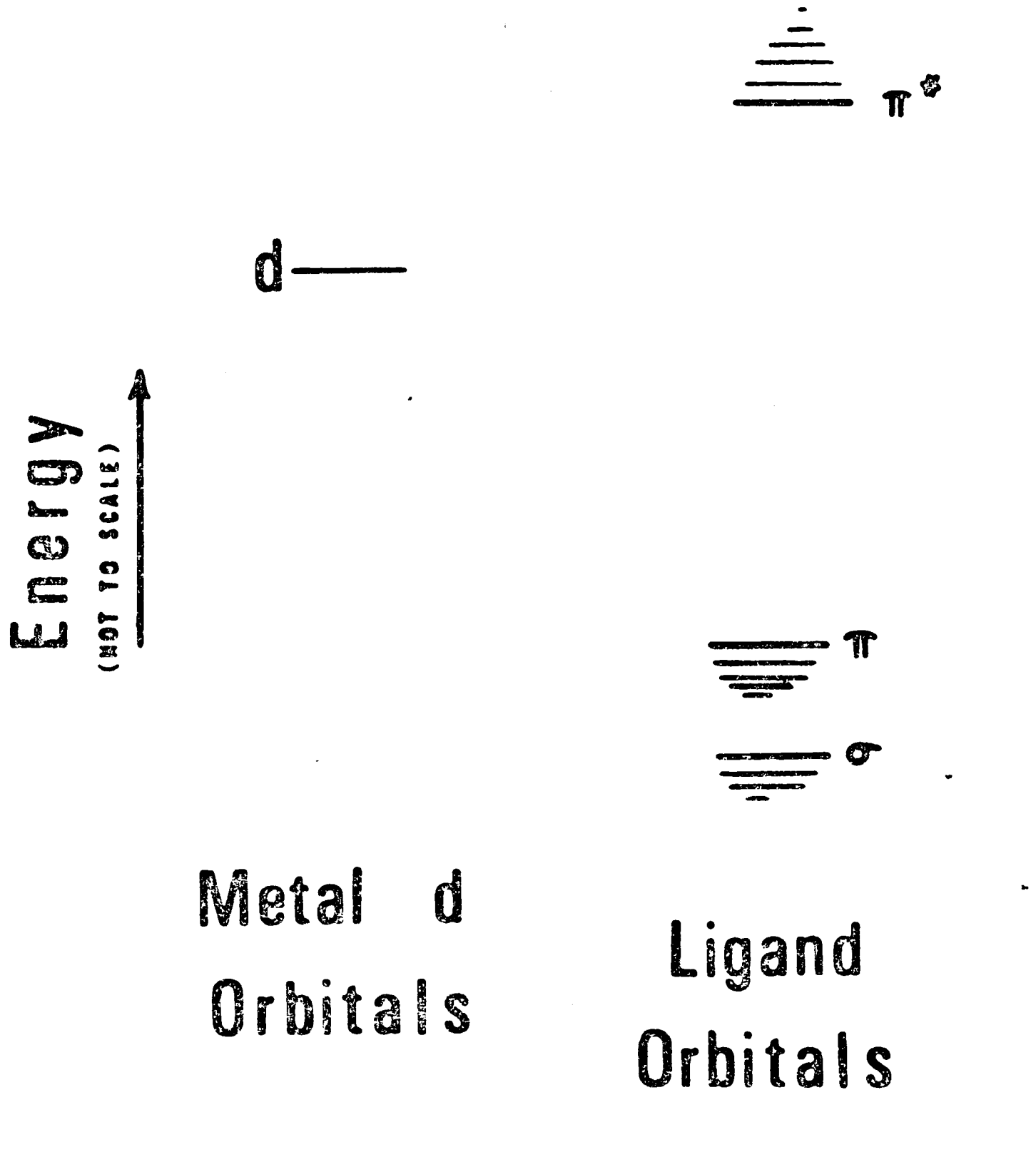
iv) Spin delocalisation via M-L π bonding

Spin transfer through a π bond usually occurs via metal-ligand dπ -pπ bonding[61,62]. Within the assumption that the π MO's for the whole complex can be described by equations (4.1) and (4.2), where the ϕ_L are the MO's for the free ligand, the directly transferred spin will distribute itself over the aromatic framework according to the nature of the particular ϕ_L involved in the bonding. In contrast to σ MO's, where usually a single ligand MO is important, there are generally several π MO's with energies which permit significant mixing with the d orbitals. Hence the net spin distribution will reflect the vector sum of the spin densities in the various contributing MO's. Furthermore, there are both filled π and vacant π * ligand MO's to be considered, allowing direct spin transfer by both L → M and M → L charge transfer. This multiplicity of possible delocalisation mechanisms usually makes it very difficult to describe quantitatively the observed spin density distribution unless a single ligand π MO is overwhelmingly favoured in the M-L π bonding.

For transition metal ions in their more stable oxidation states, the d orbitals have energies which place them well above the ligand filled π MO's. The vacant π * MO's can range in energy from below to above the d orbitals. Due to the $^1/\Delta E$ dependence (ΔE is as in Figure 4.1) of the M-L mixing[70] it may be anticipated that the most important ligand π MO involved in L → M charge transfer is the highest filled orbital (HFO), while the dominant ligand MO involved in M → L charge transfer would be the lowest vacant orbital (LVO).

It may be expected from Figure 4.3 that, for a fixed metal ion, raising the energies of all π MO's will facilitate L → M charge transfer. Keeping the ligand system fixed and raising the energy of metal d orbitals will favour M → L over L → M charge transfer[81]. Thus, in the ions of the first transition series, M → L should be

FIG. 4.3 Relative energies of metal d orbitals and ligand σ, π (filled) and π^* (vacant) molecular orbitals.



favoured for the first part of the series, whilst the L → M mechanism should dominate the latter part. A similar increase in the importance of M → L over L → M charge transfer mechanisms is expected if the oxidation state of the metal ion in a given complex is lowered[82].

It is a characteristic of π spin delocalisation that both positive and negative shifts and hyperfine coupling constants are found, and there is no particular tendency toward attenuation of shift magnitudes as the distance of the resonating proton from the paramagnetic metal is increased. Hyperfine constants tend to alternate in sign between adjacent positions and the largest shifts often occur at positions far removed from the co-ordination site.

The behaviour of the hyperfine shift upon substitution of a methyl group for a proton can also be diagnostic of π spin delocalisation. A proton attached to a carbon atom of an aromatic system has a hyperfine coupling constant given by 2.21 in Chapter 2, where Q_H is negative. This leads to upfield shifts for protons attached to carbon atoms whose pπ orbital contains positive (↑) spin density, and to downfield shifts when negative (↓) spin density is adjacent. For a methyl group attached to an aromatic carbon the analogous expression is 2.22 in Chapter 2, where Q_{CH_3} is positive. Thus if methyl substitution does not affect the π spin density distribution, an assumption made in computing Q_{CH_3}, then methyl groups and protons attached to a given aromatic carbon atom will exhibit hyperfine constants and shifts of opposite sign.

N.B. It has been shown[83], however, that the inversion of sign of isotropic shift on methyl substitution may occur even when the unpaired electron occupies (in a one electron sense) a MO of σ symmetry (see above).

4. Theoretical models of delocalisation systems

As is the case for most physical measurements, ideally, experimental results would be described in terms of a valid theory and, if possible, predictions made based on this theory. For systems involving transition metal complexes, since unpaired electron spins originate on the metal, the most desirable quantum mechanical approach to spin delocalisation would involve a complete calculation of all metal and ligand orbitals with full allowance for electron correlation. The level of theory for which it is feasible to include a transition-metal atom is relatively low. The extended Hückel molecular orbital (EHMO) theory, which does take account of the metal atom, is one example of such a crude semi-empirical theory. The approximations involved in EHMO theory render it of limited usefulness in describing spin delocalisation, but the reasonable agreement of calculations of spin densities for metallocenes[84] with experimental results suggests the theory may be a fair approximation.

A more common procedure has been to carry out calculation on a molecular fragment (either a ligand or a radical derived from the ligand), to compare the relative spin densities at different positions, and hence to deduce the fraction of an electron delocalised which gives a measure of the metal-ligand interaction. This procedure has some obvious limitations. First, the perturbation of the ligand electronic structure by the metal ion is either ignored or treated in a very approximate way. Second, and more important, is the fact that unlike an organic radical where the unpaired electron(s) occupies a particular MO, there is the possibility that more than one ligand MO is simultaneously involved in spin delocalisation. In fact, the success of many of the calculations in the literature can be attributed to the fact that, in the particular cases treated, a single ligand MO dominates the spin delocalisation.

There is some experimental evidence which suggests that it is the ligand electronic structure rather than the metal-ligand interaction,

which dominates spin delocalisation in a ligand moiety. This comes from a comparison of results of three closely related phenomena: NMR contact shifts, EPR hyperfine splittings and NMR spin-spin coupling constants. Contact shifts and EPR hyperfine splittings arise from the same physical interaction and the close resemblance of contact shift ratios for coordinated pyridine and the ratios of hyperfine coupling constants obtained from the EPR spectrum of the phenyl radical (iso-electronic with the pyridine cation radical) was pointed out some years ago[78].

The close theoretical relationship between NMR spin-spin splittings and electron-nuclear hyperfine interactions has been pointed out by several authors[85,86], e.g. a parallelism between the spin-spin coupling constants of benzene and toluene and contact shifts of coordinated pyridine and various picolines has been observed[83]. These analogies suggest that some degree of success may be achieved in describing spin delocalisation in coordinated molecules by calculations on molecular fragments.

5. Aim of the work

It has been shown[87] that redox properties of ferric metalloporphyrins are dependent on the axial ligand coordinated to the central metal ion and on substituents on the porphyrin ring, since these affect electron transfer from the chelated metal ion. A series of hexa-coordinate iron (III) metalloporphyrins in which

(a) substituents on the porphyrin ring,

(b) substituents on the axial ligand,

(c) the axial ligand

are varied will be studied by PMR spectroscopy.

The work reported here was undertaken with several objectives:

(i) the PMR spectra of hemin derivatives are useful as models in understanding the PMR spectra of more complex proteins;

(ii) it is hoped to achieve a better understanding of the transmission of electronic effects in iron (III) metalloporphyrins, and interpretation of the PMR spectra of hemins and hemin complexes placed on a qualitative basis.

The paramagnetic shifts will be interpreted to try and give information about the electronic structure of hemins, and thereby the nature of the metal-ligand bonding. The effectiveness and mechanism of transmission of unpaired electron spin from the paramagnetic iron to protons at the periphery of the porphyrin ring and on the coordinated axial ligand will be observed. The influence of the axial ligand on the bonding interactions between porphyrin and iron, and the influence of the porphyrin ligand on bonding interactions between axial ligand and iron will be monitored. Hyperfine coupling constants for some porphyrin and axial ligand protons will be calculated and the experimental results described in terms of a valid theory for spin delocalisation.

4.2 Experimental

1. Apparatus and materials

i) NMR measurements

^{1}H NMR spectra were recorded on the JEOL JNM-C-60HL spectrometer at 60 MHz and on the Bruker HX 90 90 MHz spectrometer. Solutions were prepared by dissolution of the iron (III) porphyrin, in most cases the dimethyl ester form, in deuterochloroform (0.4 ml) followed by addition of 20-40 µl of the substituted pyridine or 20-40 mg of the substituted imidazole. Either 50 or 100 mM solutions of porphyrin were used. Most of the porphyrins were not completely soluble in deuterochloroform alone, but all were immediately taken up into solution on addition of the heterocyclic base to form brownish-red solutions. Chemical shifts are quoted in parts per million relative to TMS, negative values indicating low field shifts.

ii) Solvents

The solvents used for NMR measurements were as follows: $CDCl_3$, isotopic purity 99.5% D, as supplied by Beta Scientific Ltd.; Pyridine (A.R.) as supplied by B.D.H. Ltd.; d_5-Pyridine, isotopic purity 99% D, as supplied by C.I.B.A. Ltd.; β-Picoline (3-methylpyridine), as supplied by B.D.H. Ltd.

γ-Picoline (4-methylpyridine), supplied by B.D.H. Ltd., was purified as follows[88]. A solution of nickel chloride (9g) in water (3 - 4.5 ml) was added with vigorous stirring to γ-picoline (30 ml) at room temperature. The suspension was filtered, the blue-green nickel complex washed thoroughly with n-butanol and then refluxed with n-butanol (22.5 ml). After cooling the mixture was filtered, the solid dried and recrystallised from ethanol containing a little methanol. The complex was decomposed with excess sodium hydroxide, the mixture steam distilled, the aqueous distillate strongly alkalised with sodium hydroxide, and the separating oil distilled to give γ-picoline, b.p. 139-140°, free from β-picoline and 2,6-lutidine.

2,6-d_2-Pyridine was prepared as follows[89,90]. Pyridine N-oxide was redistilled under nitrogen, and the fraction distilling at 148-152°C collected. Freshly distilled Pyridine N-oxide (2g) was heated under reflux with 5% sodium deuteroxide (20 ml) for 3 hours. The mixture was extracted with chloroform (4 x 25 ml), the combined extracts dried over anhydrous sodium sulphate and evaporated to dryness. This yellow-white oxide was heated under reflux with chloroform (30 ml) and phosphorus trichloride (7.5 ml) for 2 hours. The mixture was concentrated to about 5 ml in vacuo, water (25 ml) added, the solution basified with sodium carbonate and then allowed to stand for 30 mins. The mixture was filtered, the filtrate extracted with chloroform (4 x 25 ml) and the combined extracts dried overnight over anhydrous sodium sulphate. After filtering

off the drying agent, the solvent was removed to give 2,6-d_2-pyridine, which was redistilled on a vacuum line. The extent of deuteration was monitored by comparison of the NMR spectrum of this product with that of pyridine (Figure 4.4). Deuteration takes place almost exclusively at the 2- and 6-positions, and to a small extent at the 3- and 5-positions.

iii) Other materials

Imidazole, benzimidazole, quinoline and isoquinoline as supplied by B.D.H. Ltd. and 5,6-dimethylbenzimidazole as supplied by Koch-Light Laboratories Ltd.

Hemin chloride, as supplied by Fluka A.G., mesoporphyrin dimethyl ester and deuteroporphyrin dimethyl ester as supplied by Koch-Light Laboratories Ltd. Etioporphyrin was a gift from Dr. P.J. Sadler.

2. Preparation of compounds

i) Esterification of ferric protoporphyrin chloride[91]

Fe(III)-protoporphyrin (hemin) chloride (0.5 g) was shaken with a portion of 5% ($^{v}/v$) sulphuric acid in methanol for about 20 mins. The mixture was filtered, the residue treated with a further portion of 5% ($^{v}/v$) sulphuric acid in methanol and filtered, etc. This was repeated about four times (200 mls of solvent); some residue remained at the end. The combined extracts were left in a refrigerator overnight, in order for esterification to be complete. Thin layer chromatography studies in chloroform confirmed that esterification was complete; only the ester moved up the plate, leaving any acid at the origin. Equal volumes of both toluene and 2N potassium carbonate were added (100-150 mls of each) and the mixture centrifuged. The toluene layer was washed with 2N potassium carbonate (100 mls), twice with distilled water, twice with 2N potassium chloride (pH 2), and the toluene removed under vacuum to

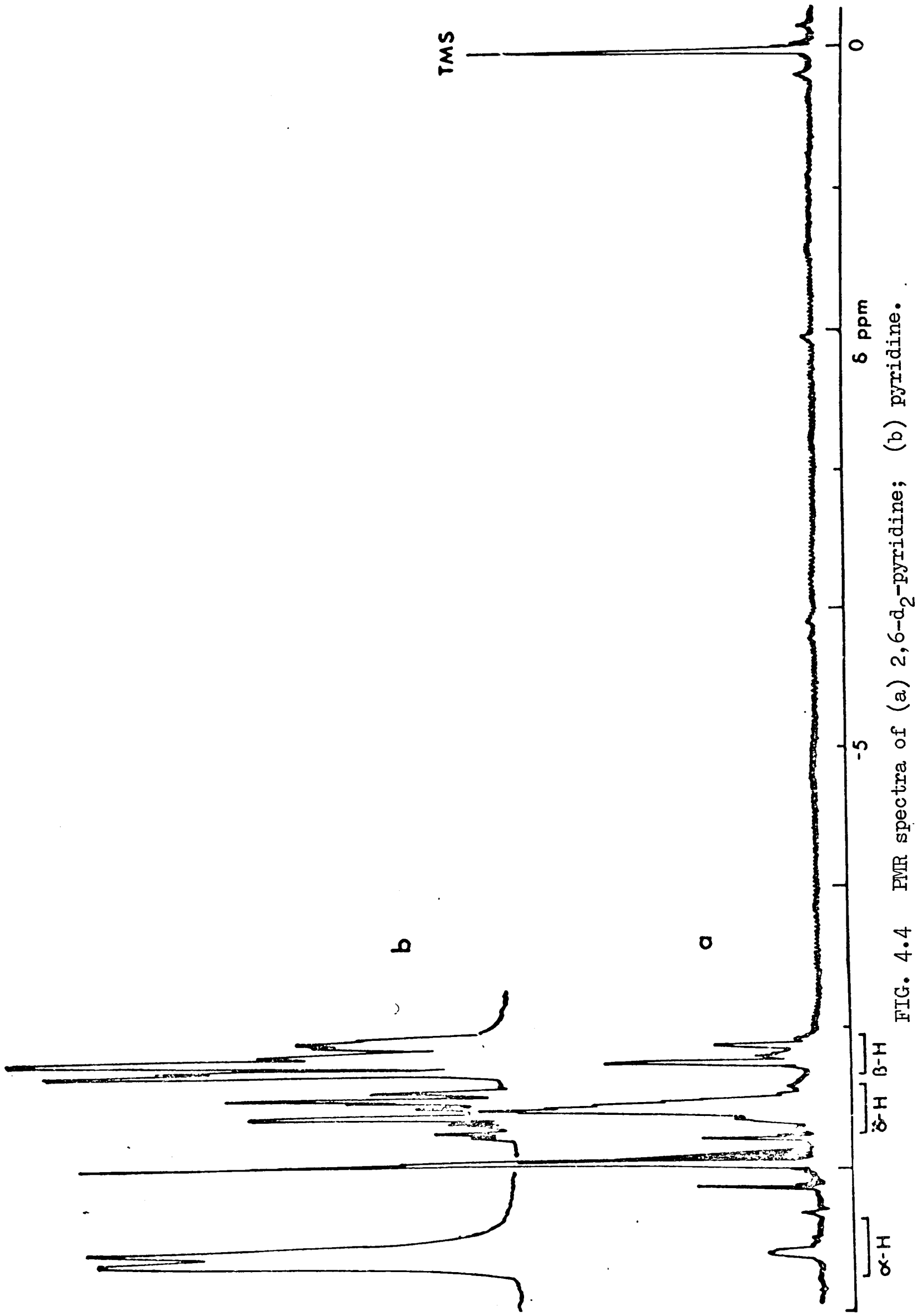


FIG. 4.4 PMR spectra of (a) 2,6-d_2-pyridine; (b) pyridine.

give the crude ester. The latter was dissolved in the minimum quantity of chloroform, the remaining potassium chloride filtered off, and the chloroform removed under vacuum. The ester was finally recrystallised from a chloroform/carbon tetrachloride mixture by the method of Erdman and Corwin[92]. Yield 0.23 g.

ii) Synthesis and purification of porphin[93]

(a) Synthesis of pyrrole alcohol

Pyrrole 2-carboxaldehyde (45 g) was added to water (550 ml) and ethanol (15 ml) contained in a 2 l, 3-necked flask fitted with a dropping funnel, thermometer, condenser and magnetic stirrer. A solution of sodium borohydride (23 g) in water (200 ml) and ethanol (8 ml) was added to this dropwise over a period of 2 hours and the solution became pale yellow. After addition was completed, the solution was saturated with potassium carbonate (1000 g) and the pyrrole alcohol, which separated as the upper layer, was extracted with ether (5 x 200 ml). The combined ether extracts were dried overnight over anhydrous sodium sulphate, filtered and the ether removed under vacuum. Pyrrole alcohol was obtained as a red-brown oily liquid.

(b) Synthesis of porphin

Xylene (1250 ml) and glacial acetic acid (100 ml) were placed in a 2l, 3-necked flask fitted with a mechanical stirrer, condenser and thermometer and heated to 110°C in a mantle. Pyrrole alcohol (0.2 ml), prepared as above, was added and 0.2 ml aliquots of pyrrole alcohol were added at intervals of a minimum of 2 hours until a total of 3 ml of pyrrole alcohol had been added. After all of the pyrrole alcohol had been added, the reaction mixture was stood at 110° for ca 1 week in order to oxidise chlorin present to porphin. Absorption spectra of the reaction mixture were taken during this time to determine when the maximum amount of chlorin had been eliminated, as shown by the gradual

disappearance of the absorption maximum at 635 nm due to chlorin. The absorption maximum at 616 nm due to porphin was relatively constant during this time.

The cooled and filtered reaction mixture was evaporated to remove xylene and acetic acid, and the reddish-brown residue was redissolved in benzene (ca 1l) so that the porphin absorbance at 616 nm was about 0.4. The benzene solution was stirred over sodium hydroxide pellets (150 g) until the chlorin absorbance at 635 nm was zero. The solution was quickly filtered from the pellets using suction and sodium hydroxide in solution was removed by twice extracting with distilled water. The benzene layer changed colour due to hydrolysis of the sodium salt of porphin (purple) forming the free base porphin (cherry red). The benzene solution was dried over anhydrous, granular calcium chloride for 1 hour, concentrated to a volume of 200 ml and the porphin crystallised slowly from solution. Yield 67 mg of red crystals.

iii) Insertion of iron into porphyrins[94]

N,N-dimethyl formamide (50 ml) was brought to reflux. The porphyrin was added, 1 minute allowed for complete solution to occur, and then a stoichiometric amount of ferrous chloride was added and the reaction allowed to proceed. After a few minutes, completion of the reaction was checked spectrophotometrically by withdrawing a small aliquot and monitoring the disappearance of the free porphyrin band at 560-600 nm. If the reaction was not found complete more ferrous chloride was added, the reaction allowed to proceed for another few minutes, and then re-checked for completion.

The reaction vessel was removed from the heat source and cocled in an ice-water bath for 15 mins. An equal volume of chilled distilled water was added and the partially crystalline black precipitate filtered on a Buchner funnel until the filtrate was clear. The filtered material was washed with water and air dried.

TABLE 4.1

Analytical Data for Porphyrin Compounds

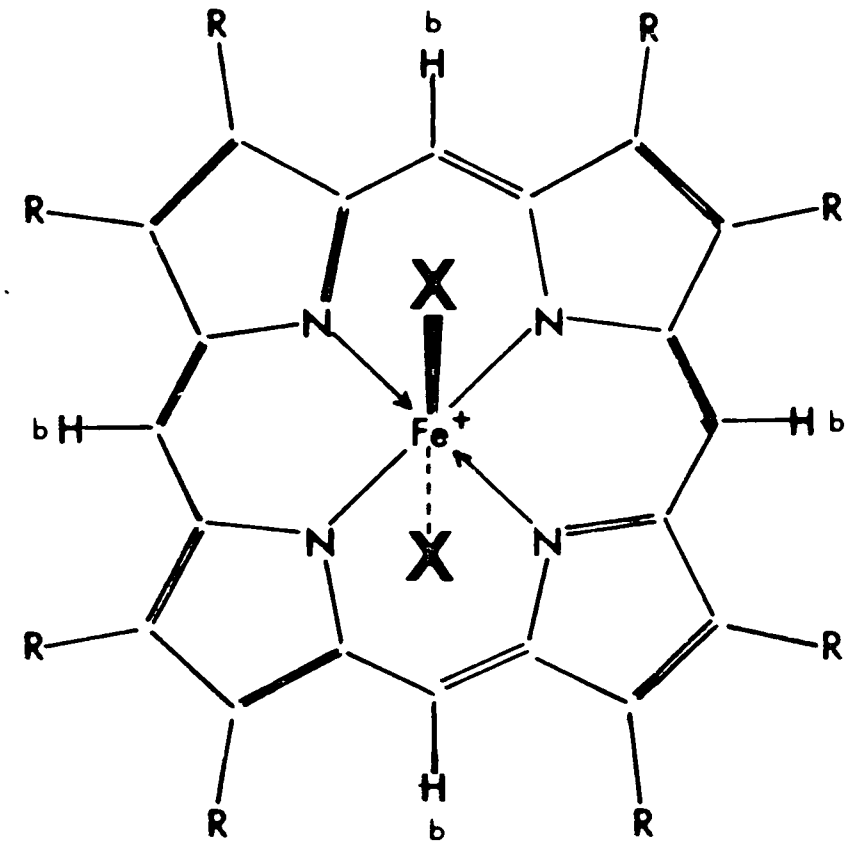
COMPOUND	REQUIRED (%)			FOUND (%)		
	C	H	N	C	H	N
Porphin	77.4	4.51	18.05	76.3	4.70	18.52
Fe(III) porphin chloride	60.0	3.00	14.00	58.9	3.10	14.76
Fe(III) deuteroporphyrin dimethylester chloride	61.2	5.23	9.01	61.1	5.18	9.11
Fe(III) etioporphyrin chloride	67.6	6.34	9.86	67.7	6.56	9.74
Fe(III) protoporphyrin dimethylester chloride	63.6	5.33	8.23	63.2	5.23	8.87
Fe(III) mesoporphyrin dimethylester chloride	63.3	5.85	8.19	63.3	5.77	8.31

4.3 Results

1. Pyridinato complexes

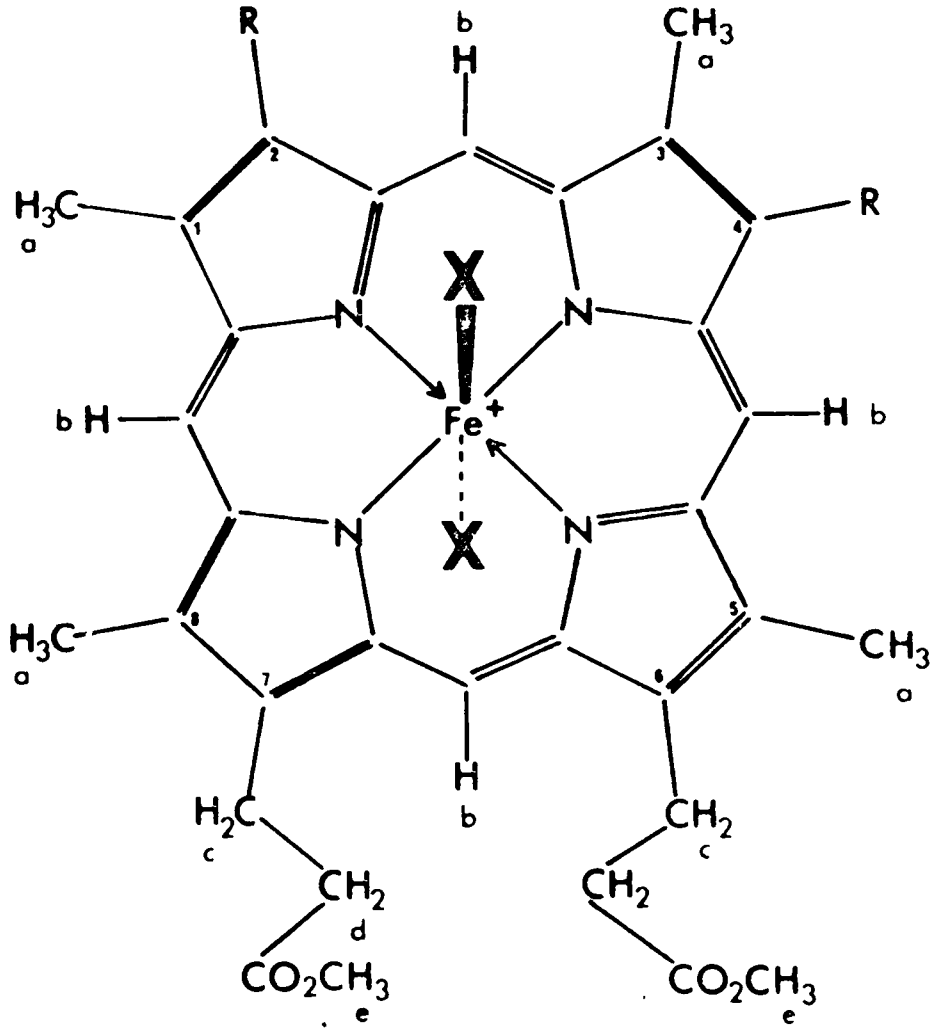
The PMR spectra of 100 mM solutions of Fe(III) porphin chloride + γ-picoline and Fe(III) etioporphyrin chloride + γ-picoline at 225°K are shown in Figure 4.6. The assignments are given in Figure 4.5, and are based on relative intensities and comparison of the two spectra. The two temperature dependent peaks of the porphin complex which occur downfield from TMS are assigned to the γ-methyl and β-protons of two complexed γ-picoline molecules per iron atom. The corresponding shifts of these particular resonances for the etioporphyrin complex are about the same. These resonances are not observed at room temperature but are observed as broad peaks at ca. 290°K and as sharp peaks below 280°K for the porphin complex and below 250°K for the etioporphyrin complex. The two high-field signals of the porphin complex are assigned to the 8 pyrrole and 4 methene bridge ("meso") protons from their relative intensities. The additional downfield signal and the signal just upfield from TMS in the etioporphyrin complex are assigned to resonances f and g of the peripheral ethyl groups respectively. The broad resonance common to both complexes at ca. +10 ppm is assigned to the α-protons of the complexed γ-picoline molecule.

The PMR spectrum of Fe(III) protoporphyrin dimethylester chloride with various complexed axial ligands at 219°K is shown in Figures 4.7 and 4.8. The assignments of the porphyrin ligand protons are based on comparison with those for cyanoiron (III) protoporphyrin IX dimethyl ester[48] and those of Hill and Morallee[49]. The four ring methyl groups are individually assigned for the bispyridine complex on the basis of results using chromium (III) tris-biguanide trichloride as a broadening agent[95] and syntheses involving selective deuteration[96]. Thus, the two methyl group resonances furthest downfield are assigned to the



$R = \acute{R} = H_a$ Fe^{III} PORPHIN

$R = CH_3{}_a$; $\acute{R} = CH_2{}_f CH_3{}_g$ Fe^{III} ETIO



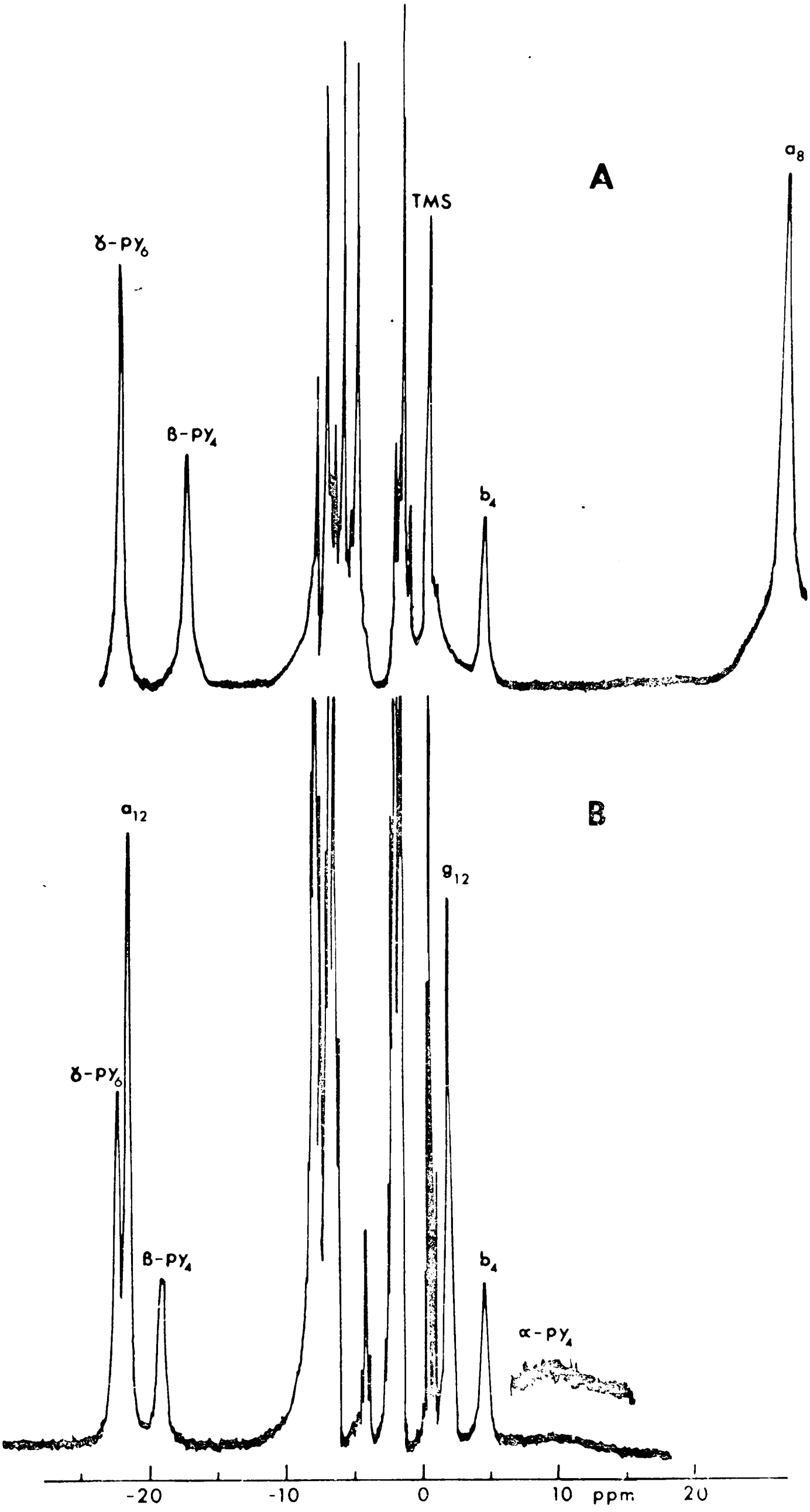
$R = H_f$ Fe^{III} DEUTERO

$R = CH{:}CH_2{}_f{}_g$ Fe^{III} PROTO

$R = CH_2CH_3{}_f{}_g$ Fe^{III} MESO

FIG. 4.5 Porphyrin structures and assignment nomenclature.

FIG. 4.6 PMR spectra of Fe-porphin chloride (A) and Fe-etioporphyrin chloride (B) + 4-methylpyridine at 225°K.



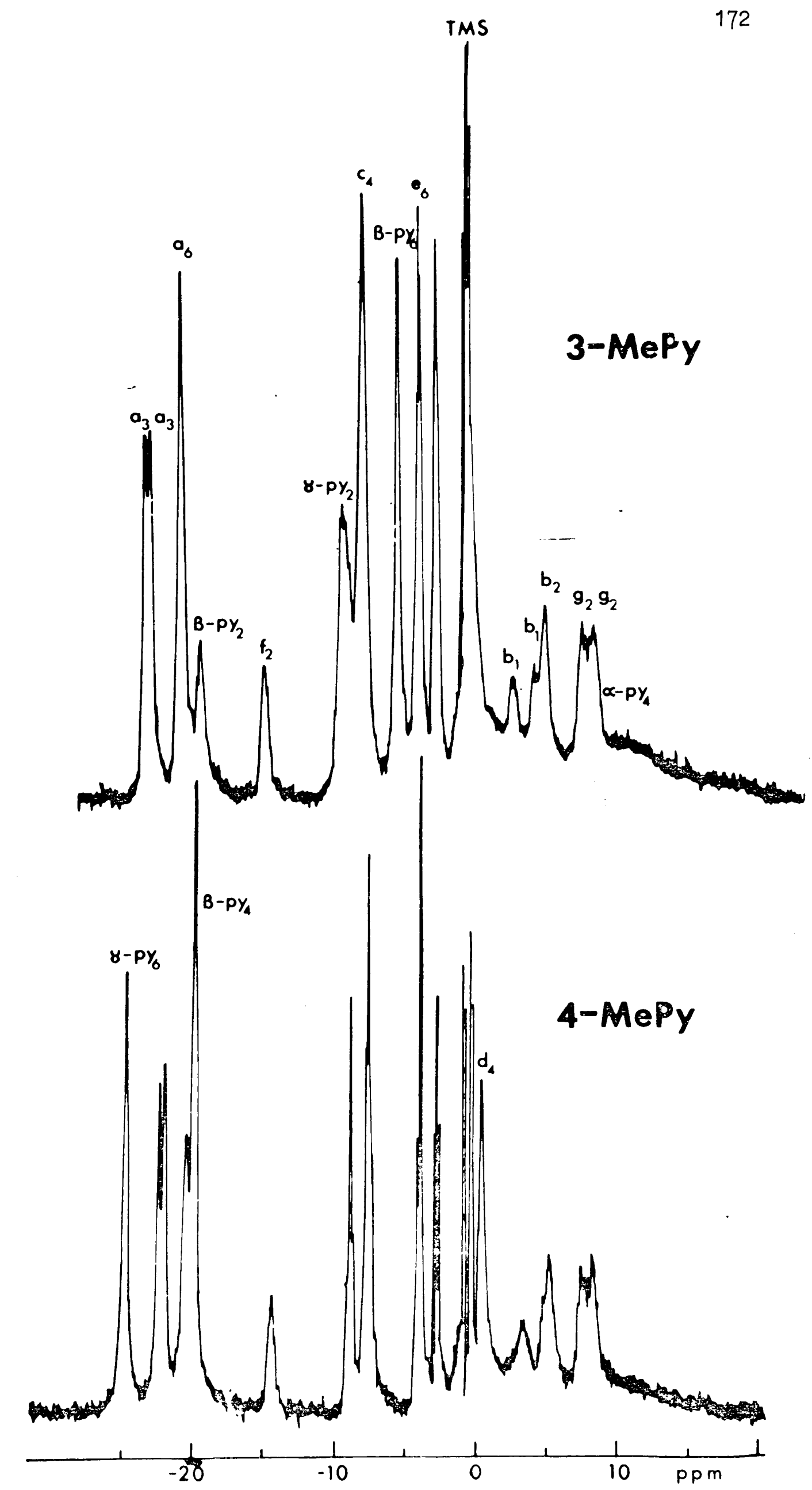


FIG. 4.7 PMR spectra of Fe-protoporphyrin dimethyl ester chloride + 3-methylpyridine and 4-methylpyridine at 219°K.

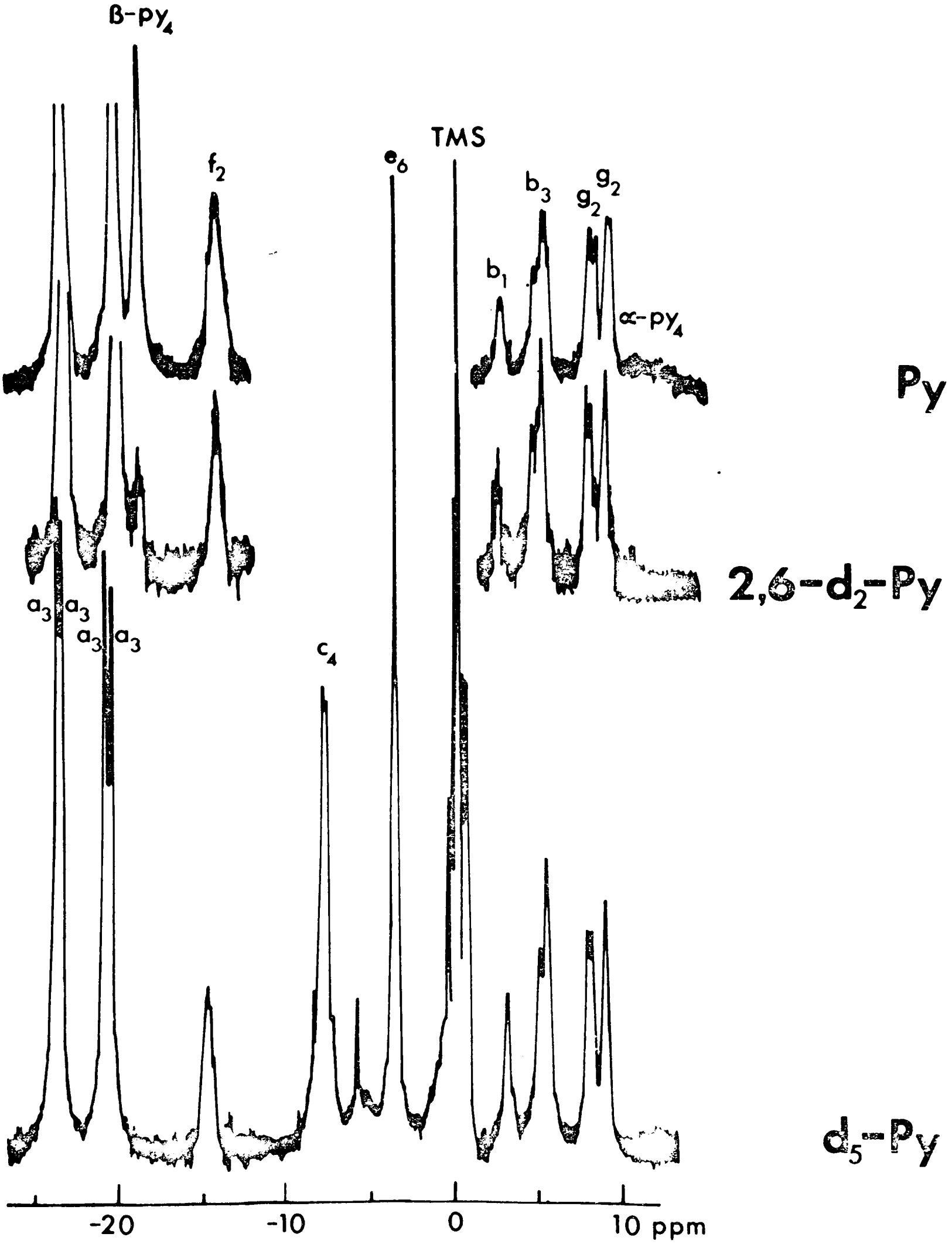


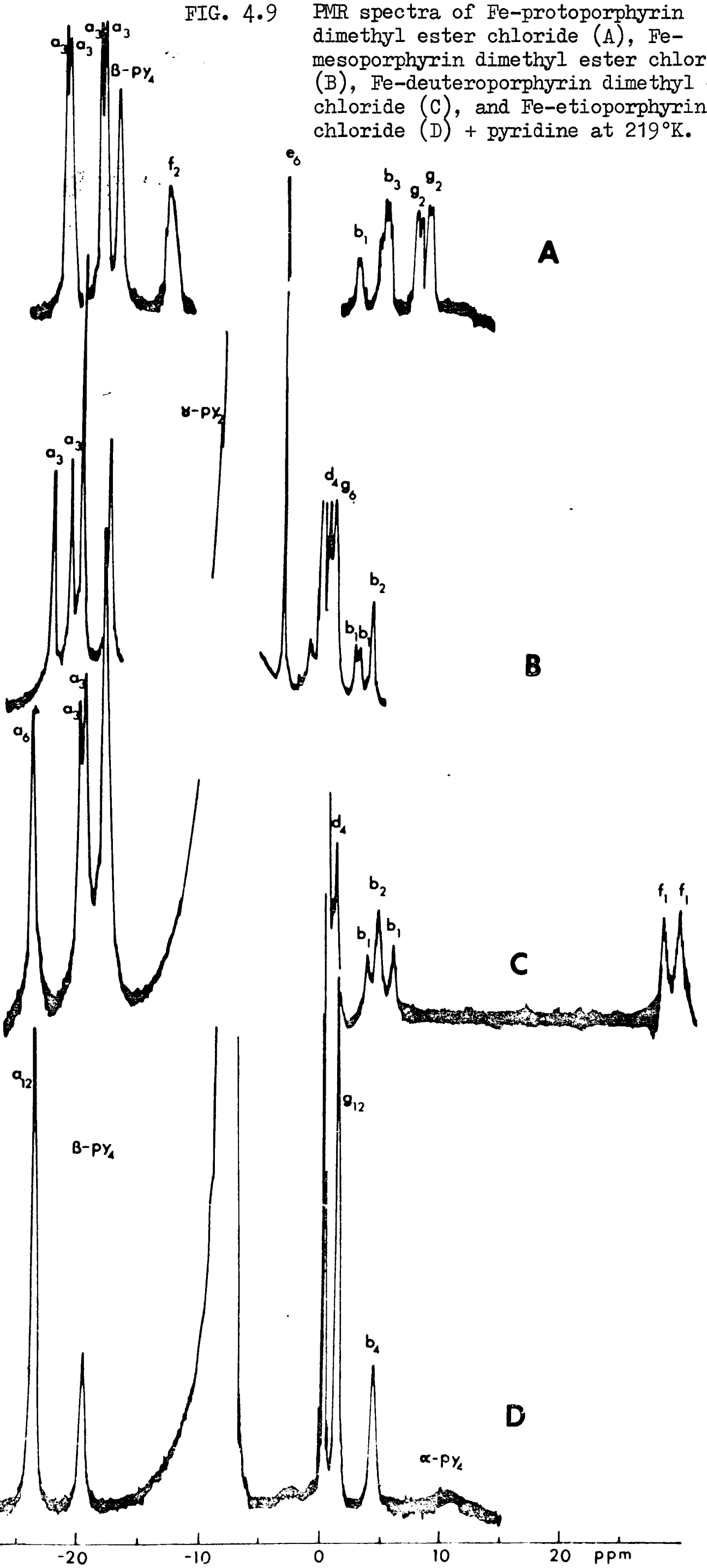
FIG. 4.8 PMR spectra of Fe-protoporphyrin dimethyl ester chloride + 2,6-d_2-pyridine, d_5-pyridine and pyridine at 219°K.

methyl groups at positions 5 and 8 on the porphyrin ring, i.e. adjacent to the propionic acid groups. Of the other two ring methyl resonances, the downfield one is that of the methyl group at position 3 whilst the other is that of the methyl group at position 1. These 4 resonances are most clearly resolved in the spectrum of the bis pyridine complex. By reference to the line broadening studies of Brassington[95], the methene resonance at lowest field is that of the proton at the γ-position on the porphyrin ring. The resonances g are those of the vinyl CH_2 protons at positions 2 and 4, those at position 2 being shifted to highest field.

The format of the spectra can be seen to be dependent on the axial ligand attached to the iron atom. Thus, the resonances of all four porphyrin ring methyl groups are resolved for the bispyridine complex, but two of these resonances coincide for the bis γ-picoline and bis β-picoline complexes. Similarly, the vinyl group resonances g are better resolved in the former complex. All of the expected axial ligand resonances are present, although the γ-protons only emerge from underneath unbound ligand and solvent resonances at temperatures below 210°K. The α-proton resonances are very broad and in some cases at some temperatures are masked by resonances g. That these are the resonances of the α-protons is proved conclusively by the spectrum of the bis 2,6-d_2-pyridine complex, in which the broad signal at ca. 9-12 ppm upfield from TMS, present in the bis pyridine complex, is absent. A diminution in intensity of the resonance corresponding to the β-protons is also observed with the deuterated pyridine complex, and this may be attributed to partial deuteration at the β-positions, as remarked on earlier.

A comparison of the PMR spectra of the bispyridine complexes of a number of natural bispyridinato ferric porphyrins at 219°K is shown in Figure 4.9. Again, a difference in format of the spectra is observed, this time by varying the porphyrin ligand. Thus, the form of the ring

FIG. 4.9 PMR spectra of Fe-protoporphyrin dimethyl ester chloride (A), Fe-mesoporphyrin dimethyl ester chloride (B), Fe-deuteroporphyrin dimethyl ester chloride (C), and Fe-etioporphyrin chloride (D) + pyridine at 219°K.



methyl and meso proton resonances is dependent on the porphyrin, for example the spread of the ring methyl shifts is greatest for deuteroporphyrin, whilst for mesoporphyrin 2 resonances coincide and for etioporphyrin all 4 resonances coincide. Assignments are based on relative intensities of resonances, and by comparison with P.M.R. data for the corresponding biscyano complexes[11]. The empirical observation that protons on carbon atoms bound directly to the porphyrin ring are shifted to the low-field side of their positions in diamagnetic complexes, whilst protons bound directly to the porphyrin ring, or to carbon atoms one atom removed from the porphyrin ring, are shifted to the high-field side of their positions in diamagnetic complexes, is an additional aid in assignment.

All spectra were recorded at temperatures between 300 and 200°K. The spectrum of Fe(III) mesoporphyrin IX dimethyl ester chloride + β-picoline at various temperatures is shown in Figure 4.10 and the dependence of the observed shifts on the reciprocal of the temperature is shown in Figure 4.11. There is a linear dependence on T^{-1} only at low temperatures, and in fact this departure from linearity of the observed shift versus T^{-1} relationship is shown by all the complexes but at different temperatures. This non-linear behaviour is most marked for the ring methyl protons of the porphyrin ligand, for which the slope of the temperature plot changes sign. A complete summary of observed shift data at various temperatures for all the complexes studied is given in Appendix V.

2. Miscellaneous complexes

i) Imidazole

The PMR spectra of the imidazole complexes of Fe(III) porphin chloride and Fe(III) mesoporphyrin IX dimethyl ester chloride at 246°K and 252°K, respectively, are shown in Figure 4.12, and the shift data

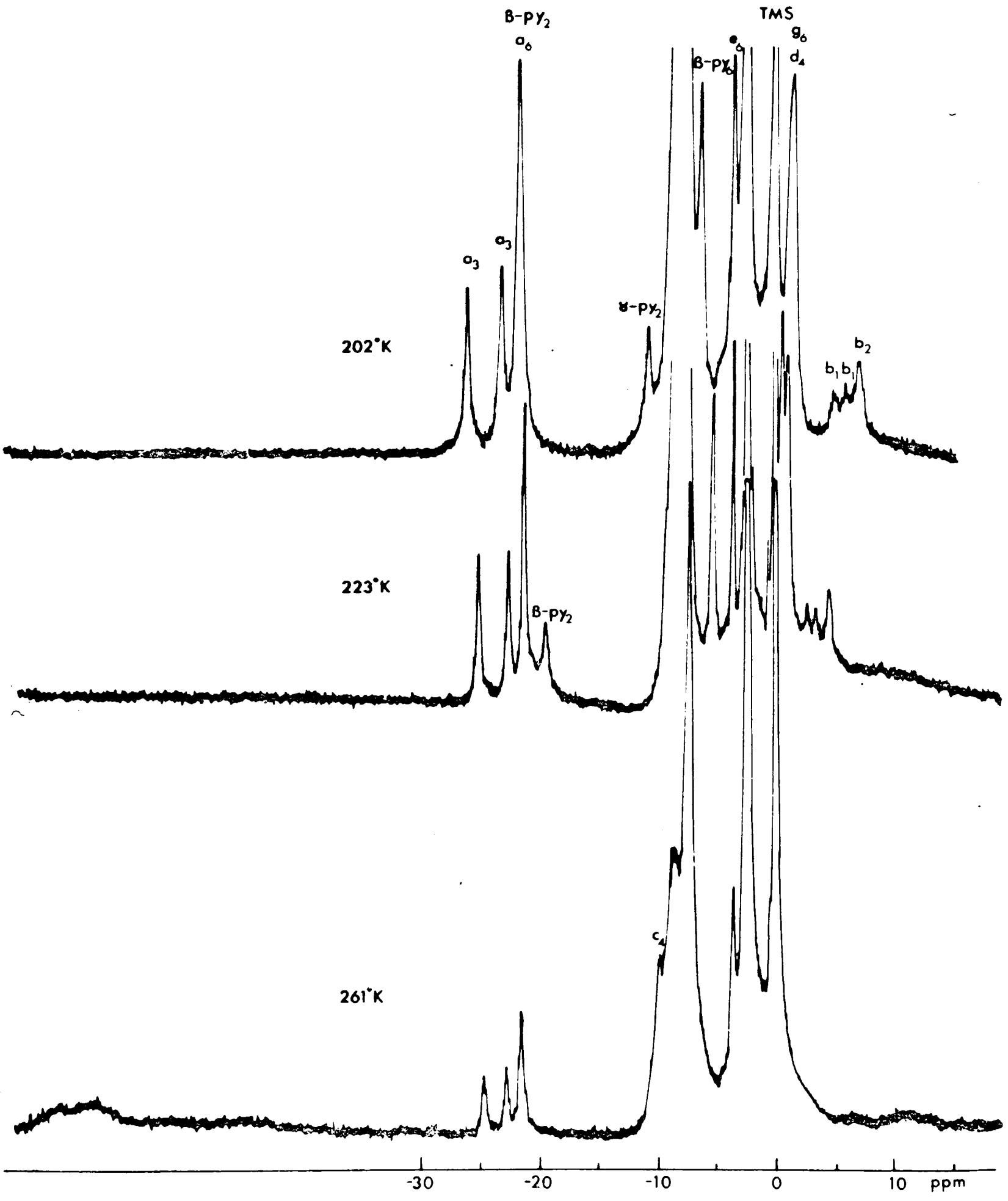
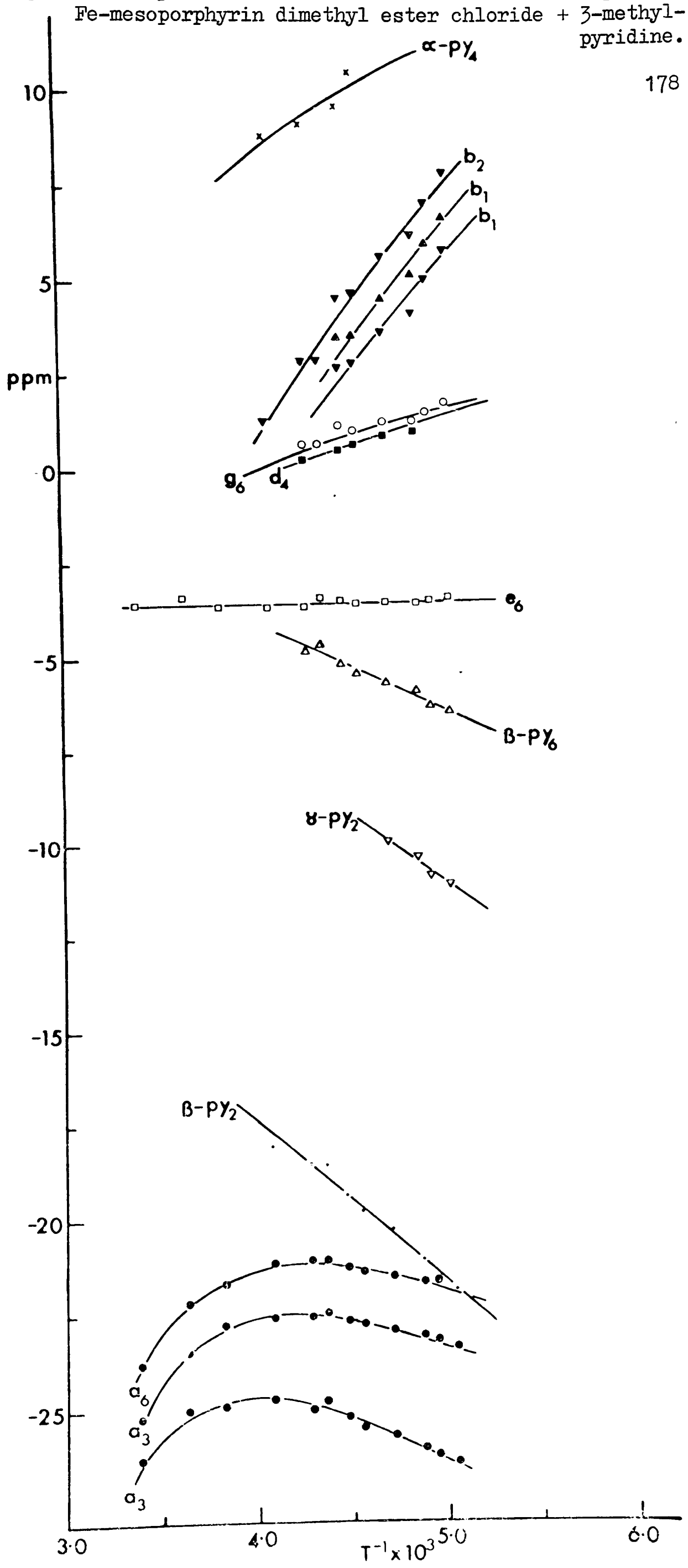


FIG. 4.10 PMR spectrum of Fe-mesoporphyrin dimethyl ester chloride + 3-methylpyridine at various temperatures.

FIG. 4.11 Temperature dependence of observed PMR shifts from spectrum of Fe-mesoporphyrin dimethyl ester chloride + 3-methyl-pyridine.



are given in Appendix V, Tables M and N. The spectra are similar to those of the corresponding bispyridine complexes, except that the magnitude of the observed shifts is smaller for the former than for the latter complexes. Assignments are determined for the porphyrin protons by comparison with bis pyridinato complexes. For the porphin complex this is fairly straightforward. In the case of the meso-porphyrin complex, assignment is a little more difficult. At 252°K, the resonance at -4.0 ppm can readily be assigned to the e_6 protons, and the resonances at -1.0 and +0.7 ppm to the b_4 and d_4/g_6 protons respectively on the basis of relative intensity and analogy with the pyridinato species. The three resonances at lowest field similarly correspond to the a_n protons of the pyridinato species. There are therefore three unassigned resonances at -10.0 ppm, -8.9 ppm and +9.3 ppm.

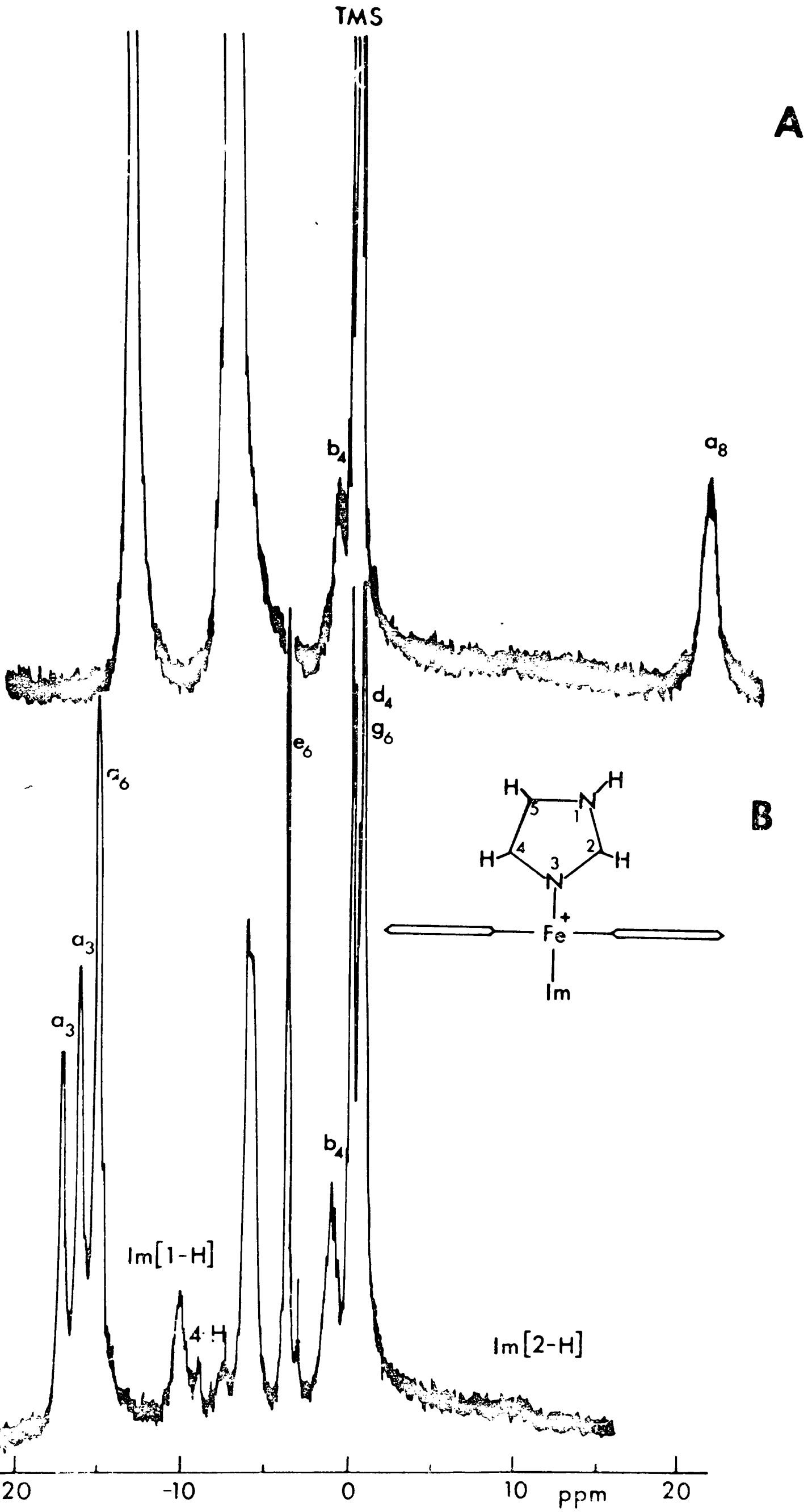
The latter broad resonance is present for the porphin complex, and must therefore arise from an imidazole proton, since the porphyrin resonances are fully assigned for the porphin complex. The resonances at -10.0 and -8.9 ppm are in the region where the c_4 and f_4 resonances would be expected. However these resonances shift downfield as the temperature is lowered, contrary to the trend anticipated for the c_4 and f_4 proton resonances. These observed resonances must therefore arise from imidazole protons. This assignment has been confirmed recently by La Mar and Walker[108].

Plots of the observed shifts against T^{-1} are reproduced in Figure 4.13. Within the limits of experimental error, a linear relationship between the observed shift and T^{-1} is found.

ii) Benzimidazole

The P.M.R. spectrum of Fe(III) mesoporphyrin IX dimethyl ester chloride with benzimidazole at various temperatures is shown in Figure 4.14. A quite dramatic change in the spectrum is observed as the temperature

FIG. 4.12 PMR spectra of Fe-porphin chloride (A) and Fe-mesoporphyrin dimethyl ester chloride (B) + imidazole at 246, 252°K respectively.



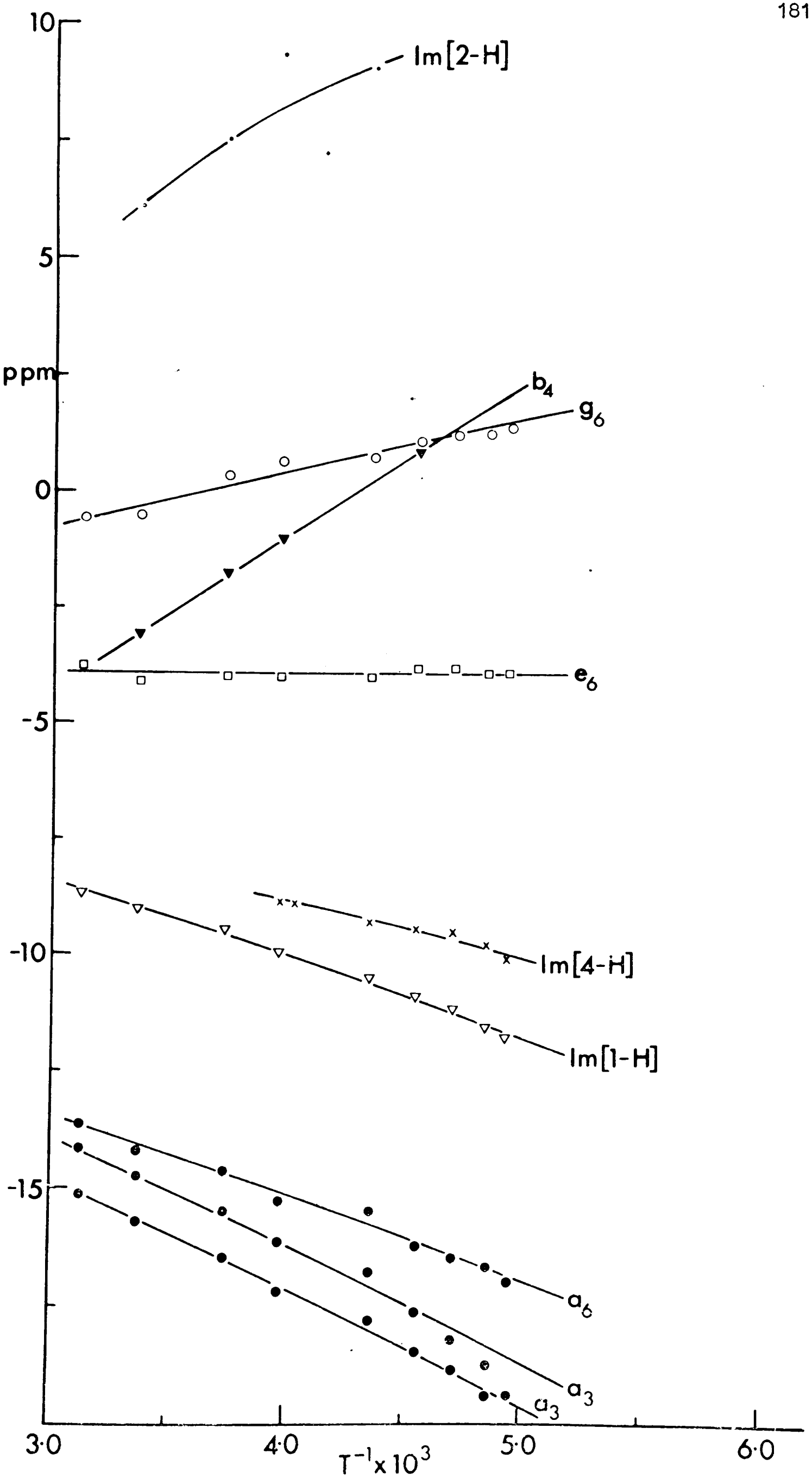


FIG. 4.13 Temperature dependence of observed PMR shifts from spectrum of Fe-mesoporphyrin dimethyl ester chloride + imidazole.

is lowered, and this may be due to a decrease in the ligand exchange rate.

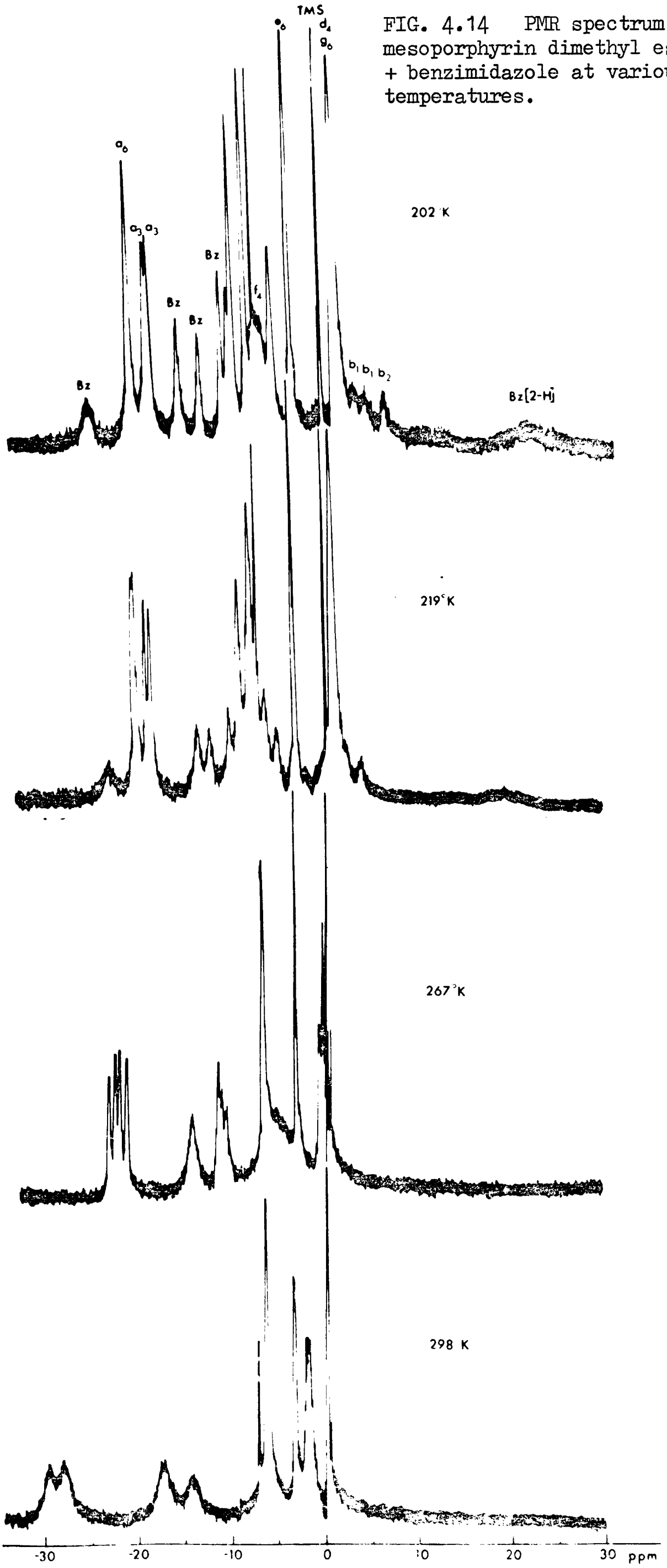
The resonances of the porphyrin ligand protons are easily assigned at lower temperatures by comparison with the corresponding bisimidazole complex, but a number of extra resonances are observed which are assumed to arise from axial ligand protons. In order to help with assignment of the resonances, the 5,6-dimethylbenzimidazole complex spectrum was also examined. The PMR spectra of benzimidazole and 5,6-dimethylbenzimidazole complexes of Fe(III) protoporphyrin IX dimethyl ester chloride have also been studied, and the spectra of these complexes at 216°K are illustrated in Figure 4.15. All the shift data are tabulated in Tables P, Q, R and S of Appendix V.

The assignment of a number of the axial ligand resonances can be made by comparison with the bis-imidazole complex spectrum. Thus the broad resonance in the region +15 to +20 ppm upfield from TMS can be attributed to the protons at position 2. The resonance of these protons might be expected to be broadened considerably due to the proximity of the protons to the metal. The peak at lowest field is assigned to proton 1 by comparison with the imidazole complex spectrum. Three unassigned peaks remain to be considered for the benzimidazole mesoporphyrin complex, two of which shift downfield as the temperature is lowered and the other resonance shifting upfield. Only the two resonances which shift downfield are present for the 5,6-dimethylbenzimidazole complex. The resonance which shifts upfield is tentatively assigned as that of the f_4 protons of the porphyrin ring. Two resonances are also observed for the benzimidazole/protoporphyrin complex which are not specifically assigned although these must both correspond to axial ligand protons.

iii) Quinoline and isoquinoline

The PMR spectra of Fe(III) mesoporphyrin IX dimethyl ester chloride + isoquinoline and Fe(III) protoporphyrin IX dimethyl ester chloride + isoquinoline at 200°K are illustrated in Figure 4.16 and the shift data at

FIG. 4.14 PMR spectrum of Fe-mesoporphyrin dimethyl ester chloride + benzimidazole at various temperatures.



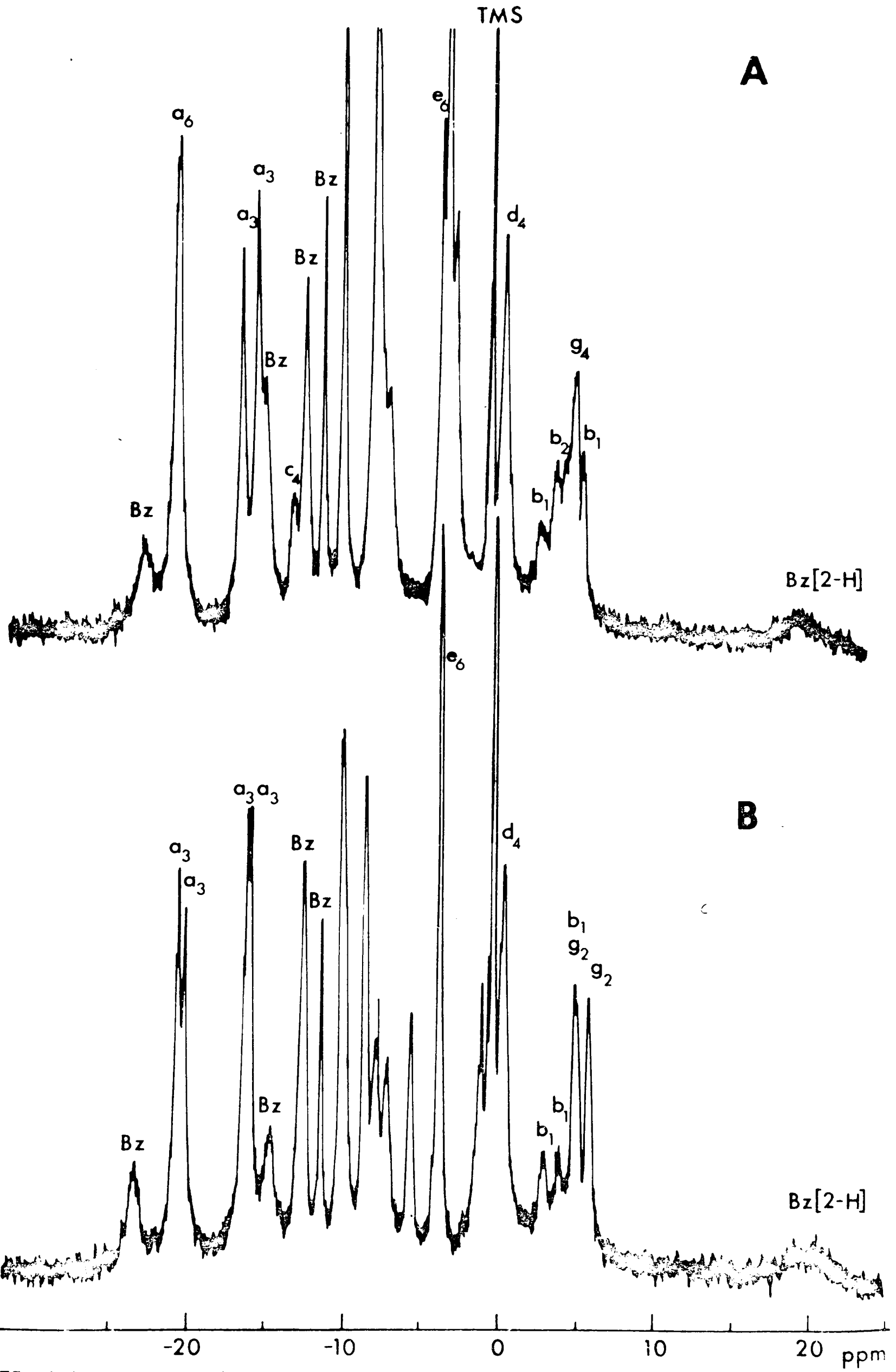


FIG. 4.15 PMR spectra of Fe-protoporphyrin dimethyl ester chloride + 5,6-benzimidazole (A) and benzimidazole (B) at 216°K.

various temperatures are given in Tables T and U in Appendix V. As with the benzimidazole complexes, assignment of the porphyrin ligand protons is straightforward but the axial ligand proton resonances pose some difficulty. Four temperature dependent resonances corresponding to bound isoquinoline protons are observed, and these broaden considerably as the temperature is raised. Above 260°K it is no longer possible to observe them. The relative intensities of the bound isoquinoline resonances provide proof that the species present in solution is the bisisoquinoline complex, since each resonance integrates as two protons.

Although the change is not as dramatic as with the bispyridinato complexes, the plot of observed shift against T^{-1} is not a linear one for some resonances, especially the ring methyl protons. For these protons, the slope of the temperature plot changes sign, as with the bispyridinato complexes.

No similar results were obtained using quinoline instead of isoquinoline. With a very large excess of quinoline, some broad resonances corresponding to low-spin ferric porphyrin ring protons were observed, but no resonances which could be attributed to bound quinoline protons were observed.

4.4 Discussion

1. Pyridinato complexes

i) General features

The results show conclusively that at low temperatures the investigated species in solution are bispyridinato iron (III)-porphyrin complexes. At higher temperatures approaching room temperature, it was not possible to observe sharp resonances due to the coordinated pyridines. Broad resonances present in the region -40 to -50 ppm suggest that the high spin ($S = {}^{5}/_{2}$) iron(III) porphyrin chloride complex is present, due tc dissociation of the axial pyridinato ligands. The exchange

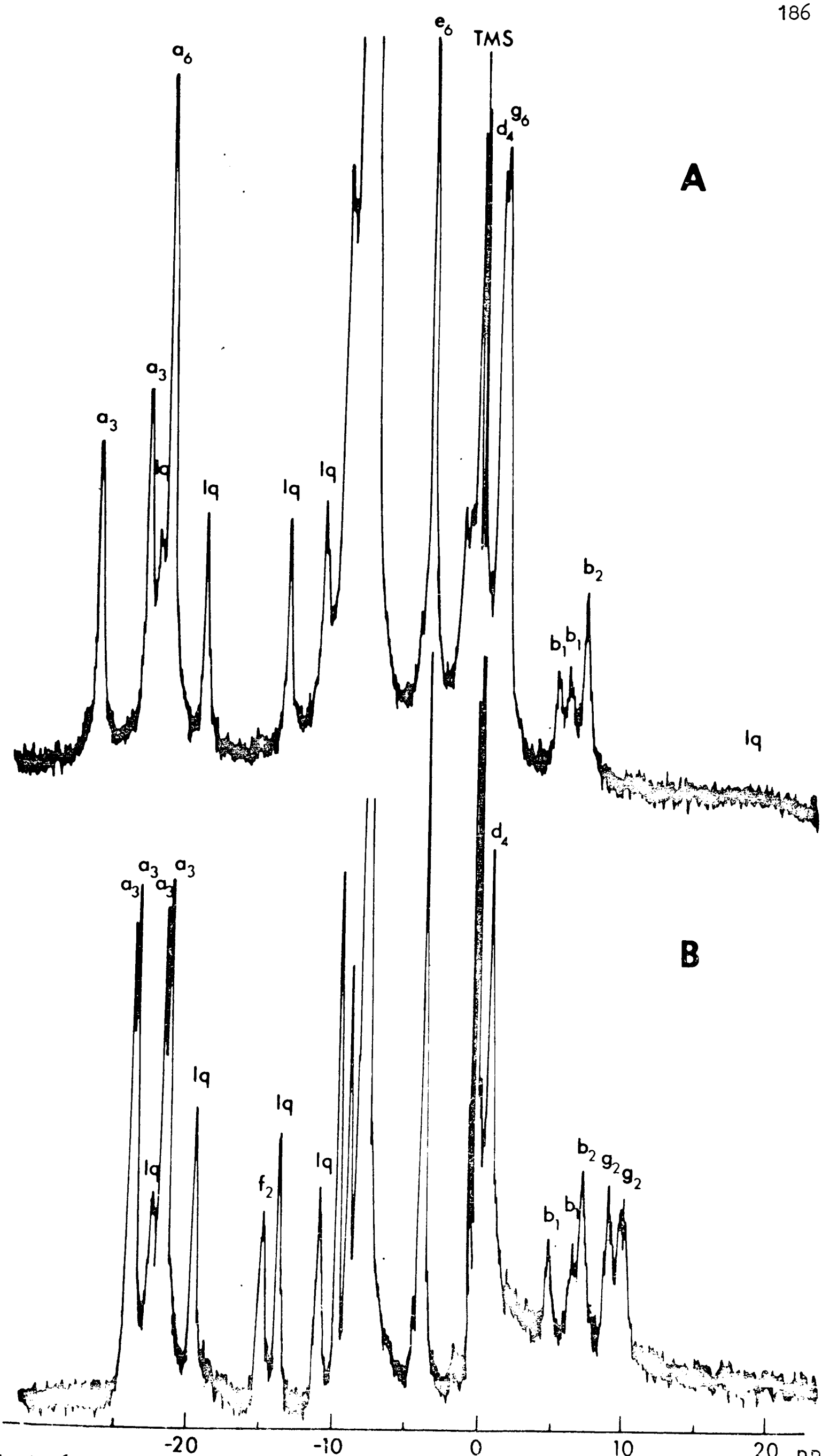


FIG. 4.16 PMR spectra of Fe-mesoporphyrin dimethyl ester chloride (A) and Fe-protoporphyrin dimethyl ester chloride (B) + isoquinoline

rate of free and complexed pyridine at and below 260°K must be much smaller than the frequency shift differences between the protons in the two environments ($< 5 \times 10^{-2}$ sec^{-1}) as separate resonances are observed for free and complexed pyridines.

Above ca. 260°K, the exchange rate of free and complexed pyridine increases rapidly with increase in temperature so that separate resonances for free and complexed pyridines first broaden and then coalesce. Similarly, the resonances of the porphyrin protons broaden above 260°K but because the frequency shift differences of porphyrin protons in the two environments are greater than the frequency shift differences of the two pyridine proton environments, two separate sets of resonances for the porphyrin protons are observed right up to room temperature.

The observation of sharp spectral lines in most of the spectra at 200°K indicates that the complexes are low spin ($S = {}^1/_2$) by analogy with the results of Wüthrich et al[11,48] on the low-spin cyanohemes. Much broader lines are expected for high-spin complexes[42-46] due to the longer electron spin-lattice relaxation time T_{1e}.

ii) Origin of shifts

Both contact and pseudocontact interactions can contribute to the shifts. The general equations for these contributions in axial symmetry have been given in (2.18) and (2.24) respectively. More specifically, in the case of a single populated spin level with negligible contribution from the second order Zeeman (SOZ) term, equations (2.18) and (2.24) may be reduced to

$$\left[\frac{\Delta H}{H_o}\right]^C = \Delta_i^C = \frac{-2\pi a_i \beta S(S+1)(g_{\parallel} + 2g_{\perp})}{\gamma_H \, 9kT} \qquad (4.3)$$

$$\left[\frac{\Delta H}{H_o}\right]^D = \Delta_i^D = -\beta^2 \frac{S(S+1)}{9kT}(g_{\parallel}^2 - g_{\perp}^2)\left(\frac{3\cos^2\theta - 1}{r^3}\right) \qquad (4.4)$$

At low temperature, the observed chemical shifts vary linearly with the inverse of the absolute temperature, T^{-1}, suggesting that the proton resonances are shifted by isotropic interactions represented by equations (4.3) and (4.4) above. According to these equations, extrapolation of the linear portions of the temperature dependence curves to $T^{-1} \longrightarrow 0$ should bring the resonances close to the values observed in diamagnetic complexes.

The chemical shifts of the protons in a number of porphyrins in $CDCl_3$ are given in Table 4.2[11,37,40]. The diamagnetic values for a bis pyridinato Co(III) porphyrin are also given and these do not differ by more than 0.2 ppm from the metal-free porphyrin. In fact, the shift between metal-free and metallo-porphyrin is very small compared to the observed paramagnetic shift, and the values for the metal-free porphyrin resonances were taken as the diamagnetic values throughout.

TABLE 4.2

Diamagnetic porphyrin shifts* relative to TMS

(assignment nomenclature corresponds to Figure 4.5)

PORPHYRIN	a	b	c	d	e	f	g
Porphin	-9.8	-10.6					
Deuteroporphyrin dimethylester	-3.5	-9.9	-4.2	-3.2	-3.6	-8.9	-
Etioporphyrin	-3.6	-10.1				-4.1	-1.9
Protoporphyrin dimethylester	-3.4	-9.6	-4.3	-3.2	-3.6	-6.4	-5.9
Mesoporphyrin dimethylester	-3.5	-10.1	-4.3	-3.2	-3.6	-3.9	-1.8
$(X\text{-py})_2$Co(III)mesoporphyrin dimethylester chloride	-3.7	-10.1	-4.4	-3.2	-3.5	-4.1	-1.9

*in ppm

Most of the resonances do not, however, extrapolate to the diamagnetic values. For example, in Figure 4.11 resonances a extrapolate to ca -15 ppm, d to -6.9, b to -25 and g to -5.6. The pyridine resonances extrapolate

to -1.3 ppm (α-py_4), -0.2 (β-py_2), -5.2 (β-py_6) and -7.6 (γ-py_2).

These results are similar to those obtained by Wüthrich et al[11,48] for the cyanohemes, which were attributed to temperature-dependent changes in conformation. However, a number of other explanations for this non-Curie behaviour present themselves and these are discussed below together with the deviation of the shift/temperature plots from linear behaviour at higher temperatures.

The pseudocontact contributions to the observed isotropic shifts can be estimated from equation (4.4) with a knowledge of molecular geometry and information on magnetic anisotropy. Although many physical properties of metalloporphyrins are known to be sensitive to the pattern of peripheral substitution, alternations in the bond parameters of the porphyrinato core that arise from this source are apparently too small to be certainly identified in any existing X-ray determination of crystalline structure. Thus listed values of the averaged parameters of methoxyiron(III)-mesoporphyrin IX dimethyl ester[4] differ insignificantly from those reported for hemin chloride[97]. Furthermore the spin state of the iron atom has little appreciable effect upon the bond parameters of the porphyrinato core, as the values[5] for low spin ferric tetraphenyl-porphin bisimidazole chloride demonstrate.

Data on g values for bispyridinato iron (III)-porphyrins are scarce. The E.P.R. spectrum of bispyridinato iron(III)-protoporphyrin IX chloride in frozen solution in $CHCl_3$ at 22°K has been obtained[98]. This was found to be typical polycrystalline material with $g_{\parallel} = 3.4$ and $g_{\perp} = 0.58$, an identical $g_{\parallel}$ value to that found for bispyridinato iron(III)-octaethyl-porphin perchlorate (Chapter 3). In the absence of further information on g values, those found for the protoporphyrin complex have been used to calculate pseudocontact shifts, since g values for other porphyrin complexes will not differ widely from these.

iii) Hyperfine shifts of the porphyrin ligand protons

The isotropic shifts Δ_i (in ppm from the diamagnetic values given in Table 4.2) for porphyrin ligand protons of various complexes at 200°K are shown in Table 4.3. Pseudocontact shifts calculated from equation (4.4) are given in Table 4.4, using the g values above and values of r and θ as appropriate. The temperature 200°K was chosen because in this region, the observed chemical shifts vary linearly with the inverse of the absolute temperature. The assumption is made that only the ($S = {}^1/_2$)spin state of the iron atom is populated at this temperature and thus equation (4.4) is applicable for this case.

The pseudocontact values are very much larger than those estimated for the cyanohemes by Wüthrich et al[48], and somewhat larger than those calculated for cyanohemes by Shulman et al[32]. Comparison with experimental values of the isotropic shifts suggests that pseudocontact effects are far too large to be neglected and indeed may constitute the major contribution to the observed shift of some proton resonances. Wüthrich et al[48] observed that there were no shifts in the positions of the methyl and ethyl ester resonances in biscyano complexes of deuterohemin dimethylester and hemin diethylester, as compared to their positions in analogous diamagnetic compounds. From this it was concluded that the experiments indicated $\Delta_i^D < 0.2$ ppm for the methyl ester position, as contact effects were regarded as negligible, and it was concluded that Δ_i^D was negligible for all positions. The reason why the ester groups are not shifted could be that in solution they are out of the porphyrin ring plane, so that $(3\cos^2\theta - 1)$ is small. Also, recent studies[31] have shown that Δ_i^D is not negligible in cyanomyoglobin.

Shulman et al[32], in their analysis of the PMR shifts of cyanohemes, included an orbital reduction factor of 0.75 in the dipolar shift equation to take account of unpaired spin in the iron orbitals. As has been pointed out since[58,59], the application of an orbital reduction

TABLE 4.3

Isotropic shifts* of protons in $(X\text{-}Py)_2Fe(III)$ porphyrin chloride complexes in $CDCl_3$ at 200°K

PORPHYRIN	X	a				b			c	d	e	f		g
Porphin	4-CH_3	+43.7				+18.2			-	-	-	-		-
	(Imid	+38.1				+11.9								)
Deutero	H	-23.3	-18.7	-18.4	-16.7	+15.9	+16.9	+18.3		+5.1	-	+43.6	+45.2	
	4-CH_3	-22.2	-17.5	-16.8	-15.5	+16.1	+16.5	+17.2	+18.5	+5.5	-	+43.0	+44.7	
Etio	H	-21.2				+17.0					-	-3.6	+3.5	
	4-CH_3	-19.8				+17.2					-	-2.8	+3.9	
Proto	H	-21.3	-20.9	-17.8	-17.1	+15.0		+17.6	-2.7	+5.0		-7.4	+15.5	+16.5
	3-CH_3	-20.7	-20.4	-17.9		+14.9	+16.6	+17.4		+4.3		-7.8	+15.5	+16.5
	4-CH_3	-19.8	-16.6	-16.3	-15.8	+15.4		+17.8		+5.4		-6.4	+15.3	+16.3
Meso	H	-21.8	-20.2	-19.1		+15.3	+15.9	+17.1	-3.0	+4.7		-4.1	+3.3	
	3-CH_3	-22.9	-19.9	-18.4		+15.5	+16.4	+17.4		+4.6			+3.4	
	4-CH_3	-20.6	-18.5	-17.6		+15.9	+16.5	+17.8	-1.4	+5.2			+3.8	
	(Imid	-15.9	-15.2	-13.3		+12.5							+3.5	)

Imidazole complex data in parentheses for comparison.

*ppm from diamagnetic values.

TABLE 4.4

Calculated pseudocontact shifts of porphyrin protons in $(X\text{-}Py)_2$ Fe(III)-porphyrin chloride complexes at 200°K

Porphyrin		a	b	c	d	e	f	g
	r(Å)	5.7	4.5					
Porphin	θ°	90	90					
	Δ_i^D(ppm)	+15.7	+32.0					
	r(Å)	6.4	4.5	6.4	7.4	10.1	5.7	
Deutero	θ°	90	90	90	75	90	90	
	Δ_i^D(ppm)	+11.1	+32.0	+11.1	+5.7	+2.8	+15.7	
	r(Å)	6.4	4.5				6.4	7.4
Etio	θ°	90	90				90	75
	Δ_i^D(ppm)	+11.1	+32.0				+11.1	+5.7
	r(Å)	6.4	4.5	6.4	7.4	10.1	6.4	
Proto	θ°	90	90	90	75	90	90	
	Δ_i^D(ppm)	+11.1	+32.0	+11.1	+5.7	+2.8	+11.1	
	r(Å)	6.4	4.5	6.4	7.4	10.1	6.4	7.4
Meso	θ°	90	90	90	75	90	90	75
	Δ_i^D(ppm)	+11.1	+32.0	+11.1	+15.7	+2.8	+11.1	+5.7

factor in this manner appears to be an incorrect procedure since the measured g-values reflect the behaviour of the electronic paramagnetic in an applied magnetic field and any orbital reduction effects are embodied therein.

The hyperfine (contact) shifts, Δ_i^C, given in Table 4.5 are found by subtraction of pseudocontact shifts calculated at 200°K in Table 4.4 from the corresponding isotropic shifts in Table 4.3. A dependence of the hyperfine shifts on the nature of the substituent X is observed. Thus the magnitudes of hyperfine shifts are in the order pyridine > 3-methylpyridine > 4-methylpyridine compared with the pK_a order 4-methylpyridine > 3-methylpyridine > pyridine.

The hyperfine constants may be calculated using equation (4.3) since apart from a_i, all other parameters are known. From these constants, π-electron spin densities can be derived from the McConnell relationships (2.21) and (2.22). However, the assumptions built into (2.22) as described in Chapter 2 restrict its general applicability, and the spin densities quoted are only a qualitative guide. A value for Q_H of -6.5×10^7 Hz was taken. The value of Q_{CH_3} is known not to be constant for methyl groups attached to an aromatic ring, as explained in Chapter 2. A value for Q_{CH_3} of 4×10^7 Hz was taken, which is smaller than the oft-quoted value of 7×10^7 Hz but not outside the range of previous assignments[32,49]. The hyperfine interaction data are given in Table 4.6.

TABLE 4.5

Hyperfine shifts of porphyrin protons in $(X\text{-}Py)_2Fe(III)$-porphyrin chloride complexes in $CDCl_3$ at 200°K

PORPHYRIN	X	a				b			c	d	e	f		g
Porphin	4-CH_3	+28.0				-13.8								
	(Imid	+30.3				-3.9								)
Deutero	H	-34.4	-29.8	-29.5	-27.8	-16.1	-15.1	-13.7		-0.6		+27.9	+29.5	
	4-CH_3	-33.3	-28.6	-27.9	-26.6	-15.9	-15.5	-14.8 -13.5		0		+27.3	+29.0	
Etio	H	-32.3				-15.0						-14.7		-2.2
	4-CH_3	-30.9				-14.8						-13.9		-1.8
Proto	H	-32.4	-32.0	-28.9	-28.2	-17.1		-14.5	-13.8	-0.7		-18.5		
	3-CH_3	-31.8	-31.5	-29.0		-17.1	-15.4	-14.6		-1.4		-18.9		
	4-CH_3	-30.9	-27.7	-27.4	-26.9	-16.6		-14.2		-0.3		-17.5		
Meso	H	-32.9	-31.3	-30.2		-16.7	-16.2	-14.9	-14.1	-1.1		-15.2		-2.5
	3-CH_3	-34.0	-31.0	-29.5		-16.5	-15.6	-14.6		-1.1				-2.3
	4-CH_3	-31.7	-29.6	-28.7		-16.1	-15.5	-14.2	-12.5	-0.6				-2.0
	(Imid	-21.4	-20.7	-18.8				-9.9						-0.5)

TABLE 4.6

Hyperfine interaction data for some porphyrin protons of $(X\text{-}Py)_2Fe(III)$-porphyrin chloride complexes in $CDCl_3$ at 200°K

Porphyrin	Parameter	X	a	b	f	g
	Δ_i^c (ppm)	4-CH_3	+28.0	-13.8		
Porphin	a_i (10^5 Hz)	4-CH_3	-9.36	+4.61		
	ρ_c^π (% of 1 unpaired electron)	4-CH_3	+1.4	-0.71		
	Δ_i^c (ppm)	H	-34.4 -29.8 -29.5 -27.8	-16.1 -15.1 -13.7	+27.9 +29.5	
		4-CH_3	-33.3 -28.6 -27.9 -26.6	-15.9 -15.5 -14.8 -13.5	+27.3 +29.0	
Deutero	a_i (10^5 Hz)	H	+11.5 +9.96 +9.86 +9.29	+5.38 +5.05 +4.58	-9.32 -9.86	
		4-CH_3	+11.1 +9.56 +9.32 +8.89	+5.31 +5.18 +4.95 +4.51	-9.12 -9.69	
	ρ_c^π (% of 1 unpaired electron)	H	+2.9 +2.5 +2.5 +2.3			
		4-CH_3	+2.8 +2.4 +2.3 +2.2			
	Δ_i^c (ppm)	H	-32.3	-15.0	-14.7	-2.2
		4-CH_3	-30.9	-14.8	-13.9	-1.8
Etio	a_i (10^5 Hz)	H	+10.8	+5.01	+4.91	+0.74
		4-CH_3	+10.3	+4.95	+4.64	+0.60
	ρ_c^π (% of 1 unpaired electron)	H	+2.7			
		4-CH_3	+2.6			

(Cont.)

TABLE 4.6 (Cont.)

Porphyrin	Parameter	X	a			b			f	g
Proto	Δ_i^c (ppm)	H	-32.4	-32.0	-28.9 -28.2	-17.1		-14.5		
		3-CH_3	-31.8	-31.5	-29.0	-17.1	-15.4	-14.6		
		4-CH_3	-30.9	-27.7	-27.4 -26.9		-16.6	-14.2		
	a_i (10^5 Hz)	H	+10.8	+10.7	+9.66 +9.42	+5.71		+4.85		
		3-CH_3	+10.6	+10.5	+9.69	+5.71	+5.15	+4.88		
		4-CH_3	+10.3	+9.26	+9.16 +8.99		+5.55	+4.74		
	ρ_c^π (% of 1 unpaired electron)	H	+2.7	+2.7	+2.4 +2.4					
		3-CH_3	+2.7	+2.6	+2.4					
		4-CH_3	+2.6	+2.3	+2.3 +2.3					
Meso	Δ_i^c (ppm)	H	-32.9	-31.3	-30.2	-16.7	-16.2	-14.9	-15.2	
		3-CH_3	-34.0	-31.0	-29.5	-16.5	-15.6	-14.6		
		4-CH_3	-31.7	-29.6	-28.7	-16.1	-15.5	-14.2		
	a_i (10^5 Hz)	H	+11.0	+10.5	+10.1	+5.58	+5.41	+4.98	+5.08	
		3-CH_3	+11.4	+10.4	+9.86	+5.51	+5.21	+4.88		
		4-CH_3	+10.6	+9.89	+9.59	+5.38	+5.18	+4.74		
	ρ_c^π (% of 1 unpaired electron)	H	+2.8	+2.6	+2.5					
		3-CH_3	+2.9	+2.6	+2.5					
		4-CH_3	+2.7	+2.5	+2.4					

iv) Hyperfine shifts of the pyridinato ligand protons

The diamagnetic shifts of complexed pyridine protons in porphyrin complexes are given in Table 4.7 below. The values given for the pyridine complex are those quoted[99] for the bispyridinatocobalt(III) mesoporphyrin IX dimethyl ester acetate, whilst those for the methylpyridine complexes are for the bismethylpyridinatocobalt(III)mesoporphyrin IX dimethyl ester chloride.

TABLE 4.7

Diamagnetic shifts* of pyridine protons of pyridinatocobalt(III) porphyrin complexes

Axial Ligand	α-py$_4$	β-py$_2$	β-py$_4$	β-py$_6$	γ-py$_2$	γ-py$_6$
Pyridine	0		-4.7		-5.9	
3-Methylpyridine	0	-4.7		-0.6	-5.6	
4-Methylpyridine	0		-4.6		-1.3	

*ppm from TMS

The diamagnetic values of pyridine protons complexed with porphyrins other than mesoporphyrin are not expected to differ very widely from these values. The isotropic shifts Δ_i (in ppm from the diamagnetic values given in Table 4.7) for pyridinato ligand protons of various complexes at 200°K are given in Table 4.8, and pseudocontact shifts calculated from equation (4.4) at 200°K given in Table 4.9 using values of r and θ shown.

In calculating r and θ, a bond length of 2.0 Å for the Fe-pyridine bond was assumed. This seems reasonable in view of typical values quoted in the literature for complexing bond lengths of 1.97 Å (for bisimidazole Fe(III)-tetraphenylporphin chloride[5]) and 2.13 Å (for bispiperidine Fe(II)-tetraphenylporphin[6]). It might be expected that steric interactions of

TABLE 4.8

Isotropic shifts* of pyridine protons in $(X\text{-}Py)_2Fe(III)$-porphyrin chloride complexes in $CDCl_3$ at 200°K

PORPHYRIN	X	α-py$_4$	β-py$_2$	β-py$_4$	β-py$_6$	γ-py$_2$	γ-py$_6$
Porphin	4-CH_3	+12.1		-17.8			-26.9
Deutero	H	+11.7		-17.6			
	4-CH_3	+10.4		-18.9			-26.7
Etio	H	+10.9		-17.7		-5.0	
	4-CH_3	+10.2		-18.1			-25.3
Proto	H	+11.9		-16.7		-3.9	
	3-CH_3	+12.0	-16.5		-5.3	-5.1	
	4-CH_3	+11.4		-18.4			-26.4
Meso	H	+11.0		-17.0		-4.7	
	3-CH_3	+11.2	-17.0		-5.7	-5.3	
	4-CH_3			-17.9			-25.4

*ppm from diamagnetic values.

TABLE 4.9

Calculated pseudocontact shifts of pyridinato protons in $(X\text{-}Py)_2$-Fe(III)-porphyrin chloride complexes at 200°K

X	Parameter	α-py$_4$	β-py$_2$	β-py$_4$	β-py$_6$	γ-py$_2$	γ-py$_6$
	r (Å)	3.0		5.1		5.9	
H	θ°	44		25		0	
	Δ_i^D (ppm)	-59.6		-32.1		-28.4	
	r (Å)	3.0	5.1		5.8	5.9	
3-CH_3	θ°	44	25		30	0	
	Δ_i^D (ppm)	-59.6	-32.1		-18.7	-28.4	
	r (Å)	3.0		5.1			6.8
4-CH_3	θ°	44		25			9
	Δ_i^D (ppm)	-59.6		-32.1			-17.9

the porphinato core with the neighbouring pair of hydrogen atoms on each pyridine ring would be greater than with the imidazole complex, but not as great as those with the piperidine complex. Furthermore, π back bonding might be expected to decrease the Fe-N distance in pyridine complexes from that in piperidine complexes where π back bonding is not feasible. Thus, a Fe-N bond distance of about 2.0 Å is indicated for the bispyridine complex.

The hyperfine (contact) shifts, Δ_i^c, for pyridinato ligand protons given in Table 4.10 are found by subtracting the pseudocontact shifts calculated in Table 4.9 from the corresponding isotropic shifts in Table 4.8.

TABLE 4.10

Hyperfine shifts of pyridinato protons in $(X\text{-}Py)_2Fe(III)$-porphyrin chloride complexes in $CDCl_3$ at 200°K

PORPHYRIN	X	α-py$_4$	β-py$_2$	β-py$_4$	β-py$_6$	γ-py$_2$	γ-py$_6$
Porphin	4-CH_3	+71.7		+14.3			-9.0
Deutero	H	+71.3		+14.5			
	4-CH_3	+70.0		+13.2			-8.8
Etio	H	+70.5		+14.4		+23.4	
	4-CH_3	+69.8		+14.0			-7.4
Proto	H	+71.5		+15.4		+24.5	
	3-CH_3	+71.6	+15.6		+13.4	+23.3	
	4-CH_3	+71.0		+13.7			-8.5
Meso	H	+70.6		+15.1		+23.7	
	3-CH_3	+70.8	+15.1		+13.0	+23.1	
	4-CH_3			+14.2			-7.5

TABLE 4.11

Hyperfine interaction data for some pyridinato protons of $(X\text{-}Py)_2$-Fe(III)-porphyrin chloride complexes in $CDCl_3$ at 200°K

PORPHYRIN	Parameter	X	α-py$_4$	β-py$_2$	β-py$_4$	β-py$_6$	γ-py$_2$	γ-py$_6$
Porphin	Δ_i^c(ppm)	4-CH_3	+71.7		+14.3			-9.0
	$a_i(10^5$ Hz)	4-CH_3	-24.0		-4.78			+3.01
	ρ_c^π (% of 1 unpaired electron)	4-CH_3	+3.7		+0.74			+0.75
Deutero	Δ_i^c(ppm)	H	+71.3		+14.5			
		4-CH_3	+70.0		+13.2			-8.8
	$a_i(10^5$ Hz)	H	-23.8		-4.85			
		4-CH_3	-23.4		-4.41			+2.94
	ρ_c^π (% of 1 unpaired electron)	H	+3.7		+0.75			
		4-CH_3	+3.6		+0.68			+0.74
Etio	Δ_i^c(ppm)	H	+70.5		+14.4		+23.4	
		4-CH_3	+69.8		+14.0			-7.4
	$a_i(10^5$ Hz)	H	-23.6		-4.81		-7.82	
		4-CH_3	-23.3		-4.68			+2.47
	ρ_c^π (% of 1 unpaired electron)	H	+3.6		+0.74		+1.2	
		4-CH_3	+3.6		+0.72			+0.62
Proto	Δ_i^c(ppm)	H	+71.5		+15.4		+24.5	
		3-CH_3	+71.6	+15.6		+13.4	+23.3	
		4-CH_3	+71.0		+13.7			-8.5
	$a_i(10^5$ Hz)	H	-23.9		-5.15			
		3-CH_3	-23.9	-5.21		-4.48	-8.19	
		4-CH_3	-23.7		-4.58		-7.79	+2.84
	ρ_c^π (% of 1 unpaired electron)	H	+3.7		+0.79			
		3-CH_3	+3.7	+0.80		-1.12	+1.3	
		4-CH_3	+3.6		+0.71		+1.2	+0.71

(Cont.)

TABLE 4.11 (Cont.)

PORPHYRIN	Parameter	X	α-py$_4$	β-py$_2$	β-py$_4$	β-py$_6$	γ-py$_2$	γ-py$_6$
Meso	Δ_i^c (ppm)	H	+70.6		+15.1		+23.7	
		3-CH_3	+70.8	+15.1		+13.0	+23.1	
		4-CH_3			+14.2			-7.5
	a_i(10^5 Hz)	H	-23.6		-5.05		-7.92	
		3-CH_3	-23.7	-5.05		-4.34	-7.72	
		4-CH_3			-4.74			+2.51
	ρ_c^π (% of 1 unpaired electron)	H	+3.6		+0.78		+1.2	
		3-CH_3	+3.6	+0.78		-1.09	+1.2	
		4-CH_3			+0.73			+0.63

v) Non-Curie behaviour of chemical shifts

Equations (4.3) and (4.4) show that both contact and pseudocontact shifts should vary inversely with the absolute temperature. Thus it follows that a plot of observed chemical shift against $^1/T$ should be linear and extrapolation to $T^{-1} \longrightarrow 0$ should bring the resonances close to the values observed in diamagnetic complexes. That neither of these occurs demonstrates either false assumptions in derivation of these equations or else the presence of factors not taken into account by the underlying theory.

a) Deviation of the temperature dependence plots from linearity

In nearly all cases, plots of observed shift against $^1/T$ become non-linear as the temperature rises above ca. 220°K. The deviations from linearity are most marked for the ring methyl protons (a), where the slopes of the curves become zero at a particular temperature, T_c, and thereafter are positive up to room temperature. The values of T_c observed for the $(X\text{-}Py)_2Fe(III)$-porphyrin dimethyl ester chloride complexes are given in Table 4.12 below.

TABLE 4.12

Values of T_c observed for $(X\text{-}Py)_2Fe(III)$-porphyrin dimethyl ester chloride complexes

PORPHYRIN	pK_3*[100]	AXIAL LIGAND	pK_a[101]	T_c
Proto	4.8	Pyridine	5.17	250
		3-methylpyridine	5.60	250
		4-methylpyridine	6.02	255
Deutero	5.5	pyridine	5.17	265
		4-methylpyridine	6.02	275
Meso	5.8	pyridine	5.17	255
		3-methylpyridine	5.60	250
		4-methylpyridine	6.02	265

*These data pertain to the equilibrium between neutral porphyrin and monocation in 2.5% sodium dodecyl sulphate at 25°.

These values are dependent on the nature of the substituent, a decrease being observed with decrease in pK_a of the base, and are also slightly dependent on the porphyrin, a decrease being observed with decrease in pK_3 of the porphyrin.

A dependence of the resonance line widths on temperature is also observed. The broadening of lines at low temperature may be attributed to an increase in the electron relaxation time, T_{1e}, but the broadening near room temperature cannot be explained in this way. The latter broadening begins at about $T = T_c$ and increases so that lines are no longer observable at about $T = T_c + 40^{o}K$.

These observations may be explained by either (a) exchange effects or (b) the presence of a spin equilibrium.

As the temperature is increased, the rate of exchange between bound and unbound pyridinato species would be anticipated to increase as a result of the increase in kinetic energy of the pyridinato species in bulk solution. As a result, all resonances would be expected to sharpen if the exchange rate situation changed from the intermediate to the fast exchange situation. This might be countered by a tendency that greater dissociation of the complexed axial ligand at higher temperature would produce more porphyrin species with metal spin state $S = {}^{5}/_{2}$, i.e. akin to the five coordinate complex. However, the fact that separate broad resonances corresponding to those of the high spin 5-coordinate chloro-complex are observed at room temperature would seem to disprove this theory.

The observations are consistent with the formation of a high spin complex as the temperature increases, with the rate of exchange between the two spin states being very much greater than the frequency shift difference of the protons in the two environments, so that a single resonance is observed for each set of protons. Increase in pK_a of the

axial ligand would be expected to favour formation of the low-spin complex with respect to the high-spin complex, since the positive charge on the iron atom is thereby decreased, thus raising the energy of the metal orbitals (see later). A similar result might be expected for increase in pK_3 of the porphyrin ligand.

Formation of a high-spin complex would almost certainly result in a greater metal-axial ligand bond distance due to increased electron-electron repulsion terms. Thus continuous change in the geometric parameters in (4.4) over a temperature range could lead to deviations from linearity for the pyridinato proton resonance temperature dependences. The metal-porphinato bond distances are more fixed than those of the metal-pyridinato distances, in view of the constraints exerted by the "hole" in the porphyrin skeleton occupied by the metal. It is possible though that with a high-spin bis axial complex, the iron atom is no longer centrally situated but displaced, thus affecting bonding parameters.

N.B. It must be stressed that these deviations from Curie behaviour must arise from <u>intrinsic</u> spin-equilibrium properties of the complexes and not from temperature-dependent equilibria between <u>different</u> species, since the phenomena are observed even at temperatures where the co-ordinated pyridine to porphyrin ratio is known to be 2:1 from relative intensities of proton resonances.

In line with the results from the synthetic porphyrin complexes of Chapter 3, a spin equilibrium is proposed.

b) <u>Extrapolation anomalies in the temperature dependence plots</u>

In nearly all cases, extrapolation of the linear portion of the plot of observed shift against T^{-1} to infinitely high temperature (i.e. $T^{-1} \longrightarrow 0$) fails to produce that value of the NMR shift observed in comparable diamagnetic complexes, in general the value at $T^{-1} = 0$ being

more negative than the diamagnetic value. These results are similar to those obtained by Wüthrich et al[11,48] for the cyanohemes, for which temperature-dependent changes in conformation were invoked.

A recent investigation[59] of theoretical predictions for the temperature dependences of both dipolar and contact contributions to isotropic shifts in low-spin iron (III) systems concluded that such anomalies in the extrapolation to $T^{-1} = 0$ were both expected and explicable. The basis of these apparent anomalies is a non-Curie behaviour of the total axial anisotropy arising from three sources:

(a) a SOZ anisotropy contribution which is opposite in sign from the FOZ term and relatively independent of temperature;

(b) thermal depopulation of the lowest Kramers doublet which increases with temperature;

(c) thermal population of the first excited Kramers doublet which has a FOZ anisotropy opposite in sign from that of the ground doublet.

Effects (b) and (c), which amplify one another, can cause significant non-Curie behaviour even in the absence of SOZ effects. As explained more fully in Chapter 3, non-zero extrapolated intercepts of plots of isotropic shift against T^{-1} on the T^{-1} axis are to be expected. For pure contact shifts such intercepts will generally be negative. For dipolar shifts, intercepts of either sign may be obtained, with positive ones likely in highly anisotropic systems.

In this case, all the intercepts are negative and this would indicate a predominance by the contact interaction.

vi) Bonding interactions in porphyrin complexes

a) Porphyrin-metal bonding

A simple description[102,103] of the orbital energies is given in Figure 4.17. Since the orbital ground state for low-spin ferric porphyrins is ^2E in effective fourfold symmetry, this $(b_{2g})^2(e_g)^3$ state

places the unpaired electron in either the π bonding d_{xz} or d_{yz} orbitals and can be delocalised into any e(π) orbital on the porphyrin.

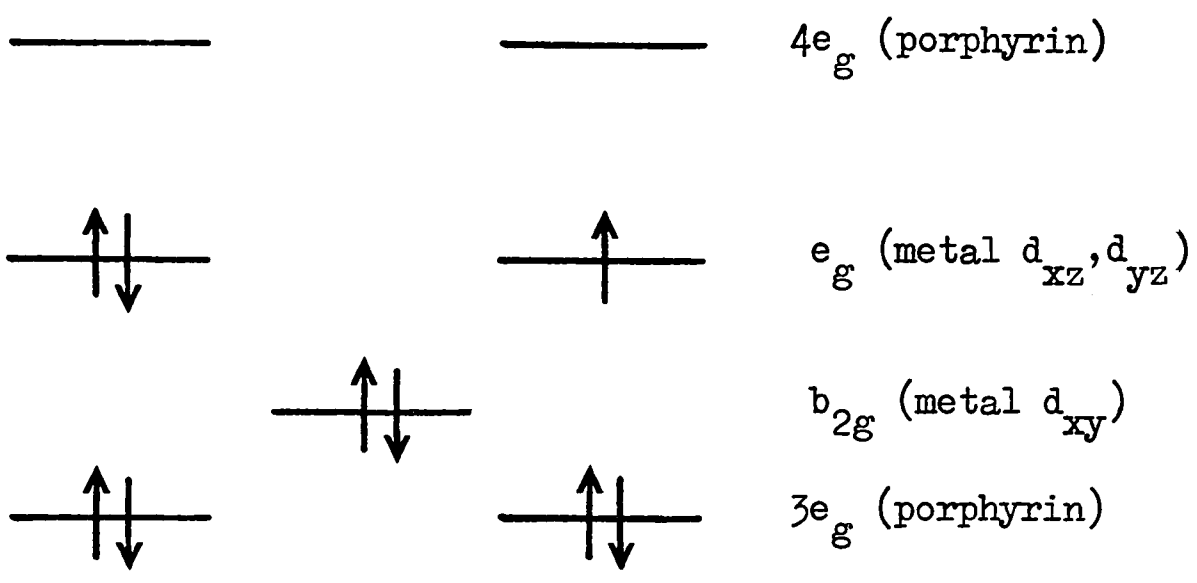


Figure 4.17: Top-filled and lowest empty π orbitals of iron (III)-porphyrin complexes.

The spin can be delocalised via interaction between metal e_g and filled porphyrin $3e_g$ (which can be stated as "ligand to metal charge transfer") or by interaction of the metal e_g with $4e_g$ of the porphyrin ("metal to ligand charge transfer"). (The symmetry labels for the D_{4h} point group are used although the real symmetry is lower.) Out of these ligand e(π) orbitals with energies suitable for significant metal-ligand mixing, simple Hückel MO calculations[102] predict large meso-carbon spin density and much smaller pyrrole carbon spin density for the lowest vacant π MO $4e_g(\pi^*)$, whilst the highest filled MO, $3e_g(\pi)$, possesses nodes through the meso carbons and should exhibit large positive pyrrole spin density.

The hyperfine interaction data for the porphyrin ligand protons, although capable of interpretation in terms of either mechanism, are more consistent with a prevailing spin transfer involving ligand to metal charge transfer out of the highest filled π MO, $3e_g$. Thus in

Table 4.6 the contact shifts and hyperfine constants for pyrrole protons (a) of the porphin complex are more than twice as large as those for the meso-protons (b).

Such a mechanism might be expected for ferric iron. It was noted earlier that M → L charge transfer should be favoured in the first part of the transition series whilst L → M transfer should dominate the latter part. Iron, being intermediate in the series, might be anticipated to be more conducive to L→M charge transfer, if not entirely dominated by this mechanism. In addition, evidence for a π delocalisation mechanism is provided by the facts that in Tables 4.5 and 4.6, contact shifts and hyperfine constants are found to alternate in sign for adjacent positions, within the conjugated system, viz. the meso- and pyrrole positions. The observation that substitution of a methyl group for a proton leads to a change in sign of the hyperfine shift is also diagnostic of a π spin delocalisation mechanism. Unfortunately, the latter evidence is not rigidly conclusive as this inversion of sign of hyperfine shift on methyl substitution is also found in cases where a σ spin delocalisation mechanism operates, although somewhat rarer in incidence.

It is interesting to note that the mechanism of spin transfer, and hence the π bonding, appears to differ significantly for the high-spin[45,46] and low-spin complexes. The former complexes yielded contact shifts indicative of sizeable positive π spin density only at the meso position, which is consistent with a dominant M→L charge transfer into the lowest vacant π MO, 4e(π^*). Calculations on ferrous porphyrins by Gouterman and Zerner[103,104] indicate that the metal e orbitals are higher in energy for a configuration with the metal out of the plane (high spin) relative to the planar form (low spin). Another factor which must be considered is that the large displacement of the metal out of the

porphyrin plane in the high-spin species permits metal-ligand π bonding with a number of different metal orbitals. In the absence of more detailed quantitative calculations, a deeper analysis of the relative hyperfine constants will not be undertaken.

b) Pyridine-metal bonding

A more detailed analysis of the contact shifts and hyperfine constants for pyridine ligand protons is possible, in view of the recognition that the behaviour of complexed pyridine ligands is intimately associated with the spin density distributions in related radicals. An attempt to correlate theory and experiment may be made by calculating the spin density distribution on a ligand by the method of "intermediate neglect of differential overlap" (INDO) developed by Pople et al[74].

In a paramagnetic metal complex, as with the porphyrin ligand, net unpaired spin density can arise on the pyridinato ligand as a result of electron transfer in either of two directions.

1) Transfer from metal atom to ligand: the unpaired spin is in a previously empty (antibonding) orbital of the ligand.

2) Transfer from ligand to metal atom: the unpaired spin thus left on the ligand is in a previously fully occupied (bonding) orbital.

If a whole electron were transferred, then (1) would produce an anionic ligand radical, whereas (2) would produce a cationic ligand radical species.

INDO spin densities calculated for molecular fragments derived from the ligand are compared with spin densities obtained from contact shifts in Table 4.13. Since the contact shift technique does not normally yield absolute spin densities, but rather relative spin densities, it is necessary to use a reference shift (or reference spin density) within each molecule in order that valid comparisons can be made from one molecule to another. The arbitrary reference used here is the α-proton

TABLE 4.13

Relative spin density distributions in molecular moieties

PORPHYRIN	X	α	β_2	β_4	β_6	γ_2	γ_6
A. Experimental							
Porphin	4-CH_3	1.0		+0.20			-0.13
Deutero	H	1.0		+0.20			
	4-CH_3	1.0		+0.19			-0.13
Etio	H	+1.0		+0.20		+0.33	
	4-CH_3	+1.0		+0.20			-0.11
Proto	H	+1.0		+0.22		+0.34	
	3-CH_3	+1.0		+0.22	+0.19	+0.33	
	4-CH_3	+1.0		+0.19			-0.12
Meso	H	+1.0		+0.21		+0.34	
	3-CH_3	+1.0		+0.21	+0.18	+0.33	
	4-CH_3						
B. Calculated							
Phenyl radical	H	+1.0		+0.33		+0.21	
	3-CH_3	+1.0	0.31		+0.09	+0.23	
	4-CH_3	+1.0		+0.34			-0.06
Pyridine cation	H	+1.0		+0.28		+0.58	
	3-CH_3	+1.0	0.25		+0.08	+0.56	
	4-CH_3	+1.0		+0.30			-0.06
Pyridine anion	H	+1.0		-0.06		+2.3	
Hybrid	H	+1.0		+0.33		+0.34	

spin density of the pyridinato moiety.

In all calculations, the metal atomic orbitals were completely neglected in forming molecular orbitals, and the metal atom was considered simply as an electron source or sink for the ligand. In addition, the effect of other ligands in the complex was neglected. Neglect of the metal orbitals is equivalent to assuming that the order of the orbitals calculated for the ligand radical ion would be retained if they were combined with metal orbitals to form molecular orbitals for the complex. If this is not the case, the predicted spin densities will be incorrect.

The observation that the experimental relative spin densities do not alternate in sign between adjacent positions provides an indication that, contrary to the situation with the porphyrin moiety, unpaired spin density may be delocalised through the σ electron system, to the pyridine moiety. In these ligands σ - and π-orbitals could lie quite close together, and a mechanism involving σ-electron delocalisation as well as a mechanism involving $\sigma - \pi$ space polarisation leading to non-zero distribution of the spin density in the π system can result in the appearance of spin density on the atoms. The second mechanism becomes particularly significant in the case of atoms which are situated far from the orbitals of the unpaired electron by virtue of the fact that delocalisation of an unpaired electron in a system of σ bonds attenuates rapidly with distance as well as during calculation of the spin density on atoms of groups which participate in hyperconjunction with the π system of electrons.

Calculations of the distribution of spin density in the π system of a phenyl radical, obtained under the assumption that the unpaired electron is localised in the σ system, are shown at the top of Table 4.13B[80,83,105]. Whilst these calculations predict the experimental signs, the relative magnitudes of the spin densities do not agree with experiment. The calculated order is $\alpha > \beta > \gamma$ whereas the observed order is $\alpha > \gamma > \beta$.

The INDO spin densities calculated[106,107] for pyridine cations, shown in Table 4.13B, are all positive for ring atoms, in agreement with experiment, whereas the anion leads to an alternation of sign around the ring. In the pyridine cation, the unpaired electron is calculated to be in a σ-orbital, although there are π-orbitals quite close to it in energy. In the 3-methyl and 4-methyl substituted pyridines all spin densities on protons are of correct sign and of approximate agreement with experiment. Replacement of hydrogen by a methyl group reverses the sign of the spin density at the 4-(γ) position but not for the 3-(β) position. Apart from this, methyl substitution has only a marginal effect on the remaining spin densities.

If a hybrid of pyridine cation and anion moieties is considered, significant improvement in the agreement of the calculated spin distributions with the experimental values is obtained. A hybrid representing a composition of 60% cation and 40% anion reproduces the experimental distribution at the α and γ positions, and the value for the β-position is of the correct order. A hybrid of cation and anion forms implies that L$\rightarrow$M and M$\rightarrow$L spin transfer are occurring simultaneously. Both L$\rightarrow$M and M$\rightarrow$L spin transfer are expected to be important for pyridine as it has both a lone pair for transfer to the metal and low-lying vacant π^* antibonding orbitals capable of accommodating spin from the metal (π "back-bonding").

In summary, it may be stated that unpaired electron spin on the metal is transmitted to the pyridine moiety of the porphyrin complexes through the σ-bonding framework. The actual spin density distribution is influenced by $\sigma - \pi$ spin polarisation within the pyridine orbitals and also by a measure of π back-bonding from the metal. Both ligand to metal and metal to ligand charge transfer are important.

The simple mesomeric model of a hybrid of both ionic forms of the pyridine ligand explains the observed results satisfactorily. The INDO

method allows for electron correlation and spin polarisation and as it is an "all-valence electron" method, is capable of calculating spin densities at all those nuclei which are accessible to experimental measurement, and not just those which are round the carbon framework. Hence no empirical McConnell type relations are needed to calculate spin densities from hyperfine coupling constants. Undoubtedly, some of the discrepancies arise from treating molecular orbitals for the ligand fragment alone. To treat the contact shifts fully adequately, a molecular orbital method for the entire complex would be needed.

vii) Substituent effects

From the results compounded in Table 4.14, it can be seen that increase in basicity of the axial ligand is concomitant with a decrease in spin density in the porphyrin ring. This can readily be interpreted in terms of the delocalisation mechanism propounded earlier. Increase in basicity of the axial ligand would be expected to decrease positive charge on the iron, thus raising the energy of the e_g orbitals. Ligand to metal charge transfer would be less favoured and a decrease in spin density in the porphyrin ring would be observed since interaction between the metal e_g and porphyrin $3e_g$ orbitals will decrease. Conversely, increasing the basicity of the porphyrin ligand would favour charge transfer from porphyrin to metal and also increase back bonding interactions, leading to an increase in spin density on the porphyrin. This is indeed found.

Owing to the duality of charge transfer mechanisms operating between pyridinato ligand and metal, and the delocalisation of the unpaired spin to the pyridinato ligand through a σ-framework, no facile interpretation of the spin densities on the pyridine is apparent. However, the insensitivity of the spin density on the axial ligand to variation in basicity of the porphyrin ligand is somewhat surprising.

TABLE 4.14

Comparison of ligand basicity with spin density for particular $(X\text{-}Py)_2$-Fe(III)-porphyrin chloride complexes

PORPHYRIN	pK_3	AXIAL LIGAND	pK_a	TOTAL RING METHYL SPIN DENSITY*	SPIN DENSITY* AT A β-PYRIDINE POSITION
Porphin	-	4-methylpyridine	6.02	-	+0.73
Deutero	5.5	pyridine	5.17	+10.2	+0.74
		4-methylpyridine	6.02	+9.7	+0.68
Etio	-	pyridine	5.17	+10.8	+0.74
		4-methylpyridine	6.02	+10.4	+0.72
Proto	4.8	pyridine	5.17	+10.2	+0.79
		3-methylpyridine	5.60	+10.1	+0.80
		4-methylpyridine	6.02	+9.5	+0.71
Meso	5.8	pyridine	5.17	+10.4	+0.78
		3-methylpyridine	5.60	+10.5	+0.78
		4-methylpyridine	6.02	+10.0	+0.73

*% of 1 unpaired electron.

2. Other complexes

In view of the insufficiency of NMR and geometric data for diamagnetic porphyrin complexes with most of the ligands, an analysis of the observed results is only possible for the bisimidazole complexes. The diamagnetic porphyrin proton shifts are assumed to be as in Table 4.2. A metal-ligand distance of 1.97 Å was taken from the X-ray data of Hoard[5] for bis-imidazole tetraphenylporphinatoiron (III) chloride, and the geometric parameters were calculated from this same source.

By comparison with the bispyridinato complexes, the hyperfine constants of the porphyrin protons in the imidazole complexes are smaller in magnitude. Again, the spin densities at the pyrrole ring carbon and methene carbon atoms are opposite in sign. The implication of this is either that the filled $3e_g$ orbitals of the imidazole complexes are lower in energy than those for the pyridinato complexes, or that the metal e_g orbitals are higher in energy for the former than for the latter. This latter hypothesis could be expected, in that imidazole, being a stronger base than say pyridine itself, would be expected to reduce the positive charge on the metal more and thus raise the energy of the predominantly metal orbitals.

Broad resonances attributed to complexed imidazole protons are observed. This is probably due to the fact that the iron-axial bond is shorter here than in the pyridinato complexes because of the stronger base. Hence metal-proton distances are shorter and the resonances are broadened more.

At low temperatures, the benzimidazole complexes are present as the bis-form, confirmed by comparing the relative intensities of the Bz (1-H) and a_6 resonances which are in the ratio of 1:3 which is consistent with the binding of two axial benzimidazole ligands. As the temperature is raised, however, the form of the NMR spectrum changes and it is not possible to determine the number of benzimidazole ligands

TABLE 4.15

Calculated pseudocontact shifts of protons in $Im_2Fe(III)$-porphyrin chloride complexes at 200°K

Porphyrin		a	b	α	β
Porphin	r(Å)	5.7	4.5	3.2	5.1
	θ°	90	90	40	14
	Δ_i^D(ppm)	+7.8	+15.8	-33.5	-19.8
Meso	r(Å)	6.4	4.5	3.2	5.1
	θ°	90	90	40	14
	Δ_i^D(ppm)	+5.5	+22.4	-33.5	-19.8

TABLE 4.16

Hyperfine interaction data for some porphyrin protons of $(Im)_2Fe(III)$porphyrin complexes in $CDCl_3$ at 200°K

Porphyrin	Parameter	a			b
Porphin	Δ_i^c(ppm)	+30.3			-3.9
	a_i(10^5 Hz)	-6.7			+0.87
	ρ_c^π (% of 1 unpaired electron)	+1.03			-0.13
Meso	Δ_i^c (ppm)	-21.4	-20.7	-18.8	-9.9
	a_i(10^5 Hz)	+4.7	+4.6	+4.2	+2.2
	ρ_c^π (% of 1 unpaired electron)	+1.2	+1.2	+1.1	-0.34

bound per porphyrin. It would appear that exchange of the axial ligands between the bound and free states increases to such a rate that it is no longer possible to observe separate resonances for the bound and free states. Replacing the benzimidazole ligand with 5,6-dimethylbenzimidazole does not appreciably help with the assignment of bound ligand resonances.

The influence of steric factors on the bonding of axial ligands is very noticeable, as evidenced by the difference in behaviour of quinoline and isoquinoline as bases. The isoquinoline molecule is no different in regard to its steric interactions with the porphyrinato atoms than the pyridine molecule, the main hindrance sterically presumably arising through the protons located in a position alpha to the basic nitrogen atom. In the case of the quinoline molecule though, the proton at position 8 would be expected to hinder the close approach of the quinoline molecule to the metalloporphyrin. This is borne out by the PMR spectrum, which does show some evidence for the existence of a low-spin ferric porphyrin, but only with the addition of a large excess of quinoline. No resonances are observed which can be attributed to bound quinoline protons. This is probably to be explained in terms of a very low concentration of the bis quinoline complex, coupled with a fairly rapid exchange between this small quantity of bound quinoline and free base. Besides these kinetic factors it is also true that quinoline (pK_a 4.94) is a weaker base than isoquinoline (pK_a 5.14), although this difference in basicity is no more than marginal, and it is undoubtedly the steric factor which leads to the difference in binding behaviour.

3. Comparison with heme-proteins and enzymes

The main difference between the PMR spectra of hemins and heme-proteins is the presence in the latter of overlapping resonances corresponding to amino-acid residues in the diamagnetic region. However,

paramagnetically shifted resonances of the heme unit protons of heme-proteins are observed to be of the same order as those of the simple hemins. The similarity of the NMR data for the hemin complexes and for the heme-proteins suggests that these smaller and simpler complexes may serve as reliable models for interpretation of the NMR spectra of more complicated heme-proteins in terms of magnetic properties and electronic structure.

One essential disparity between the bispyridine porphyrin complexes and the heme-proteins is the presence of a rhombic perturbation. It is known that the g factor is highly anisotropic e.g. for ferricyanohemoglobin at 1.4°K, $g_x = 0.75$, $g_y = 1.88$ and $g_z = 3.41$ and for such an anisotropic g factor both a tetragonal and a rhombic perturbation must be present. With the assumption that g_z is perpendicular to the heme plane, the b_{2g} (d_{xy}) orbital is lowest in energy of the metal orbitals, and the e_g orbital degeneracy is lifted, with d_{xz} more stable than d_{yz}. In order to account for the effective symmetry close to D_{4h} at room temperature, Shulman et al[32] proposed two distinct geometries for the liganded heme. One geometry has the ϕ_2 orbital ($\sim d_{xz}$) more stable than ϕ_1 ($\sim d_{yz}$) and the other has the reverse order, with a small difference in energy ($\leqslant 50$ cm^{-1}) between the lowest states of the two geometries. Then at 1.4°K, the more stable of the two geometries is frozen in (i.e. that with the "hole" in d_{yz}), whilst at 300°K there is a rapid thermal equilibrium with approximately equal populations in the two states.

It was postulated[32] that the rhombic low-temperature E.P.R. data resulted not from the static low-symmetry field of the asymmetrically substituted porphyrin, but from the "locking-in" of one of the two distorted forms by a perturbation of the protein in the form of π-bonding with the basal histidine. The observation that the EPR signals obtained for bispyridine iron (III)-protoporphyrin IX dimethyl ester appear to

reflect axial symmetry, whilst those obtained for bisimidazole iron (III)-octaethyl porphin (see Chapter 3) reflect a rhombic perturbation, strongly reinforces the theory that these low-temperature EPR spectra of proteins result from an inherent distortion of the porphyrin skeleton rather than the perturbation of the in-plane ligand field by the asymmetrically placed substituents.

The difference between the bispyridine and bisimidazole EPR spectra may arise as a result of the greater axial field of the imidazole ligand, which lifts the degeneracy of the e_g orbital. This degeneracy is not lifted then for the bispyridine complex, and hence the EPR spectrum reflects only a tetragonal and not a rhombic distortion.

The situation in the proteins themselves will be even more complex since a_i, the hyperfine constant, is expected to be temperature dependent owing to significant thermal population of the excited orbital state (d_{xz} vacancy configuration), which will affect contact contributions by altering the spin delocalisation pattern. In protein systems the low-symmetry distortions giving rise to the rhombic g-tensor are locked in by the polypeptide matrix, producing an effective solid-state environment for the heme moiety. In isolated hemin complexes, equatorial distortions evidenced in the EPR spectra at low temperatures in the solid state will necessarily be averaged out in solution at higher temperatures. Equal numbers of rapidly interconverting distorted complexes, which place the unpaired electron alternately in the d_{yz} and d_{xz} orbitals, would render a_i effectively independent of temperature. On the other hand, for the static distortion present in the proteins, a_i will be considerably temperature dependent if the excited orbital state is significantly populated in the experimental temperature range.

4.5 ADDENDUM A

STUDIES ON PIPERIDINE COMPLEXES OF A NATURAL PORPHYRIN

1. Introduction

In comparison with the considerable amount of work published on pyridine complexes of metalloporphyrins, adducts of metalloporphyrins with the corresponding saturated six-membered ring heterocycle, piperidine, have received little attention.

It has been shown, using spectrophotometric techniques, that copper and nickel mesoporphyrin IX form, respectively, a mono and a dicomplex with piperidine[109]. Bis-piperidine complexes with a variety of nickel porphyrins have subsequently been established[110]. However, doubts on the accuracy of the spectrophotometric method of determining the ligand coordination number were expressed[111] and complex formation between nickel (II) mesoporphyrin IX dimethyl ester and piperidine has been studied by proton magnetic resonance methods. Subsequent studies[112,113] have shown that the predominant paramagnetic form of Ni(II) porphyrins is in most cases the 6-coordinate bis-amine form, and that the apparent 1:1 stoichiometry of the nickel mesoporphyrin dimethyl ester piperidine complex[111] resulted from the use of the H-bonding solvent $CDCl_3$.

Throughout this study of the physical properties of metallo-porphyrins, attention has been directed towards the iron containing porphyrins. It has previously been observed[114] that the addition of piperidine to ferric porphyrins caused spontaneous reduction of the iron without the addition of a reducing agent. No explanation for this reducing property of piperidine has been forthcoming. It has been proposed that only the ferrous porphyrin/piperidine adduct is obtained, and indeed crystal parameters[6] and Mössbauer properties[114] have been published for a complex stated to be the dipiperidine derivative.

The interesting observation that addition of piperidine to ferric porphyrin complexes appeared to cause spontaneous reduction was con-

sidered to be worth investigating further. The effect of temperature on ferric porphyrin systems has been noted earlier in Chapter 3 and Chapter 4 of this work. Accordingly the examination of piperidine addition to ferric porphyrin complexes at low temperature springs to mind, as previous references to the reducing effect of piperidine relate to room temperature studies.

2. Experimental

NMR spectra were recorded on the JEOL JNM-C-60HL spectrometer at 60 MHz. Absorption spectra were recorded on a Cary 17 spectrophotometer with variable temperature facility as described in Chapter 3.

Piperidine was purified as follows[115]. Piperidine (50 ml) was added to potassium hydroxide pellets (20 g), the mixture shaken and the piperidine distilled at 102°C. The distillate was collected, partially crystallised in acetone cooled by liquid nitrogen at -30°C, the liquid remaining decanted and the solid piperidine allowed to melt. The crystallisate was then redistilled and the fraction distilling at 104°C collected (30 ml).

3. Results

i) NMR spectroscopy

The addition of piperidine to ferric protoporphyrin IX dimethyl ester chloride at about 200°K is found to radically alter the PMR spectrum, and indeed spectra characteristic of low-spin ferric porphyrin complexes are observed with particular experimental conditions. It is found that for a 50 mM porphyrin solution in $CDCl_3$, the addition of 20 microlitres of piperidine, which represents a porphyrin/piperidine concentration ratio of 1:100, is found to produce PMR spectra similar in form to those of bispyridine adducts of ferric porphyrins.

The 60 MHz PMR spectrum of such a solution at 212°K is illustrated

in Figure 4.18. Comparing this spectrum with that of the corresponding bispyridine complex in Figure 4.8, a fairly close resemblance is to be seen and several resonances can be assigned by analogy. Thus the two pairs of downfield shifts at -19.3, -18.9 ppm and -16.6, -16.0 ppm are assigned as the ring methyl protons (a_3), the resonance at -3.4 ppm as the methyl ester protons(e_6), the resonance at +2.3 ppm as the propionic ester β-methylene protons (d_4) and the resonance at +10.1 ppm as the vinyl methylene protons (g_4). The resonance at -10.5 ppm may arise from the vinyl methene (f_2) protons. Other resonances are observed at -13.9, -17.5, -24.2, and -38 ppm.

The first two resonances shift downfield as the temperature is lowered, and the shift and temperature behaviour of these resonances is not unlike that of the γ- and β-proton resonances of the corresponding bis pyridine complex. More definitive assignment is not possible. The remaining two resonances are rather broader than the other resonances and shift downfield as the temperature is lowered. The broadness of these lines would suggest that they do not arise from a low-spin ferric complex. On the other hand they do not appear to correspond to the resonances of the high spin ferric protoporphyrin IX dimethyl ester chloride complex, which for the most part tend to occur at lower field. One possibility is that they could arise due to the exchange of piperidine between bound and free states at an intermediate rate, that is to say in a condition where neither fast nor slow exchange is present. Separate resonances for the complexes with and without bound piperidine will be observed at positions which are intermediate between those of the two types which would be observed in a condition of slow exchange.

At temperatures higher than 212°K, resonances are observed upfield of TMS which may arise from the meso protons (b_4). These appear to coalesce with the g_4 resonance at 212°K, since the g_4 resonance is somewhat larger than the d_4 resonance which represents 4 protons. The full

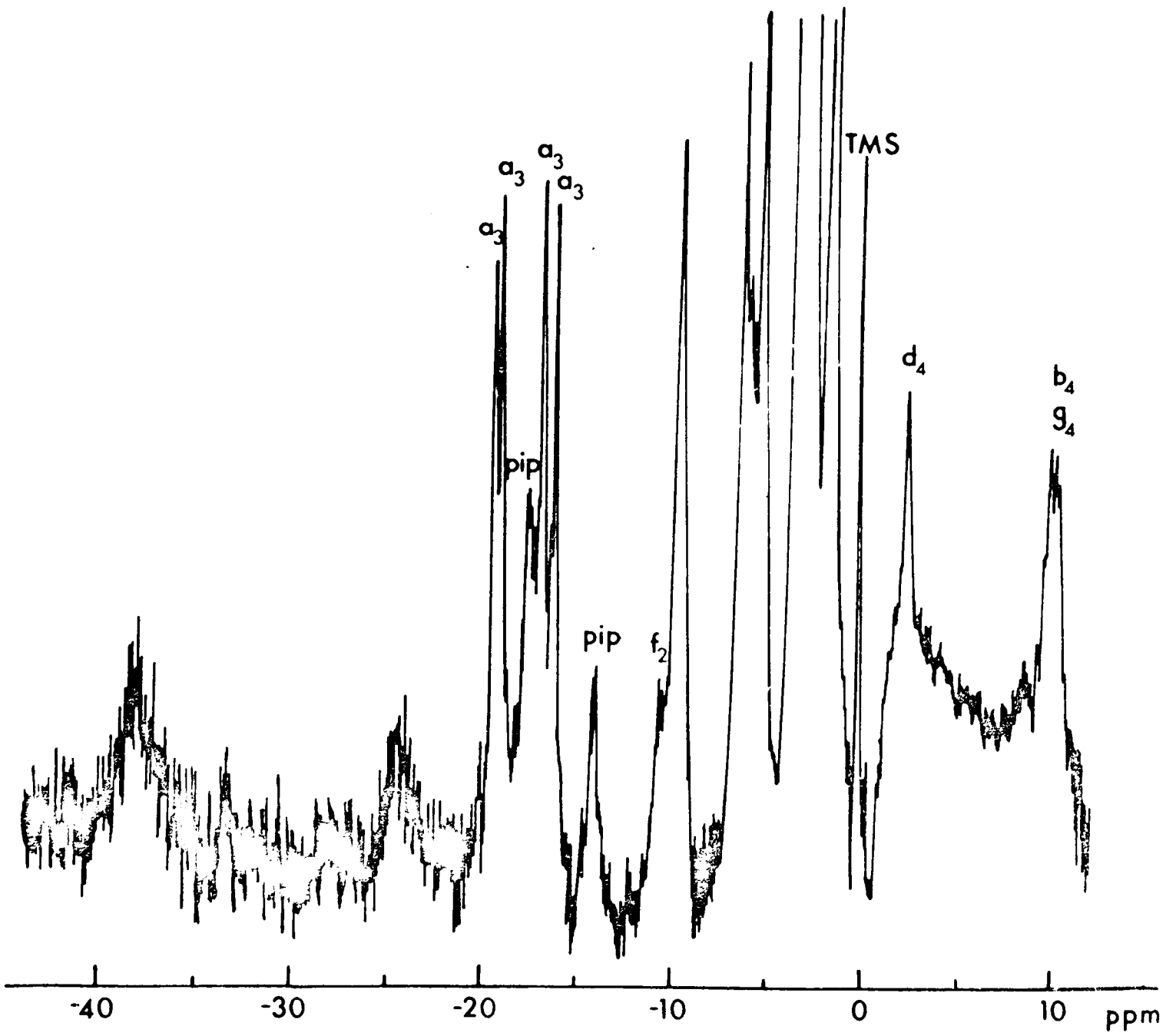


FIG. 4.18 PMR spectrum of Fe-protoporphyrin dimethyl ester chloride + piperidine at 212°K.

PMR data at a variety of temperatures are given below in Table 4.17.

On progressively raising the ambient temperature, the peaks shifted to low and high field broaden and eventually disappear.

ii) Absorption spectroscopy

The addition of aliquots of piperidine to a solution of ferric protoporphyrin IX dimethyl ester chloride (1×10^{-4} M) is seen to affect the absorption spectrum. By varying the amount of added piperidine and the temperature of the solution, a number of different spectra types are observed. Thus by adding 300 microlitres of piperidine (porphyrin/piperidine concentration ratio 1:30,000) at room temperature, a visible spectrum characteristic of dipyridine ferrous porphyrin complexes is obtained, with the α-band at 565 nm and the less intense β-band at 525 nm. This compares with an α-band at 555 nm and a β-band at 523 nm for the spectrum of the bis pyridine iron (II) protoporphyrin IX dimethyl ester in pyridine-benzene solution[116].

By addition of 40 microlitres of piperidine (porphyrin/piperidine concentration ratio 1:4000) at 217°K, a spectrum is obtained which bears a striking resemblance to those of the bispyridinato iron (III) porphyrin complexes at comparable temperature described in Chapter 3. Absorption maxima are found at 515 nm and 565, 575 nm. On allowing the ambient temperature of the solution to rise to room temperature, the spectrum changes and a spectrum with maxima at 475 nm and 588 nm is obtained. This spectrum is also obtained by adding 1 microlitre of piperidine (porphyrin/piperidine concentration 1:100) to the porphyrin solution at 216°K. The evidence would seem to suggest that this is a monopiperidine iron (II) complex spectrum.

These three spectrum types are illustrated in Figure 4.19, together with the spectrum at room temperature of the initial porphyrin solution.

TABLE 4.17

PMR shift* data for ferric protoporphyrin IX dimethyl ester chloride in the presence of piperidine

T	pip	pip	$(a_3)_2$		$(a_3)_2$		pip	pip	f_2	e_6	d_4	b_4	g_4
249				-11.9						-3.4			
242	-24.9		-15.0		-13.2			-9.3		-3.3		+2.2 +3.0	+5.2
233	-29.0		-16.8	-16.6	-14.8	-14.3	-13.6	-10.7		-3.4		+5.9 +6.8	+7.7
219	-34.4	-21.9	-18.6	-18.3	-16.2	-15.6	-15.6	-12.8	-10.8	-3.4	+1.7	+6.9	+8.9
212	-38	-24.2	-19.3	-18.9	-16.6	-16.0	-17.5	-13.9	-10.5		+2.3		+10.1
202	-41	-26.2	-19.7	-19.2	-17.0	-16.1	-19.2	-15.4			+2.8		+11.1

*observed shift in ppm from TMS.

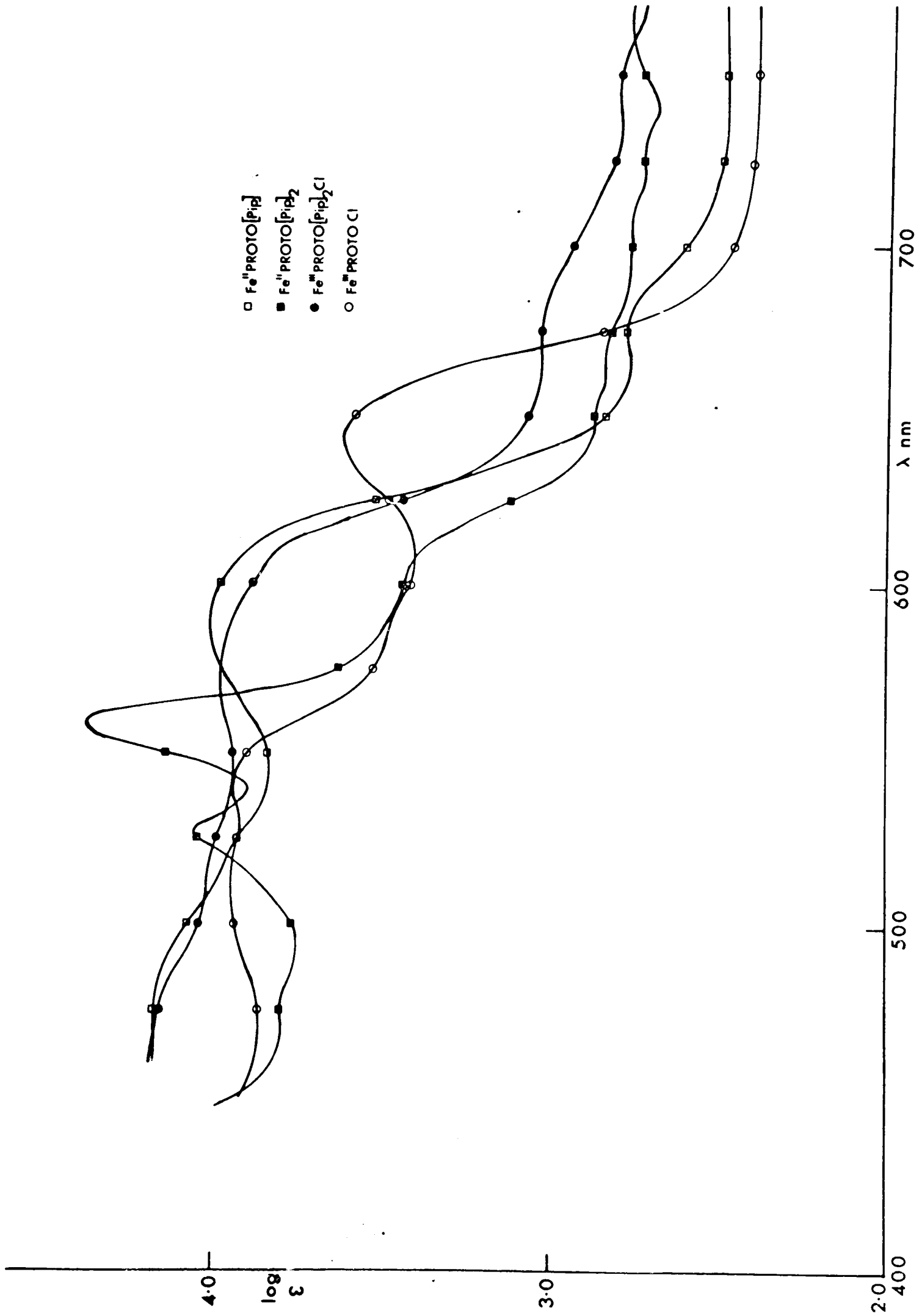


FIG. 4.19 Absorption spectra of complexes of piperidine with Fe-protoporphyrin dimethyl ester chloride.

4. Discussion

The appearance and form of the PMR spectrum of ferric protoporphyrin IX dimethyl ester chloride in the presence of piperidine at low temperature suggests that a low-spin ferric bis piperidine complex is formed. This complex is unstable at higher and room temperature being reduced to a ferrous porphyrin complex. Presumably, the reason why the bis piperidine iron (III) complex has never previously been identified is that the addition of piperidine has always been made at room temperature. The reduction of iron (III) to iron (II) with increase in solution temperature is found to be irreversible, since the low spin ferric porphyrin PMR spectrum never reappears on cooling the solution down from room temperature. Other than a tentative assignment of the PMR resonances, no further analysis of the spectra is really worthwhile.

A similar story is told by the absorption spectra. Here however both mono and bis piperidine iron (II) porphyrin complexes can be characterised, as well as the bis piperidine iron (III) complex at low temperature. Whilst it should in theory be possible to add aliquots of piperidine at a given temperature to the porphyrin solution, in practice it is not easy to obtain absorption spectra corresponding to different quantities of added piperidine. The design of the cryostat is such that the cell has to be withdrawn in order to add aliquots, and in the process condensation occurs on the cold cell. The practical outcome is that the baselines of the absorption spectra measured tend to wander and no meaningful comparison can be made. No assesment of the equilibrium constant for formation of the bis piperidine complex can therefore be undertaken.

Both the PMR and absorption spectral data provide conclusive evidence for the existence of the bis piperidine iron (III) porphyrin species. It is strange that the iron (III) species should be "spontaneously reduced" to the iron (II) species at room temperature but with the limited experimental information at hand no explanation of this can be advanced.

4.6 ADDENDUM B

STUDIES ON A DIPYRIDINE FERRIC PORPHYRIN COMPLEX

1. Introduction

Association phenomena which result in multiple species are well known to occur with heme porphyrin complexes. The structures of many of these species remain poorly understood, some forms being extensively aggregated.

Investigations into the possibility of there being metal-metal interactions between isolated metal centres linked by bridging ligands have taken place. A number of oxo-bridged iron porphyrin complexes have been studied and their properties reviewed[117], and these will be examined further in Chapter 6. The ability of pyrazine and its methyl-substituted derivatives to form monomeric, dimeric and polymeric species has been demonstrated, and there has been evidence that pyrazine can act as a bridging ligand such that there is spin-spin interaction between the metal centres[118-120], although these studies have not been carried out with porphyrin complexes. Returning to porphyrin species, a copolymer of ferroheme, 4,4'-dipyridine and poly(L-lysine) has been synthesised[121]. A tunnelling calculation showed that the frequency of electron transfer between two neighbouring Fe(III) heme units through the bridging di-pyridyl group is $\geq 6 \times 10^{9}$ sec^{-1}. Since this frequency is much larger than the rate of oxidation of the Fe(II) heme copolymer by oxygen, the Fe(II) heme units of the copolymer could cooperate in the reduction of O_2.

In the main part of this chapter, attention was focussed on complexes formed by addition of pyridine and derivatives to ferric porphyrins. It is a natural extension of this work to study the possibility of forming polymeric ferric porphyrin species with the pyridine derivative 4,4'-dipyridyl as a bridging ligand. As reported above[121], a polymer with ferroheme has been obtained and these studies represent an attempt to examine a comparable ferric heme complex.

2. Experimental

NMR spectra were recorded on the JEOL JNM-C-60HL spectrometer at 60 MHz. Absorption spectra were recorded on a Cary 17 spectrophotometer with variable temperature facility as described in Chapter 3.

3. Results

i) NMR spectroscopy

At room temperature, the NMR spectrum of a solution of ferric mesoporphyrin IX dimethyl ester chloride to which 4,4'-dipyridyl has been added is typical of a high spin ferric porphyrin species. Thus 4 broad bands are found in the -50 to -35 ppm region downfield from TMS, with other broad bands in the -10 to 0 ppm region downfield from TMS.

On lowering the temperature to 240°K and below, the form of the NMR spectrum is radically altered, and spectra more characteristic of low-spin ferric porphyrin complexes are obtained, in a similar fashion to those obtained with the pyridinato complexes. The 60 MHz PMR spectrum of a 25 mM solution of ferric mesoporphyrin IX dimethyl ester chloride with 19.5 mg of 4,4'-dipyridyl added (porphyrin:dipyridyl concentration 1:2.5) at 223°K is shown in Figure 4.20. This spectrum appears typical of low spin ferric spectra, except for the extra peaks occurring in the ring methyl proton region at -20 to -30 ppm downfield from TMS.

From the format of the low field resonances, there is a suggestion that the ring methyl proton resonances comprise two separate sets. Thus the resonances at -27.4, -24.7 and -23.0 ppm appear to originate from one source whilst the more intense resonances at -26.1, -23.7 and -22.0 ppm appear to originate from another source. The peak at -19.3 ppm is in position and intensity (integrating as 4 protons relative to the ring methyl peaks) comparable to the β-py_4 peak present for bispyridinato complexes. Accordingly this resonance is assigned to those protons on bound 4,4'-dipyridyl ligands in the β-position relative to the basic nitrogen atom.

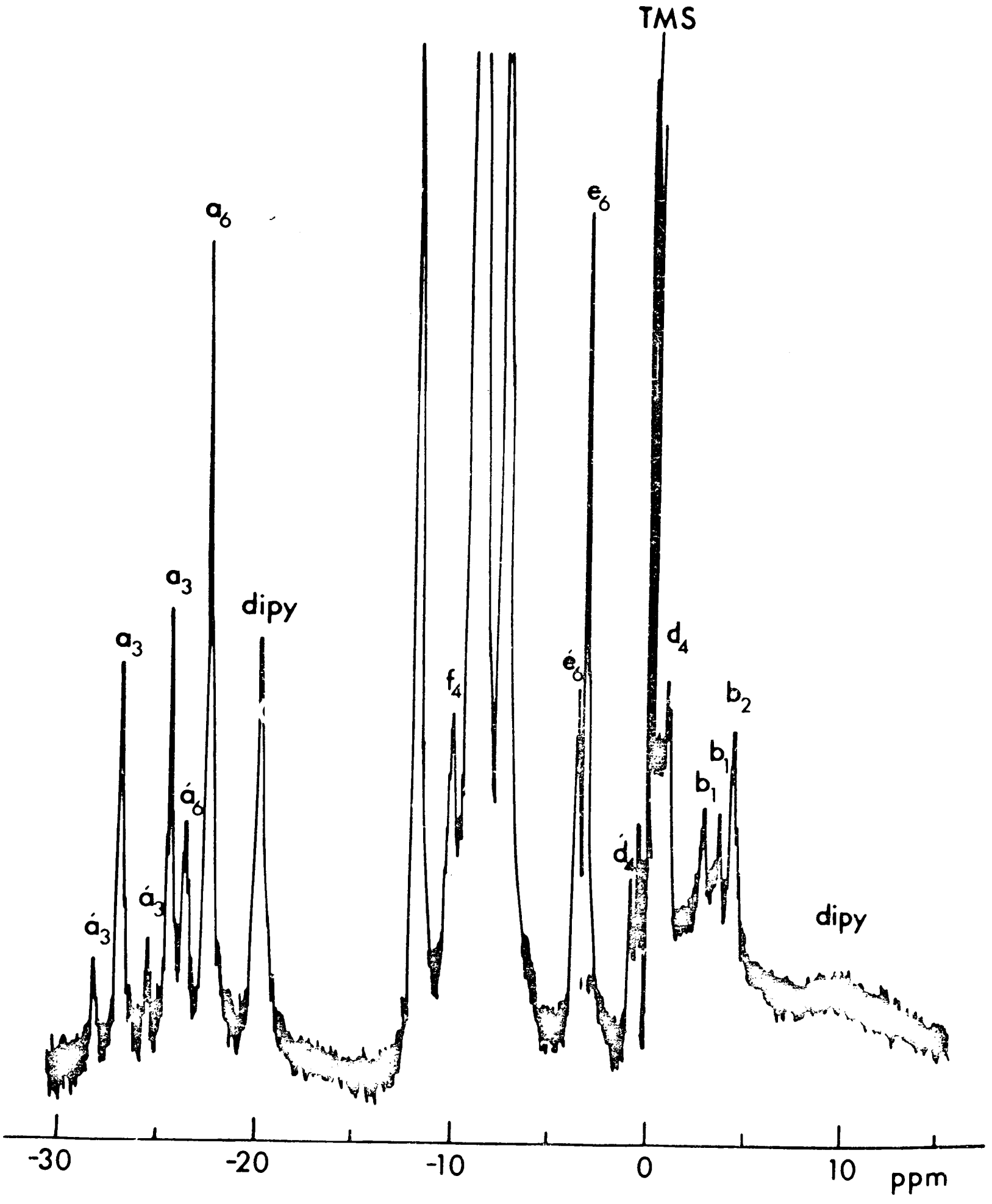


FIG. 4.20 PMR spectrum of Fe-mesoporphyrin dimethyl ester chloride + 4,4'-dipyridyl at 223°K.

The resonance at -9.8 ppm could be attributed as arising either from the c_4 or f_4 protons by comparison with the PMR spectrum of the bispyridine ferric mesoporphyrin dimethyl ester chloride complex. Two resonances occur with shifts comparable to that expected for the methyl ester group proton resonance, at -3.6 and -3.2 ppm. In common with the ring methyl proton resonances, these two peaks are of different intensity and appear to originate from two different sources. The peaks upfield from TMS are straightforward to assign by direct comparison with the corresponding bispyridinato complex spectrum. It is interesting that a broad resonance can be observed at ca. +9.3 ppm, in a position not dissimilar from the resonance α-py_4 seen with bispyridine complexes. This resonance must correspond to those protons of the bound 4,4'-dipyridyl ligand in the position α to the basic nitrogen atom which binds to the iron, and is represented as α-pyr_4.

The behaviour of the resonances with variation of temperature is as expected and similar in manner to that observed previously with bispyridinato complexes. The results are reproduced fully in Table 4.18. In order to examine the effect of the 4,4'-dipyridyl, the PMR experiments were repeated on the 25 mM ferric porphyrin solution with only 3.5 mg of 4,4'-dipyridyl added (porphyrin:dipyridyl concentration 2:1). The spectra obtained are fairly similar to those with the higher concentration of added base, except that the two sets of ring methyl proton resonances and two methyl ester proton resonances are more closer in intensity than before.

ii) Absorption spectroscopy

Absorption spectroscopy studies were undertaken in an attempt to characterise the species present on addition of the 4,4'-dipyridyl base. It was found that the addition of 4,4'-dipyridyl produced an appreciable change in the absorption spectrum observed.

TABLE 4.18

PMR shift* data for ferric mesoporphyrin IX dimethyl ester chloride in the presence of 4,4'-dipyridyl

$T^{\circ}K$					a_3'	a_3'	a_6'	a_3	a_3	a_6	β-pyr$_4$	f_4	e_6'	e_6	g6 d_4	b_1	b_1	b_2	α-pyr$_4$
300	-49	-49	-42	-38															
284		-53	-47	-42															
269		-55	-48	-43															
252	-63	-60	-52	-46				-25.4	-23.6	-21.8	-17.1			-3.3					
236					-26.9	-24.7	-23.0	-25.7	-23.6	-21.8	-18.4			-3.4	-0.6		+1.7	+2.6	
233					-27.6	-25.2	-23.5	-26.4	-24.1	-22.3	-19.1	-10.6	-4.1	-3.7		+1.2	+2.0	+2.6	+9.1
229					-27.5	-24.9	-23.2	-26.3	-24.0	-22.3	-19.2	-10.3	-3.8	-3.6	+0.5	+2.0	+2.7	+3.4	
223					-27.4	-24.7	-23.0	-26.1	-23.7	-22.0	-19.3	-9.8	-3.6	-3.2	+1.0	+2.8	+3.6	+4.3	+9.3
212					-28.0	-25.2	-23.5	-26.9	-24.2	-22.3	-20.4	-9.7	-4.1	-3.2	+1.0	+3.9	+4.9	+5.5	+9.3
206					-28.2	-25.2	-23.3	-27.0	-24.2	-22.3	-21.2	-9.2	-3.9	-2.8	+1.5	+5.2	+6.1	+6.9	

*observed shift in ppm from TMS

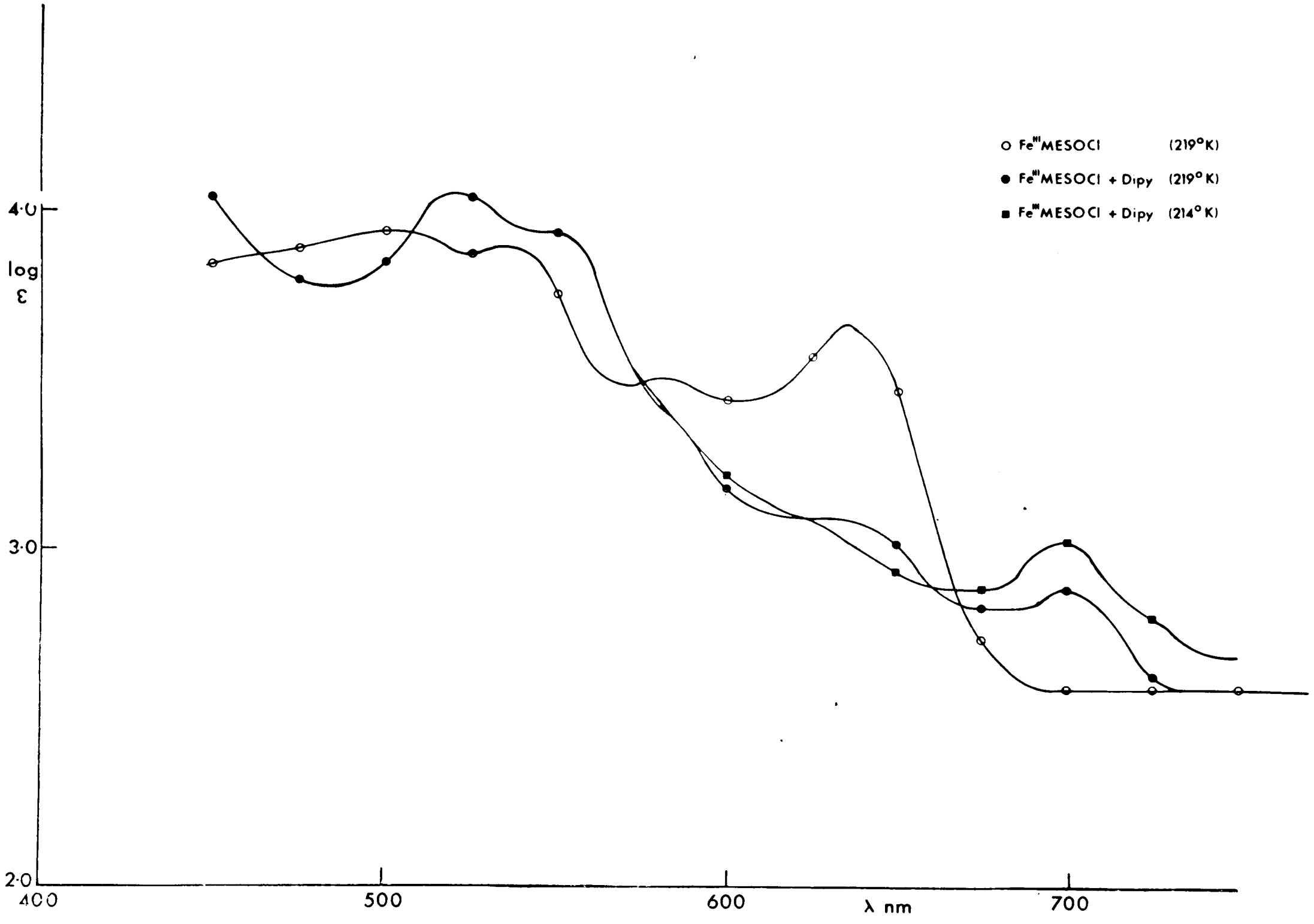
Spectra characteristic of those obtained are reproduced in Figure 4.21. The spectrum of a solution of ferric mesoporphyrin IX dimethyl ester chloride (1.03×10^{-4} M) in chloroform at 219°K is typical of high spin ferric porphyrin spectra, with 4 absorption bands at 505, 535, 580 and 635 nm. The addition of 40 microlitres of a solution of 1.56 mg of 4,4'-dipyridyl in 1 ml of chloroform (porphyrin: dipyridyl concentration 1:2) at 219°K causes a change in the visible spectrum, a new spectrum being obtained as illustrated in Figure 4.21. This spectrum has absorption bands at 520, 550 and 700 nm, together with a shoulder at 635 nm which arises from the uncomplexed high spin ferric porphyrin complex, and is typical in form of low spin ferric porphyrin complex spectra. On cooling the solution to 214°K and remeasuring the spectrum, the shoulder at 635 nm is hardly in evidence and the band at 700 nm is appreciably more pronounced.

On warming the solution progressively, the spectrum of the 4,4'-dipyridyl species gradually merges into that of the high spin ferric porphyrin complex, and at room temperature there is no evidence of the existence of any absorption bands other than those of the high spin species. At these higher temperatures it is presumed that bound 4,4'-dipyridyl dissociates from the ferric porphyrin increasingly as complexation becomes more unfavourable.

4. Discussion

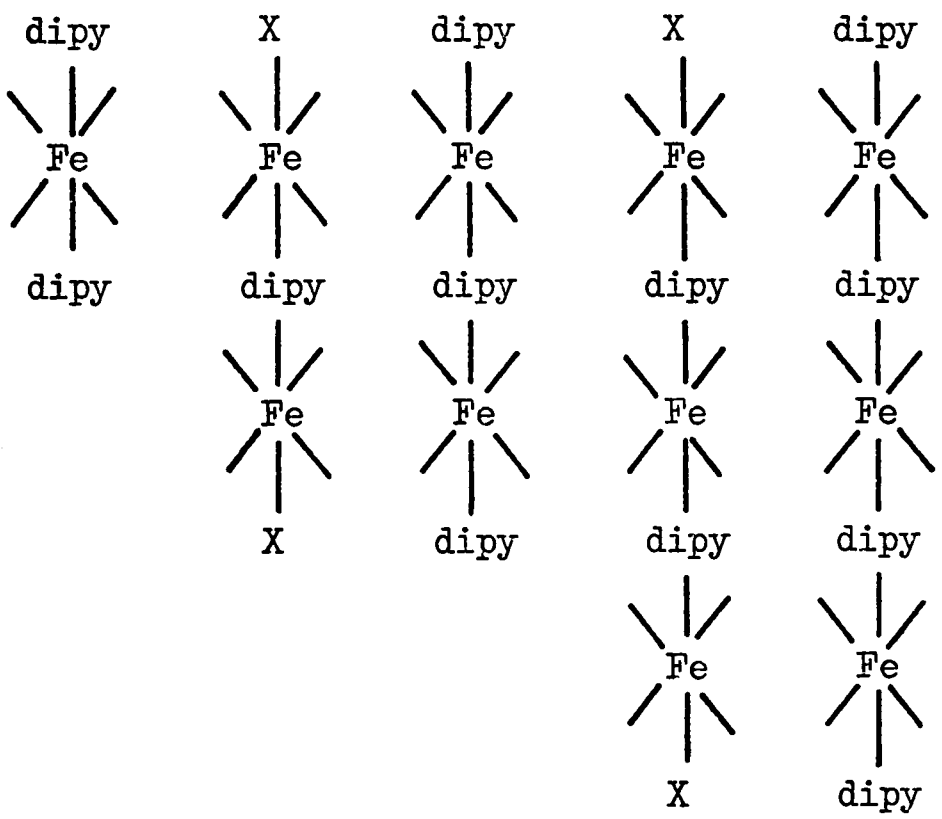
It seems clear from the PMR evidence that more than one low-spin ferric porphyrin/dipyridyl derivative is present at lower temperatures, since two sets of resonances a and e are observed. It is perhaps surprising that only two types of proton resonances are duplicated, but many of the other resonances are slightly broader than is found with corresponding bispyridinato derivatives. Higher resolution spectroscopy

FIG. 4.21 Absorption spectra of complex of 4,4'-dipyridyl with Fe-mesoporphyrin dimethyl ester chloride.



might resolve some of these latter peaks into split resonances.

These results are consistent with the formation of polymeric porphyrin species with the 4,4'-dipyridyl base acting as a bridging ligand. The PMR spectra suggest that there are only two different porphyrin types. A number of species can be considered as likely possibilities present. Some of these are shown below, where dipy represents the 4,4'-dipyridyl ligand and X represents other possible ligands such as chloride ion or solvent.



I II III IV V

The fact that two different porphyrin types appear to exist could mean that two species with dissimilar iron porphyrin entities co-exist or that two dissimilar iron porphyrin entities exist in one polymeric species. As the amount of base added is increased, one of the porphyrin entities is seen to reduce in concentration in comparison to the other entity, in that the set of ring methyl proton resonances at lower field reduces in intensity by comparison with the set at higher field.

As base is added, it is a fair assumption that the degree of aggregation increases. Species such as IV and V might exhibit distinct

resonances characteristic of protons attached to the two different porphyrin entities, that is one porphyrin with two bridging dipyridyl ligands bound and one porphyrin with only one bridging dipyridyl ligand bound. On closer examination of these species, it is readily apparent that as the length of the polymer increases, that is as aggregation increases, the number of terminal porphyrin groups decreases in proportion to the number of "bridging" porphyrin groups.

An alternative way of accounting for the relative variation in intensity between the sets of resonances is possible. As base is added, the prevalence of species such as type III would be expected to increase at the expense of species such as type I. Spin-spin interaction between the metal centres is a possibility for complexes such as type III, and the presence of such spin-spin interaction would manifest itself in terms of a change in spin density at the porphyrin periphery in comparison to the spin density at the periphery of the porphyrin in complexes like species I. In turn, this might be expected to give rise to more than one set of NMR resonances characteristic of, say, the ring methyl groups.

In Figure 4.20, the intensities of the two sets of ring methyl proton resonances are in the approximate ratio of 1 to 4 (lower field set:higher field set), whilst the resonances of the higher field set and the β-pyr$_4$ resonance integrate in the approximate ratio of 3:3:6:5. Whilst there is probably no unique set of species which accord with these observations, the existence of species I and III in the ratio 1:2 would reproduce the spectra found with $2\frac{1}{2}$ equivalents of added 4,4'-dipyridyl to each equivalent of ferric porphyrin. One postulate therefore may be that species I is first formed as the base is added, and on further addition of base, species I is converted to species III.

The absorption spectra at low temperatures indicate that some form of complexation of 4,4'-dipyridyl and ferric mesoporphyrin takes place

in that a low-spin ferric spectrum is observed. Unfortunately it is not really feasible to propose the existence of a bridging dipyridyl ligand on the basis of the absorption spectra observed. The spectrum at 214°K is not dissimilar in form to that observed for μ-oxo-bis meso-hemin dimethyl ester[122], although for the latter the absorption bands in benzene are at higher wavelength at 564 and 590 nm, but the evidence is not conclusive in itself.

In summary, whilst the results in this section are not sufficiently conclusive nor definitive in themselves, there is a reasonable argument which can be advanced to support the existence of polymeric ferric porphyrin species bridged by the 4,4'-dipyridyl ligand. Further studies would be useful in attempting to characterise the species formed under particular experimental conditions.

REFERENCES

1. K. Wüthrich, R.G. Shulman and J. Peisach. Proc. Nat. Acad. Sci. U.S., 1968, 60, 378.

2. J.L. Hoard. Science, 1971, 174, 1295.

3. T.A. Hamor, W.S. Caughey and J.L. Hoard. J. Amer. Chem. Soc., 1965, 87, 2305.

4. J.L. Hoard, M.J. Hamor, T.A. Hamor and W.S. Caughey. J. Amer. Chem. Soc., 1965, 87, 2312.

5. D.M. Collins, R. Countryman and J.L. Hoard. J. Amer. Chem. Soc., 1972, 94, 2066.

6. L.J. Radonovitch, A. Bloom and J.L. Hoard. J. Amer. Chem. Soc., 1972, 94, 2073.

7. A.B. Hoffman, D.M. Collins, V.W. Day, E.B. Fleischer, T.S. Srivastava and J.L. Hoard. J. Amer. Chem. Soc., 1972, 94, 3620.

8. J.L. Hoard. Ann. N.Y. Acad. Sci., 1973, 206, 18.

9. E.B. Fleischer. Acc. Chem. Res., 1970, 3, 105.

10. A. Takenaka, Y. Sasada, E. Watanabe, H. Ogishi and Z. Yoshida. Chem. Lett., 1972, 1235.

11. K. Wüthrich. Struct. Bonding, 1971, 8, 53.

12. W.D. Phillips and M. Poe, in "Iron-Sulphur Proteins", Ed. W. Lovenberg, Academic Press, New York, 1972.

13. D.R. Eaton and W.D. Phillips. Advan. Magnetic Resonance, 1965, 1, 103.

14. M. Poe, W.D. Phillips, J.D. Glickson, C.C. McDonald and A. San Pietro. Proc. Nat. Acad. Sci. U.S., 1971, 68, 68.

15. M. Poe, W.D. Phillips, C.C. McDonald and W. Lovenberg. Proc. Nat. Acad. Sci. U.S., 1970, 65, 797.

16. A. Kowalsky. Biochem., 1965, 4, 2382.

17. K. Wüthrich. Proc. Nat. Acad. Sci. U.S., 1969, 63, 1071.

18. R.K. Gupta and A.G. Redfield. Biochem. Biophys. Res. Commun., 1970, 41, 273.

19. R.K. Gupta and A.G. Redfield. Science, 1970, 169, 1204.

20. S. Ogawa and R.G. Shulman. Biochem. Biophys. Res. Commun., 1971, 42, 9.

21. R.G. Shulman, S. Ogawa, K. Wüthrich, T. Yamane, J. Peisach and W.E. Blumberg. Science, 1969, 165, 251.

22. S. Ogawa, R.G. Shulman, P.A.M. Kynoch and H. Lehmann. Nature, 1970, 225, 1042.

23. D.G. Davis, S. Charache and C. Ho. Proc. Nat. Acad. Sci. U.S., 1969, 63, 1403.

24. D.G. Davis, N.L. Mock, V.R. Laman and C. Ho. J. Mol. Biol., 1969, 40, 311.

25. R.G. Shulman, J. Peisach and B.J. Wyluda. J. Mol. Biol., 1970, 48, 517.

26. D.J. Patel, L. Kampa, R.G. Shulman, T. Yamane and B.J. Wyluda. Proc. Nat. Acad. Sci. U.S., 1970, 67, 1109.

27. K. Wüthrich, R.G. Shulman and T. Yamane. Proc. Nat. Acad. Sci. U.S., 1968, 61, 1199.

28. K. Wüthrich, R.G. Shulman and J. Peisach. Proc. Nat. Acad. Sci. U.S., 1968, 60, 373.

29. R.G. Shulman, K. Wüthrich, T. Yamane, E. Antonini and M. Brunori. Proc. Nat. Acad. Sci. U.S., 1969, 63, 623.

30. C.C. McDonald and W.D. Phillips. J. Amer. Chem. Soc., 1967, 89, 6332.

31. B. Sheard, T. Yamane and R.G. Shulman. J. Mol. Biol., 1970, 53, 35.

32. R.G. Shulman, S.H. Glarum and M. Karplus. J. Mol. Biol., 1971, 57, 93.

33. J.P. Jesson. J. Chem. Phys., 1967, 47, 582.

34. G.N. La Mar, J.P. Jesson and P. Meakin. J. Amer. Chem. Soc., 1971, 93, 1286.

35. E.D. Becker and R.B. Bradley. J. Chem. Phys., 1959, 31, 1413.

36. J. Ellis, A.H. Jackson, G.W. Kenner and J. Lee. Tetrahedron Letters, 1960, 2, 23.

37. E.D. Becker, R.B. Bradley and C.J. Watson. J. Amer. Chem. Soc., 1961, 83, 3743.

38. R.J. Abraham. Mol. Phys., 1961, 4, 145.

39. R.J. Abraham, A.H. Jackson and G.W. Kenner. J. Chem. Soc., 1961, 3468.

40. W.S. Caughey and W.S. Koski. Biochemistry, 1962, 1, 923.

41. D.R. Eaton, and E.A. LaLancette. J. Chem. Phys., 1964, 41, 3534.

42. R.J. Kurland, D.G. Davis and C. Ho. J. Amer. Chem. Soc., 1968, 90, 2700.

43. W.S. Caughey and L.F. Johnson. Chem. Commun., 1969, 1326.

44. R.J. Kurland, R.G. Little, D.G. Davis and C. Ho. Biochemistry, 1971, 10, 2237.

45. G.N. La Mar, G.R. Eaton, R.H. Holm and F.A. Walker. J. Amer. Chem. Soc., 1973, 95, 63.

46. F.A. Walker and G.N. La Mar. Ann. N.Y. Acad. Sci., 1973, 206, 328.

47. H.A. Degani and D. Fiat. J. Amer. Chem. Soc., 1971, 93, 4281.

48. K. Wüthrich, R.G. Shulman, B.J. Wyluda and W.S. Caughey. Proc. Nat. Acad. Sci. U.S., 1969, 62, 636.

49. H.A.O. Hill and K.G. Morallee. J. Amer. Chem. Soc., 1972, 94, 731.

50. G.N. La Mar and F.A. Walker. J. Amer. Chem. Soc., 1972, 94, 8607.

51. G.N. La Mar and F.A. Walker. J. Amer. Chem. Soc., 1973, 95, 1782.

52. I. Salmeen and G. Palmer. J. Chem. Phys., 1968, 48, 2049.

53. H. Hori. Biochim. Biophys. Acta., 1971, 251, 227.

54. C. Mailer and C.P.S. Taylor. Can. J. Biochem., 1972, 50, 1048.

55. W. de W. Horrocks. Inorg. Chem., 1970, 9, 690.

56. R.J. Kurland and B.R. McGarvey. J. Magn. Resonance, 1970, 2, 286.

57. B.R. McGarvey. J. Chem. Phys., 1970, 53, 86.

58. W. de W. Horrocks and E.S. Greenberg. Biochim. Biophys. Acta., 1973, 322, 38.

59. W. de W. Horrocks and E.S. Greenberg. Mol. Phys., 1974, 27, 993.

60. C.J. Ballhausen. "Introduction to Ligand Field Theory", McGraw-Hill, New York, 1962, Chapter 7.

61. C.J. Ballhausen and H.B. Gray. "Molecular Orbital Theory", Benjamin, New York, 1965, Chapter 8.

62.

63. H.M. McConnell. J. Chem. Phys., 1956, 24, 764.

64. H.M. McConnell. Proc. Nat. Acad. Sci. U.S., 1957, 43, 721.

65. S.I. Weissman. J. Chem. Phys., 1956, 25, 890.

66. R. Bersohn. J. Chem. Phys., 1956, 24, 1066.

67. H.S. Jarrett. J. Chem. Phys., 1956, 25, 1289.

68. B. Venkataraman and G.K. Fraenkel. J. Chem. Phys., 1956, 24, 737.

69. M. Karplus and G.K. Fraenkel. J. Chem. Phys., 1961, 35, 1312.

70. J. Owen and J.H.M. Thornley. Rep. Prog. Phys., 1966, 29, 675.

71. R.G. Hayes, in "Electron Spin Resonance in Chemistry", Methuen, London, 1967, Chapter 3.

72. L.E. Orgel. Disc. Faraday Soc., 1958, 26, 92.

73. L.E. Orgel. J. Chem. Phys., 1959, 30, 1617.

74. J.A. Pople, D.L. Beveridge and P.A. Dobosh. J. Amer. Chem. Soc., 1968, 90, 4201.

75. P.B. Ayscough. "Electron Spin Resonance in Chemistry", Methuen, London, 1967, Chapter 8.

76. J.A. Happe and R.L. Ward. J. Chem. Phys., 1963, 39, 1211.

77. R.W. Kluiber and W.D. Horrocks Jr. Inorg. Chem., 1967, 6, 166.

78. R.H. Holm, G.W. Everett Jr. and W.D. Horrocks Jr. J. Amer. Chem. Soc., 1966, 88, 1071.

79. G.M. Zhidomirov, P.V. Schastnev and N.D. Chuvylkin. J. Struct. Chem., 1969, 10, 800.

80. G.M. Zhidomirov, P.V. Schastnev and N.D. Chuvylkin. J. Struct. Chem., 1970, 11, 458.

81. D.R. Eaton. J. Amer. Chem. Soc., 1965, 87, 3097.

82. G.N. La Mar, E.O. Sherman and G.A. Fuchs. J. Coord. Chem., 1971, 1, 289.

83. W. de W. Horrocks Jr. and D.L. Johnston. Inorg. Chem., 1971, 10, 1835.

84. M.F. Rettig and R.S. Drago. J. Amer. Chem. Soc., 1969, 91, 1361.

85. Z. Luz. J. Chem. Phys., 1968, 48, 4186.

86. J.W. McIver Jr. and G.E. Maciel. J. Amer. Chem. Soc., 1971, 93, 4641.

87. J-H. Fuhrhop. Structure and Bonding, 1974, 18, 1.

88. Chem. Abs., 1962, 56, 3746i.

89. T. Okamoto and Y. Kawazoe. Chem. Pharm. Bull. Japan, 1964, 12, 1384.

90. R.M. Acheson and B.J. Jones. J. Chem. Soc., 1970, 1301.

91. J.E. Falk. "Porphyrins and Metalloporphyrins", Elsevier, Amsterdam, 1964.

92. J.G. Erdman and A.H. Corwin. J. Amer. Chem. Soc., 1947, 69, 750.

93. A.D. Adler, L. Sklar, F.R. Longo, J.D. Finarelli and M.G. Finarelli. Unpublished manuscript.

94. A.D. Adler, F.R. Longo, F. Kampas and J. Kim. J. Inorg. Nucl. Chem., 1970, 32, 2445.

95. J.G. Brassington, Part II Thesis, Oxford, 1974.

96. J.A.S. Cavaleiro, A.M. d'A. Rocha Gonsalves, G.W. Kenner, K.M. Smith, R.G. Shulman, A. Mayer and T. Yamane. Chem. Commun., 1974, 392.

97. D.F. Koenig. Acta. Crystallogr., 1965, 18, 663.

98. Dr. R.C. Bray. Private communication.

99. C.B. Storm. J. Amer. Chem. Soc., 1970, 92, 1423.

100. J.N. Phillips. Rev. Pure Appl. Chem., 1960, 10, 35.

101. K. Schofield. "Heteroaromatic Nitrogen Compounds - Pyrroles and Pyridines", Butterworth, 1967, Table 5.10.

102. H.C. Longuet-Higgins, C.W. Rector and J.R. Platt. J. Chem. Phys., 1950, 18, 1174.

103. M. Zerner and M. Gouterman. Theor. Chim. Acta., 1966, 6, 363.

104. M. Gouterman and M. Zerner. "Hemes and Hemoproteins". Ed. B. Chance, R.W. Estabrook and T. Yonetani, Academic Press, New York, 1966, p.589.

105. W. de W. Horrocks Jr. Inorg. Chem., 1973, 12, 1211.

106. M.J. Scarlett, A.T. Casey and R.A. Craig. Aust. J. Chem., 1970, 23, 1333.

107. M.J. Scarlett, A.T. Casey and R.A. Craig. Aust. J. Chem., 1971, 24, 31.

108. G.N. La Mar and F.A. Walker. Private communication.

109. E.W. Baker, M.S. Brookhart and A.H. Corwin. J. Amer. Chem. Soc., 1964, 86, 4587.

110. B.D. McLees and W.S. Caughey. Biochem, 1968, 7, 642.

111. R.J. Abraham and P.F. Swinton. J. Chem. Soc., B, 1969, 903.

112. F.A. Walker. Unpublished results.

113. J.D. Satterlee and G.N. La Mar. Unpublished results.

114. L.M. Epstein, D.K. Straub and C. Maricondi. Inorg. Chem., 1967, 6, 1720.

115. A.J. Gordon and R.A. Ford. "The Chemist's Companion". Wiley-Interscience, New York, 1972, p.434.

116. J.O. Alben, W.H. Fuchsman, C.A. Beaudreau and W.S. Caughey. Biochem., 1968, 7, 624.

117. K.S. Murray. Coord. Chem. Rev., 1974, 12, 1.

118. J.F. Villa and W.E. Hatfield. J. Amer. Chem. Soc., 1971, 93, 408.

119. R.W. Mathews and R.A. Walton. Inorg. Chem., 1971, 10, 1433.

120. S.A. Cotton and J.F. Gibson. J. Chem. Soc., A., 1971, 1969.

121. J.H. Wang. Accounts Chem. Res., 1970, 3, 90.

122. C.H. Barlow and W.S. Caughey. Unpublished results.

CHAPTER 5

NUCLEAR MAGNETIC RESONANCE STUDIES OF SOME MIXED LIGAND FERRIC OCTAETHYLPORPHIN COMPLEXES

5.1 Introduction

1. Mixed ligand heme systems

One vital feature of hemeproteins and enzymes which has not received overmuch attention is the question of the ligands and groups attached to the iron atom axial to the heme plane. Whereas most biological and biochemical systems contain dissimilar ligands bound at the axial positions in hexa-coordinate structures, most model systems have tended to overlook this and have comprised two similar ligands bound at these positions. "Mixed ligand" model systems tend to have been studied exceptionally rather than as a rule.

The most extensively studied hemeproteins such as the hemoglobins, myoglobins and cytochromes all contain the iron atom in either a five-coordinate or more usually a hexa-coordinate environment with two dissimilar ligands bound axially. Although the axial ligand in hemoproteins[1-5] in their native states is most frequently the histidyl imidazole, and either another histidyl imidazole, the methionine sulphur, water or O_2, hemeproteins have also been characterised[4] with a wide variety of other axial ligands (halide, azide, cyanide, carbonyl, etc.). In fact the stereochemistry and spin-state in both protein and model compounds are largely determined by the number and nature of the axial ligands.

It has been found most difficult[6] to prepare and to identify metalloporphyrins which contain either mixed anionic, mixed anionic and neutral, or mixed neutral axial ligands. Neutral ligands of mixed anionic and neutral axial ligand species are easily lost and some ligations not unambiguously defined. In the case of mixed neutral ligand species, these mixed complexes are only isolable because the two axial ligands

strongly differ in their σ-donor-π-acceptor balance. The strong π-acceptors exert a trans effect preventing the binding of a second ligand of the same type.

A number of heme porphyrin complexes which have been prepared with mixed axial ligands are listed below in Table 5.1.

TABLE 5.1

Examples[6] of heme-porphyrin complexes with mixed axial ligands

Porphinato ligand	Axial ligands	
Protoporphyrin IX di-Me ester	N_3	Py
	CO	Py
	CO	N-MeIm
Mesoporphyrin IX di-Me ester	CO	Py
Tetraphenylporphin	NO	N-MeIm
	CO	Py, N-MeIm, Pip
	C_6H_5S	N-MeIm

A number of porphyrin complexes which have not been isolated have been studied in solution as mixed ligand complexes, for example the pyridine/water/hemin system of Degani and Fiat[7]. Metastable six co-ordinate complexes involving a hemin/benzenethiol/Lewis base system have been suggested to exist[8], the Lewis base including ligands such as benzenethiol, N-methylimidazole, tetrahydrofuran, etc.

A number of physical techniques have been employed to study heme model systems. This work is particularly concerned with the effect of the axial ligand on structure-function correlations in model systems. In this regard, physical methods which have previously been utilised in the study of such systems include electron paramagnetic resonance[8], electronic and infra-red[9], and nuclear magnetic resonance spectroscopies.[10-14] In this work ligation properties will be studied by means of NMR spectroscopy.

2. Effect of axial ligands

As was indicated in Chapter 1, a number of factors acting in combination control and account for the physical, chemical and electronic properties of heme complexes. Factors which affect the functioning of heme model systems include some of the following: spin state of central metal; Fe(III)/Fe(II) redox potential of the metal; position of metal in relation to porphyrin plane; substituents on porphyrin periphery; nature of axial ligands.

In this chapter particular attention will be addressed to the influence of the axial ligands. Axial ligands have a crucial role in determining the nature of a number of physical properties, although clearly in conjunction with a number of other factors. Some of the physical effects which hinge upon the nature and type of axial ligands are discussed below.

i) Cis and trans effects

These were touched upon in Chapter 1, but it is of special interest to look at the way in which these effects manifest themselves in NMR spectroscopy. Analysis of the origins of ligand effects on chemical shifts is often complex, but factors which merit consideration are the influence of a change in ligand on the ring current field strength, on the bonding interaction between axial ligand and iron and on the strength of porphyrin-iron bonding interactions which, in turn, determine the magnitude of contact shifts due to spin delocalisation from iron into the porphyrin ring system.

One example of both cis and trans effects is found in a comparison of monocyano and dicyano protohemins in aqueous pyridine solutions by IR and NMR spectroscopy. The spectral data are given below in Table 5.2.

TABLE 5.2

Spectral Data[15] for Cyanoprotohemins in Aqueous Pyridine

Species	Infrared ν_{CN} (cm^{-1})	Observed NMR shift of 1,3,5,8-CH_3 protons (ppm)
Py-Fe-CN	2125	-20.2 -19.7 -15.3 -13.6
NC-Fe-CN	2112	-17.5 -17.0 -13.1 -11.4

The replacement of the trans-pyridine ligand by a second cyanide ligand produces a shift in ν_{CN} from 2125 cm^{-1} to 2112 cm^{-1}, which indicates a decrease in bond strength of the C-N bond. This is consistent with the greater sigma donor ability of a trans cyanide ligand compared with a trans pyridine ligand with concomitant increase in π back bonding from iron to the cyanide ligand.

This change in ligand also causes a cis effect in that the PMR shifts found for the ring methyl group protons are markedly less in the dicyanide than in the cyanide/pyridine species. The weaker porphyrin nitrogen to iron bonding in the dicyanide complex is a result of stronger bonding between the iron and the axial ligands. The stronger the interaction between iron and the axial ligands, the weaker will be the interaction between porphyrin and iron. Spin density is less effectively delocalised into porphyrin orbitals and thus the contact shift contribution to the observed shift is reduced, reducing the total observed shift values.

ii) Position of metal

One factor which cannot be ignored is the effect of axial ligands on the position of the metal. It is known from X-ray crystallographic work[16] that in low-spin bis axial ferric heme complexes the iron atom is generally coplanar with the four nitrogen atoms of the porphyrin moiety. Whilst the iron atom can undergo a dynamic movement along the axis between the two axial ligands, its centre of harmonic motion will be in the plane of the four nitrogen atoms.

In the case of a mixed ligand complex however, the circumstances may alter. In fact it would be surprising if with two different axial ligands the iron atom was centred in the porphyrinato nitrogen plane, at least in solution. In the event this would have an influence on the PMR shifts.

Crystallographic data reveal that the iron atom is displaced out of the plane of the porphyrinato nitrogen atoms by about 0.4 Å in high spin ($S = {}^{5}/_{2}$) ferric porphyrin complexes and proteins, e.g. chloro-hemin[17], methoxyiron (III) mesoporphyrin IX dimethyl ester[18] and ferri-myoglobin[19]. The iron atom is about 0.3 Å out of the plane of the porphyrin in high-spin Fe(III) myoglobin derivatives whose X-ray structures have been determined[20,21] and the iron is thought to remain out of the plane in some low-spin complexes[22-25].

The extent to which the iron atom lies outside the plane of the porphyrin ligand is critically dependent upon the nature of the ligands to which the iron is bound perpendicular to this plane. In model complexes two main factors are relevant: the electronic interaction between the ligand and the metal which can affect the spin-state of the iron, and steric hindrance between the incoming ligand group and the planar porphyrin ligands. In a protein the situation is more involved for there are the additional steric requirements of the conformation of the protein itself. It is apparent that in a number of hemeproteins the inability of the ligand side-chains of the protein to come to the best distance relative to the iron (i.e. that distance which would be achieved in models in the absence of the restrictions imposed by the protein) is a source of the reactivity of the protein.

In conclusion it may be germane to regard the metal position relative to the porphyrin plane-metal spin state interrelationship from another viewpoint. Rather than examining the iron spin state as the

cause of the out of plane displacement effect, it is probably more accurate to consider the displacement of the iron atom out of the heme plane as determining the electronic properties of the entity. The exact position of the iron atom is dependent on the axial ligands and a conformational change in a protein involving a movement of the iron atom along the axial axis could be expected to result in a change in the planar interactions. The iron atom being sensitively poised at different distances from the heme plane in different proteins then implies that rather small steric strains in the heme complex could be manifested in terms of substantial changes in magnetic properties.

3. Aim of the Work

The aim of the work described in this chapter is to monitor and evaluate the effect of incremental addition of base on the PMR spectrum of a bis axial heme model system. In particular, the system will be studied for evidence of the existence of mixed ligand species. Such mixed ligand species will be examined from the standpoint of certain features which are of relevance to more complex biological species, for example position of the metal, and with regard to certain physical effects which are of interest in themselves, namely cis/trans effects, spin density additivities, etc.

The heme model system which will be considered for this study is the bis 4-methylpyridinato iron (III) octaethylporphin perchlorate complex. Two different bases will be utilised, pyridine and N-methylimidazole, and this will enable the effect of addition of both a stronger base (N-methylimidazole) and a weaker base (pyridine) than the 4-methylpyridine ligand as base to be monitored.

5.2 Experimental

1. Apparatus and materials

NMR measurements

^{1}H NMR spectra were recorded on the JEOL JNM-C-60HL spectrometer operating at 60 MHz. The solutions used were prepared at 25 mM ferric porphyrin concentration (ca. 11 mg of porphyrin), the solvent being $CDCl_3$ (0.5 ml), isotopic purity 99.5% D, as supplied by Beta Scientific Ltd. Pyridine or N-methylimidazole was added to the solution contained in an NMR tube and the NMR spectrum immediately taken. This was undertaken at a number of temperatures and with a variety of added aliquots ofthe particular base. In some instances it was necessary to add base diluted with $CDCl_3$. TMS was used as an internal standard in all cases.

Bases

Pyridine as supplied by B.D.H. Ltd. and N-methylimidazole as supplied by Fluka A.G. were used.

2. Preparation of compounds

$Fe(OEP)(4\text{-}MePy)_2ClO_4$ was prepared as described in Section 3.2.2.

5.3 Results

1. Addition of pyridine to $Fe(OEP)(4\text{-}MePy)_2ClO_4$

The effect of the addition of pyridine on the spectrum of $Fe(OEP)(4\text{-}MePy)_2ClO_4$ is shown in Figure 5.1, which demonstrates the spectrum changes in the -25 to -20 ppm region resulting at a constant temperature (216°K) from increased amounts of added pyridine. With 11.4 mg of $Fe(OEP)(4\text{-}MePy)_2ClO_4$ present (1.3×10^{-5} moles), each microlitre of added pyridine represents approximately one equivalent of base.

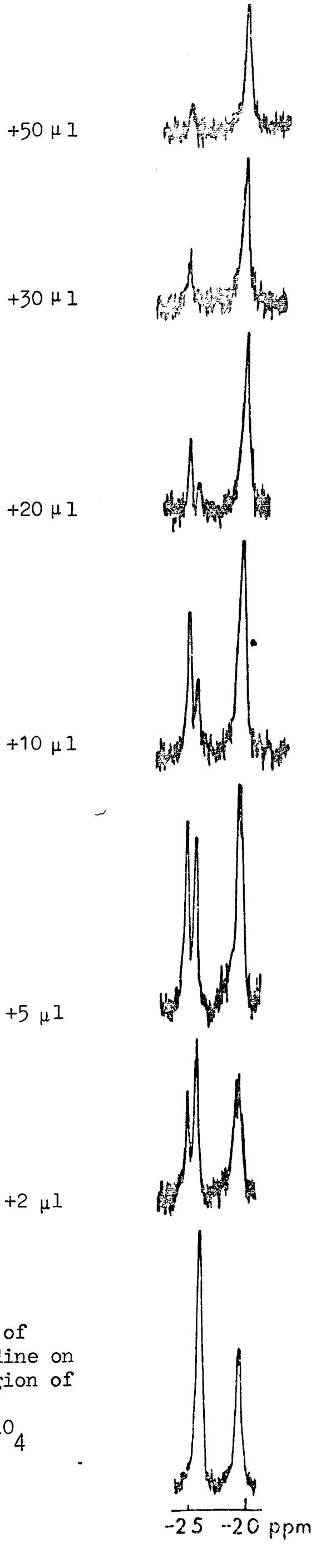


FIG. 5.1 Effect of additions of pyridine on -20 to -25 ppm region of PMR spectrum of $Fe(OEP)(4\text{-}MePy)_2ClO_4$ at 216°K.

The spectrum of $Fe(OEP)(4\text{-}MePy)_2ClO_4$ at 216°K can be easily assigned as was done in Chapter 3. Thus the peaks to low field represent $\gamma\text{-}py_6$ (-24.1 ppm) and $\gamma\text{-}py_4$ (-20.6 ppm) protons whilst the peaks to high field of TMS represent c_{24} (+1.5 ppm), a_4 (+4.3 ppm) and $\alpha\text{-}py_4$ (+9.9 ppm) protons. The remaining peak at -7.6 ppm represents the b_{16} protons. All these assignments correspond to the nomenclature given in Figure 3.5.

On addition of 1 µl of pyridine, a small peak appears downfield of the $\gamma\text{-}py_6$ peak, the $\beta\text{-}py_4$ and a_4 peaks broaden appreciably, and the b_{16} peak splits into two. With the presence of 2 equivalents of pyridine, the peak downfield of the $\gamma\text{-}py_6$ peak is enhanced in intensity relative to the $\gamma\text{-}py_6$ peak, and the original $\beta\text{-}py_4$ peak is split. These results are entirely consistent with the formation of a mixed-ligand complex, that is $Fe(OEP)(4\text{-}MePy)(Py)ClO_4$. The resonance to low-field of the $\gamma\text{-}py_6$ resonance can safely be assigned to the $\gamma\text{-}py_3$ protons of the mixed ligand complex. The broadening or splitting of the peaks assigned to porphyrin ring protons, i.e. a_4, b_{16} and c_{24}, is consistent with the presence of two different porphyrin environments described by the bis-4-methylpyridine and mixed pyridine/4-methylpyridine complexes. The broadening of the $\beta\text{-}py_4$ proton peak, which in some of the spectra where resolution is particularly good is manifested as a splitting, is caused by the different environments of the protons at the β-position of the pyridine ring. In point of fact there are three different environments possible for these protons, one for the $Fe(OEP)(4\text{-}MePy)_2ClO_4$ complex and two for the $Fe(OEP)(4\text{-}MePy)(Py)ClO_4$ complex, but only two resonances are clearly defined.

These assignments are confirmed by observing the effect of further additions of pyridine. The $\gamma\text{-}py_3$ resonance gains in intensity at the expense of the $\gamma\text{-}py_6$ resonance, and a small peak appears at about -11 ppm

(at 216°K) which can be assigned as the γ-py_1 resonance of the mixed ligand complex. With 3 equivalents of added pyridine the order of intensity of resonances is γ-py_6 > γ-py_3 whilst with 5 equivalents of added pyridine the order is γ-py_3 > γ-py_6. With 4 equivalents of added pyridine it would seem that the intensities of the γ-py_6 and γ-py_3 resonances would be about equal.

On continued addition of pyridine to the solution at a constant temperature, the γ-py_6 resonance steadily declines in intensity and with 30 equivalents of added pyridine, the resonance has all but disappeared. The resonances of the a_4 and β-py_4 protons clearly sharpen and become less broad. With 50 equivalents of added pyridine present, the γ-py_3 resonance has appreciably diminished in intensity in relation to the resonance corresponding to the β-py_4 protons, and this latter resonance is considerably sharper than that with only 3 equivalents of pyridine present. These observations are quite explicable in terms of the complete conversion of the bis-4-methylpyridine complex to the mixed ligand pyridine/4-methylpyridine complex, concomitant with conversion of the mixed ligand complex to a bis pyridine complex.

The NMR spectra data are set out in Table 5.3. Two different experimental effects on the spectra are monitored by means of these data.

i) The effect of varying quantities of added base at a fixed temperature;

ii) the effect of varying temperature at a fixed quantity of added base.

With 1 equivalent of base added, the effect of temperature change on the spectrum is broadly similar to the situation where only a bis ligand complex is present. As the temperature is lowered, the resonances of the a_4, b_{16} and c_{24} resonances move upfield whilst the resonances of the protons at the β- and γ-positions of the axial ligand move downfield. Unfortunately the resonances of the protons at the β- and γ-positions of the axial ligand are not observed at the higher temperatures where in bis-complexes these actually shift upfield as the temperature is lowered at first. This is presumably due to the exchange between complexed and

TABLE 5.3

PMR shift data for $Fe(OEP)(4\text{-methylpyridine})_2ClO_4$ + pyridine

Variation of quantity of pyridine added at fixed temperature (216°K)

Equivs. of py added	γ-py_3	γ-py_6	β-py_4		γ-$py_{1/2}$	b_{16}	c_{24}	a_4
0		-24.1	-20.6			-7.6	+1.5	+4.4
1	-25.0	-24.2	-20.7			-7.8	+1.4	+4.0
2	-25.2	-24.4	-20.8	-20.6	-11.1	-8.1	+1.4	+4.2
3	-24.9	-24.2	-20.6	-20.3	-11.0	-8.1	+1.4	+4.1
5	-25.2	-24.4	-20.6			-8.2	+1.1	+3.9
10	-24.9	-24.2		-20.2			+1.3	+4.0
15	-25.2	-24.4		-20.2			+1.1	+4.0
20	-25.0	-24.1		-20.2			+1.1	+3.9
30	-25.2			-20.3			+1.0	+3.9
50	-24.9			-20.2			+1.1	+3.9
Bis py complex				-20.1	-9.6	-8.5	+1.1	+3.8

Variation of temperature at fixed quantity of added pyridine (~1 equiv.)

Temp. (°K)	γ-py_3	γ-py_6	β-py_4	b_{16}	c_{24}	a_4
300				-11.8	-0.7	-4.3
273				-9.8		-1.0
252		-20.4	-17.9	-8.9	+0.7	
237		-22.5	-19.3	-8.4	+0.9	+2.3
231	-24.0	-23.4	-20.0	-8.1	+1.2	+3.2
226	-24.5	-23.7	-20.2	-7.9 -7.7	+1.3	+3.9
216	-25.0	-24.2	-20.7	-7.8	+1.4	+4.0
212	-26.4	-25.5	-22.1 -21.8	-7.4	+1.7	+5.4
208	-27.6	-26.6	-23.4 -22.6	-7.3 -7.2	+1.9	+6.4

uncomplexed base which is prevalent in the situation where base has been added and occurs at a rate which is sufficiently fast to broaden the resonances of the complexed ligand protons so that these are not well defined.

The effect of successive additions of pyridine on the observed spectrum has been described above. The effect of base on the observed shifts is not clear. There is a suggestion that the shifts of the resonances of the a_4 and c_{24} protons become less positive as the quantity of pyridine present is increased, that is the resonances are shifted downfield slightly relative to the situation with no pyridine present. However the total change in shift of 0.5-0.6 ppm is marginally greater than the range of experimental error, but the change in shift of all the other resonances is encompassed within the range of experimental error.

2. Addition of N-methylimidazole to $Fe(OEP)(4\text{-}MePy)_2ClO_4$

With the addition of neat N-methylimidazole, it is found that with only 1 µl of the base added, the observed PMR spectrum changes dramatically and a number of extra resonances appear. (See Figure 5.2 cf. Fig. 3.8). On addition of a further 1 µl, it is found that the spectrum changes dramatically again, many of the resonances of the previous spectrum disappearing. Comparison of this latter spectrum with that of the $Fe(OEP)(N\text{-}MeIm)_2ClO_4$ spectrum described in Chapter 3 demonstrates without question that the two are the same, and that the species present is the $Fe(OEP)(N\text{-}MeIm)_2ClO_4$ complex. Thus only 2 µl of added N-methylimidazcle is required to convert the $Fe(OEP)(4\text{-}MePy)_2ClO_4$ complex completely. With 11.2 mg of $Fe(OEP)(4\text{-}MePy)_2ClO_4$ originally present ($\sim 1.3 \times 10^{-5}$ moles), this represents about 2 equivalents of added base.

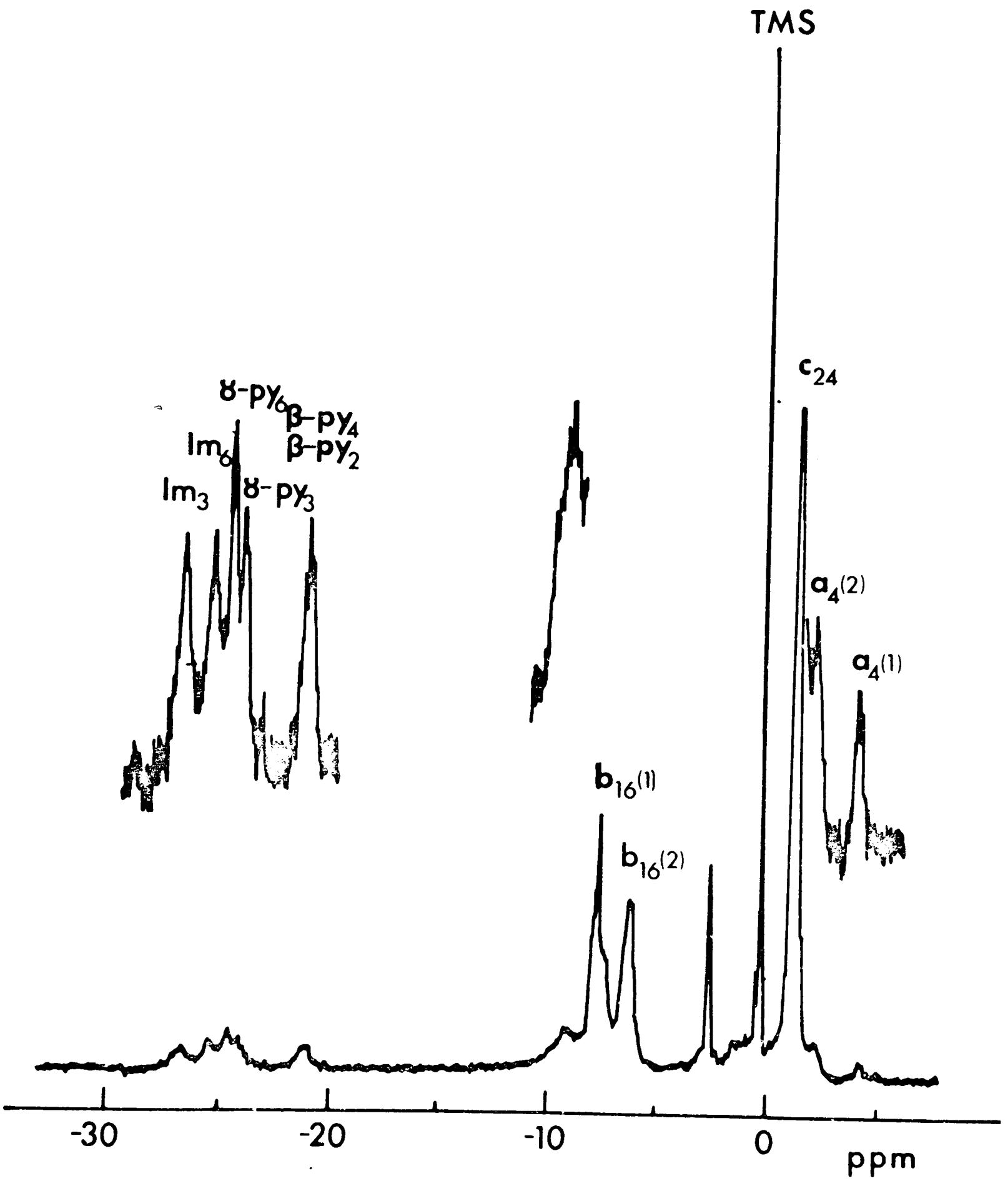


FIG. 5.2 PMR spectrum of $Fe(OEP)(4\text{-}MePy)_2ClO_4$ + N-methylimidazole.

To study more closely the effect of additions of base, the N-methylimidazole was diluted tenfold in $CDCl_3$ and 1 µl aliquots of this solution added. Figure 5.3 illustrates the change in the PMR spectrum of $Fe(OEP)(4\text{-}MePy)_2ClO_4$ at 221°K in the -25 to -20 ppm region as aliquots of diluted base are added. Three extra peaks in the 20-27 ppm downfield region, a new peak at +2.3 ppm and new peaks at -7.8, -6.3, -2.5 ppm all appear. Some of these peaks disappear again as further base is added.

With the spectra of $Fe(OEP)(4\text{-}MePy)_2ClO_4$ and $Fe(OEP)(N\text{-}MeIm)_2ClO_4$ at 221°K both assigned, it is immediately possible to assign some of the resonances in the spectra under consideration here. The resonances at -24.2, -20.7, -7.8, +1.5 and +4.4 ppm coincide with resonances present for the $Fe(OEP)(4\text{-}MePy)_2ClO_4$ complex and can be assigned accordingly as those of $\gamma\text{-py}_6$, $\beta\text{-py}_4$, b_{16}, c_{24} and a_4 protons respectively. In a similar fashion the resonances at -25.0 and -6.0 ppm correspond to resonances of the $Fe(OEP)(N\text{-}MeIm)_2ClO_4$ complex and can be assigned as those of the Im_6 and b_{16} protons. The resonance at +1.4 ppm is very much in the same position as stated earlier and can only arise from the c_{24} protons.

The resonances present in the intermediate spectra can then only arise from the mixed ligand complex, i.e. $Fe(OEP)(4\text{-}MePy)(N\text{-}MeIm)\ ClO_4$. These occur at -26.4, -23.6, -6.3 and +2.3 ppm. The two lowest field resonances are obviously those of the two axial-CH_3 group protons, the only problem being to distinguish which is which. It is apparent that with the mixed ligand complexes, one of the resonances moves upfield and one downfield from its position in the appropriate bis complex. The methyl resonance in the bisimidazole complex is further downfield than the methyl resonance in the bis-4-methylpyridine complex. By substituting a N-methylimidazole ligand for a 4-methylpyridine ligand, it might be assumed that the order of resonances remains the same,

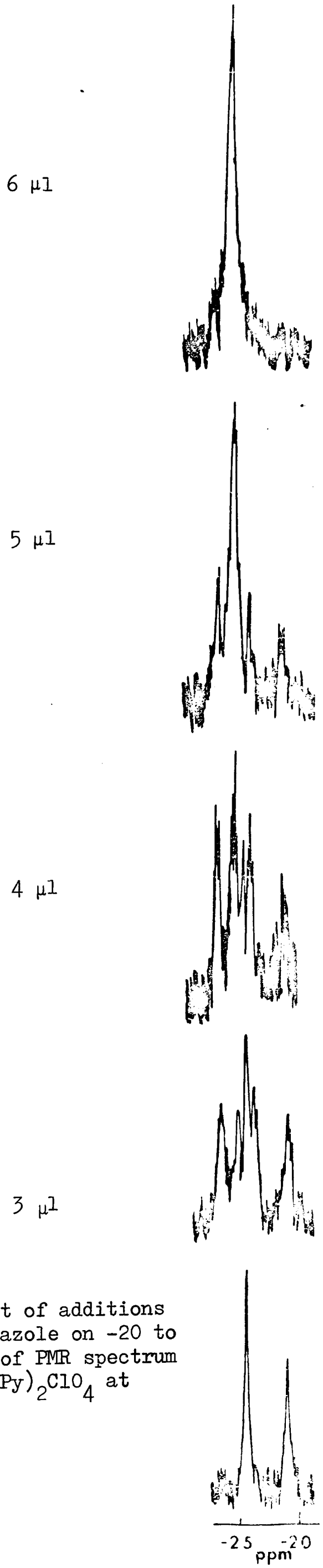


FIG. 5.3 Effect of additions of N-methylimidazole on -20 to -25 ppm region of PMR spectrum of $Fe(OEP)(4\text{-}MePy)_2ClO_4$ at 221°K.

that is the imidazole methyl resonance remaining at lower field to the pyridine methyl resonance. If this assumption is made, then the -26.4 ppm resonance is assigned to the methyl protons of the N-MeIm ligand, designated Im_3, and the -23.6 ppm resonance is assigned to the methyl protons of the 4-MePy ligand, designated γ-py_3.

The resonance at -6.3 ppm lies between the positions of the b_{16} resonance in the two bis complexes and it seems a fair assumption that this resonance arises from the b_{16} protons of the mixed ligand complex. Similarly the resonance at +2.3 ppm could reasonably be assigned to the a_4 protons of the mixed ligand complex, since this resonance lies between the known positions of the a_4 resonance in the two bis complexes. The intensity of the peak in comparison with that of the other a_4 peak present at +4.3 ppm appears about right, examining Figure 5.2, since these peaks are of almost equal area and from a comparison of the Im_3, γ-py_3 and γ-py_6 peaks it is estimated that the ratio of bis-4-MePy complex to 4-MePy/N-MeIm complex is about 1:1 in this case.

The resonances at -7.5, -6.0 and -2.5 ppm are assigned to uncomplexed 4-methylpyridine which is dissociated from the porphyrin complex by the addition of N-methylpyridine which is the more powerful base. The resonance at -8.9 ppm is present in the spectrum of the $Fe(OEP)(N\text{-}MeIm)_2ClO_4$ complex studied in Chapter 3, even at higher temperatures where the Im_6 resonance is broadened. It is therefore most unlikely that this resonance arises from complexed ligand protons and is more likely to arise from the small amount of uncomplexed ligand present.

With all the resonances assigned it is interesting to note the effect of successive aliquots of added base at a fixed temperature, in this case 221°K. Resonances at -26.6, -23.7 and +2.3 ppm first appear which are characteristic of the mixed ligand complex. On further

addition of base, the intensities of the γ-py_6 and β-py_4 resonances decrease in relation to the intensities of the γ-py_3 and Im_3 resonances, and a new resonance attributable to the Im_6 protons of the bis-N-MeIm complex appears at -24.8 ppm. This resonance progressively increases in intensity with further aliquots of added base whilst the γ-py_6 resonance at -24.2 ppm eventually disappears. The resonance of the β-pyridinato protons decreases more slowly, since the resonance of the β-py_2 protons of the mixed ligand complex is coincidental. Finally, the mixed ligand complex is converted completely to the bis-N-MeIm complex and the resonances at -26.4, -23.6 and -21.0 ppm characteristic of the mixed ligand complex disappear entirely and only the resonance of the Im_6 protons at -25.0 ppm remains. The resonance of the a_4 protons of the bis-4-MePy complex at +4.4 ppm also progressively decreases in intensity as the a_4 resonance of the mixed ligand complex appears at +2.3 ppm, and this in turn diminishes in intensity and eventually disappears as the bis N-MeIm complex is formed. The a_4 resonance of this latter complex is probably masked by the TMS and c_{24} resonances.

The NMR spectral data are set out in Table 5.4. The effect of varying quantities of added base at a fixed temperature has been described above. The effect of varying temperature at a fixed quantity of added base is very much as expected, that is the axial ligand proton resonances move downfield and the porphyrin proton resonances move upfield as the temperature is reduced. Warming the solution at 221°K up to 267°K is found to change the spectrum. Thus, with 0.8 equivalents of base added, the spectrum characteristic of a mixture of all 3 possible species, i.e. the bis-4-MePy, bis-N-MeIm and 4-MePy/N-MeIm complexes, at 221°K changes to that characteristic of only the bis-N-MeIm species at 267°K. On recooling however, the original spectrum at 221°K results.

TABLE 5.4

PMR shift data for Fe(OEP)(4-methylpyridine)$_2$ClO$_4$ + N-methylimidazole

Variation of quantity of N-methylimidazole added at fixed temperature (221°K)

Equivs. of N-MeIm added	Im_3	Im_6	γ-py_6	γ-py_3	β-py_4 β-py_2	$b_{16}(1)$	$b_{16}(3)$	c_{24}	$a_4(2)$	$a_4(1)$
0			-24.2		-20.7	-7.8		+1.5		+4.4
0.2			-24.2		-20.7	-7.8		+1.4	+2.3	+4.4
0.4	-26.6		-24.2	-23.7	-20.9	-7.8		+1.4	+2.3	+4.3
0.6	-26.4	-24.8	-24.2	-23.3	-20.6			+1.5	+2.4	+4.4
0.8	-26.4	-25.0	-24.2	-23.6	-20.8			+1.4	+2.3	
1.0	-26.4	-25.0		-23.6	-21.0			+1.4		
1.2		-25.0						+1.3		
Bis N-MeIm		-25.1					-6.0	+1.4		

(Cont.)

Table 5.4 (cont.)

Variation of temperature at fixed quantity of added N-methylimidazole (~ 1 equiv.)

Temp. (°K)	Im_3	Im_6	γ-py_6	γ-py_3	β-py_4 β-py_2	$b_{16}(1)$	$b_{16}(2)$	c_{24}	$a_4(2)$	$a_4(1)$
267						-9.6 -8.2	-6.7	+0.5		
253						-8.8 -7.9	-6.4	+0.8		-1.4
236	-24.6	-23.4			-19.6	-8.3 -7.5	-6.4	+1.2		+2.5
223	-26.6	-25.4	-24.4	-23.8	-20.8	-7.6	-6.2	+1.4	+2.1	+4.2
212	-27.8	-26.4	-25.5	-25.0	-21.8	-7.4	-6.0	+1.7	+3.0	+5.4
202	-29.2	-27.7	-26.8	-26.2	-23.1	-7.1	-5.8	+2.1	+4.4	+7.0

(1) $Fe(OEP)(4\text{-}MePy)_2ClO_4$ complex

(2) $Fe(OEP)(4\text{-}MePy)(N\text{-}MeIm)ClO_4$ complex

(3) $Fe(OEP)(N\text{-}MeIm)_2ClO_4$ complex.

5.4 Discussion

1. Equilibrium processes

In view of the finding that warming and recooling the test solution does not lead to any permanent change in the PMR spectrum, the reactions occurring must be fully reversible, at least with N-methylimidazole as the added base. It is reasonable to assume that this is also the case with pyridine as added base, since cooling the temperature from 223°K to 202°K and then rewarming does not lead to any permanent change in the spectrum. The reactions occurring may be generally described by the following equilibria

$$Fe(OEP)(X)_2ClO_4 \underset{-Y}{\overset{+Y}{\rightleftharpoons}} \underset{(1)}{Fe(OEP)(X)(Y)ClO_4} + X \underset{-Y}{\overset{+Y}{\rightleftharpoons}} \underset{(2)}{Fe(OEP)(Y)_2ClO_4} + 2X \qquad (5.1)$$

where X and Y are aromatic bases.

It is possible to obtain approximate values of K_1 and K_2 by a simple treatment of the equilibria processes as follows.

$$Fe(OEP)(X_2)ClO_4 + Y \overset{K_1}{\rightleftharpoons} Fe(OEP)(X)(Y)ClO_4 + X \qquad (5.2)$$

Initially	A	B	0	0
After reaction	A-α	B-α	α	α

$$K_1 = \frac{\alpha^2}{(A-\alpha)(B-\alpha)} \qquad (5.3)$$

$$Fe(OEP)(X)(Y)ClO_4 + Y \overset{K_2}{\rightleftharpoons} Fe(OEP)(Y_2)ClO_4 + X \qquad (5.4)$$

Initially	α	B-α	0	0
After reaction	α-β	B-α-β	β	β

$$K_2 = \frac{\beta^2}{(\alpha-\beta)(B-\alpha-\beta)} \qquad (5.5)$$

From the PMR spectra, it is possible to measure concentrations of the bis complexes and the mixed ligand complex from areas of peaks corresponding to particular species. Thus values of $(\alpha-\beta)$, β and α can be found for a known value of A and with a particular value of B. Substitution of these values in (5.3) and (5.5) leads to evaluation of K_1 and K_2 respectively. These measurements and calculations were kindly undertaken by Dr. N. Zarb-Adami.

It is readily apparent that the equilibrium constants of these two reactions differ greatly according to whether pyridine or N-methylimidazole is the aromatic base used, since the spectral forms observed are dissimilar. When pyridine is used, the bispyridine complex is not formed to any great degree until an appreciable amount of the bis 4-methylpyridine complex has been converted to the mixed ligand complex. This means that the amount of the mixed ligand complex present has to be fairly large before any appreciable amount of the bispyridine complex is formed. These effects are represented graphically in Figure 5.4, which demonstrates the change in concentration of species present as pyridine is added. From these results, the following equilibrium constant values are calculated:

$$K_1 = 1.0 \pm 0.3$$
$$K_2 = 0.11 \pm 0.06$$

When N-methylimidazole is used as the added base, virtually all the bis 4-methylpyridine complex is converted to the mixed ligand complex before conversion to the bis N-methylimidazole complex begins. The results are illustrated graphically in Figure 5.5. From these results, the following equilibrium constant values are calculated:

$$K_1 \approx \infty$$
$$K_2 = 17 \pm 5.$$

FIG. 5.4 Titration of pyridine into $Fe(OEP)(4\text{-}MePy)_2ClO_4$

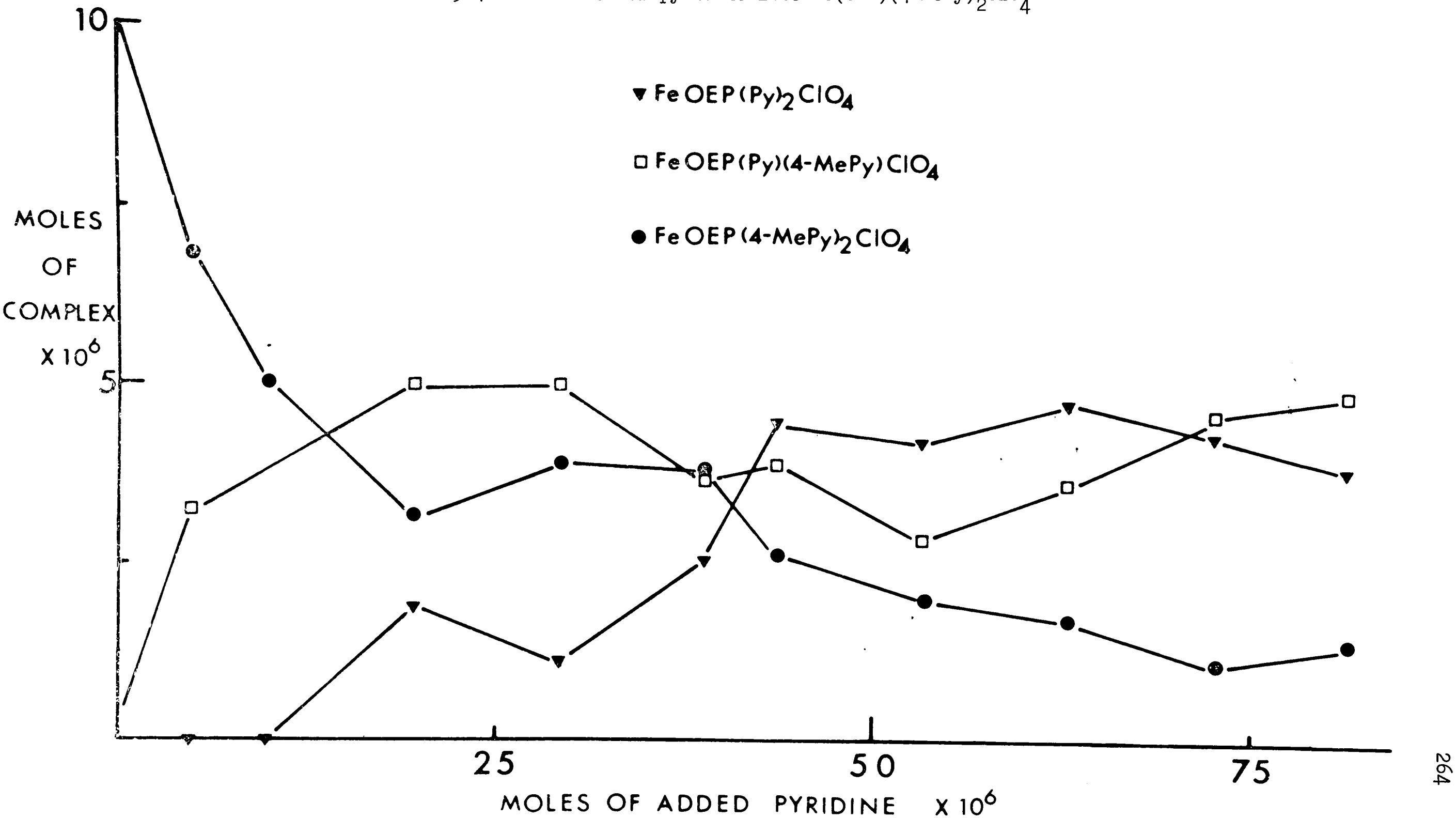
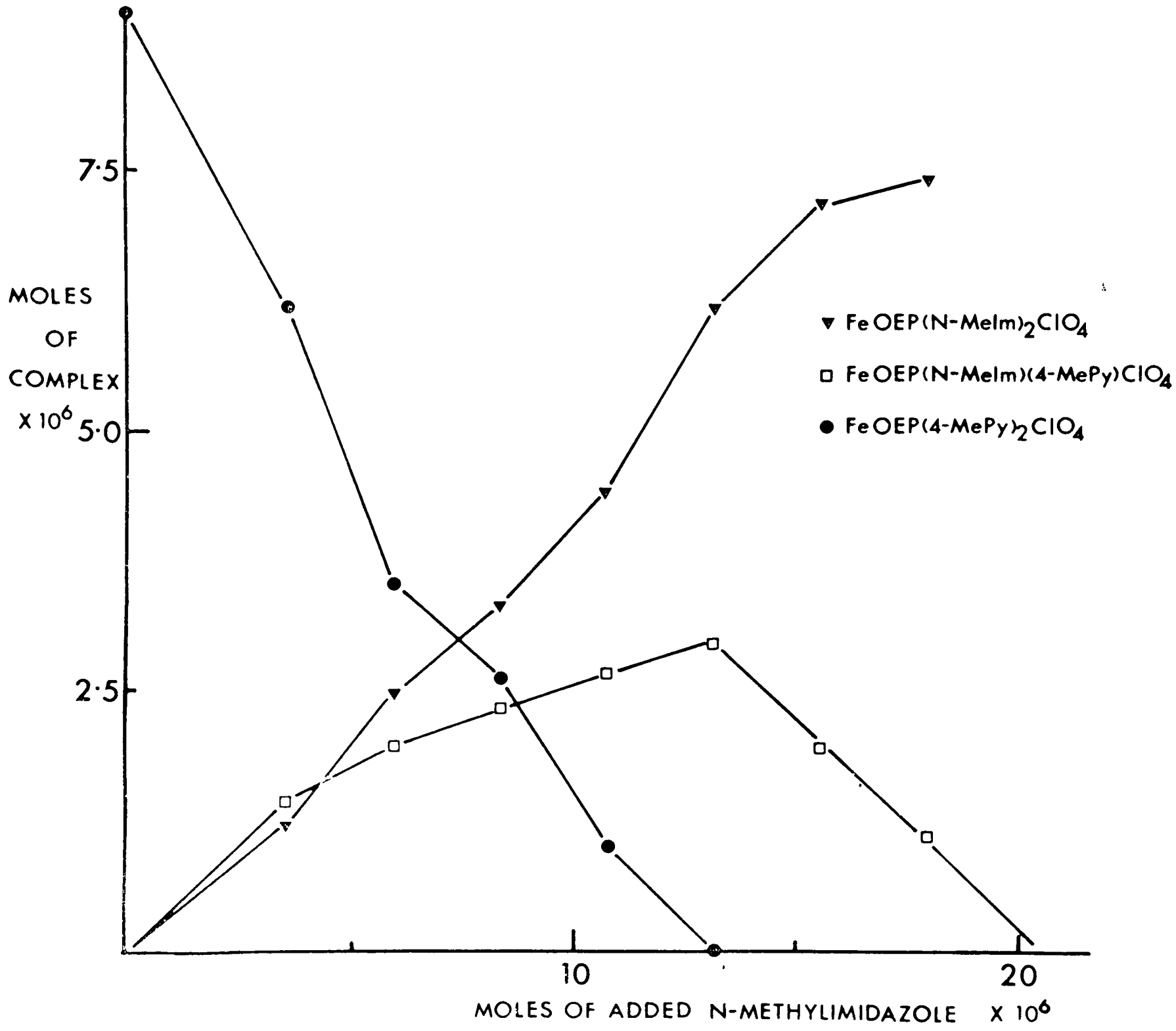


FIG. 5.5 Titration of N-methylimidazole into $Fe(OEP)(4\text{-}MePy)_2ClO_4$



For both systems, $K_1 \gg K_2$, so that the mixed ligand intermediates form fairly readily. The relative pK_a's of the bases are in the order N-methylimidazole > 4-methylpyridine > pyridine. N-methylimidazole thus displaces the weaker base 4-methylpyridine with greater ease than does pyridine, which has to displace a stronger base.

Errors in the results are in the main due to the method of measurement of the concentrations by peak areas. The peaks tend to be fairly small and overlap considerably. This inaccuracy in the measurement of concentration is estimated to be about 10%.

2. NMR shifts

A number of features of the NMR data deserve more than a passing comment. It is immediately apparent that for the 4-MePy/Py system, separate axial ligand proton resonances are observed for the bis-4-MePy and mixed ligand complexes, and yet only one resonance is observed for each of the porphyrin ring protons a, b and c. A fairly steady gradation is observed in the shifts of these latter three resonances on passing from the bis-4-MePy complex through the mixed ligand complex to the bis-Py complex as aliquots of pyridine are added.

In the case of the 4-MePy/N-MeIm system however, separate axial ligand proton resonances are observed for the two bis complexes and the mixed ligand complex, and two separate resonances are also observed for the a_4 and b_{16} porphyrin ring protons. Again though, only one c_{24} resonance is observed throughout.

These effects could arise from one of two causes, either through exchange effects or through lack of resolution. In general, the complexed base at the axial position will be exchanging with free base in solution, and there is the possibility of either the added base (pyridine or N-methylimidazole) or displaced 4-methylpyridine exchanging

with the complexed base. In order for separate resonances to be observed for a particular proton or group of protons in two different environments, the exchange rate of free and complexed base must be much smaller than the frequency shift difference between the protons in the two environments. If the exchange rate of free and complexed base is about the same or greater than the shift difference between the protons in the two environments, a broadening or coalescing of the resonances takes place. Clearly this exchange effect could be responsible for the observations described above. It would be expected that the exchange rate of free and complexed base would increase with increase in temperature. An examination of the behaviour of the resonances on variation of the temperature might be expected to cast light on the origin of the resonance anomalies, since the tendency for resonances to broaden or coalesce due to the exchange effect would diminish with decrease in temperature.

The other possible explanation of the difference in form of the particular resonances is a lack of resolution. If, with the 4-MePy/Py system for example, the shifts of the a_4 resonances characteristic of the three different complexes are very close, then the resolution of the NMR instrument may not be good enough to separate the resonances. Variation of the temperature of the sample may affect the resolving of superimposed resonances due to change in the linewidth of the resonances if the electronic spin-lattice relaxation time alters.

On examination of the spectra and spectral data of the two systems under study, it would appear that both the above-described effects contribute. At the higher temperatures, the axial ligand proton resonances are broadened so much that they are not observable, and this can demonstrably be attributed to the effect of exchange between complexed and free base. As the temperature is lowered, more resonances become discernible as the rate of exchange decreases.

For example, on cooling the Fe(OEP)(4-MePy)$_2$ClO$_4$/Py system from 237°K to 231°K, the resonance originally centred at -22.5 ppm shifts downfield and two separate resonances at -24.0 and -23.4 ppm are readily observed at the lower temperature. At the lower temperatures a splitting of the b_{16} proton resonance is observed for this system at certain temperatures. In the case of the b_{16} proton resonance, the shift difference between the two bis complexes at 216°K is of the order of 1 ppm, whereas for the a_4 and c_{24} proton resonances, the difference in shifts is of the order of 0.5 ppm. A combination of base exchange and lack of sufficient resolution therefore causes these latter two resonances to appear as single unsplit resonances.

In the case of the Fe(OEP)(4-MePy)$_2$ClO$_4$/N-MeIm system, the difference in shifts between the bis 4-MePy and the mixed ligand complex a_4 proton resonances is of the order of 2 ppm, and this frequency shift difference is sufficiently greater than the exchange rate between complexed and uncomplexed base to ensure that separate resonances are observed. Similarly separate resonances are observed for the b_{16} proton resonances, even at the higher end of the temperature range. Only the c_{24} proton resonance appears as a single resonance, in all probability a combination of factors combining since the paramagnetic shifts are probably not very different in the three systems and the resonances are exchange broadened such that the spectrometer resolution is not sufficient to enable them to be seen as separate peaks.

3. Cis and trans effects

The NMR spectral data for the two systems under study effectively illustrate the cis and trans effects operating. Cis effects are experienced by porphyrin ring protons influenced by the axial ligand presence. Trans effects are experienced by the protons of one axial ligand in response to the presence of the other axial ligand.

In the case of the $Fe(OEP)(4\text{-}MePy)_2ClO_4$/Py system, it can be seen that the a_4 and c_{24} resonances are further upfield for the bis-4-MePy complex than for the bis-Py complex. On replacing one axial ligand of the bis-4-MePy complex with a pyridine ligand, this axial ligand can readily be observed to exert a cis effect on the porphyrin ligand, as evidenced by the smaller upfield shift of the a_4 and c_{24} proton resonances. Again, on replacing the 4-methylpyridine ligand of this mixed complex with another pyridine ligand, a cis effect is exerted as evidenced by the further decrease in upfield shift of the a_4 and c_{24} proton resonances. Similar effects are observed for the b_{16} proton resonance, in that the resonance shifts downfield on replacement of 4-methylpyridine ligands by pyridine ligands.

In the case of the $Fe(OEP)(4\text{-}MePy)_2ClO_4$/N-MeIm system, the axial ligand(s) can be seen to be exerting a cis effect on the a_4 protons, since on replacing the 4-methylpyridine ligand with a N-methylimidazole ligand, the a_4 proton resonance of the mixed complex appears some 2 ppm downfield of the same resonance in the bis-4-MePy complex. However it is not so apparent that the axial ligand is exerting a strong effect on the b_{16} and c_{24} protons. For the b_{16} protons this is probably a result of the absence of any resonance which can be assigned conclusively to the mixed ligand complex. For the c_{24} protons, this is probably a reflection of the tailing off of an effect as the distance and number of bonds removed from the porphyrin ring increases.

Trans effects tend to be more pronounced, and give rise to some features which at first sight appear strange. Thus in the $Fe(OEP)(4\text{-}MePy)_2ClO_4$/Py system, replacing the 4-methylpyridine axial ligand with the weaker base pyridine ligand causes the resonance of the γ-methyl protons to move downfield in the mixed ligand complex. In addition, the resonances of the axial ligand protons at the β-position are found to move downfield

for the 4-methylpyridine ligand when the trans-ligand is changed from a similar ligand to the pyridine ligand. Conversely for the pyridine ligand, the resonance of the β-py_4 protons is seen to move slightly upfield when the trans-ligand is changed from a 4-methylpyridine to a weaker base pyridine ligand.

For the Fe(OEP)(4-MePy)$_2$ClO$_4$/N-MeIm system, replacing one 4-methylpyridine ligand with a stronger base N-methylimidazole ligand causes the resonance of the γ-methyl protons in the trans-4-methylpyridine ligand to move upfield. It would appear that the resonance of the β-protons shifts downfield, but the effect is smaller here and may be within the range of experimental error. Substituting the stronger base N-methylimidazole for the weaker base 4-methylpyridine causes the resonance of the N-methyl protons in the trans N-methylimidazole ligand to move upfield.

The effect of the trans ligand can be summarised as follows. Taking any particular axial ligand proton resonance, then replacing the trans axial ligand with a stronger base ligand causes the resonance to shift upfield. Replacing the trans axial ligand with a weaker base axial ligand causes the resonance to shift further downfield.

The effect of the cis ligand is less straightforward to state. It is found that taking any particular porphyrin peripheral proton resonance, replacing the cis axial ligand with a stronger base ligand may cause the resonance to shift upfield (Fe(OEP)(4-MePy)$_2$ClO$_4$/Py system) or downfield (Fe(OEP)(4-MePy)$_2$ClO$_4$/N-MeIm system).

Without analysis of the contact and pseudocontact contributions to the isotropic shift, and without a knowledge of the diamagnetic shifts in the mixed ligand complex, it is not possible to examine these cis and trans effects in any depth. Change in basicity of the axial ligand could affect both the contact and pseudocontact contributions. The former could be susceptible to change in the charge on the

iron, which would affect ligand-metal charge transfer and hence π - delocalisation. The latter could be affected if change in basicity altered the magnetic anisotropy of the complex. However it may be that the magnetic anisotropy of the complex is governed more by difference in ligand type (i.e. imidazole and pyridine type) than by change in the basicity of the ligand base.

4. Hyperfine shifts of the mixed ligand complex protons

It should be possible to examine the observed shifts of the mixed ligand complex protons and extract hyperfine interaction data as was the case for the complexes examined in Chapter 4. A number of assumptions and extrapolations will of necessity have to be introduced, but nevertheless it is of interest to compare the hyperfine interaction data for the mixed ligand complex with equivalent data for each of the bis--complexes.

Taking the experimental results for the $Fe(OEP)(4\text{-}MePy)_2ClO_4$/Py system and using the PMR results for the $Fe(OEP)(Py)_2ClO_4$ and $Fe(OEP)(4\text{-}MePy)_2ClO_4$ complexes obtained in Chapter 3, the observed shifts are plotted at various temperatures and extrapolated to produce the observed shift at a temperature of 200°K. Although there are no diamagnetic data for any bis-pyridinato complexes, it is reasonable to suppose that the data for the metal-free porphyrin will not be very different. The diamagnetic values for the pyridinato protons are taken from Table 4.7 and here again it is not expected that the values for say a cobalt(III)-octaethylporphin complex would be substantially different. The observed PMR shifts of particular protons at 200°K, the corresponding diamagnetic shifts and the resultant isotropic shifts (equal to observed minus diamagnetic shift) are given in Table 5.5.

TABLE 5.5

Hyperfine parameters for $Fe(OEP)(4\text{-}MePy)(Py)ClO_4$ mixed ligand complex at 200°K

	γ-py$_3$	γ-py$_6$	β-py$_2$	β-py$_2$	β-py$_2$	γ-py$_1$	γ-py$_2$	$b_{16}^{(3)}$	$b_{16}^{(2)}$	$b_{16}^{(1)}$	$c_{24}^{(3)}$	$c_{24}^{(2)}$	$c_{24}^{(1)}$	$a_4^{(3)}$	$a_4^{(2)}$	$a_4^{(1)}$
Observed shift(ppm)	-28.4	-26.8	-22.7	-23.7	-23.2	-13.8	-11.5	-8.1	-7.4	-7.1	+1.7	+2.0	+2.2	+6.0	+6.7	+6.9
Diamagnetic shift(ppm)	-1.3	-1.3	-4.7	-4.7	-4.6	-5.9	-5.9	-4.2	-4.2	-4.2	-2.0	-2.0	-2.0	-10.2	-10.2	-10.2
Isotropic shift(ppm)	-27.1	-25.5	-18.0	-19.0	-18.6	-7.9	-5.6	-3.9	-3.2	-2.9	+3.7	+4.0	+4.2	+16.2	+16.9	+17.1
Pseudocontact shift(ppm)	-17.9	-17.9	-32.1	-32.1	-32.1	-28.4	-28.4	+11.1	+11.1	+11.1	+5.7	+5.7	+5.7	+32.0	+32.0	+32.0
Hyperfine shift(ppm)	-9.2	-7.6	+14.1	+13.1	+13.5	+20.5	+22.8	-15.0	-14.3	-14.0	-2.0	-1.7	-1.5	-15.8	-15.1	-14.9
a_i (10^5 Hz)	+3.1	+2.5	-4.7	-4.4	-4.5	-6.9	-7.6	+5.0	+4.8	+4.7	+0.7	+0.6	+0.5	+5.3	+5.1	+5.0
ρ_c^π (% of 1 electron)	+0.77	+0.64	+0.73	+0.67	+0.69	+1.1	+1.2							-0.81	-0.78	-0.77

(1) $Fe(OEP)(4\text{-}MePy)_2ClO_4$ complex

(2) $Fe(OEP)(4\text{-}MePy)(Py)ClO_4$ complex

(3) $Fe(OEP)(Py)_2ClO_4$ complex.

Perhaps the greatest uncertainty is in calculating values for the pseudocontact shifts for each proton type. These pseudocontact contributions can be estimated with a knowledge of molecular geometry and information on magnetic anisotropy. The molecular dimensions of the octaethylporphin entity are known[26] and good estimates can be made for the geometrical parameters of the axial ligand protons in the same way as was done for the complexes in Chapter 4. Magnetic anisotropy data is less easy to come by, and in particular no data is available for the mixed ligand complex. In the absence of the second-order Zeeman (SOZ) interaction, g values may be used instead of magnetic susceptibility (χ) values. ESR g values have been measured for the $Fe(OEP)(Py)_2ClO_4$ complex[27] and although Momenteau et al.[28] have concluded that the g-tensor is dependent on the basicity of the axial ligand, g values in practice do not vary much between porphyrin complexes with the same axial ligand type and it would seem a reasonable approximation to apply the above values of $g_{\parallel}$ and $g_{\perp}$ for the $Fe(OEP)(4\text{-}MePy)_2ClO_4$ complex, particularly as the use of g tensor values in place of magnetic susceptibility values is of suspect validity anyway. The same values are also used for the mixed ligand complex, although here there must be more doubt as to the acceptability of this assumption.

Pseudocontact shifts calculated from equation (4.4) are given in Table 5.5, using g values of 3.4 ($g_{\parallel}$) and 0.58 ($g_{\perp}$) and values of r and θ as appropriate. The assumption is made that only the doublet spin state of the iron atom is populated at this temperature. The hyperfine (contact) shifts are found by subtraction of the calculated pseudocontact shifts from the corresponding isotropic shifts. By means of equation (4.3) the hyperfine constants may be found since all the parameters are known except for a_i.

It is readily observed for the porphyrin protons that the hyperfine constants are all positive and follow the trend $(Py)_2 > (Py/4\text{-}MePy) > (4\text{-}MePy)_2$. This is consistent with the explanation given in Chapter 4 for the bis systems and explicable in terms of a π spin delocalisation mechanism. Increase in basicity of the axial ligand would be expected to decrease positive charge on the iron, thus raising the energy of the e_g orbitals. Ligand to metal charge transfer would be less favoured and a decrease in spin density in the porphyrin ring would be observed since interaction between the metal e_g and porphyrin $3e_g$ orbitals will decrease. The effect of replacing one pyridine ligand by a 4-methylpyridine ligand in forming the mixed ligand complex is to increase the overall basicity of the axial ligands, and hence reduce the spin density at the porphyrin periphery. Replacing the pyridine ligand in the mixed ligand complex by a further 4-methylpyridine ligand reinforces this effect.

The hyperfine data for the axial ligand protons are not as easy to interpret. The protons at the β-position produce hyperfine data which at first glance appears anomalous in that the hyperfine constant for the mixed ligand complex is not intermediate between those for the bis complexes. However it is likely that one of the reasonances for the β-protons of this mixed ligand complex is unresolved, since it may be expected that there should be two separate resonances, one due to the β-protons of the pyridine axial ligand and one due to the β-protons of the 4-methylpyridine axial ligand. As the resonance of the β-protons of the bis-4-MePy complex is shifted to lower field than the corresponding resonance of the bis-Py complex, it would be reasonable to suggest that for the mixed ligand complex, the β-proton resonance should be further downfield for the 4-methylpyridine axial ligand protons than for the pyridine axial ligand protons. The bonding interactions which lead to greater hyperfine shifts for β-pyridinato protons in the case of the

bis-pyridine complex as compared with the bis-4-methylpyridine complex should equally lead to greater hyperfine shifts (but less negative isotropic shifts) for the β-pyridinato protons of the pyridine ligand in relation to those of the 4-methylpyridine ligand for the mixed ligand complex.

Examination of the hyperfine data for the resonances of protons at the γ-position of the axial ligand is not particularly meaningful unless the spin densities at these positions are utilised. However this exercise involves the use of empirical McConnell type relationships (2.21) and (2.22) and the assumptions inbuilt into (2.22), restricting its general applicability, were pointed out in Chapter 2. On the basis that the spin densities calculated by this method provide something of a qualitative description, if not a quantitative description, of what is taking place, then by inserting the values of $Q_H = -6.5 \times 10^7$ Hz and $Q_{CH_3} = +4 \times 10^7$ Hz respectively into (2.21) and (2.22), the values of the spin density (ρ_C^π %) at various carbon atoms can be compared.

Perhaps the most effective approach is to compare the total spin densities at various axial ligand carbon atoms of the two bis and one mixed ligand complexes, and this is done in Table 5.6 below.

TABLE 5.6

Comparison of spin density distributions at various axial ligand positions

Complex	Total spin density (% of 1 electron)	
	β	γ
$Fe(OEP)(Py)_2ClO_4$	2.92	2.34
$Fe(OEP)(Py)(4\text{-}MePy)ClO_4$	2.68	1.82
$Fe(OEP)(4\text{-}MePy)_2ClO_4$	2.76	1.28

It is not perhaps surprising to find that the spin density at the γ-position of the mixed ligand complex is intermediate between the bis-pyridine and bis-4-methylpyridine complex. It is at first surprising

to find that this is not the case at the β-position, but this may be rationalised in terms of the earlier supposition that the resonance of the β-protons of the pyridine adduct of the mixed ligand complex is unresolved. Generally the values for the spin densities are in line with those calculated for the bis-pyridinatoferricporphyrin complexes studied in Chapter 4 (viz. Table 4.11).

A similar treatment of the experimental data for the $Fe(OEP)(4\text{-}MePy)_2ClO_4$/N-MeIm system is more difficult. Whilst it is possible to make certain assumptions about the 4-MePy/Py mixed ligand complex in regard to molecular dimensions and magnetic anisotropy, such assumptions are much more unrealistic for the 4-MePy/N-MeIm mixed ligand complex.

It was reported in Chapter 3 that the $Fe(OEP)(N\text{-}MeIm)_2ClO_4$ complex possessed a large in-plane magnetic anisotropy and three g-values were measured. As the $Fe(OEP)(4\text{-}MePy)_2ClO_4$ complex is axially symmetric possessing only two g values, there must be considerable doubt as to values of the g tensor for the mixed ligand complex. Furthermore the lengths of the metal-axial ligand bonds are likely to be significantly different from the lengths in the respective bis complexes due to the effects of the trans ligands.

5. Position of iron atom

One of the aims of this work was to examine the mixed ligand species with a view to ascertaining the position of the metal atom relative to the porphyrin ring plane. There does not however appear to be any experimental evidence which will provide any insight into this.

With the metal out of the porphyrin plane, it may be expected that the ring methylene groups which experience restricted rotation would become diastereotopic. A split resonance for the methylene group protons could then result, as is found in the case of complexes such as (OEP)FeCl.

This split resonance is indeed found under certain conditions for both systems studied. Unfortunately it is not possible to attribute this splitting uniquely to the complex conformation factors, since the splitting may also represent the methylene proton resonance exhibited by two different complexes present, that is the mixed ligand complex and either of the bis ligand complexes.

The experimental observations are therefore incapable of establishing the metal position and whether there is out-of-plane displacement.

References

1. H.A. Harbury and R.H.L. Marks. "Inorganic Biochemistry", ed. G.I. Eichhorn, Elsevier, Amsterdam, 1973, Vol. 2, Chapter 26.

2. D.C. Wharton. "Inorganic Biochemistry", ed. G.I. Eichhorn, Elsevier, Amsterdam, 1973, Vol. 2, Chapter 27.

3. B.C. Saunders. "Inorganic Biochemistry", ed. G.I. Eichhorn, Elsevier, Amsterdam, 1973, Vol. 2, Chapter 28.

4. E. Antonini and M. Brunori. "Hemoglobin and Myoglobin in their Reactions with Ligands", North-Holland, Amsterdam, 1971.

5. J.M. Rifkind. "Inorganic Biochemistry", ed. G.I. Eichhorn, Elsevier, Amsterdam, 1973, Vol. 2, Chapter 25.

6. J.W. Buchler. "Porphyrins and Metalloporphyrins", ed. K.M. Smith, Elsevier, Amsterdam, 1975.

7. H.A. Degani and D. Fiat. J. Amer. Chem. Soc., 1971, 93, 428.

8. J.P. Collman, T.N. Sorrell and B.M. Hoffman. J. Amer. Chem. Soc. 1975, 97, 913.

9. J. Peisach, W.E. Blumberg and A. Adler. Ann. N.Y. Acad. Sci. 1973, 206, 310.

10. W.S. Caughey. "Inorganic Biochemistry", ed. G.I. Eichhorn, Elsevier, Amsterdam, 1973.

11. K. Wüthrich. Struct. Bonding, 1971, 8, 53.

12. K. Wüthrich, R.G. Shulman, B.J. Wyluda and W.S. Caughey. Proc. Nat. Acad. Sci. U.S. 1969, 62, 636.

13. H.A.O. Hill and K.G. Morallee. J. Amer. Chem. Soc. 1972, 94, 731.

14. G.N. La Mar and F.A. Walker. J. Amer. Chem. Soc., 1973, 95, 1782.

15. W.S. Caughey, C.H. Barlow, D.H. O'Keeffe and M.C. O'Toole. Ann. N.Y. Acad. Sci., 1973, 206, 310.

16. J.L. Hoard. Science, 1971, 174, 1295.

17. D.F. Koenig. Acta. Cryst., 1965, 18, 663.

18. J.L. Hoard, M.J. Hamor, T.A. Hamor and W.S. Caughey. J. Amer. Chem. Soc., 1965, 87, 2312.

19. J.C. Kendrew. Science, 1962, 139, 1259.

20. B. Chance. "Probes of Structure and Function of Macromolecules and Membranes"; eds. B. Chance, T. Yonetani and A.S. Mildvan, Vol. 2, Academic Press, New York, 1971, p.321.

21. H.C. Watson and B. Chance. "Hemes and Hemoproteins", eds. B. Chance, R.W. Estabrook and T. Yonetani, Academic Press, New York, 1966, p.149.

22. L. Stryer, J.C. Kendrew and H.C. Watson. J. Mol. Biol. 1964, 8, 96.

23. C.L. Nobbs. J. Mol. Biol. 1965, 13, 325.

24. B.P. Schoenborn. J. Mol. Biol. 1969, 45, 297.

25. B.P. Schoenborn. Ref. 20, p.181.

26. A. Takenaka, Y. Sasada, E. Watanabe, H. Ogoshi and Z. Yoshida. Chem. Lett., 1972, 1235.

27. P.D. Skyte. Unpublished result.

28. M. Momenteau, J. Mispetter and D. Lexa. Biochim. Biophys. Acta., 1973, 320, 652.

CHAPTER 6

NUCLEAR MAGNETIC RESONANCE STUDIES OF PORPHODIMETHENE FERRIC COMPLEXES

6.1 Introduction

1. Redox activities in the biological context

The presence of several metalloporphyrins as participants in various types of biologically important electron exchange reactions has been recognised for some time. Amongst these are iron porphyrins which are components of cytochromes, catalase and peroxidase, a cobalt porphyrin derivative which is an essential component of vitamin B_{12}, and chlorophyll, a dihydroporphyrin containing magnesium. These electron exchange reactions are in essence a direct function of the redox properties of the metalloporphyrins and in attempting to define an exchange mechanism, it is usually helpful to concentrate on the oxidation and reduction characteristics of the metalloporphyrin entity.

The classification of the redox reactions for metalloporphyrins includes four main types, according to the occurrence of:

1) Reversible changes in the formal oxidation number of the metal ("inorganic" redox reactions).

2) Reversible changes of the oxidation state of the porphyrin ("organic" reversible redox reactions).

3) Reversible or irreversible redox reactions of the central metal ion with axial ligands.

4) Reversible or irreversible redox reactions of the porphyrin ligand, in particular addition of oxygen or hydrogen.

The biological activities of metalloporphyrins corresponding to each of the above redox types can be classified similarly.

1. Electron transport is, by virtue of a reversible valency change of the heme iron, the main biological function of the cytochromes in

various biological redox reactions (e.g. respiration, photosynthesis). The porphyrin ligand can participate in the sequence of reactions.

2. The chlorophylls contain redox inert magnesium as the central ion and form π-cation radicals on oxidation. Such radicals play a prominent role in photosynthesis and the biosynthesis of photochlorophyll.

3. Some hemoproteins function in the transport and activation of molecular oxygen as well as in the decomposition of hydrogen peroxide (e.g. hemoglobin, tryptophan, dioxygenase, cytochrome P450, catalases).

4. The metabolism of naturally occurring tetrapyrrole metal complexes includes irreversible oxygenation and hydrogenation reactions (bile pigment formation, protochlorophyll hydrogenation).

This Chapter will be primarily concerned with two aspects of redox activities of the iron porphyrin entity:

i) The effect of hydrogen addition to the porphyrin ligand, and the influence of this on metal-porphyrin interactions, resulting from the break in conjugation of the porphyrin ring π-electron system.

ii) The effect of oxo-bridges between iron porphyrins on the metal-porphyrin interactions and on the metal-metal interactions. This event can be regarded as a partial reduction of the oxygen molecule to a peroxo bridge.

2. Redox properties of the porphyrin ligand

The oxidation and reduction potentials of some non-metallic porphyrin derivatives are given in Tables 6.1 and 6.2. Electron-donating substituents lower the oxidation potential but also lower the reduction potential to more negative values (inductive effect). Protonation of the methene bridges of porphyrins invariably occurs when reduction is carried out in protic media and is usually fully reversible with a rise in the redox potential of the solution.

TABLE 6.1

Oxidation potentials[1] of some non-metallic porphyrin derivatives

Porphyrin	OX $E_{\frac{1}{2}}(1)$	OX $E_{\frac{1}{2}}(2)$
OEP	0.81	1.30
$OEPH_2^{2+}$	1.65	-
ETIO	0.77	-
PROTO	0.83	-
TPP	0.97	1.12

TABLE 6.2

Reduction potentials[1] of some non-metallic porphyrin derivatives

Porphyrin	RED $E_{\frac{1}{2}}(1)$	RED $E_{\frac{1}{2}}(2)$
OEP	-1.46	-1.86
ETIO	-1.37	-1.80
MESO	-1.34	-1.73
TPP	-1.08	-1.52

The reduction of a porphyrin by the addition of two electrons and two protons results in the formation of two classes of isomeric dihydroporphyrins - chlorins and phlorins[2] (Figure 6.1). These two classes have quite different chemical and physical properties, for example the chlorins are relatively stable to air-oxidation whereas the phlorins are not. Further reduction of the dihydroporphyrins by two more electrons and two protons produces 3 classes of isomeric tetrahydroporphyrins[3]: bacteriochlorins, chlorin-phlorins[4] and porphomethenes[5]. In an analogous manner to the dihydroporphyrins, the bacteriochlorins are the most stable tetrahydroporphyrins with respect to air oxidation. This particular property of stability toward oxidation could be related to the fact that chlorins and bacteriochlorins are saturated in peripheral ring positions whereas phlorins and chlorin-phlorins involve methene bridge saturation. The reduction pathway is followed until all four methene bridges are reduced.

Closs[6] first described the reductive protonation of (TPP)Zn to $(H_2TPP)Zn$. This reaction has been extended to complexes $(OEP)MX_K$ by Buchler et al[7-9]. Electron transfer from sodium anthracenide in tetrahydrofuran at 20° furnishes, in subsequent steps, the green porphin monoanion and the red porphin dianion (Reaction 6.1). Protonation yields orange-red, air-labile α,γ-dihydroporphins (porphodimethenes, reaction 6.2) of general formula

Reduction stage

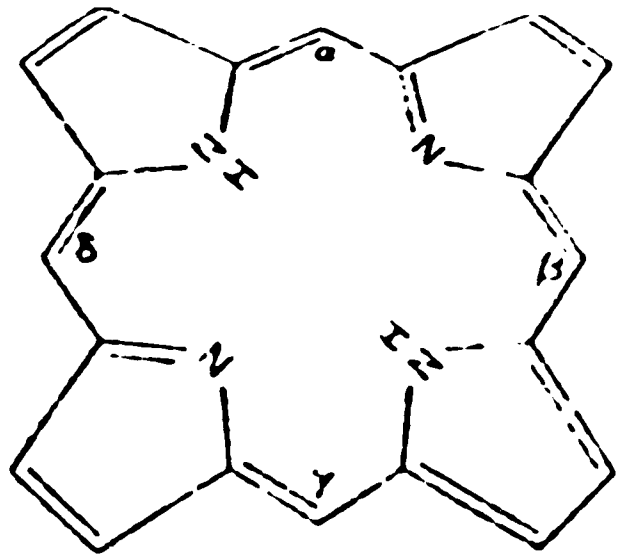
$$(OEP)MX_K \xrightarrow[-\ C_{14}H_{10}]{NaC_{14}H_{10}} Na[(OEP)MX_K] \xrightarrow[-\ C_{14}H_{10}]{NaC_{14}H_{10}} Na_2[(OEP)MX_K] \qquad (6.1)$$

Protonation stage

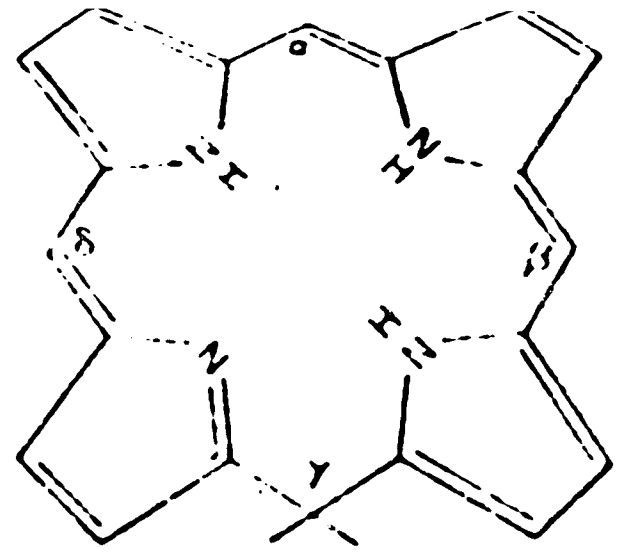
$$Na_2[(OEP)MX_K] \xrightarrow[-2NaOCH_3]{2CH_3OH} (OEPH_2)MX_K \qquad (6.2)$$

Reaction (6.2) can be modified to yield reaction (6.3) which represents a reductive alkylation with an alkyl iodide.

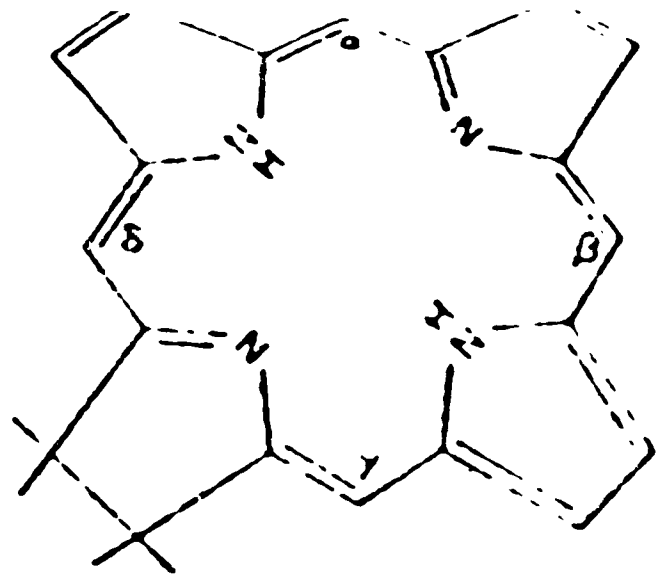
$$Na_2[(OEP)MX_K] \xrightarrow[-2NaI]{2RI} (OEPR_2)MX_K \qquad (6.3)$$



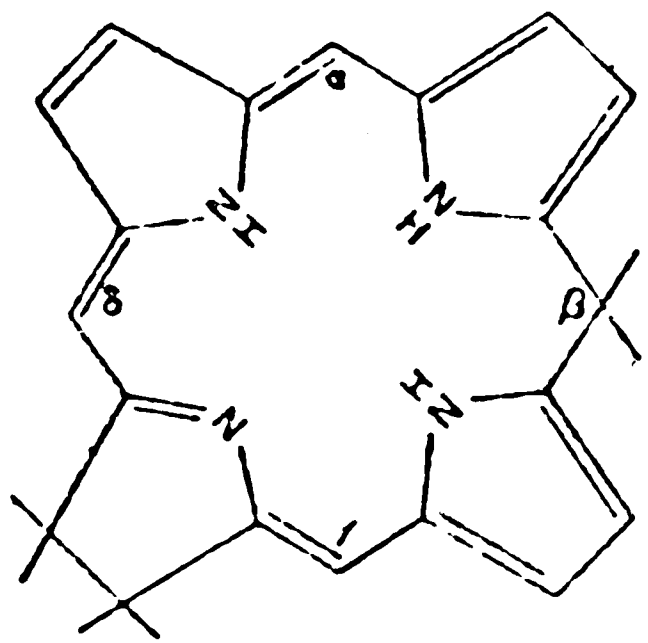
PORPHYRIN



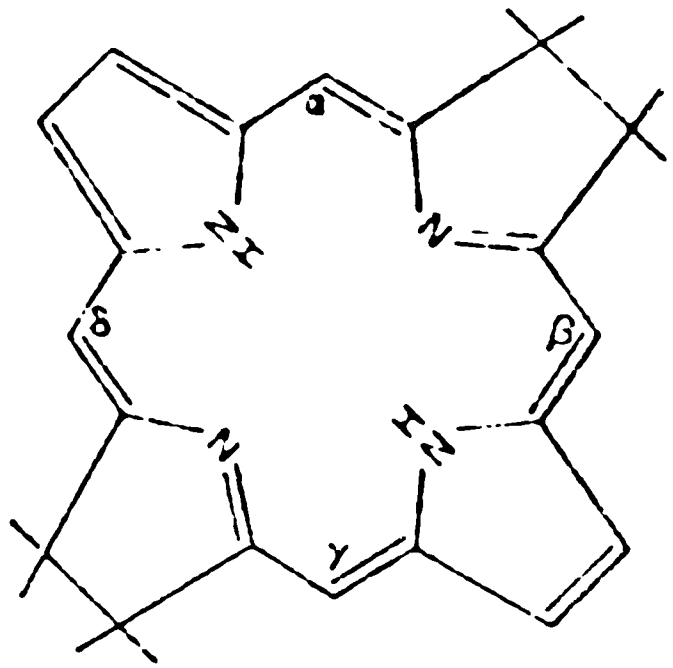
PHLORIN



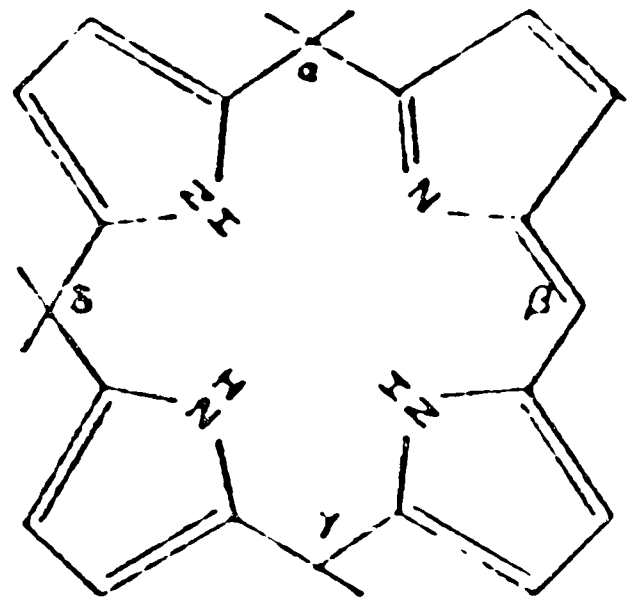
CHLORIN



CHLORIN-PHLORIN



BACTERIOCHLORIN

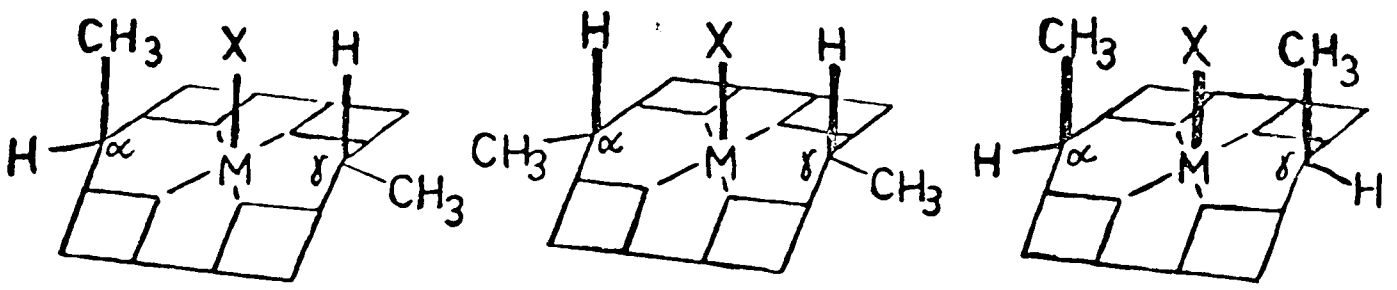


PORPHOMETHENE

FIG. 6.1 Structures of chlorins and phlorins.

Contrary to their α,γ-unsubstituted analogues these compounds are not dehydrogenated by oxygen and do not rearrange to chlorins. This can be attributed to steric constraints imposed upon the ligand by introduction of the two additional alkyl groups.

The saturation of C_α and C_γ with concomitant reductive alkylation offers the tetrapyrrole ligand a certain flexibility. In the presence of a central metal, a rather strainless geometry is attained by a roof-like folding of the macrocycle about the line penetrating C_α and C_γ. Thus, the coplanarity of the two pyrromethene systems can be kept to a large degree. This folding is further aided by an axial ligand X residing in a "chimney position". Three isomers denoted (i), (ii) and (iii) in Figure 6.2 below are then possible.



anti
X

syn–equatorial
Y

syn–axial
Z

(i) anti (ii) syn-equatorial (iii) syn-axial

Figure 6.2: Stereoisomers of folded complexes $(OEPR_2)MX$.

The shape of the roof makes an approach by alkyl groups from above more easy than from below, leading to the expectation that two alkyl groups should enter the porphin ligand in the two chimney positions

neighbouring the axial ligand. Stereoisomer (iii) should therefore be the most probable product.

3. Oxo bridging in heme systems

Polynuclear iron clusters are widely accepted as important entities in the metal binding sites of a number of proteins and enzymes. It is well established that in many systems more than one iron porphyrin moiety, as well as other metal ions, may be cooperatively involved, and antiferromagnetic spin coupling between metal centres is operative in a variety of important biological macromolecules[10-19]. Although Fe-S-Fe bridging has been characterised by X-ray methods in non-heme iron-sulphur proteins[20,21], and exchange interactions across this sulphur bridge have been recognised using magnetic[12,22] and spectroscopic measurements[11,23], there is less concrete evidence for Fe-O-Fe bridging in native proteins. However it seems likely that this latter system does occur in view of its proven existence in a number of model systems.

Caughey[24-26] and Fleischer[27,28] and their respective co-workers have characterised a number of oxo-bridged iron (III) complexes with porphyrins such as TPP, deuteroporphyrin IX dimethyl ester and proto-porphyrin IX dimethyl ester. X-ray structure determinations have confirmed the binuclearity and Fe-O-Fe bridging[29]. Highly characteristic physical properties result from the presence of the Fe-O-Fe linkage[30]. Certain resonances in NMR spectra exhibit broadening and small paramagnetic shifts (see below). The antiferromagnetic character of these compounds is illustrated by magnetic susceptibilities measured from 1.4 to 293°K for μ-oxo-bis-(protoporphyrin IX dimethyl ester iron (III)) which were consistent with strong coupling between high-spin ($S = {}^{5}/_{2}$) iron (III) atoms[31]. Crystal structures for this compound[32] and for the related TPP compound[27] reveal a stereochemistry of the high-spin iron (III) type

with each iron out of the porphyrin plane by ca. 0.5 Å toward the bridging oxygen atom. Mössbauer[25,33] and electronic spectra[24,25,33] of these complexes have also been determined.

Cytochrome c oxidase is considered to possess two heme a groups and two copper atoms at the active site. The mode of oxygen bonding is not fully established, although Caughey considers that Fe-O-Fe bridging exists between heme a groups in the fully oxidised oxidase, despite the large bulky C_{17} side chain on the porphyrin[30]. The NMR spectrum of the oxidase is very similar to that of the μ-oxo-bis-proto-porphyrin complex[34]. The significance of this bridging in cytochrome c oxidase and possibly other hemeproteins is made more likely by the evidence that a μ-oxo-linkage can be formed from hemin a[30,35], and from 2,4-bis(ethoxycarbonylcyclopropyl)deuterohemin[36] despite the presence of such bulky groups on the porphyrin ring.

It has been shown that one of the hemerythrin proteins, which are involved in oxygen transport in certain invertebrates, possesses a Fe-O-Fe linkage. Klotz, Williams and co-workers[15,16] and Gray and co-workers[17] demonstrated that the active sites in the sub-units of the oxy and met forms consist of exchange-coupled ($S = {}^{5}/_{2}$) iron (III) pairs with Fe-O-Fe bridging.

4. NMR studies of oxo-bridged heme systems

NMR studies on a number of oxo-bridged porphyrin systems have been reported. μ-Oxotetraphenylporphin iron(III)[37] and μ-oxo-bis protohemin dimethyl ester[30] have been tried and the contact shifts used as a direct measure of the antiferromagnetic coupling constant J. The spectra are unusual for iron porphyrin NMR spectra in that although the chemical shifts fall within the usual range for diamagnetic metal porphyrins, most resonances are broader and shifted somewhat from the case of low-spin iron (II) porphyrins. Furthermore the lines are well-resolved and

are quite narrow (~ 50 Hz) as compared with the spectra of iron (III) porphyrin complexes commonly observed. These features are amply demonstrated in Figure 6.3 and are most likely a result of the strong magnetic exchange interactions which give rise to majority population of the diamagnetic $S' = 0$ ground state. That sufficiently strong coupling between iron (III) atoms occurs to make these complexes essentially diamagnetic is shown also by the absence of changes in the NMR shifts as the temperature is varied.

In a later work, La Mar et al[38] put forward the view that some of the interpretations of the NMR data relied on a number of assumptions which had not been adequately tested. They asserted that the assumption that the contact shift had the same temperature dependence as the paramagnetic susceptibility was identical with the assumption that the coupling constant, A, for any given nucleus is independent of the spin state for the dimer. Data was presented to substantiate a dependence of A on spin state.

Secondly it had previously been implied that the isotropic shifts were purely contact in origin and that the shifts arising from the high-spin ($S = {}^5/_2$) metal ions followed the Curie law accurately. The theoretical treatment of Kurland and McGarvey[39] casts doubt on this assumption in that significant dipolar shifts can arise in high-spin d^5 systems due to the presence of zero-field splittings. These dipolar shifts resulting from a lifting of electronic degeneracy in the absence of an applied field are predicted[39] to vary as T^{-2}, where T is the absolute temperature. Thus the temperature dependence of the isotropic shift for such a system may be expected to exhibit both T^{-1} and T^{-2} components even though the bulk susceptibility may follow the Curie law accurately over the same temperature range. Even were A identical for each spin-state of the dimer, the antiferromagnetic coupling constant J may not be extracted from the temperature dependence of the isotropic

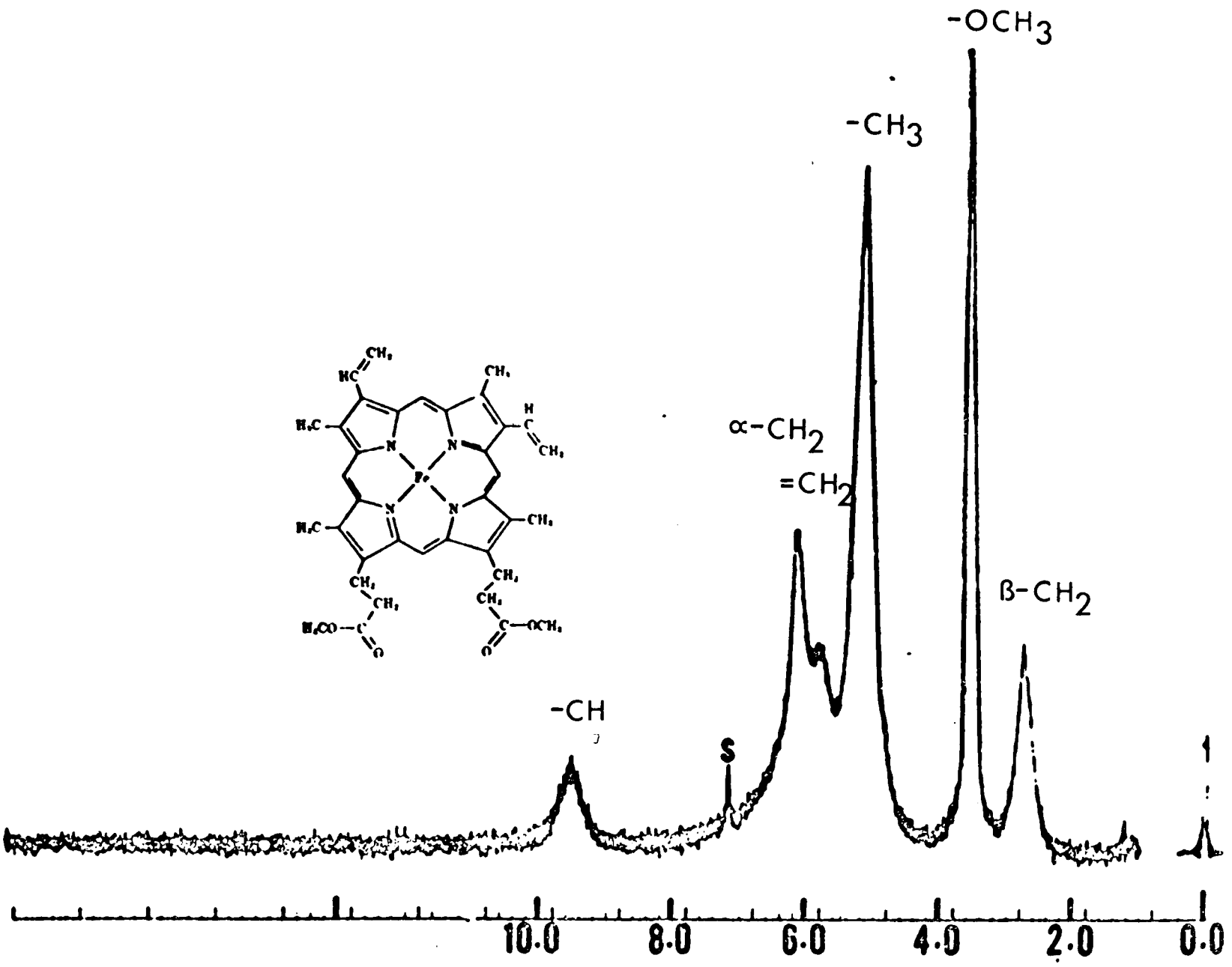


FIG. 6.3 PMR spectrum of μ-oxo-bis ferric protoporphyrin IX dimethyl ester at 308°K.

shift without explicit consideration of the contributions from the zero field splittings for each thermally accessible spin state. La Mar and co-workers demonstrated that these contributions can be substantial in some of the previously studied systems.

5. Aim of the work

It was demonstrated in Chapter 4 that electron transfer from the chelated iron atom is affected by substituents on the porphyrin periphery in ferric metalloporphyrin systems. Electron transfer from the iron atom in turn is related to the redox properties of a particular iron metalloporphyrin and these two factors have a close bearing on the participation of the iron porphyrin entity in electron exchange reactions when this entity is incorporated as a heme unit in proteins.

Redox reactions of the porphyrin ligand involving addition of oxygen or hydrogen occur in vivo as was pointed out earlier. Addition to the porphyrin ring clearly disrupts the ring conjugation, and the π electron system has been shown in Chapter 4 to play a crucial role in the mechanism of spin transfer between metal and porphyrin, particularly for high-spin iron (III) porphyrin systems. Accordingly it would be useful to examine porphyrin systems involving a degree of saturation at the porphyrin periphery in order to monitor the effect of this on electron spin transfer from the iron atom.

To this end a number of substituted α,γ-dihydromethenes will be studied by means of PMR spectroscopy and the role of the alkyl substituent in the iron-porphyrin interaction determined. The effectiveness of transmission of unpaired electron spin from the paramagnetic iron to protons at the porphyrin periphery in comparison with the corresponding unsubstituted iron octaethylporphin will be observed and it is desirable to relate this to the role of these systems in vivo.

These substituted α,γ-dihydromethenes in oxo-bridged systems will also be examined by PMR spectroscopy in order to find out the effects of the peroxo bridge and any antiferromagnetic coupling on the transmission of unpaired electron spin from one iron to the porphyrin ring to which it is chelated. The theoretical background to oxo-bridging will not be of primary concern here but interest will be directed at the effect of saturation on the antiferromagnetic coupling phenomenon, insofar as this may be governed by the iron-porphyrin interaction, in conjunction with the results obtained with the corresponding monomer.

6.2 Experimental

1. Apparatus and materials

i) NMR measurements

^{1}H NMR spectra were recorded on the Bruker HX 90, Bruker WH 90 and Bruker 270 MHz spectrometers. 50 mM solutions were used in all cases.

The α,γ-dialkyl-α,γ-dihydrooctaethylporphinato iron (III) methoxo complexes were dissolved in dideuterodichloromethane (0.2 ml) and an excess of deuteromethanol (0.3 ml) added. This mixed solvent is necessary since in the presence of CD_2Cl_2 alone the condensation reaction

$$2(OEPR_2)FeOMe + H_2O \rightleftharpoons [(OEPR_2)Fe]_2O + 2MeOH$$

takes place[40]. The presence of excess CD_3OD drives the reaction to the left, thus minimising the degree of dimerisation.

Deuterochloroform was used as the solvent for the μ-oxo-α,γ-dialkyl-α,γ-dihydrooctaethylporphinato iron (III) complexes. Chemical shifts are quoted in parts per million relative to TMS as internal standard. Negative values indicate low field shifts.

ii) Solvents

The solvents used for the NMR measurements were obtained from the following sources.

$CDCl_3$, isotopic purity 99.5% D, as supplied by Beta Scientific Ltd.; d_4-methanol, isotopic purity 99.0% D, as supplied by B.D.H. Ltd.; d_2-dichloromethane, isotopic purity 99.5% D, as supplied by Stohler Isotope Chemicals Ltd. Tetramethylsilane was supplied by Stohler Isotope Chemicals Ltd.

2. Preparation of complexes

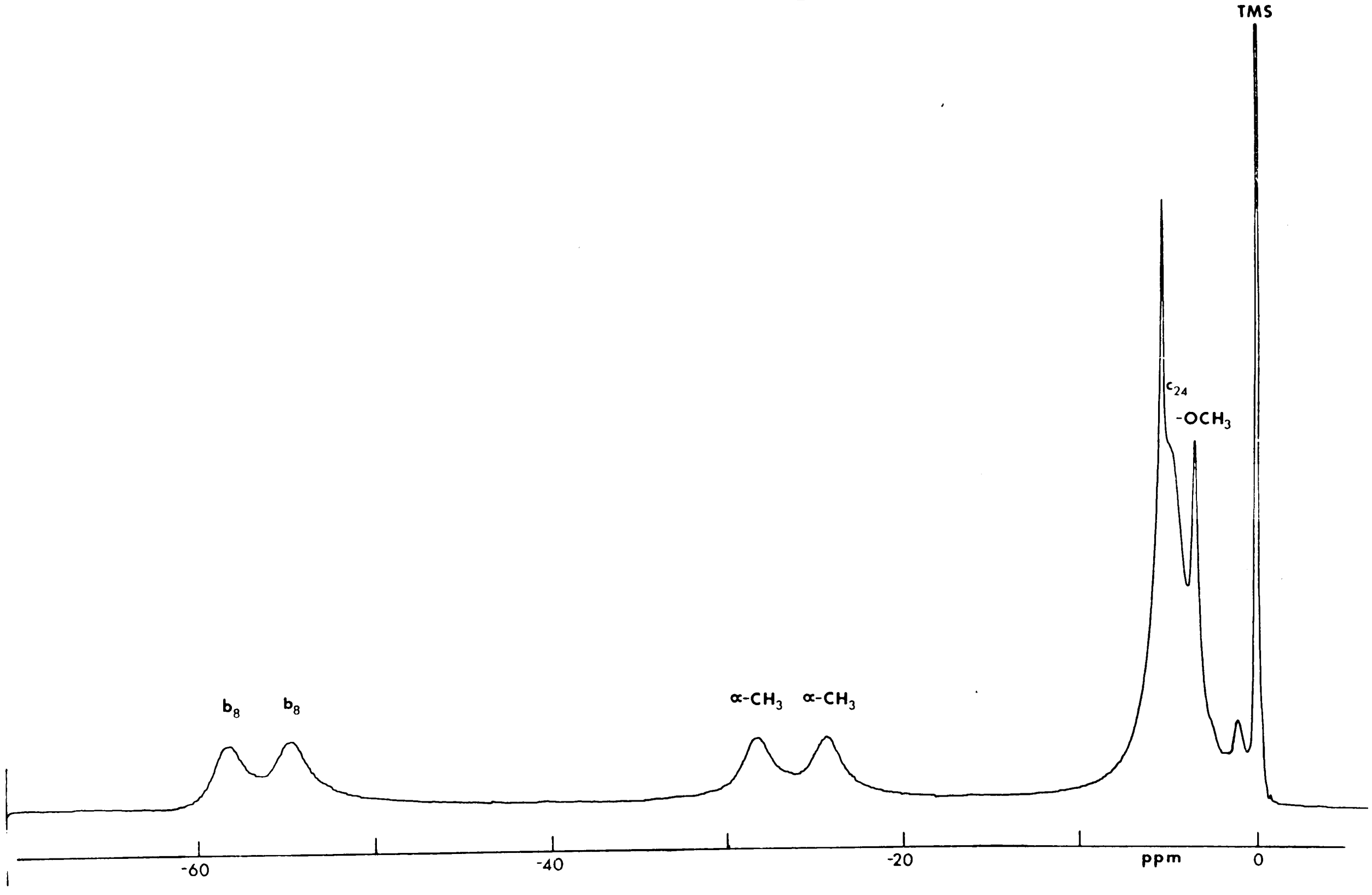
Complexes of $(OEPR_2)FeOMe$ where R is a methyl, ethyl, n-propyl or iso-propyl group were kindly supplied by Dr. J.W. Buchler, as were the μ-oxo species $[(OEPR_2)Fe]_2O$ where again R represents a methyl, ethyl, propyl or isopropyl group. All the complexes are black and dissolve to give brown-black solutions.

6.3 Results

1. Monomers

The 90 MHz PMR spectrum of $(OEPMe_2)FeOMe$ at 297°K is illustrated in Figure 6.4. The assignment nomenclature is taken from Figure 6.5. Comparing the spectrum with the published spectrum[41] of OEPFeCl (see Figure 6.6), assignment of several of the resonances is immediately obvious. The resonances at -3.4 ppm and -5.3 ppm are residual methyl and methylene proton resonances arising from the deuterated solvents CD_3OD and CD_2Cl_2 respectively. The two resonances shifted downfield in the region -55 to -60 ppm (b_8) are assigned to the α-CH_2 proton resonances. The intense resonance at -4.9 ppm is assigned to the β-CH_3 protons (c_{24}), leaving the pair of resonances in the region -25 to -30 ppm to the two α,γ-methyl groups. At first glance the relative

FIG. 6.4 PMR spectrum of $(OEPMe_2)FeOMe$ at 297°K.



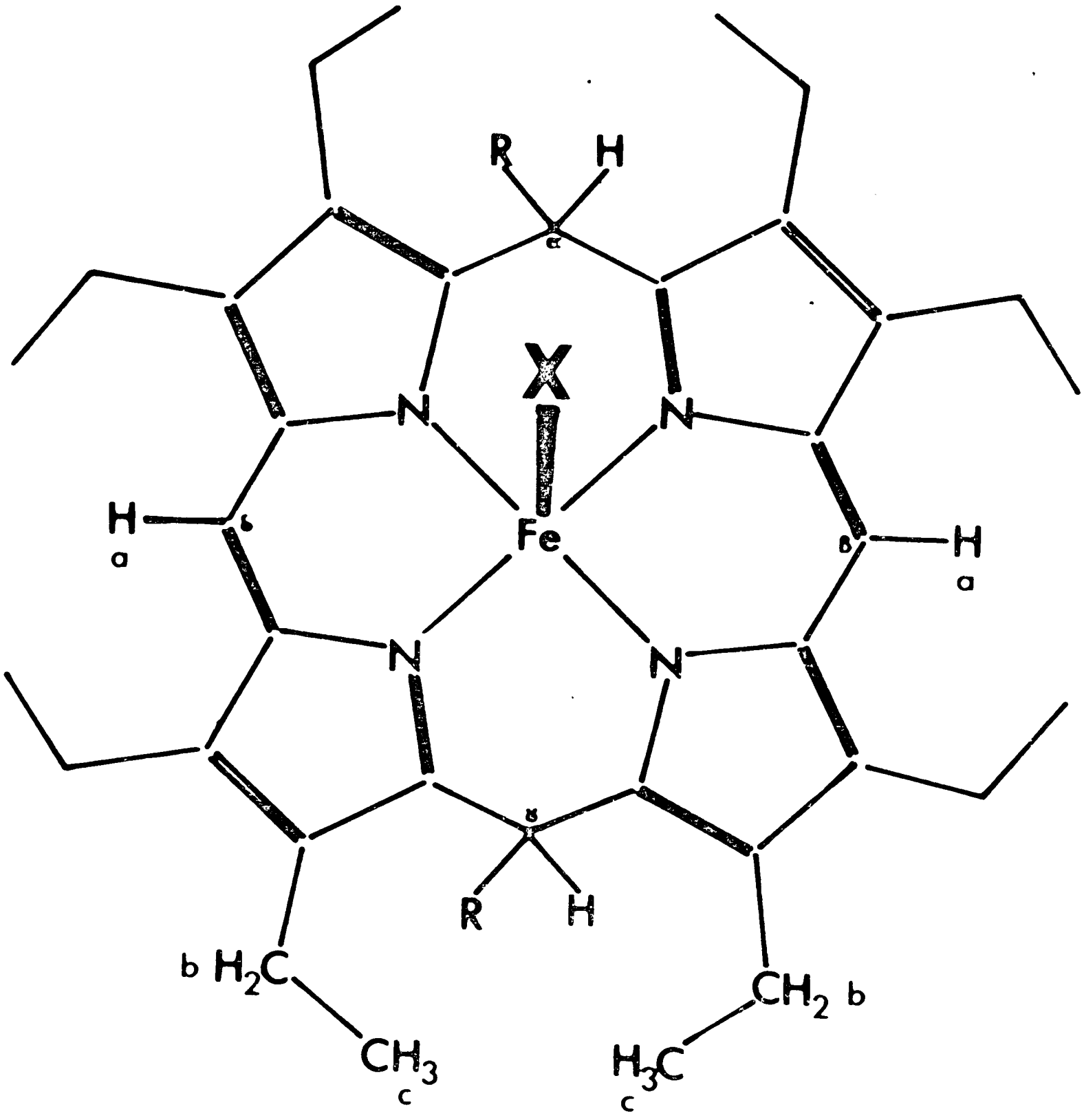


FIG. 6.5 α,γ-Dialkyl-α,γ-dihydroferric octaethylporphin complex structures and assignment nomenclature.

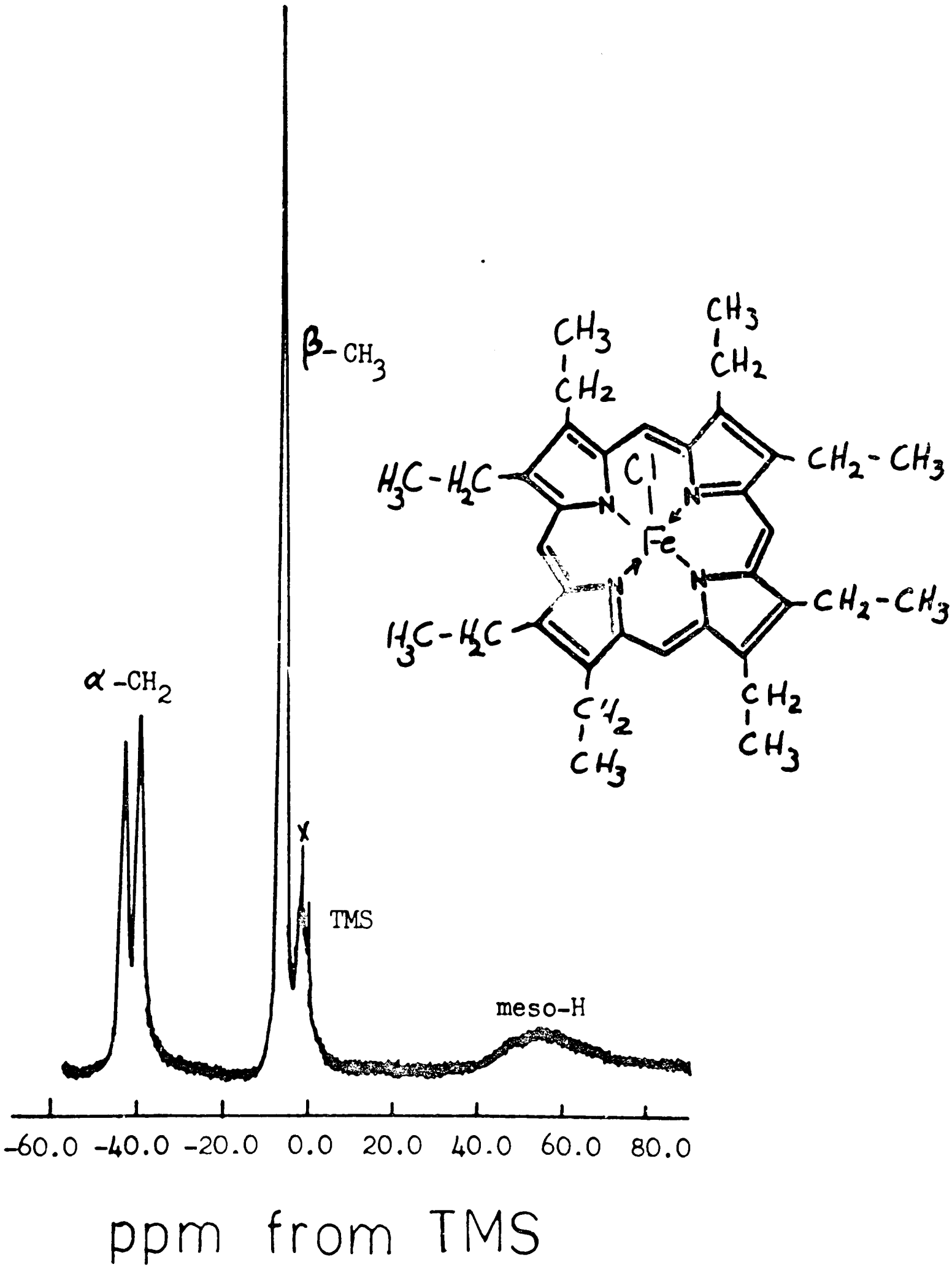


FIG. 6.6 PMR spectrum of FeOEPCl at 302°K.

areas of the two downfield pairs of resonances would not appear to be in the requisite ratio of 8:3 respectively for the 16 methylene protons of the ethyl groupsand the 6 methyl protons of the α,γ-methyl groups. However the broadness of the peaks makes accurate integration difficult and this above assignment would seem to be borne out by comparison with the spectra of the other ($OEPR_2$)FeOMe complexes where R is other than a methyl group (see later).

No resonances which can obviously be assigned to the α,γ-meso protons or the β,δ-meso protons are observed. In the published spectrum[41] of OEPFeCl, a broad hump centred at about +55 ppm but extending over a range of probably 25 ppm is assigned as the meso proton resonance. In this latter case there are 4 equivalent meso protons but in all the cases under study here, there are two pairs of equivalent protons. It is therefore quite reasonable to expect the resonances of these two pairs of protons to be very broad indeed and ill-defined. Unfortunately, the FT method is not as sensitive to broad peaks as is the CW method, but yet the FT spectrometer is necessary for these studies in order to resolve a number of the resonances which are closely grouped, especially in the 0 to -10 ppm region.

No resonance corresponding to that of the -OMe axial ligand protons is observed. This may be due to the resonance being obscured by the resonances in the -3.4 to -5.3 region, that is the solvent resonances at -3.4 ppm and -5.3 ppm, and the c_{24} resonance at -4.9 ppm. (The methoxy proton resonance of the complex ($OEPMe_2$)AlOMe occurs at -3.3 ppm[42].)

The 270 MHz spectra of the other ($OEPR_2$)FeOMe complexes at 299°K are shown in Figures 6.7 - 6.9. All three complexes show the two low-field resonances corresponding to the 16 α-CH_2 protons of the ethyl groups. The α,γ-di-isopropyl complex spectrum is the most straightforward to analyse. Thus the resonance at -27.1 ppm is assigned to the 12 methyl protons of the isopropyl groups by comparison of the intensity

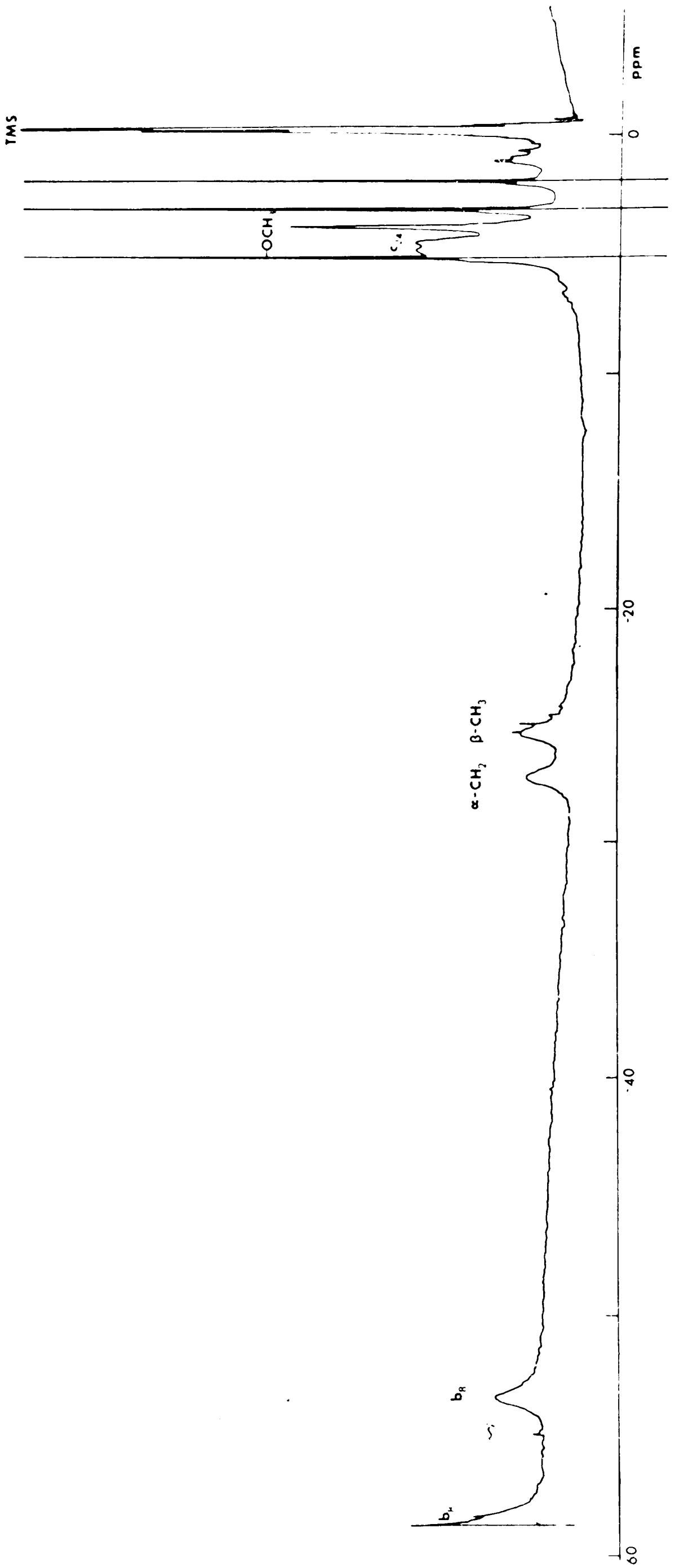


FIG. 6.7 PMR spectrum of $(OEPEt_2)FeOMe$ at 299°K.

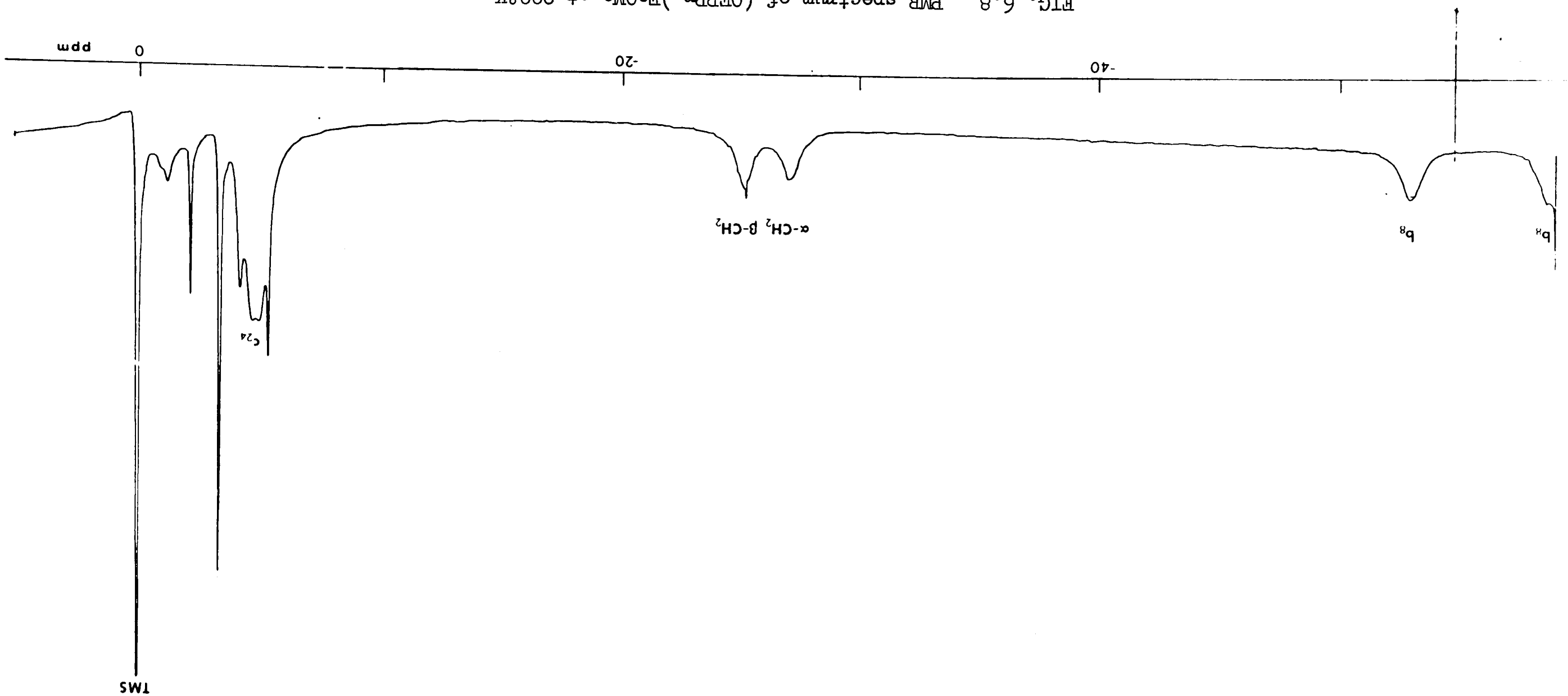


FIG. 6.8 PMR spectrum of $(OEPFr_2)FeOMe$ at 299°K.

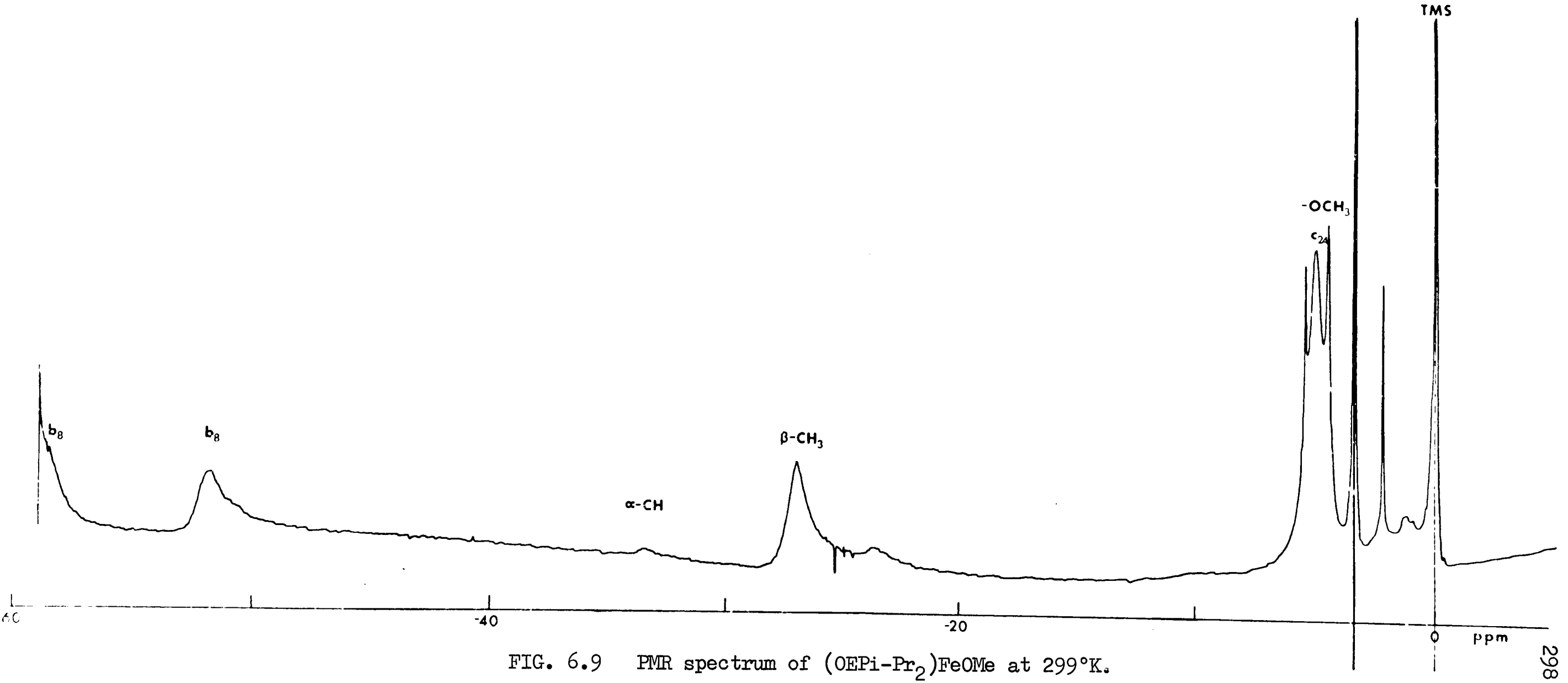


FIG. 6.9 PMR spectrum of (OEPi-Pr_2)FeOMe at 299°K.

with the intensities of the α-CH_2 resonances further downfield. Of the two resonances occurring in the 4-5 ppm downfield region, the more downfield one is considerably the broader of the two and is therefore assigned to the 24 β-CH_3 protons of the ethyl groups, leaving the more upfield one to be assigned to the 3 protons of the methoxy group. Three resonances in the diamagnetic region arise from residual protons in the solvents.

Two small peaks on either side of the isopropyl methyl proton resonance are observed. These resonances appear to be of similar intensity. In the PMR spectrum of FeOEPCl, the meso proton resonance is reported[41] to occur at around +60 ppm, and it is a reasonable assumption that in these complexes under study the β, δ-proton resonance should occur in the same region. The two resonances at -24 and -34 ppm can then be attributed to resonances of the α,γ-dihydro protons and the α-CH protons of the isopropyl groups. Both of these peaks seem about right in area compared with the area under the isopropyl methyl proton peak that is in the ratio 2:12.

It is true for all the ferric porphyrin spectra observed in this work that in complexes with side chains attached to the porphyrin ring, the resonance of protons attached to the α-carbon atom is shifted further downfield than the resonance of protons attached to the β-carbon atom. It is therefore a reasonable supposition to attribute the resonance at about -34 ppm to the α-CH protons of the isopropyl group, since this resonance is downfield of that assigned to the β-CH_3 protons of the isopropyl group. This leaves the resonance at about -24 ppm to be assigned to the α,γ-dihydro protons.

The spectra of the α,γ-diethyl and α,γ-dipropyl complexes are more difficult to assign. Two peaks at -23 to -27 ppm are present for both complexes, together with a doublet at ca. -4.6 ppm and a peak slightly upfield of this. This latter peak corresponds to that assigned to the methoxy protons of the isopropyl complex, and this peak is therefore

assigned accordingly. It might be expected that an extra peak would be present for the propyl complex as compared with the ethyl complex but this does not appear at first sight to be true. With the isopropyl complex the two peaks at -23 to -27 ppm have been assigned to the protons attached to the α- and β-carbon atoms of the α,γ-alkyl groups. It seems reasonable to assume then that in the spectra of the ethyl and propyl complexes the resonances at -23 to -27 ppm correspond to protons attached to the α- and β-carbon atoms as well. For the ethyl complex this then leaves the doublet at -4.5 ppm which is assigned to the β-CH_3 groups of the pyrrole ring ethyl groups. Comparing the intensity of this split peak with the corresponding split peak for the propyl complex, it is readily apparent that the latter peak is more intense, particularly in relation to the neighbouring peak assigned to the methoxy protons. It could therefore be that the resonance of the γ-CH_3 protons of the n-propyl groups coincides with the resonance of this β-CH_3 resonance from the octaethyl groups.

An explanation for the non-appearance of a resonance which can be assigned to the α,γ-dihydro protons could be that according to the assignment for the isopropyl complex, this resonance would in fact be obscured by the resonances of the side chain protons of the α,γ-dialkyl groups present in the methyl, ethyl and propyl complexes.

The observed PMR shifts are set out for all four complexes in Table 6.3.

TABLE 6.3

Observed PMR shift data for some α,γ-dialkyl-α,γ-dihydroferric porphin complexes (observed shifts in ppm from TMS)

$(OEPMe_2)FeOMe$

Temp.	b_8	b_8	α-CH_3	α-CH_3	c_{24}
297	-58.5	-55.0	-28.7	-24.3	-4.9
280	-63.8	-59.7	-31.3	-26.8	-5.3
263	-72.8	-67.5	-36.4	-30.9	-6.3
258	-76.5	-70.8	-38.6	-32.5	-6.4
253	-78.1	-72.3	-39.5	-33.2	-6.6
243	-83.8	-77.3	-43.1	-35.7	-7.4
233	-90.6	-83.1	-47.1	-38.8	-8.0

$(OEPEt_2)FeOMe$

Temp.	b_8	b_8	α-CH_2	β-CH_3	c_{24}	$-OCH_3$
314	-55.3	-50.4	-25.6	-23.8	-4.5 -4.4	-3.8
299	-58.6	-53.2	-27.6	-25.7	-5.0 -4.7	-4.0
261	-68.4	-61.0	-32.0	-30.0		
241	-74.3	-66.6				

$(OEPnPr_2)FeOMe$

Temp.	b_8	b_8	α-CH_2	β-CH_2	γ-CH_2 c_{24}	$-OCH_3$
314	-55.9	-50.7	-26.0	-24.4	-4.7 -4.4	-4.0
299	-58.4	-53.1	-27.3	-25.4	-5.0 -4.7	-4.2
261	-67.7	-60.7				
241	-73.4	-66.2				

$(OEPiPr_2)FeOMe$

Temp.	b_8	b_8	α-CH	β-CH_3	α,γ-H	c_{24}	$-OCH_3$
314	-56.1	-49.3	-31.5	-25.5	-22.4	-4.7	-4.3
299	-58.8	-51.7	-33.6	-27.1	-23.8	-4.9	-4.4
261	-68.1	-58.8		-31.1			
241	-74.2	-63.8		-34.0			

2. Dimers

The 270 MHz PMR spectra of $[(OEPR_2)Fe]_2O$ complexes at 291°K are illustrated in Figure 6.10, where R represents the alkyl groups present in each particular complex, that is methyl (Me), ethyl (Et), n-propyl (Pr) or iso-propyl (i-Pr). The observed shifts for the four complexes are given in Table 6.4. The chemical shifts for the $[(OEP)Fe]_2O$ complex have been reported[38] and a superficial comparison of the spectra of the complexes under study here with that of the $[(OEP)Fe]_2O$ complex enables some of the resonances to be immediately assigned.

The pair of resonances in the -5.8 to -7.3 region are assigned to the α-CH_2 protons of the octaethyl groups, whilst the intense resonance(s) at -1.1 to -1.3 ppm is (are) assigned to the β-CH_3 protons of the octaethyl groups. In all cases the α-CH_2 proton resonances are split and in the case of the ethyl and n-propyl complexes the β-CH_3 resonance is split as well. In the case of the $[(OEP)Fe]_2O$ complex, the authors reported that the meso proton signal was not clearly resolved, being present in the form of a broad resonance coincident with the α-CH_2 proton resonances. A poorly resolved broad resonance downfield from the α-CH_2 resonances is observed in the spectra of the methyl, ethyl and n-propyl complexes which may tentatively be assigned to the two β,δ-meso protons. No resonance in this region appears to be present in the spectra of the iso-propyl complex.

The peak at -3.7 ppm present in the methyl complex spectra can unquestionably be assigned as that of the six α,γ-dimethyl protons, although at first sight it would not appear to integrate as six protons in comparison with the two peaks each representing eight α-methylene protons of the octaethyl groups. In a similar fashion the peak at -4.4 ppm present in the spectra of the iso-propyl complex can be unambiguously assigned as that of the twelve α,γ-isopropyl protons since this peak could not arise from any other source and be so intense.

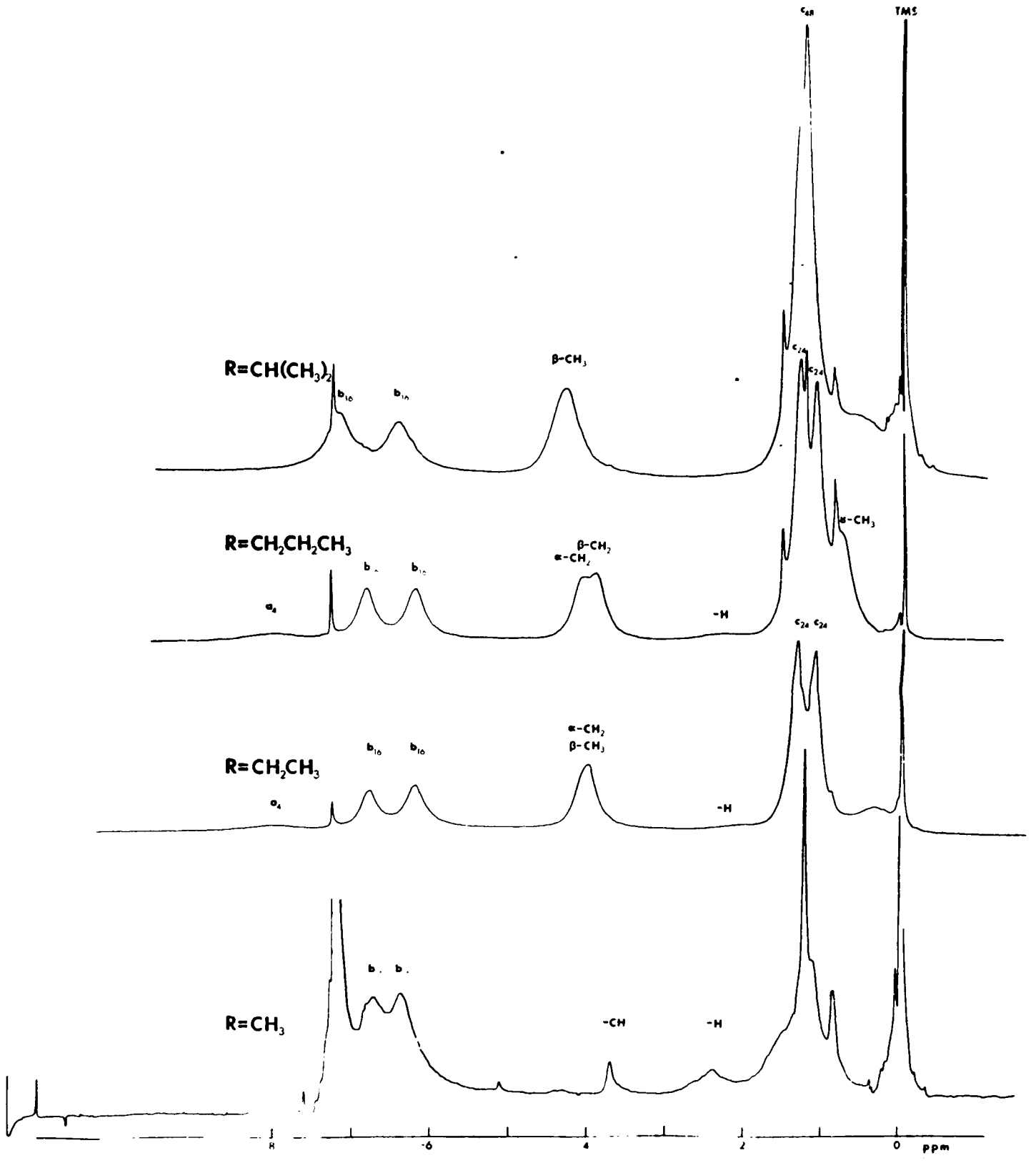


FIG. 6.10 PMR spectra of $[(OEPR_2)Fe]_2O$ complexes at 291°K.

TABLE 6.4

Observed PMR shift data for some α,γ-dialkyl-α,γ-dihydroferric porphin μ-oxo bridged dimers (observed shifts in ppm from TMS)

$[(OEPMe_2)Fe]_2O$

Temp.	a_4	$(b_{16})_2$	α-CH_3	α,γ-H	c_{48}
314	-7.3	-6.2 -5.8	-3.7	-2.4	-1.2
291		-6.7 -6.4	-3.7	-2.4	-1.2
280		-6.9 -6.7	-3.7	-2.4	-1.2

$[(OEPEt_2)Fe]_2O$

Temp.	a_4	$(b_{16})_2$	α-CH_2 β-CH_3	α,γ-H	$(c_{24})_2$
314	-8.0	-6.9 -6.3	-4.1	-2.1	-1.4 -1.1
291	-8.0	-6.8 -6.2	-4.0		-1.4 -1.1
280	-8.0	-6.8 -6.2	-4.0		-1.4 -1.1

$[(OEPPr_2)Fe]_2O$

Temp.	a_4	$(b_{16})_2$	α-CH_2	β-CH_2	α,γ-H	$(c_{24})_2$	γ-CH_3
314	-8.1	-6.9 -6.3	-4.2	-4.0	-2.4	-1.3 -1.1	-0.8
291	-8.0	-6.8 -6.2	-4.1	-3.9	-2.3	-1.3 -1.1	-0.8
280	-8.1	-6.8 -6.2	-4.1	-3.9	-2.2	-1.3 -1.1	-0.8

$[(OEPiPr_2)Fe]_2O$

Temp.	$(b_{16})_2$	α-CH	?	c_{48}	?
314	-7.3 -6.6	-4.5		-1.3	
291	-7.2 -6.4	-4.3	-1.55	-1.3	-0.7
280	-7.2 -6.4	-4.3	-1.6	-1.3	-0.5

The peaks occurring in this approximate region for the ethyl and n-propyl complexes are not as simple to assign. For the ethyl complex a single peak is observed at about -4 ppm which is not split. This peak is quite large in comparison with the two α-CH_2 peaks from the octaethyl groups representing eight protons each. An explanation of this could be that this peak at -4 ppm is due to separate overlapping resonances of the $-CH_2$ and $-CH_3$ protons of the two α,γ-ethyl groups, the whole peak integrating as ten protons. No other peak is observed which could be assigned to say the methyl protons alone of these ethyl groups, giving some substance to the above argument.

In the case of the n-propyl complex, the peak at about -4 ppm is slightly split, and a further broad peak is observed as a shoulder at about -0.8 ppm. By analogy with the spectra of the ethyl complex, it may be expected that the resonances of the protons attached to the α- and β-carbon atoms of the α,γ-dialkyl groups will overlap. In this case of course the protons attached to the α- and β-carbon atoms are all methylene protons, and the split peak at -4 ppm is therefore assigned to the α- and β-methylene protons. This leaves the shoulder at -0.8 ppm to be assigned to the γ-methyl protons (6) of the two propyl groups. Qualitatively the spectrum of the n-propyl complex is related to that of the oxo-bridged dimer of ferric tetra-n-propylporphin ($[Fe(TPP)]_2O$) as measured by La Mar and co-workers[38] in that the order of observed shifts is α-CH_2 > β-CH_2 > γ-CH_3, although the scale of the shifts differs.

By means of the resolution enhancement techniques expounded by Campbell et al[43] better spectra can be reproduced in which the narrower resonances at least are well-defined. Deconvoluted spectra of the α,γ-diethyl and α,γ-dipropyl complexes are shown in Figure 6.11. In Figure 6.11(B) the peak at -0.8 ppm is clearly resolved and the intensity of this resonance in comparison with the two overlapping peaks at about -4 ppm looks to be of the correct order (i.e. in the ratio 6:8) to

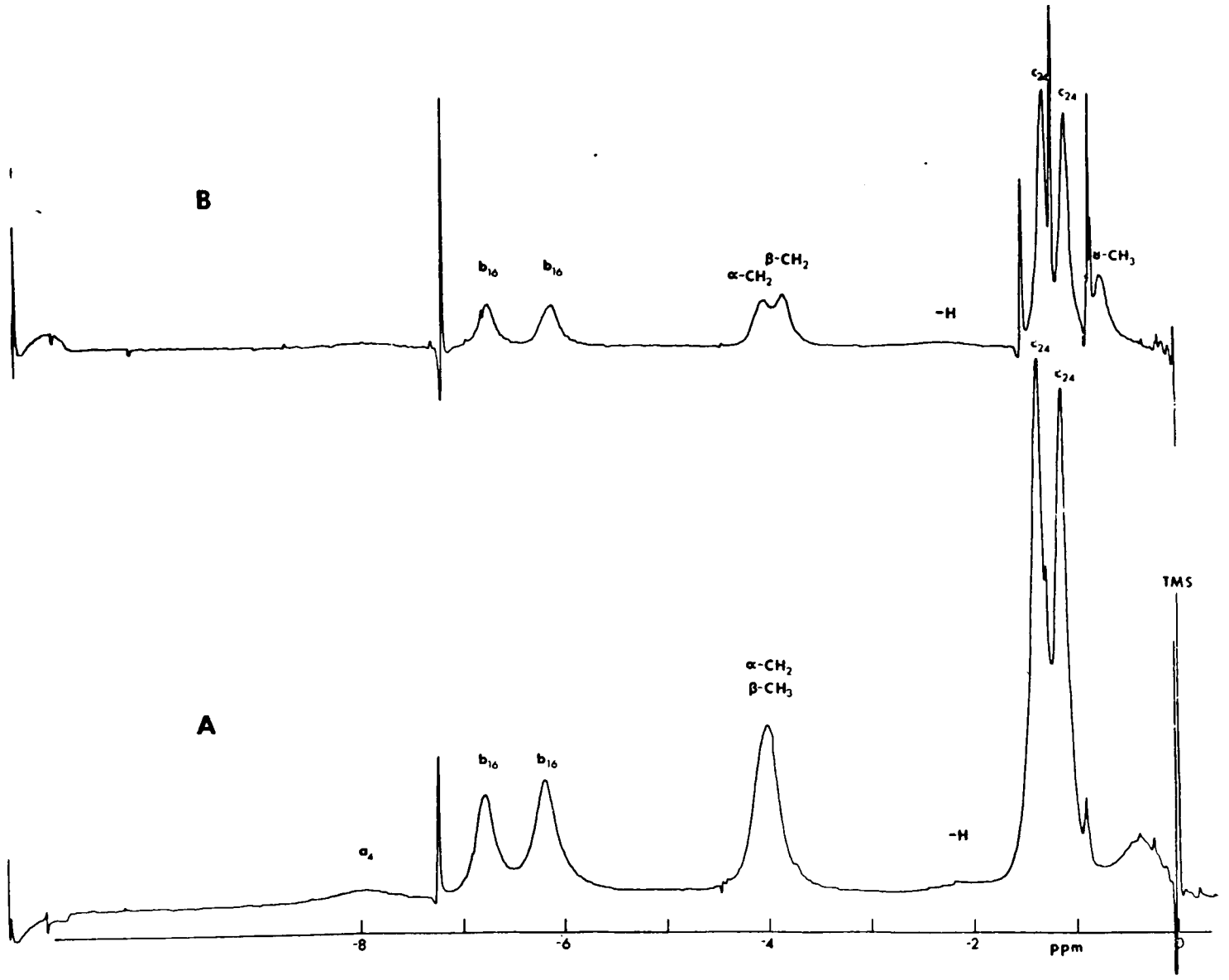


FIG. 6.11 Deconvoluted PMR spectra of $\{(OEPEt_2)Fe\}_2O$ (A) and $\{(OEPPr_2)Fe\}_2O$ (B) at 291°K.

support the assignments made.

The outstanding doubts concern the attribution of resonances to the two α,γ-dihydroprotons in all cases and the α-CH protons of the isopropyl groups in the isopropyl complex. In the cases of the methyl and propyl complexes a broad hump is found at about -2.3 ppm which may or may not be real. In the case of the ethyl complex, the spectrum at 314°K shows a broad doublet at -5.57 and -5.78 ppm which does not seem to be present at the other two temperatures at which spectra are measured. It would seem more likely that this latter doublet represents some impurity in view of its non-occurrence in the spectra of the other complexes, and a high-spin monomer is one possibility. In addition, the two α,γ-dihydro protons are equivalent and only one signal is expected. It might therefore be that the broad hump at -2.3 ppm is due to the α,γ-dihydro protons, but no degree of certainty can be attached to this assignment.

6.4 Discussion

1. Monomers

Comparing the results here with those for the OEPFeCl complex, it can be seen that the doublet furthest downfield arising from the octaethyl α-methylene protons is common to all spectra. Displacement of the iron atom out of the plane removes the mirror plane through the porphyrin plane containing the methylene carbon, rendering the protons diastereotopic. A splitting of the resonance which has been assigned to the β-CH_3 protons of the octaethyl groups is also observed for the ethyl and n-propyl complexes but not for the methyl and iso-propyl complexes. This is an observation that deserves a closer examination.

With the iron atom displaced from the porphyrin plane, it would be expected that both the methylene and methyl protons of the octaethyl groups would be rendered diastereotopic. A possible explanation for the difference in observed behaviour of the methylene and methyl protons is the presence of restricted rotation. It is reasonable to suppose that rotation about the α-CH_2/pyrrole carbon bond might be more restricted than rotation about the α-CH_2/β-CH_3 bond, since the α-CH_2 is closer to other groups attached to the porphyrin ring and also axial ligands. Free rotation around the α-CH_2/β-CH_3 bond would lead to an averaging out of various alternative positions of the protons with respect to the metal, and hence only one resonance would be observed. In the absence of free rotation, a situation proposed for the α-CH_2 group with respect to the α-CH_2/pyrrole carbon bond, then the metal would "see" two different sets of methylene protons and hence two resonances would result.

The above explanation adequately provides a reason for the expected observation of two resonances for the α-CH_2 protons but only one resonance for the β-CH_3 protons. However it does not explain why one resonance for the c_{24} protons is found in the α,γ-dimethyl and α,γ-diisopropyl cases but two resonances (or rather a split resonance) are found in the α,γ-diethyl and α,γ-dipropyl cases. One possible postulate is that in these latter two cases, the β-CH_3 group is not able to freely rotate around the methyl-methylene bond, whereas in the former two cases free rotation of the group is possible. Why this should be so is not obvious, since although the α,γ-dimethyl groups would not be expected to hinder the rotation of the β-CH_3 groups, there should not be an appreciable difference in effect between α,γ-diethyl groups and α,γ-diisopropyl groups.

One aspect of the stereochemistry which has not so far been considered is the question of the configuration about the c_α and c_γ atoms

of the porphyrin ring. It has been determined by Buchler and co-workers[42,44] that the syn-axial stereoisomer(Figure 6.2(iii)) is the most likely conformer, and here C_{2v} symmetry would be present. However if the anti-conformer were the stereoisometric form (Figure 6.2(i)), then folding along the c_α-c_γ axis would reduce the symmetry to C_5 and the octaethyl groups would no longer be isochronous or equivalent, and two resonances representative of each group would be observed. This question of stereoisomers will be returned to later.

2. Dimers

As in the case of the monomer complexes, a doublet is observed to arise from the octaethyl α-methylene protons. A similar splitting phenomenon for the resonance of the octaethyl β-methyl protons is also observed in that this resonance is observed as a doublet for the α,γ-diethyl and α,γ-dipropyl complexes but only as a singlet for the di-methyl and di-isopropyl complexes. Clearly, common effects must be operating for both the monomer and dimer complexes to produce this parallel behaviour, and it is suggested that as with the monomer complexes, restricted rotation of the octaethyl methylene groups about the α-CH_2/pyrrole carbon bond causes the observed doublet for the α,γ-diethyl and α,γ-dipropyl complexes.

It is surprising that two resonances are observed for the α-CH_2 and β-CH_2 protons of the α,γ-dipropyl groups whereas only one combined resonance is observed for the α-CH_2 and β-CH_3 protons of the α,γ-diethyl groups. This may reflect inappropriate assignment, or there may be some effect present which acts differently in the two complexes.

3. Comparison of monomers and dimers

The PMR shifts of the monomer complexes are fairly typical of high spin ferric porphyrin complexes in being quite large and the resonances are spread over a range of 60 ppm at room temperature. In contrast the shifts of the dimer complexes are typical of those of complexes exhibiting antiferromagnetic coupling, the resonances being spread over a range of less than 10 ppm..

Although the line widths of the monomer complex resonances are quite broad (up to 0.9 ppm) the chemical shifts are large enough to realise a well-resolved spectrum in each case. The line widths of the dimer complex resonances are much smaller (maximum about 0.25 ppm). Variation of the alkyl substituent at the α,γ- positions does not appear to have any marked effect on the line widths of the resonances for either the monomers or the dimers.

One feature of the spectra of the α,γ-dimethyl complexes which is present in both the monomer and dimer complexes is that the resonances assigned as b_8 behave markedly different to the b_8 resonances in spectra of the other three complexes. In the spectra of the monomer complexes, the b_8 resonances are shifted appreciably further downfield for the α,γ-dimethyl complex than for the other three complexes. This effect becomes increasingly pronounced as the temperature is lowered. Thus at 243°K the b_8 resonances are shifted to -83.8 and -77.3 ppm downfield of TMS for the $(OEPMe_2)FeOMe$ complex, as against -74.3, -66.6 ppm ($(OEPEt_2)FeOMe$), -73.4, -66.2 ppm ($(OEPnPr_2)FeOMe$) and -74.2, -63.8 ppm ($(OEPiPr_2)FeOMe$) for the other complexes, at the slightly lower temperature of 241°K. In addition, the shift difference between the b_8 resonances increases by almost 100% in the α,γ-dimethyl complex case whereas this difference increases by something less than 50% in the case of the other three monomer complexes.

In the case of the oxo-bridged dimer complexes, the presence of antiferromagnetic coupling scales down the effect, but again the α,γ-dimethyl complex behaves anomalously in comparison with the other three complexes. In the spectrum of the $[(OEPMe_2)Fe]_2O$ complex, the resonances labelled b are not shifted as far downfield as is the case in the spectra for the other three oxo-bridged dimeric complexes. Furthermore in reducing the ambient temperature at which the spectra are measured from 314°K to 280°K, the shifts in the spectrum of $[(OEPMe_2)Fe]_2O$ of resonances b change appreciably, in that the resonances are shifted to lower field by about 0.8 ppm. The shift change is not the same for the two resonances and as a result there is a tendency towards coalescence of the peaks. Such an effect is not observed in the spectra of the α,γ-diethyl, α,γ-dipropyl and α,γ-di-isopropyl dimeric complexes on corresponding change in temperature, and in fact temperature change has virtually no effect on the observed shifts.

It would therefore seem as though the methyl groups in the α,γ-dimethyl complexes influence the electronic environment of the iron atom in a manner which does not occur in the other α,γ-dialkyl complexes. It was noted previously that the resonance of the octaethyl β-methyl protons was observed as a doublet for the α,γ-diethyl and α,γ-dipropyl complexes in both the monomer and dimer examples, but only as a singlet for the α,γ-dimethyl and α,γ-di-isopropyl complexes. In fact the behaviour of the α,γ-diethyl and α,γ-dipropyl complexes is to all intents and purposes identical, and whilst the α,γ-di-isopropyl complexes differ marginally in behaviour, they do not differ radically in the way that the α,γ-dimethyl complexes do. Attention must be focussed on the α,γ-dimethyl complexes in view of the somewhat different behaviour observed.

Two aspects may be relevant to these experimental observations. The bonding interactions may be influenced firstly by structural or

steric effects and secondly by the substitution and the partial saturation in the porphyrin ring.

4. Stereochemistry of the porphodimethene complexes

It has been proposed by Buchler et al[44] that the syn-axial stereoisomer, denoted as (iii) in Figure 6.2, is the most probable conformer. The spatial structures of ($OEPMe_2$)Ni and ($OEPMe_2$)TiO have been determined[45] and in these complexes it is found that the syn-axial configuration is indeed taken up. Whether this is always the case is determined by the ease of formation and also by steric factors. Essentially this is dependent on the form of control of the formation reaction, that is kinetic or thermodynamic control.

It was stated in the Introduction that the shape of the roof, caused by the folding of the porphyrin macrocycle about the axis linking C-α and C-γ, makes the approach of incoming groups easier from above than from below. If this kinetic effect were the dominant control exercised, then the syn-axial stereoisomer would be favoured. It has been claimed[44] that the syn-axial form is also favoured against the syn-equatorial form on thermodynamic (steric) grounds. For the ($OEPMe_2$)MX complex shown in Figure 6.2, the syn-axial stereoisomer implies only two methyl-axial ligand contacts whereas the syn-equatorial stereoisomer contains four eclipsed methyl-ethyl contacts. This reasoning is supported by the crystal and molecular structures determined, as mentioned above.

No crystal or molecular structures have been determined for complexes other than α,γ-dimethyl complexes. It is pertinent here to discuss the configuration of complexes which contain α,γ-dialkyl groups other than the methyl group. In particular, the possibility of syn-equatorial stereoisomers occurring should be discussed.

Whereas the methyl group is small in bulk, the ethyl and n-propyl groups are longer in length and the iso-propyl group is a fairly bulky

group in comparison. It may be that with these larger groups in the syn-axial configuration, steric interference with other groups such as the axial methoxy group in the monomer case or the second porphyrin moiety in the dimer case, is more prevalent than in the case of dimethyl groups. If this is so, then a different configuration would be favoured on thermodynamic grounds; either an anti- or a syn-equatorial stereoisomer would be the result. The approach of incoming groups in the formation process from above the roof macrocycle may not be as easy for alkyl groups other than the methyl group. Kinetic factors may dictate that the more bulky groups approach the α,γ-positions at the porphyrin ring from below the roof.

It has already been noted that the α,γ-dimethyl complexes exhibit PMR spectra which are different in form from those of the other complexes. As has been stated, the structures of certain nickel and titanium dimethyl porphodimethenes show that the syn-axial configuration is taken up, and it is probably reasonable to extend this determination to the dimethyl complexes under study here. It is probably not a reasonable assumption to propose that the complexes with di-ethyl, di-propyl and di-isopropyl substituents have a similar configuration. Indeed the experimental observations, whilst not conclusive in themselves, may be indicative of a stereoisomer which is not that of the syn-axial type in these latter complexes.

The anti-isomer which is of C_s symmetry would be expected to exhibit separate PMR resonances for the α- and γ-alkyl groups as these are diastereotopic in this conformation. There is no clear evidence from the observed spectra that separate resonances are obtained, and the presence of this form must therefore be doubtful. If the ethyl, n-propyl and isopropyl porphomethene derivatives do take up a different configuration from that of the methyl derivative, it would seem likely then that this would be syn-equatorial.

There is no obvious way in which such a configurational effect, if it does exist, can be qualitatively related to the bonding and electronic interactions within the porphodimethene molecule. There is a conformational effect though, which can more clearly be understood to influence the bonding interactions, namely the effect of the folding of the porphyrin macrocycle about the line joining C-α and C-γ. The actual angle of folding is bound to influence the character of the orbitals at C-α and C-γ, which in turn may be expected to have a bearing on both the ease and manner in which unpaired electron spin is transmitted from the iron atom to the orbitals characteristic of the α,γ-substituents. Spin delocalisation through the ring conjugation will be affected by the bonding interaction of the central iron atom and the four nitrogen atoms of the porphyrin ring. This interaction is likely to be critically dependent on the angle of folding of the macrocycle, which allows for a variation in orientation of electronic orbitals, variation in Fe-N bond distance etc.

The substitution of increasingly larger alkyl groups at the α- and γ-positions is bound to have an effect on the angle of folding since the macrocycle will attempt to take up that conformation which minimises geometric strain and reduces steric compression and interference. The difference in behaviour of the dimethyl derivative in comparison with the other derivatives could well reflect this change in the angle of folding with consequential change in the bonding interactions within the molecular macrocycle.

5. Effect of partial reduction of the porphyrin ring on electronic interaction

It was demonstrated in Chapter 4 that the π-electron system of the porphyrin entity played a vital role both in bonding interactions and in the mechanism of transfer of unpaired spin between metal and porphyrin. One of the aims of the examination of this particular model system was to observe whether saturation at the porphyrin periphery interfered with the electronic interactions of bonding and electron spin transfer.

Ideally this aim would be achieved by comparison of the hyperfine shifts of the $(OEPR_2)FeOMe$ and $[(OEPR_2)Fe]_2O$ complexes with those of (OEP)FeOMe and $[(OEP)Fe]_2O$. Unfortunately this comparison is not feasible owing to the lack of any geometric or magnetic susceptibility data for the former complexes. A comparison can be made for the monomers between the isotropic shifts referenced against a comparable diamagnetic complex[46]. Although no PMR data are available for the (OEP)FeOMe complex, data are obtainable for the (OEP)FeCl complex and these will be used.

Representative isotropic shift data for some α,γ-dialkyl-α,γ-dihydroferric porphin complexes and two high-spin ferric porphyrin chloride complexes are given in Table 6.5. Many of the isotropic shifts of the porphodimethene complexes are of approximately the same order as those of the ferric porphyrin chloride complexes. Thus the isotropic shifts of the b protons are of the order -35 to -40 ppm in the (OEP)FeCl complex as against -49 to -56 ppm in the porphodimethene complexes. This difference may reflect the different axial ligands bonded, or it may reflect some feature of the folding of the porphyrin macrocycle in the latter case.

TABLE 6.5

Representative isotropic shift data for some α,γ-dialkyl-α,γ-dihydroferric porphin and high-spin ferric porphyrin chloride complexes

Complex	b				c	a
(OEP)FeCl[38]	-39.4	-35.4			-4.7	+65.1
			α-CH_3	α-CH_3		
(OEPMe_2)FeOMe	-55.9	-52.4	-27.2	-22.8	-3.7	
			α-CH_2	β-CH_3		
(OEPEt_2)FeOMe	-56.0	-50.6	-25.3	-24.7	-3.8	-3.5
				β-CH_2		
(OEPnPr_2)FeOMe	-55.8	-50.5		-23.9	-3.8	-3.5
			α-CH	β-CH_3		
(OEPiPr_2)FeOMe	-56.3	-49.2	-31.0	-26.1	-3.8	

	α-CH_2	β-CH_2	γ-CH_3
(T-nPrP)FeCl[38]	-57.2	~ 0	-1.3

Shift data measured at 299°K with the exception of:

(OEP)FeCl and (T-nPrP)FeCl data measured at 302°C.

(OEPMe_2)FeOMe data measured at 297°K.

A folding of the porphyrin about the line joining the C-α and C-γ atoms increases the angle between the metal-proton vector and the unique magnetic axis for many protons. This angle is one of the factors which determine the pseudocontact shift, and any increase in its value over 90° will effectively mean that the pseudocontact shift becomes more and more negative, all other factors being equal. The more negative isotropic shifts for the porphodimethene complexes may be indicative of this, although there is no quantitative knowledge of the contact shifts in the porphodimethene cases, and the influence of the contact shift cannot be ruled out.

The isotropic shifts of the c protons are fairly similar for both (OEP)FeCl and the porphodimethene complexes. It would be interesting to compare the isotropic shifts of the α,γ-dialkyl protons of the (OEPnPr$_2$)FeOMe complex with those of the n-propyl protons of the (T-nPrP)FeCl complex. Unfortunately the assignments of the alkyl group proton resonances in the case of the former are uncertain. Nevertheless there does appear to be an appreciable difference between the magnitudes of the shifts in the respective complex types. This is perhaps not unexpected. Although the pseudocontact shift might be assumed not to vary greatly with folding of the molecule along the α-γ axis, it is very likely that the direct transfer of metal spin density into the methene carbon pπ orbitals will be substantially affected by reduction at the methene carbon, breaking up the full conjugation of the porphyrin ring, and hence altering the contact shift contribution. This possible change in the contact shift contribution could well produce significant variation in the isotropic shifts of the alkyl group protons between the (T-nPrP)FeCl and (OEPnPr$_2$)FeOMe complexes.

No direct comparison between the isotropic shifts of the oxo-bridged α,γ-dialkyl-α,γ-dihydroferric porphin dimers and those of unsubstituted complexes is possible since diamagnetic reference data

for the former complexes are not available. A brief examination of the observed shifts given in Table 6.6, although not particularly meaningful in itself, nevertheless does appear to indicate that many of the observed shifts are fairly close in magnitude. Whilst there is some variation in shifts between the α,γ-dialkyl and the unreduced complexes, this variation includes a contribution from the change in substituent at the α,γ-positions as well as any possible effect from the partial reduction of the porphyrin ring. In this regard it is perhaps worth noting that in the work of La Mar et al[38] it was found that the observed shift of the pyrrole protons changed from -13.6 ppm in $[(TPP)Fe]_2O$ to -14.9 ppm in $[(T\text{-}nPrP)Fe]_2O$, that is an increase in the magnitude of the shift by 1.3 ppm on substitution of the phenyl group by the n-propyl group.

Detailed analysis of the PMR shifts of the α,γ-dialkyl-α,γ-dihydro-ferric porphin complexes is not realistic for either the monomers or the dimers. No quantitative assessment of the origin of isotropic shifts of the monomers can be made because of a lack of geometric and structural data, and also because the Fermi coupling constant is likely to be temperature dependent, if rotation of any of the groups is sterically hindered, since the Fermi coupling constant depends on the rotational angle[47]. It has been suggested that a straightforward analysis of isotropic shifts of porphyrin dimers assuming negligible pseudocontact interactions and zero field splitting effects is an over-simplification. A more detailed analysis of dimer shifts to elicit a value for J, the antiferromagnetic coupling constant, akin to that of Boyd and Smith[37] is therefore neither advisable nor in fact possible without a knowledge of the molecular geometry, value of zero field splitting and an expanded theoretical treatment.

Superficial examination of the α,γ-dialkyl complexes and unreduced porphyrin complexes by way of the isotropic and observed PMR shifts

TABLE 6.6

Observed PMR shift data for some oxo-bridged α,γ-dialkyl-α,γ-dihydroferric porphin and ferric porphyrin dimer complexes

Complex	a	b				c			
[(OEP)Fe]$_2$O[38]	-5.5	-6.6	-5.1				-1.75		
[(OEPMe$_2$)Fe]$_2$O	-7.3	-6.2	-5.8	α-CH$_3$ -3.7	α,γ-H -2.4		-1.2		
[(OEPEt$_2$)Fe]$_2$O	-8.0	-6.9	-6.3	α-CH$_2$ β-CH$_3$ -4.1	α,γ-H -2.1		-1.4	-1.1	
[(OEPnPr$_2$)Fe]$_2$O	-8.1	-6.9	-6.3	α-CH$_2$ -4.2	β-CH$_2$ -4.0	α,γ-H -2.4	-1.3	-1.1	γ-CH$_3$ -0.8
[(OEPiPr$_2$)Fe]$_2$O		-7.3	-6.6	α-CH -4.5			-1.3		
	Pyrrole H			α-CH$_2$	β-CH$_2$				γ-CH$_3$
[(T-nPrP)Fe]$_2$O[38]	-14.9			-6.2	-1.8				-1.1

Shift data measured at 314°K with the exception of:

[(OEP)Fe]$_2$O and [(T-nPrP)Fe]$_2$O data measured at 302°K.

appears to indicate that full conjugation throughout the porphyrin ring periphery is not essential for transmission of the unpaired electron spin on the metal to ligand orbitals. Values of the isotropic shifts shown by, for example, the octa-ethyl group protons, suggest that the creation of two pyrromethene-like "half-unit" systems as a consequence of the break in full conjugation of the porphyrin ring π-electron system does not significantly affect the metal-ligand bonding interactions. Only at the α- and γ-positions where the reductive alkylation takes place is there any apparent change in the spin density due to reduction at the porphyrin ring, although this change is not well characterised due to paucity of experimental shift information and uncertainty in assignment.

Curiosity is aroused as to the effect of further breaks in the two "half-unit" conjugated systems on the metal-ligand interactions. Reduction at the β- and δ-positions on the porphyrin ligand would lead to the formation of a porphyrinogen derivative with four isolated pyrrole units. It would be interesting to speculate whether the creation of "quarter-unit" π-electron systems produced a major change in the electronic properties observed!

6. Relevance of the work to biological systems

The observations of this work, that reduction at the porphyrin periphery can take place without seemingly altering the spin density transmission from the metal to the porphyrin ligand, must surely cast some light on the redox reactions of metalloporphyrins in biological systems.

The concept of photosynthetic and respiratory systems is that they are based on the rapid flow of electrons through a graded sequence of redox steps mediated by a continuous sequence of carriers. One

hypothesis that has been proposed for the mechanism of action of the cytochromes is that electron transfer takes place primarily over exposed heme edges, especially when the iron atom is blocked by the protein matrix[43]. Evidence has also been produced that, during a redox cycle in which the iron is reduced and re-oxidised, the methene protons exchange with the solvent[49]. From this it has been postulated that the primary peripheral attack is on the porphyrin ring with the formation of phlorin radicals in the reduction of iron (III) hemoproteins.

It may also be true that if it can conclusively be established that the reduction of the porphyrin ring to form porphodimethene species does not radically affect the bonding interactions of the metallo-porphyrinic macrocycle, as is intimated in this work, then here is another possible model for electron transfer systems. Further work on the redox properties of these porphodimethene complexes would be useful in this connection. It is however known that protonation of the methene bridges invariably occurs when the reduction of porphyrins is carried out in protic media and is usually fully reversible with a rise in the redox potential of the solution, much like electron addition and removal[3-6]. This therefore suggests that the possibility of this reversible reduction at the porphyrin ring has mechanistic implications in terms of the role and manner of operation of electron transfer agents.

It is unfortunate that no further analysis of the μ-oxo-bridged dimer results beyond that of a superficial examination of the observed PMR shifts was possible.

Earlier studies of antiferromagnetic oxo-bridged systems have realised valuable information on the electronic states of the coupled metal centres in that monitoring of the temperature dependence of the isotropic shifts of nuclei close to the metal centres permits characterisation of the local spin magnetisation without interference from the

bulk diamagnetism of a protein or paramagnetic impurities. The possible relevance of these systems to certain biological agents such as cytochrome c oxidase mentioned earlier thus highlights the importance of pursuing enquiries into the nature of electronic properties of oxo-bridged complexes since the electron exchange ability is a function of the redox properties and manner of electron transfer within the complex.

REFERENCES

1. J-H. Fuhrhop. Structure and Bonding, 1974, 18, 1.

2. R.B. Woodward. J. Pure Appl. Chem., 1961, 2, 383.

3. G. Peychal-Heiling and G.S. Wilson. Anal. Chem., 1971, 43, 550.

4. H.H. Inhoffen. J. Pure Appl. Chem., 1968, 17, 443.

5. D. Mauzerall. J. Amer. Chem. Soc., 1962, 84, 2437.

6. G.L. Closs and L.E. Closs. J. Amer. Chem. Soc., 1963, 85, 818.

7. J.W. Buchler, L. Puppe and H.H. Schneehage. Liebigs Ann. Chem., 1971, 749, 134.

8. J.W. Buchler and H.H. Schneehage. Tetrahedron Lett., 1972, 3803.

9. J.W. Buchler and H.H. Schneehage. Angew. Chem., 1969, 81, 912.

10. W.D. Phillips. "Iron Sulphur Proteins", Ed. W. Lovenberg, Academic Press, New York, 1972, Chapter 17.

11. A.J. Bearden and W.R. Dunham. Struct. Bonding, 1970, 8, 1.

12. T.H. Moss, D. Petering and G. Palmer. J. Biol. Chem., 1969, 244, 2275.

13. T. Kimura, A. Tasaki and H. Watari. J. Biol. Chem., 1970, 245, 4450.

14. G. Palmer, W.R. Dunham, J.A. Fee, R.H. Sands, T. Iizuka and T. Yonetani. Biochim. Biophys. Acta., 1971, 245, 201.

15. K. Garbett, D.W. Darnell, I.M. Klotz and R.J.P. Williams. Arch. Biochem. Biophys., 1969, 135, 419.

16. M.Y. Okamura, I.M. Klotz, C.E. Johnson, M.R.C. Winter and R.J.P. Williams. Biochemistry, 1969, 8, 1951.

17. J.W. Dawson, H.B. Gray, H.E. Hoenig, G.R. Rossman, J.M. Shredder and R-H. Wang. Biochemistry, 1972, 11, 461.

18. B.F. Van Gelder and H. Beinert. Biochim. Biophys. Acta., 1969, 189, 1.

19. J.S. Griffith. Mol. Phys., 1971, 21, 141.

20. L.C. Sieker, E. Adman and L.H. Jensen. Nature, 1972, 235, 40.

21. C.W. Carter, S.T. Freer, Ng.H. Xuong, R.A. Alden and J. Kraut. Cold Spring Harbour Symp. Quant. Biol., 1971, 36, 381.

22. J.S. Griffith. Struct. Bonding, 1972, 10, 87.

23. M. Poe, W.D. Phillips, J.D. Glickson, C.C. McDonald and A. San Pietro. Proc. Nat. Acad. Sci. U.S., 1971, 68, 68.

24. J.O. Alben, W.H. Fuchsman, C.A. Beaudreau and W.S. Caughey. Biochemistry, 1968, 7, 624.

25. N. Sadasivan, H.I. Eberspaecher, W.H. Fuchsman and W.S. Caughey. Biochemistry, 1969, 8, 534.

26. T.H. Moss, H.P. Lillienthal, C. Moleski, G.A. Smythe, M.C. McDaniel and W.S. Caughey. Chem. Commun., 1972, 263.

27. E.B. Fleischer and T.S. Srivastava. J. Amer. Chem. Soc., 1969, 91, 2403.

28. E.B. Fleischer, J.M. Palmer, T.S. Srivastava and A. Chatterjee. J. Amer. Chem. Soc., 1971, 93, 3162.

29. L.O. Atovmyan, O.A. D^{s}yachenko and S.V. Soboleva. J. Struct. Chem. (U.S.S.R.), 1970, 11, 517.

30. W.S. Caughey. Adv. Chem. Ser., 1971, 100, 248.

31. T.H. Moss, H.R. Lillienthal, C. Moleski, G.A. Smythe, M.C. McDaniel and W.S. Caughey. J. Chem. Soc. (D), in press.

32. L.J. Radonovitch, C.H. Barlow, W.S. Caughey and J.L. Hoard. Unpublished.

33. I.A. Cohen. J. Amer. Chem. Soc., 1969, 91, 1980.

34. K.S. Murray. Coord. Chem. Rev., 1974, 12, 1.

35. G.A. Smythe and W.S. Caughey. Federation Proc., 1970, 29, 464.

36. W.S. Caughey in "Inorganic Biochemistry", Vol. 2, Ed. G. Eichhorn, Elsevier, Amsterdam, 1973, Chapter 24.

37. P.D.W. Boyd and T.D. Smith. Inorg. Chem., 1971, 10, 2041.

38. G.N. La Mar, G.R. Eaton, R.H. Holm and F.A. Walker. J. Amer. Chem. Soc., 1973, 95, 63.

39. R.J. Kurland and B.R. McGarvey. J. Magn. Resonance, 1970, 2, 286.

40. J.W. Buchler. Private communication.

41. F.A. Walker and G.N. La Mar. Ann. N.Y. Acad. Sci., 1973, 206, 328.

42. J.W. Buchler and L. Puppe. Liebigs Ann. Chem., 1974, 1046.

43. I.D. Campbell, C.M. Dobson, R.J.P. Williams and A.V. Xavier. J. Mag. Reson., 1973, 11, 172.

44. J.W. Buchler, L. Puppe, K. Rohbock and H.H. Schneehage. Ann. N.Y. Acad. Sci., 1973, 206, 116.

45. W.R. Scheidt. Unpublished results.

46. J.W. Buchler. Private communication and unpublished results.

47. C. Heller and H.M. McConnell. J. Chem. Phys., 1960, 32, 1535.

48. B. Chance, L. Mela and D. de Vault, in "Structure and Function of Cytochromes", University Tokyo Press, 1968, p.475.

49. C.E. Castro and H.F. Davis. J. Amer. Chem. Soc., 1969, 91, 5405.

APPENDIX I

FOURIER TRANSFORM NMR SPECTROSCOPY

The principal advantage of this technique is the much improved signal to noise ratio obtained compared with the conventional continuous wave technique. In a conventional NMR experiment the spectrum is recorded by sweeping either the field or the frequency so that at any given time only one point in the spectrum is being observed. In Fourier Transform NMR spectroscopy neither the field nor the frequency is swept but instead a radio-frequency pulse is applied which contains a large number of discrete frequencies separated by a small amount and covering the whole spectrum. Thus the whole spectrum is examined simultaneously.

In the presence of the magnetic field the magnetisation of the nuclei will be aligned parallel to the field. A 90° pulse is applied along the x-axis which turns the magnetisation into the xy-plane. As transverse relaxation occurs the signal decays and if only one type of nucleus is present the observed signal is a free induction decay for just that nucleus. If several nuclei are present, a free induction decay representing the sum of all the individual decays is observed. These free induction decays contain the same information as the conventional spectrum because their shape depends on the Larmor frequency of the nucleus and the relaxation time T_2.

The free induction decay is a complex waveform and is measured as a function of time, f(t); Fourier transformation is a mathematical technique used for separating a complex wave function into its spectral components as a function of frequency, $F(\omega)$. It can be shown that f(t) and $F(\omega)$ are a Fourier transform pair and hence

$$f(t) = {}^{1}/_{2\pi}\int_{-\infty}^{+\infty} F(\omega)\, \exp(i\omega t)\, d\omega$$

$$F(\omega) = \int_{-\infty}^{+\infty} f(t)\, \exp(-i\omega t) dt$$

In the particular case of a Lorentzian function, given by the left hand side of the equation below, a relationship can be derived relating it to the free induction decay, thus

$$\frac{T_2}{1 + T_2^2(\omega - \omega_o)^2} = \int_o^\infty \exp(-t/T_2)\cos(\omega - \omega_o)t.dt$$

In a Fourier Transform experiment the free induction decay, which is the sum of the decays of all the resonating nuclei in the sample, is converted to the conventional spectrum by means of a digital computer which performs the Fourier transform operation described in the equation above.

In practice, application of the radio-frequency pulse and measurement of the free induction decay takes only a few seconds, so a number of measurements are made and the decays added. This reduces the noise in the same way as a CAT (a computer averaging of transients) in which the signal accumulated increases linearly with the number of scans, whilst the noise being a random function with respect to time increases only as the square root of the number of scans taken.

REFERENCES

1. T.C. Farrar and E.D. Becker. "Pulse and Fourier Transform N.M.R. An Introduction to Theory and Methods". Academic Press, New York, 1971.

2. R.R. Ernst. Rev. Sci. Instr., 1966, 37, 93.

APPENDIX II

OBSERVED ^{1}H NMR SHIFT DATA FOR Fe(III) OCTAETHYLPORPHIN X_2ClO_4 COMPLEXES

TABLE	X
A	3-chloropyridine
B	4-acetylpyridine
C	3-acetylpyridine
D	pyridine
E	4-methylpyridine
F	4-aminopyridine
G	N-methylimidazole

All shifts in ppm from TMS

TABLE A

T°K	β-py_2	b_{16}	γ-py_2	a_4	c_{24}
330		-32.8			-5.0
322		-32.9			-5.4
302		-32.5	+0.8	-16.4	-5.1
298		-31.6			-4.9
273		-26.6	-2.2		-3.7
252		-23.2		-12.8	-2.9
246		-21.6	-4.6	-11.4	-2.4
237		-19.5	-5.6	-8.7	-1.8
228		-17.7	-6.7	-6.7	-1.4
223		-16.4	-7.2	-4.6	-0.9
216		-14.9	-8.3	-2.3	-0.3
209	-24	-13.8	-9.2		+0.1
205	-23.8	-13.2	-10.2		+0.4

TABLE B

T°K	β-py$_4$	b_{16}	γ-py$_6$	c_{24}	a_4
316	-28.9	-25.0	-2.0	-3.6	
303	-26.8	-22.6	-2.6	-3.0	
287	-23.3	-18.7	-3.5	-2.1	-7.2
270	-21.0	-16.0	-4.5	-1.3	-4.5
261	-20.3	-14.8	-5.1	-1.0	-3.5
252	-19.7	-13.3	-5.3	-0.5	-1.9
244	-19.4	-12.9	-5.6	-0.3	-1.0
236	-19.5	-12.1	-6.1	0	+0.6
231	-19.9	-11.7	-6.5	+0.3	+1.5
221	-20.4	-11.1	-7.0	+0.6	+3.0
209	-21.4	-10.5	-7.9	+1.0	+5.0
204	-22.2	-10.5	-8.2	+1.1	+5.5

TABLE C

T°K	β-py_2	b_{16}	γ-py_2	β-py_6	c_{24}	a_4	α-py_4
315	-27.6	-23.7			-3.2		
304	-25.5	-20.9	-5.2		-2.5		
283	-22.0	-16.9	-6.7	-3.5	-1.5		
270	-20.9	-14.8	-7.8	-4.0	-0.9	-5.1	+5.3
263	-20.2	-13.7	-8.5	-4.4	-0.6	-3.7	
247	-20.2	-13.2	-8.7	-4.6		-2.6	
240	-20.2	-12.2	-9.7	-5.2	0		+8.7
233	-20.6	-11.5	-10.0	-5.3		+0.8	+9.3
220	-21.5	-10.4	-11.3	-6.2	+0.9	+2.6	(+8.3)
203	-22.7	-9.6	-12.9	-6.9	+1.4	+4.9	+9.3
200	-23.3	-9.5	-13.5	-7.1	+1.5	+5.6	+10.4

TABLE D

T°K	β-py_4	b_{16}	γ-py_2	c_{24}	a_4	α-py_4
315	-24.4	-19.0		-2.4	-4.4	
304	-21.8	-16.2	-5.3	-1.8		
283	-18.9	-12.5	-6.3	(-0.5)		
270	-18.2	-10.8		-1.0		+5
263	-18.3	-10.6		0		+6.3
247	-18.4	-10.1	-7.6			+6.8
240	-18.6	-9.4	-8.4	+0.6	+1.4	+8.5
233	-19.0	-9.3		+0.6	+1.8	+10.0
220	-20.1	-8.5	-9.6	+1.1	+3.8	+10.0
203	-22.0	-8.3	-11.0	+1.6	+5.6	+10.7
200	-22.7	-8.0	-11.5	$+1.7_5$	+6.4	

TABLE E

T°K	β-py_4	b_{16}	γ-py_6	c_{24}	a_4	α-py_4
318	-21.7	-15.9	-12.7	-1.8	-5.1	
304	-19.9	-13.7	-14.3	-1.0	-3.9	
286	-18.3	-11.0	-16.9		-2.0	
274	-18.1	-10.0	-18.5	0		+5.4
260	-18.1	-9.4	-19.2	+0.3		+6.0
256	-18.3	-8.9	-20.4	+0.6	+1.0	+8.2
236	-19.3	-8.2	-22.4	+1.1	+2.7	+8.2
232	-19.9	-7.9	-22.9	+1.3	+3.4	+9.2
220	-20.6	-7.6	-24.1	+1.5	+4.4	+9.9
205	-22.4	-7.2	-26.1	+2.0	+6.2	
200	-23.3	-7.1	-27.2	+2.1	+7.0	

TABLE F

T°K	β-py_4	b_{16}	γ-py_4	c_{24}	a_4	α-py_4
315	-11.9	-8.4	-4.4		-6.9	
300	-12.2	-7.6	-4.6		-4.6	
286	-13.0	-6.7	-5.2	+0.5	-2.1	
270	-14.4	-6.1		+1.0		
253	-15.7	-5.9		+1.1	+1.6	+7.5
232	-17.0	-5.5	-7.3	+1.5	+3.0	
216	-18.6	-5.1	-8.0	+2.0	+4.6	
201	-20.7	-4.7	-8.9	+2.5	+6.5	
196	-21.4	-4.5	-9.2	+2.6	+7.3	

TABLE G

T°K	Im_6	b_{16}	a_4	c_{24}	
315		-8.2	-4.0		
300		-7.6	-3.6	0	
286	-19.2	-6.8	-2.7	+0.4	
270	-20.8	-6.4	-2.1	+0.6	
253	-21.9	-6.4	-1.3	+0.8	+6.0
232	-23.4	-6.1		+1.2	
216	-25.1	-6.0		+1.4	
201	-27.2	-6.0		+1.7	+9.5
196	-27.8	-5.9		+1.9	

APPENDIX III

MAGNETIC SUSCEPTIBILITY DATA FOR Fe(III)OCTAETHYLPORPHIN X_2ClO_4 COMPLEXES

TABLE	X
A	3-chloropyridine
B	4-acetylpyridine
C	3-acetylpyridine
D	pyridine
E	4-aminopyridine
F	N-methylimidazole

χ_g mass susceptibility

χ_m molar susceptibility

χ_m^p molar paramagnetic susceptibility

μ effective magnetic moment

m mass of complex in 1 ml of solution

TABLE A

T°K	χ_g ($m^{-3}kg^{-1} \times 10^{-8}$)	χ_m ($m^{-3}kg^{-1}mole^{-1} \times 10^{-5}$)	χ_m^p ($m^{-3}kg^{-1}mole^{-1} \times 10^{-5}$)	μ (B.M.)
m = 0.027				
332	8.24	7.53	8.38	4.21
323	8.53	7.80	8.65	4.22
300	8.41	7.69	8.54	4.04
287	7.82	7.15	8.00	3.82
270	7.65	6.99	7.84	3.67
258	7.17	6.56	7.41	3.49
246	6.76	6.18	7.03	3.32
236	6.29	5.75	6.60	3.15
228	6.23	5.70	6.54	3.08
216	5.93	5.43	6.27	2.94
207	4.93	4.51	5.35	2.66
m = 0.0254				
331	8.67	7.93	8.78	4.30
324	8.79	8.04	8.89	4.28
316	8.67	7.93	8.78	4.20
313	8.54	7.81	8.66	4.15
301	8.42	7.70	8.55	4.05

(Cont.)

TABLE A (Cont.)

T°K	χ_g ($m^{-3}kg^{-1} \times 10^{-8}$)	χ_m ($m^{-3}kg^{-1}mole^{-1} \times 10^{-5}$)	χ_m^p ($m^{-3}kg^{-1}mole^{-1} \times 10^{-5}$)	μ (B.M.)
m = 0.0254 (cont.)				
289	8.29	7.58	8.43	3.94
274	7.66	7.01	7.86	3.70
267	7.35	6.72	7.57	3.59
254	6.79	6.21	7.05	3.38
244	6.41	5.86	6.71	3.23
236	6.16	5.63	6.48	3.12
223	5.97	5.46	6.31	2.99
216	5.91	5.40	6.25	2.93
m = 0.0178 + excess 3-chloropyridine				
330	8.60	7.87	8.72	4.28
323	8.34	7.62	8.47	4.17
303	8.34	7.62	8.47	4.04
287	8.34	7.62	8.47	3.93
272	8.34	7.62	8.47	3.83
252	7.62	6.97	7.82	3.54
229	6.72	6.15	7.00	3.19
219	6.19	5.66	6.50	3.01
202	6.10	5.58	6.42	2.87

TABLE B

T°K	χ_g ($m^{-3}kg^{-1} \times 10^{-8}$)	χ_m ($m^{-3}kg^{-1}mole^{-1} \times 10^{-5}$)	χ_m^P ($m^{-3}kg^{-1}mole^{-1} \times 10^{-5}$)	μ (B.M.)
m = 0.034				
321	7.30	6.79	7.64	3.95
308	6.79	6.31	7.16	3.75
292	6.51	6.05	6.90	3.58
270	5.99	5.57	6.42	3.32
252	5.85	5.44	6.28	3.17
236	5.76	5.35	6.20	3.05
221	5.85	5.44	6.28	2.97
207	6.04	5.61	6.46	2.92

TABLE C

T°K	χ_g ($m^{-3}kg^{-1} \times 10^{-8}$)	χ_m ($m^{-3}kg^{-1}mole^{-1} \times 10^{-5}$)	χ_m^p ($m^{-3}kg^{-1}mole^{-1} \times 10^{-5}$)	μ (B.M.)
320	6.18	5.75	6.59	3.66
301	5.65	5.25	6.10	3.42
283	5.12	4.76	5.60	3.18
265	4.80	4.46	5.31	2.99
252	4.69	4.36	5.21	2.89
236	4.59	4.26	5.11	2.77
219	4.80	4.46	5.31	2.72
212	4.37	4.07	4.91	2.57
208	4.80	4.46	5.31	2.65

TABLE D

T°K	χ_g ($m^{-3}kg^{-1} \times 10^{-8}$)	χ_m ($m^{-3}kg^{-1}mole^{-1} \times 10^{-5}$)	χ_m^p ($m^{-3}kg^{-1}mole^{-1} \times 10^{-5}$)	μ (B.M.)
m = 0.0416				
319	4.59	3.88	4.73	3.10
301	3.36	2.84	3.69	2.66
273	2.83	2.39	3.24	2.37
254	2.94	2.49	3.33	2.32
237	2.98	2.52	3.37	2.25
223	3.40	2.88	3.72	2.30
209	3.10	2.62	3.46	2.15
204	3.75	3.17	4.02	2.28

TABLE E

T°K	χ_g ($m^{-3}kg^{-1} \times 10^{-8}$)	χ_m ($m^{-3}kg^{-1}mole^{-1} \times 10^{-5}$)	χ_m^p ($m^{-3}kg^{-1}mole^{-1} \times 10^{-5}$)	μ (B.M.)
m = 0.0183				
329	4.51	3.95	4.79	3.17
315	4.41	3.86	4.71	3.08
306	4.21	3.68	4.53	2.97
291	4.41	3.86	4.71	2.95
275	4.51	3.95	4.79	2.90
258	4.51	3.95	4.79	2.81
242	5.11	4.48	5.32	2.86
228	5.61	4.92	5.76	2.89
215	5.92	5.18	6.03	2.87

TABLE F

T°K	χ_g ($m^{-3}kg^{-1} \times 10^{-8}$)	χ_m ($m^{-3}kg^{-1}mole^{-1} \times 10^{-5}$)	χ_m^p ($m^{-3}kg^{-1}mole^{-1} \times 10^{-5}$)	μ (B.M.)
m = 0.0288				
324	2.48	2.11	2.96	2.47
300	2.48	2.11	2.96	2.38
288	2.48	2.11	2.96	2.33
271	2.70	2.30	3.15	2.33
252	2.81	2.39	3.24	2.28
237	3.03	2.58	3.43	2.27
223	3.31	2.82	3.66	2.28
209	3.64	3.10	3.95	2.29

APPENDIX IV

MAGNETIC MOMENT DATA FOR Fe(III) OCTAETHYLPORPHIN X_2 ClO_4 COMPLEXES IN THE SOLID STATE

TABLE	X
A	3-chloropyridine
B	4-acetylpyridine
C	pyridine

TABLE A

T°K	μ (B.M.)
290	3.69
236	3.03
207	2.55

TABLE B

T°K	μ (B.M.)
290	2.93
236	2.48
207	2.44

TABLE C

T°K	μ (B.M.)
290	3.42
236	2.99
207	2.87
70	2.63

APPENDIX V

OBSERVED ^{1}H NMR SHIFT* DATA FOR X_2Fe(III)-PORPHYRIN DIMETHYL ESTER CHLORIDE COMPLEXES

TABLE	PORPHYRIN	X
A	Porphin	4-Methylpyridine
B	Deutero	Pyridine
C	Deutero	4-Methylpyridine
D	Etio	Pyridine
E	Etio	4-Methylpyridine
F	Proto	Pyridine
G	Proto	3-Methylpyridine
H	Proto	4-Methylpyridine
J	Meso	Pyridine
K	Meso	3-Methylpyridine
L	Meso	4-Methylpyridine
M	Porphin	Imidazole
N	Meso	Imidazole
P	Proto	Benzimidazole
Q	Proto	5,6-Benzimidazole
R	Meso	Benzimidazole
S	Meso	5,6-Benzimidazole
T	Proto	Isoquinoline
U	Meso	Isoquinoline

*All shifts in ppm from TMS.

TABLE A

T°K	γ-py$_6$	β-py$_4$	b_4	α-py$_4$	a_8
300					+16.0
292	-17.9	-14.9			+18.1
284	-18.7	-15.1		+10.6	+19.6
273	-19.6	-15.5			+20.4
264	-20.5	-16.2	+0.8	+11.0	+22.2
255	-21.5	-16.8	+1.7	+11.6	+23.5
249	-22.2	-17.3	+2.1	+11.6	+24.2
239	-23.1	-18.1	+3.0	+11.6	+25.8
233	-23.7	-18.5	+3.4		+26.9
225	-25.0	-19.6	+4.5		+28.7
219	-25.4	-20.1	+5.2		+29.9
214	-26.3	-20.9	+5.7		+30.8
206	-27.4	-21.9	+6.9		+32.8
198	-27.3	-21.7	+6.8		+32.3

TABLE B

T°K	a_3	a_3	a_3	a_3	β-py$_4$	c_2	c_2	e_6	d_4	b_1	b_2	b_1	α-py$_4$	f_1	f_1
320	-25.8	-23.2	-22.7	-21.9		-13.0	-10.9	-3.4						+13.3	
303						-12.5	-10.3	-3.5	-1.3	-2.3	-2.0	-1.8			
300	-24.6	-22.1	-21.2	-20.2		-11.8	-9.7							+17.1	
287						-11.2	-9.0	-3.5	-1.0		-1.3	-0.1			
284	-24.2	-21.5	-20.5	-19.6		-10.9	-8.7							+19.2	+19.8
267	-23.9	-20.9	-20.1	-19.0	-15.8	-9.8	-7.8	-3.5	-0.4	-0.9	0	+0.9		+22.8	+23.7
258					-16.6								+9.5		
254					-16.7						+1.2	+2.5	+9.9	+24.7	+25.7
250	-24.0	-20.8	-20.1	-18.9		-9.8	-7.6	-3.5	-0.2	+0.2	+1.5	+2.7		+25.5	+26.6
246					-17.1								+10.2		
242					-17.4					+1.2	+2.1	+3.4		+26.3	+27.7
236	-24.5	-20.9	-20.4	-19.0		-9.3	-7.1	-3.5	+0.2	+2.3	+3.3	+4.5		+28.3	+29.6
231	-24.6	-21.0	-20.5	-19.3	-18.2					+2.6	+3.4	+4.8	+11.4	+28.8	+30.2
223	-25.3	-21.5	-20.9	-19.6		-8.9	-6.7	-3.6	+0.6	+3.4	+4.4	+5.7		+30.4	+31.8
216	-25.8	-21.7	-21.5	-19.8	-19.8				+1.2	+4.2	+5.0	+6.5	+11.4	+31.5	+33.0
210	-25.7	-21.7	-21.2	-19.7	-20.5				+1.2	+4.8	+5.5 +5.9	+7.2		+33.2	+34.9

(Cont.)

TABLE B (Cont.)

T°K	a_3	a_3	a_3	a_3	β-py$_4$	c_2	c_2	e_6	d_4	b_1	b_2	b_2	b_1	α-py$_4$	f_1	f_1
205	-26.1	-21.6	-19.8						+1.6	+5.6	+6.4	+6.7	+7.9			
202	-26.6	-21.7	-20.0	-21.7					+1.8		+6.5		+7.9		+33.7	+35.3
198									+1.9	+5.9	+6.8	+7.2	+8.4		+35.7	+37.5
191	-27.4	-22.3	-20.1						+2.6	+7.6	+8.4	+8.8	+10.1			

TABLE C

T°K	a_3	a_3	a_3	a_3	γ-py$_6$	β-py$_4$	c_4	d_4	b_1	b_2	b_1	α-py$_4$	f_1	f_1
318	-23.9	-21.5	-20.9	-19.8			-11.7						+14.4	+14.9
303	-22.8	-20.4	-19.7	-18.7			-10.7						+14.7	+15.2
289	-22.5	-19.8	-19.3	-18.2			-9.8						+18.7	+19.3
281	-22.5	-19.8	-19.2	-18.1									+20.9	+21.7
267	-22.7	-19.8	-19.3	-18.2	-19.3	-16.6					+1.4	+9.0	+22.7	+23.6
258	-22.7	-19.8	-19.3	-18.1	-19.8	-16.8				+0.7	+1.6		+23.6	+24.6
254	-22.9	-19.8	-19.3	-18.1	-20.8	-17.4				+1.5	+2.6	+9.0	+24.8	+25.9
246	-23.1	-20.0	-19.4	-18.2	-21.3	-17.7			+1.2	+1.9	+3.0	+9.3	+25.8	+26.9
242	-23.4	-20.0	-19.4	-18.2	-22.0	-18.2			+1.6	+2.5	+3.7		+26.9	+28.0
229	-23.5	-20.1	-19.6	-18.3	-23.1	-19.0			+3.0	+3.7	+4.9	+9.9	+29.1	+30.2
219								+1.1	+4.1	+4.9	+6.3		+31.0	+32.3
216	-24.3	-20.5	-20.5	-18.7	-24.7	-20.5		+1.4	+4.2	+5.2	+5.5	+6.5		
212	-25.4	-20.9		-19.0	-26.6	-22.0		+1.6	+4.9	+5.7	+6.3	+7.4	+32.5	+34.1
202	-25.4	-20.8		-18.9	-27.2	-22.7		+2.2	+6.0	+6.5	+7.2	+8.3	+34.0	+35.6

TABLE D

T°K	a_{12}	β-py_4	f_8	γ-py_2	g_{12}	b_4	α-py_4
295	-25.4		-12.5		-0.8	-4.7	
267	-23.6		-10.4		0	-1.1	
249	-23.6	-17.7	-9.7		+0.3		+7.5
247	-23.3	-17.5	-9.4		+0.5	+1.3	+8.0
234	-23.4	-18.4			+0.8	+2.5	+9.7
229	-23.5	-18.6			+0.9	+3.1	+9.9
219	-23.8	-19.6		-9.1	+1.0	+4.3	+10.2
209	-24.2	-20.6		-10.0	+1.4	+5.5	+10.7
202	-24.6	-21.8		-10.7	+1.8	+6.8	

TABLE E

T°K	a_{12}	γ-py_6	β-py_4	f_8	g_{12}	b_4	α-py_4
298	-22.5			-10.6	-0.3		
269	-21.8		-16.8		+0.3		+8.5
249	-22.1	-20.4	-17.9		+0.5	+1.5	+8.0
242	-22.0	-21.5	-18.5	-8.4	+0.8	+2.5	+8.8
233	-22.4	-22.4	-19.1	-8.1	+0.9	+3.3	+9.4
226	-22.2	-22.9	-19.4		+1.5	+4.4	+9.6
216	-22.6	-24.1	-20.5		+1.4	+5.0	+10.0
209	-23.1	-25.3	-21.5		+1.5	+5.8	
202	-23.5	-26.7	-23.5		+2.0	+7.2	+10.5
195	-23.8	-27.3	-23.8		+2.0	+7.8	
191	-23.9	-28.1	-23.9		+2.3	+8.6	

TABLE F

T°K	a_3	a_3	a_3	a_3	β-py_4	f_2	c_4	e_6	d_4	b_1	b_3	g_2	g_2	α-py_4
300	-23.5		-21.9	-21.0		-17.8	-11.4		-1.5				+4.1	
290	-22.9	-22.7	-20.9	-20.3		-16.8	-10.3		-1.2		-1.6		+4.9	
287							-10.1	-3.6	-1.1	-3.0	-1.5			
267	-22.5	-22.3	-20.1	-19.7		-15.8	-9.1		-0.7	-1.2		+5.3 +5.6	+6.0	
264							-9.2	-3.6	-0.7	-1.3				
255	-22.0	-21.7	-19.6	-19.2	-16.6	-14.9	-8.4				+1.9	+6.0 +6.4	+6.8	+10.1
252	-22.4	-22.2	-20.0	-19.4	-17.3	-15.1					+2.5	+6.3 +6.5	+7.1	+10.1
244	-22.5	-22.3	-20.1	-19.6	-17.3	-14.9					+2.6 +2.9	+6.4 +6.7	+7.4	
236	-22.8	-22.7	-20.4	-20.0	-17.8	-14.8	-8.3	-3.6	0	+1.7	+3.3 +3.7	+6.8 +7.4	+7.8	+11.0
221							-7.9	-3.6	+0.4	+2.8				+11.3
219	-23.6	-23.2	-20.8	-20.4	-19.4	-14.6	-7.8			+3.0	+4.9 +5.5	+7.8 +8.2	+8.8	
202	-24.5	-24.0	-21.0	-20.6	-21.0	-14.1	-7.1		+1.4	+4.9	+6.9 +7.5	+9.1	+10.2	
195	-25.0	-24.6	-21.3	-20.9	-22.4	-13.6	-6.5		+1.9	+6.1	+8.2 +8.8	+10.1	+11.1	

TABLE G

T°K	a_3	a_3	a_6		β-py$_2$	f_2	γ-py$_2$	β-py$_6$	e_6	d_4	b_1	b_1	b_2	g_2	g_2	α-py$_4$
261	-22.7	-22.4	-20.5	-20.4	-17.9	-16.4			-3.8				+0.5	+5.3	+5.8	
251																+10.1
249	-22.7	-22.4	-20.3	-20.2	-17.5	-15.8		-4.2	-3.7			+1.3	+1.9	+6.1	+6.6	+10.2
223	-23.0	-22.6	-20.4		-18.4	-15.3	-8.2	-4.7	-3.5	+0.5	+1.7	+2.9	+3.7	+7.1	+7.6 +7.8	+10.2
219	-23.2	-22.8	-20.5		-19.4	-14.7	-9.0	-5.0	-3.4		+3.2	+4.7	+5.5	+8.1 +8.4	+8.9	+11.4
212	-23.7	-23.3	-20.8		-20.3	-14.6	-9.9	-5.5	-3.6	+0.7	+3.8	+5.3	+6.1	+8.4 +8.8	+9.3 +9.5	
202	-24.0	-23.6	-20.9		-20.9	-14.3	-10.3	-5.7	-3.6	+1.0	+5.0	+6.6	+7.4	+9.4	+10.3	
200	-24.2	-23.9	-21.4	-21.2	-21.3	-14.2	-10.8	-6.1	-3.4	+1.2	+5.5	+7.0	+8.0	+9.7	+10.4 +10.9	

TABLE H

T°K	a_3	a_3	a_3	a_3	γ-py$_6$	β-py$_4$	f_2	e_6	d_4	b_1	b_3	g_2	g_2	α-py$_4$
300	-22.0	-21.7	-19.8	-19.2						-1.2			+4.1	
295	-21.7	-21.5	-19.9	-19.5			-16.6	-3.4						
290	-21.5	-21.2	-19.3	-18.7						-1.0		+4.2	+4.6	
267	-21.2	-20.9	-18.9	-18.3	-19.6	-16.6	-14.9				+1.1	+5.2 +5.5	+5.9	+9.1
261	-21.3	-20.9	-18.9	-18.3	-20.3	-17.0		-3.4			+1.2	+5.2 +5.7		+9.4
255	-21.3	-21.2	-18.9	-18.3	-20.5	-17.1	-14.6				+1.9	+5.6 +5.9	+6.3	
252	-21.3	-21.2	-18.7	-18.3	-21.2	-17.4	-14.3				+2.7	+6.0 +6.4	+6.8	+9.5
244	-21.5		-18.7	-18.2	-21.5	-17.7	-14.1	-3.4			+3.0	+6.3 +6.5	+7.1	
236	-21.9	-21.5	-19.0	-18.7	-22.5	-18.7	-14.0			+1.9	+3.8	+6.7 +7.0	+7.5	+11.0
219	-22.4	-22.2	-19.3	-18.9	-24.6	-20.3	-13.5		+1.1	+3.6	+5.6 +6.0	+7.9 +8.2	+8.8	
212	-22.8	-22.4	-20.1		-25.8	-21.4		-3.6		+4.2	+6.2	+8.2	+9.1	
202	-23.1	-22.8	-19.6	-19.2	-26.6	-22.2	-13.0	-3.4	+1.9	+5.5	+7.4 +7.9	+9.1	+10.1	
195	-23.6	-23.1	-19.6	-19.3	-27.9	-23.4	-12.5	-3.4	+2.6	+6.7	+9.0	+9.5 +9.9	+11.0	

TABLE J

T°K	a_3	a_3	a_6	β-py$_4$	f_4	c_4	γ-py$_2$	e_6	d_4	g_6	b_1	b_1	b_2	α-py$_4$
313	-27.4	-26.6	-25.1		-14.4	-14.1								
303	-26.5	-25.7	-24.2		-12.9	-12.7		-3.5		-1.1			-2.0	
300	-25.8	-25.0	-23.4		-12.5			-3.6						
284	-25.0	-24.0	-22.7		-11.4	-11.1		-3.6						
267	-24.0	-22.7	-21.5		-10.4	-10.0		-3.5		-0.2	-1.2	-0.6	+0.4	+6.5
261	-24.0	-22.8	-21.5	-17.0		-9.8		-3.7						+8.0
249	-23.7	-22.3	-20.9	-17.7	-9.8	-9.3		-3.5		-0.2			+1.3	+8.5
239	-24.0	-22.7	-21.3	-18.5	-9.3			-3.7			+0.7	+1.2	+2.2	+9.5
233	-24.5	-22.8	-21.5		-9.2	-8.6		-3.5	-0.2	+0.2 +0.7	+1.8	+2.2	+3.3	+10.1
223	-25.0	-23.1	-21.7	-19.4	-8.8	-8.2		-3.5	-0.2	+0.6	+2.5	+3.0	+4.1	
212	-25.1	-23.4	-22.1	-20.4		-8.0	-9.1	-3.5	+0.3	+0.9 +1.1	+3.8	+4.4	+5.5	
205	-25.4	-23.5	-22.4	-20.8		-7.5	-10.2	-3.4	+0.5	+1.4	+4.9	+5.5	+6.8	+10.5
202	-25.5	-23.6	-22.5	-21.6		-7.5	-10.5	-3.6		+1.4	+5.2	+5.7	+6.8	
198	-25.5	-23.6	-22.5			-7.2				+1.6	+5.5	+6.0	+7.4	

TABLE K

T°K	a_3	a_3	a_6	β-py$_2$	c_4	γ-py$_2$	β-py$_6$	e_6	d_4 g_6	b_1	b_1	b_2	α-py$_4$
295	-26.3	-25.2	-23.8		-12.9			-3.6	-1.4	-4.4			
275	-25.0	-23.5	-22.2		-10.7			-3.4	-0.9				
261	-24.9	-22.8	-21.7		-9.8			-3.7					
245	-24.7	-22.6	-21.2	-18.1				-3.7				+1.3	+8.8
233	-25.0	-22.6	-21.1	-18.6			-4.8	-3.7	0	+0.3	+0.7	+2.9	+9.1
229	-24.8	-22.5	-21.1	-18.6			-4.7	-3.4			+0.7	+2.9	+10.1
223	-25.2	-22.7	-21.3	-19.4			-5.2	-3.5		+2.7	+3.6	+4.6	+9.6
219	-25.5	-22.8	-21.5	-19.8			-5.4	-3.6	+0.7 +1.0	+2.8	+3.7	+4.7	+10.5
212	-25.7	-23.0	-21.6	-20.3		-10.0	-5.7	-3.6	+0.9 +1.3	+3.7	+4.6	+5.7	
205	-26.0	-23.1	-21.7	-21.1		-10.4	-5.9	-3.6	+1.0 +1.3	+4.2	+5.2	+6.2	
202	-26.2	-23.2	-21.7	-21.7		-10.9	-6.3	-3.5	+1.5	+5.1	+6.0	+7.1	
198	-26.4	-23.4	-21.9	-21.9		-11.1	-6.5	-3.4	+1.8	+5.8	+6.7	+7.9	

TABLE L

T°K	a_3	a_3	a_6	β-py$_6$	β-py$_4$	c_4 f_4	e_6	g_6	d_4	b_1	b_1	b_2	α-py$_4$
300	-23.1	-22.1	-20.9			-10.6				-3.4			
295		-22.1	-20.8			-10.6	-3.8						
284	-22.7	-21.5	-20.4				-3.6						
264	-22.3	-20.9	-19.8	-19.4	-17.4	-9.3	-3.4						
259	-22.4	-21.0	-19.8	-19.8	-17.5		-3.5				+0.3	+0.7	
253	-22.4	-20.9	-19.8	-20.3	-17.8		-3.5				+0.6	+1.2	
249	-22.5	-20.6	-20.0	-20.6	-18.1	-8.3	-3.5			+0.3		+1.6	
236	-22.8	-21.2	-20.0	-22.3	-19.0	-7.8	-3.6		+0.7	+1.8	+2.2	+3.1	+8.8
223	-23.2	-21.5	-20.3	-23.6	-20.1	-7.2		+0.6	+1.1	+3.0	+3.4	+4.5	+10.0
216	-23.4	-21.5	-20.2	-24.2	-20.2			+0.4 +0.8	+1.2	+3.7	+4.2	+5.2	
212	-23.4	-21.5	-20.6	-24.7	-21.2		-3.6	+0.6	+1.5	+4.4	+5.0	+6.1	
202	-24.0	-22.0	-21.2	-26.5	-22.5		-3.5	+1.5		+5.3	+6.0	+7.1	
195	-24.2	-22.1	-21.5	-27.6	-23.9		-3.4	+2.2		+6.2	+7.5	+8.7	

TABLE M

T	b_4	Im(2-H)	a_8
297	-2.9	+9.5	+16.5
270	-1.8	+11.3	+19.8
246	-0.9	+12.0	+21.4
240		+11.6	+22.7
236		+13.0	+23.4
231		+12.7	+24.1
219			+24.9
202	+1.2		+27.4
195	+1.4		+29.6

TABLE N

T°K	a_3	a_3	a_6	Im(1-H)	Im(4-H)	e_6	b_4	d_4 g_6	Im(2-H)
319	-15.2	-14.2	-13.7	-8.7		-3.8	-3.8	-0.6	
297	-15.7	-14.8	-14.2	-9.1		-4.1	-3.1	-0.6	+6.1
267	-16.5	-15.5	-14.7	-9.5		-4.0	-1.8	+0.4	+7.5
252	-17.2	-16.2	-15.3	-10.0	-8.9	-4.0	-1.0	+0.7	+9.3
241					-9.1	-4.0		+0.8	+7.2
229	-17.8	-16.8	-15.5	-10.6	-9.3	-3.8		+0.8	+9.0
219	-18.5	-17.7	-16.3	-11.0	-9.5	-3.8	+0.9	+1.1	
212	-18.9	-18.3	-16.5	-11.2	-9.6	-3.9		+1.3	
206	-19.4	-18.8	-16.7	-11.6	-9.8	-3.9		+1.3	
202	-19.4		-17.0	-11.8	-10.1	-3.9		+1.4	

TABLE P

T°K	Bz	a_3	a_3	a_3	a_3	Bz	Bz	f_2	Bz	Bz	e_6	b_1	d_4	b_1	b_1	b_1	g_2	g_2	Bz(2-H)
295		-24.0		-21.2				-18.8			-3.5		-1.8					+2.2	
264		-20.4		-17.0				-14.7			-3.5						+3.2	+3.5	
247		-20.0	-19.7	-16.1				-13.5			-3.5				+0.9	+1.6	+3.5	+3.8	+4.3	+15.9
242		-20.2	-19.9	-16.1				-13.4			-3.6	-2.8		+0.6	+1.5	+2.3	+3.8	+4.0	+4.5	+16.4
234	-22.1	-20.3	-19.9	-16.0			-12.0	-13.3	-10.9		-3.4	-2.1		+1.5	+2.3	+3.3	+4.3	+4.6	+5.1	+17.8
229	-22.5	-20.2	-19.9	-16.1		-13.0	-12.1	-13.0	-11.1	-9.8	-3.7	-1.6	+0.3	+1.9	+2.8	+3.8		+4.5	+5.3	+18.2
216	-23.3	-20.7	-20.2	-16.3	-15.9	-14.6	-12.5	-12.5	-11.2	-10.0	-3.5		+0.5	+3.0	+4.1			+5.2	+5.9	+20.2
212	-24.2	-20.8	-20.3	-16.2	-15.8		-12.8	-12.3	-11.5	-10.0	-3.5		+0.5	+3.8		+5.5		+5.5	+6.4	+21.4
205	-25.0	-21.3	-20.7	-16.4	-16.0	-16.0	-13.2		-11.7	-10.3	-3.6		+0.9	+4.5				+6.0	+7.0	+22.7
202	-25.3	-21.2	-20.5	-16.3	-15.7		-13.3	-11.8	-11.8	-10.3	-3.4		+1.2	+5.0				+6.3	+7.3	+23.4

TABLE Q

T°K	Bz	a_3	a_3	a_3	a_3	c_4	f_2	Bz	Bz	Bz	e_6	d_4	b_1	b_2	b_1	g_4	Bz(2-H)
295		-21.7		-19.4	-18.9	-15.2	-17.3				-3.5	-1.3				+2.4	
264		-19.9		-16.5		-14.5	-14.5									+3.5	
247		-19.5		-16.0	-15.7	-13.4	-13.4				-3.6			+1.1		+4.0	+15.6
242		-19.6		-16.0	-15.6		-13.2	-13.2	-11.1	-10.3	-3.9	+0.3		+1.5	+3.6	+4.1	+16.0
234	-21.0	-19.7		-16.1	-15.5	-13.5	-12.8	-13.5	-11.3	-10.3	-3.5	+0.4	+1.3	+2.3	+4.5	+4.5	+17.5
229	-21.7	-19.8		-15.9	-15.2	-12.9	-12.4	-13.8	-11.6	-10.4	-3.5	+0.7	+2.2	+3.2	+5.4	+4.9	+19.0
216	-22.7	-20.7	-20.5	-16.5	-15.5	-13.2		-15.1	-12.3	-11.0	-3.4	+0.7	+2.9	+3.9	+5.7	+5.2	+19.5
212	-23.1	-20.5	-20.2	-15.9	-14.7		-11.5	-14.7	-12.0	-10.8		+1.3	+4.2	+5.3	+6.5	+5.9	+20.8
205	-24.0	-20.9	-20.5	-15.9	-14.6			-15.9	-12.6	-10.9	-3.3	+1.8	+6.0	+6.7	+7.4	+6.7	+22.9
202	-23.8	-21.2	-20.8	-16.3	-15.0			-15.8	-12.7	-11.2	-3.3	+1.5			+7.1	+6.4	

TABLE R

T°K	Bz	a_3	a_3	a_3	a_3	f_4	Bz	Bz	Bz	Bz	e_6	d_4 g_6^4	b_1	b_1	b_2	Bz(2-H)
319		-34.1		-32.1		-21.6	-13.5				-3.4	-3.4 -2.8				
298		-29.5		-28.1		-17.3	-14.1				-3.4	-2.0 -1.8				
267		-23.4	-22.8	-22.3	-21.5	-11.6	-14.4				-3.4	-0.8 -0.4				
252		-21.8	-20.9		-19.9	-9.8	-14.5				-3.3	-0.3			-1.9	
229		-20.8	-20.3	-19.7	-19.1	-8.6					-3.5	+0.7	-2.0	-0.9	+2.0	
219	-23.6	-20.8	-20.5	-19.4	-18.9	-8.1		-13.9	-12.6	-10.5	-3.7	+0.9		+2.3	+4.0	+19.2
217	-24.5	-20.8		-19.3	-18.9	-7.9					-3.4	+1.2	+2.4	+3.4	+5.1	
212	-24.2	-20.6		-19.2	-18.7	-7.3		-14.6	-12.6	-10.6	-3.5	+1.2	+2.4	+3.3	+5.1	+20.4
206	-25.0	-20.7		-19.0	-18.5	-7.1		-15.2	-12.9	-10.5	-3.4	+1.5	+3.3	+4.4	+6.4	+21.4
202	-25.2	-20.6		-18.9	-18.4	-6.3		-15.4	-13.0	-10.6	-3.3	+1.8	+3.9	+5.1	+7.1	+22.7

TABLE S

T°K	Bz	a_6	a_3	a_3	Bz	Bz	Bz	d_4 g_6^4	b_4	Bz(2-H)
295		-24.0	-22.4	-22.3						
276		-21.2	-20.0	-19.8						
264		-20.6	-19.4	-19.1						
252		-20.0	-19.0	-18.6						
242		-19.2	-18.3	-17.9						+17.9
236		-19.5	-18.8	-18.1	-12.6			+0.3	+1.0	+18.7
229	-21.2	-18.9	-18.3	-17.8	-13.3	-11.3	-9.7	+1.0	+3.4	+18.7
224	-22.4	-19.2	-18.7	-18.2	-14.0	-11.7	-10.0	+1.3	+3.9	+18.4
219	-23.0	-19.1	-18.2		-14.6	-11.8	-10.2	+1.3	+4.6	+19.3
214	-23.2	-18.8	-17.8		-14.7	-11.9	-10.0	+1.7	+5.5	+20.4
206	-24.2	-19.1	-18.3		-15.4	-12.4	-10.4		+7.2	+21.8
202	-24.5	-18.9	-18.1		-15.3	-12.5	-10.3	+2.4	+8.1	+22.5

TABLE T

T°K	a_3	a_3	a_3	a_3	Iq_2	Iq_2	f_2	Iq_2	Iq_2	e_6	d_4	b_1	b_1	b_2	g_2	g_2	Iq_4
295	-24.1		-21.9				-18.2							-1.5	+4.3		
261	-22.4	-22.3	-20.5	-20.2			-16.1			-3.7				+0.8	+5.5	+6.1	
247	-22.5	-22.4	-20.3		-18.1	-16.0	-15.8	-11.7		-3.5		+0.7	+1.7	+2.2	+6.2	+6.8	
230	-22.8	-22.5	-20.7		-19.3	-17.3	-15.5	-12.5	-9.6	-3.7		+1.7	+3.2	+3.7	+6.9	+7.7	+20.0
223	-22.9	-22.7	-20.9	-20.8	-20.0	-17.9	-15.1	-12.7	-9.9	-3.7		+2.6	+4.2	+4.8	+7.6	+8.5	+19.5
209	-23.5	-23.3	-21.4	-21.1	-21.4	-18.7	-14.9	-13.2	-10.4	-3.7	+0.7	+3.8	+5.3	+6.1	+8.4	+9.3	
198	-24.1	-23.8	-21.9	-21.5	-22.6	-19.7	-14.9	-13.8	-11.0	-3.7	+0.9	+5.0	+6.6	+7.2	+9.1	+9.9	+10.3
195	-24.4	-24.0	-22.0	-21.7	-23.3	-20.0	-14.8	-13.9	-11.1	-3.7	+1.0	+5.3	+7.1	+7.7	+9.5	+10.3	+10.6

TABLE U

T°K	a_3	a_3	a_6	Iq_2	Iq_2	Iq_2	Iq_2	e_6	d_4	g_6	b_1	b_1	b_2	Iq_4
295	-27.2	-25.8	-24.5											
264	-24.9	-22.9	-21.3					-3.5						
251	-24.8	-22.5	-21.0	-18.5	-15.7	-11.4		-3.3					+1.5	
241	-25.2	-22.7	-21.2	-19.3	-16.6	-12.2	-9.5	-3.5		+0.3	+0.5	+1.5	+2.5	+17.5
233	-25.3	-22.7	-21.2	-19.8	-17.2	-12.6	-9.6	-3.7		+0.7	+1.5	+2.0	+3.2	+18.2
226	-25.6	-22.8	-21.2	-20.1	-17.5	-12.6	-9.6	-3.5	+0.3	+0.9	+2.4	+2.9	+4.0	+18.5
222	-25.8	-22.9	-21.3	-20.8	-18.0	-12.7	-10.1	-3.7	+0.5	+1.2	+3.2	+3.8	+5.0	+19.4
217	-26.2	-23.1	-21.5	-21.5	-18.3	-13.0	-10.4	-3.4	+0.9	+1.3	+3.5	+4.3	+5.4	+20.0
207	-26.8	-23.4	-21.7	-21.7	-19.1	-13.5	-10.9	-3.6	+1.2	+1.5	+4.7	+5.5	+6.6	+20.6
202	-27.0	-23.7	-21.9	-22.9	-19.6	-13.8	-11.3	-3.6	+1.3	+1.5	+5.2	+6.1	+7.2	
200	-27.0	-23.5	-21.9	-23.5	-19.6	-13.7	-11.2	-3.4	+1.4	+1.7	+5.8	+6.4	+7.7	